AN EXPERIMENTAL AND THEORETICAL INVESTIGATION OF THE ELASTIC AND POST-ELASTIC DEFORMATION OF METALS.

BY

M. GOTTSCHALL, B.E. (Hons.)

Prepared for Submission to the Faculty of Engineering at the University of Adelaide to fulfil the Requirements for the Degree of Doctor of Philosophy.

September, 1964.

This thesis contains no material which has been accepted for the award of any other degree or diploma in any Universuty and, to the best of the writers knowledge and belief, the thesis contains no material previously published or written by any other person except where due refrence is made in the text of the thesis.

11th. Sept. 1964.

ACKNOWLEDGEMENTS

This research project was carried out with the assistance of a Commonwealth Research Fellowship Grant.

The writer is deeply indebted to his supervisor, Mr. W. D. Doble and Professor H. K. Davis for the opportunity of being able to pursue a subject somewhat on the fringe of Mechanical Engineering, for their assistance in providing critical discussion and their continued encouragement.

He is pleased to report the stimulating interest of other members of the teaching staff and the helpful advice and assistance from members of the technical staff.

INDEX

Page

1.0 SUMMARY

The dislocation and the crack are mechanisms that are fundamental to the current theory of deformation. The current view is that during deformation, these mechanisms are introduced into a crystal by a process of generation that requires the pre-existence in the deforming crystal of at least one of these mechanisms. The writer has examined the grounds for an alternative process, according to which these mechanisms are nucleated in crystals subjected to stress. This has led him to the thesis that the nucleation process occurs in real crystals. A specific nucleation hypothesis is also put forward and examined qualitatively. Experimental work , carried out in order to obtain first-hand data, also favours this thesis.

2.0 INTRODUCTION

The present phase of enquiry into the structure and mechanical properties of solids may be said to have begun about forty years ago.

An important step was taken in 1921 when A. A. Griffith[1] brought forward a theory of cracks in elastic media. This theory related the dimension of a crack to the overall stress which can cause it to be propagated. The physical properties of the material involved are surface tension and elastic modulus. He was able to explain the phenomenon that the strength of glass fibres increased with decreasing diameter on the simple assertion that the longest possible crack in such a fibre is of the order of the diameter of the fibre.

The modern ideas on shear deformation were still to come. In 1934 Polanyi[2] was still able to say that the mechanism of flow in crystals was unknown. In the same paper, he discussed the "lattice dislocation." Others had already suggested that such dislocations might be the mechanism of shear deformation in crystals. Prandtl[3] used this concept to explain the elastic after-effect, and Dehlinger[4] discussed dislocations as a cause of recrystallization.

By 1934 the concept had already become well known. Taylor[6] brought forward the hypothesis that the strength of crystals is determined by dislocation interaction. In crystals of low dislocation density the interaction is weak and the relatively free movement of dislocations permits deformation at a low stress level. In the same year Orowan[7] put forward a theory of crystal plasticity which combined the dislocation concept of Polanyi[2] with the thermal activation theory of Becker[8].

The change ushered in by this one concept was of a very fundamental nature. Previously it was generally assumed that a truly perfect array of atoms or molecules had no mechanical strength, but the presence of imperfections, "amorphous" intercrystalline zones and other "amorphous" zones produced during shear deformation were responsible for yield strength and work hardening, e.g.[9]. Griffith in the paper already cited subscribes to such a view. He suggested that the force-field about atoms and molecules is non-uniform so that in a substance whose units were oriented in a regular way strength in different directions would vary resulting in planes of weakness. Becker[8] in describing the effect of thermal activation made use of three phenomena: exchange of atoms between lattice sites, thermal stress fluctuations and strain hardening, thereby avoiding the

problem of the exact atomic mechanism of shear flow.

The earlier theory seemed to be consistent with ordinary experience. Carefully prepared and well refined crystals were after all much weaker than crystals grown rapidly and with a greater impurity content. The low strength of crystals or the high strength of "amorphous" solid were not explained. These were the basic propositions of the theory. To say that no attempt was made at all is not strictly correct. In 1921 Polanyi[10] for example proposed a quantum jump mechanism to explain the anomaly that at the stresses observed, for cleavage, the range of the attractive forces on the new surfaces being formed should be many times greater than it was believed to be.

The Griffith-crack theory and the dislocation theory called for a complete reversal of ideas about the mechanical properties of a perfect crystal. Instead of being easily deformed, the perfect lattice was assumed to possess a "theoretical" strength many times greater than that of real crystals.

The "theoretical" strength is based on the following argument. If a solid is to be broken by the application of a force, the energy required is at least as great as the surface energy associated with the new

surfaces. To pull apart two adjacent planes of atoms of a perfect crystal the surface energy associated with these planes must be provided. Now the range of the attractive forces in a crystal is known and is of the order of 10^{-7} cm. A force acting through this distance must supply the necessary energy. The magnitude of this force may therefore be estimated, and is known as the theoretical strength of the crystal.

The <u>surface energy</u> of a solid crystal may be found in several ways; namely, extrapolation of the liquid values[10], computations based on the cohesive energy of the solid[11] and direct measurement[12].

In the years following the introduction of the dislocation concept, the theory was worked out in increasing detail.

<u>Slip</u> is generally found to be concentrated into zones defined as slip bands. With some crystals such as zinc this effect is very marked as shown for example by Figure 2[13]. The only acceptable explanation of this is that dislocations are being generated during the deformation process. A satisfactory mechanism for the multiplication of dislocations was put forward by Frank and Read[14] in 1950.

Another phenomenon that required explanation is work hardening. During deformation the stress required to maintain flow increases. Several mechanisms of work hardening are available. Mott[15] proposed that obstacles, mainly sessile dislocations could cause dislocation to pile up and eventually make the generating mechanisms inactive.

Taylor[6] in 1934 suggested that during deformation dislocations are stopped at mosaic boundaries and interact with each other to increase the stress required to maintain deformation. A detailed discussion of work hardening is presented by Cottrell[16].

Another of the basic problems confronting theorists was the yield point exhibited by materials. In the case of iron for example, the transition from elastic to plastic deformation is very sudden. Cottrell and Bilby[17] suggested that crystals generally contain impurity atoms which diffuse about in the lattice, such atoms would be attracted to and concentrated in the elastic field of a dislocation. This would tend to anchor the dislocation, and before such a dislocation can move freely through the lattice it must be torn away from its "atmosphere" of impurity atoms. Sudden yielding is then a consequence of the breaking away of dislocations and

particularly generating mechanisms from their anchoring atmospheres.

The Cottrell atmosphere concept has been used also to explain strain ageing[17] and delayed yielding[18]. Others[19,20] have analyzed internal friction and the elastic modulus using the dislocation concept.

Creep is seen as thermally activated flow. For a typical specimen strain increases rapidly when the load is first applied and then increases at a uniform rate, accelerating again prior to failure.

The thermal activation process of Becker[3] which was applied to dislocations by Orowan[7] is the basis of the exhaustion theory of transient creep developed by Mott and Nabarro[21] and Smith[22]. The process is as follows: When stress is applied some of the freer dislocations are set in motion and the strain rate is high. These dislocations are eventually exhausted either running out of the crystal or encountering obstacles. The rate of strain therefore diminishes until the rate at which dislocations encounter obstacles equals the rate at which thermal activation frees them. At this point the strain rate is uniform.

After 1934 the dislocation concept dominated

literature on deformation. It is probable however that some workers in this field did consider alternative theories of deformation. One such theory that was also published is presented by Furth[23]. Furth suggested that there was an equivalence between the process of melting and the mechanical process of failure. This led him to equate the latent heat of fusion or specific melting energy to the specific elastic energy at maximum stress. He considered 10 metals and by using tensile strength values extrapolated to 0°K obtained an average value of the ratio of these two energies of 1.056 and a standard deviation of about 27%.

However Furth makes no attempt to interpret his results on an atomic scale. Hence one may conclude that rather than presenting a theory on deformation he has found a connection between melting and tensile strength which a satisfactory deformation theory must explain.

The search for more convincing experimental evidence for the dislocation concept naturally leads to the search for direct experimental evidence of dislocations. The propounders of the dislocation concept used diagramatic models at first which could eventually be analysed mathematically[24]. An analogy was developed.

using soap bubble rafts[25], which served to illustrate the properties of dislocation but could hardly support the validity of the concept (for the bubble raft could not be expected to simulate the quantum mechanical nature of the bonds in aggregates of atoms). The search for direct experimental evidence for dislocation has already borne fruit and Hirsh[26] reviewed a large body of literature on the direct evidence for dislocations in 1959.

Dislocation may be revealed in various ways. The heart of a dislocation and the lattice immediately around it is at a higher potential than the bulk of the crystal lattice. Etchants, which dissolve a crystal should remove the atoms around a dislocation at a greater rate than the rate at which they are removed from an undisturbed crystal surface. During etching, one would expect a series of pits to develop at points on a crystal surface at which dislocations emerge. The usefulness of this property of dislocations is well illustrated by the work of Gilman[27,28,29] and Johnston[30,31] who were able to study the generation, velocity, multiplication and density of dislocation in lithium fluoride crystals.

The stress field around a dislocation will also attract impurity atoms in a crystal. Bush[32]

studied dislocations in silicon by doping the silicon crystal with a trace of copper, which migrates to dislocationson heating the crystal and so makes them visible for optical examination (silicon being transparent to infra-red wavelengths). He produced crystals in which the etch pits on the surface were connected by precipitate traces, so confirming the validity of the etch-pit and precipitate method. With a technique of this kind, which permits one to study the interior of a crystal, it is possible to study the phenomenon of "dislocation-free" crystals[33], which led to the unexpected result that a crystal which appears to be dislocation free is not strikingly different from one containing dislocations.

The most direct method of observing dislocations is doubtless the observation of thin films of crystal by electron microscopes. The specimens can be subjected to stress once they are mounted in the electron microscope and the heating effect of the electron beam also generates thermal stresses which cause dislocations to move about. Whelan et al[34] working with stainless steel observed dislocation arrays, both regular and irregular, dislocation networks, groups of dislocations piled up at grain boundaries, and interactions between moving dislocations.

The sketchy outline of the development of the dislocation theory of deformation presented in the previous pages has traced the progress of the dislocation concept to date. Beginning as a possible hypothesis it found increasing application in explaining the mechanical and other properties of solids. Techniques for directly observing dislocations put the existence of dislocations beyond dispute.

The dislocation theory as it stands, however, has not been completely vindicated. Together with the indisputable proof that dislocations exist came information about their behaviour which conflicts with the dislocation theory. Dislocations have been observed to nucleate when no generating mechanism appeared to be present[25]. According to theory, the stress at which this can happen must be very great, about $\frac{1}{30}$ E (E being Young's Modulus.) For the same reason, dislocation-free crystals should be very strong. Real crystals apparently free of dislocations are not greatly different from those containing some dislocations.

It is possible that these and similar discrepancies will in time be explained within the frame-work of the existing dislocation theory. The appearances

i.e. absence of generating mechanisms may be proved to have been in error.

If this is not so, however, the dislocation theory will require some modification. It is the writer's thesis that such modification is called for. In the following sections a more detailed analysis is made of the points at which dislocation theory conflicts with experiment, and the modification to existing theory that it is claimed will remove these discrepancies is put forward.

3.0 SOME DIFFICULTIES THAT BECOME APPARENT WHEN THE DISLOCATION THEORY IS APPLIED TO EXPERIMENTAL RESULTS

A theory may differ from reality in various ways. It may be a rather inaccurate fit of the experimental results; it may suggest trends which are not found experimentally, and, finally, it may be impossible to explain some observed phenomena by the application of the theory.

The dislocation theory in its present form is usually not capable of great precision so that it is discrepancies of the second and third kind that can be employed to greatest effect when questioning the validity of the theory in its present form.

In the sections to follow, discrepancies of this kind are examined, with the purpose of testing the validity of the dislocation theory and introducing a possible modification which will lead to a theory that embraces these facts as well.

3.1 A GENERAL DISCUSSION OF INTERACTION BETWEEN DISLOCATIONS AND POINT DEFECTS

Dislocations are surrounded by stress fields. Impurity atoms, generally are also surrounded by a stress field.

A substitution atom may throw the lattice about it into a compressive or tensile stress.

An interstitial atom will generally throw the surrounding lattice into compression, but for very small atoms such as hydrogen, the reverse may be the case.

A vacancy will put the surrounding lattice into a state of tension, for the vacancy state may be likened to a soap bubble which also tends to diminish under the influence of its surface tension.

These defects are point sources of stress whereas a dislocation is a mobile line source.

Three classes of interaction are possible:

(1) Interaction between fixed point sources and an otherwise mobile dislocation.

(2) Interaction between mobile point sources of stress and an otherwise mobile dislocation.

(3) Both fixed and mobile point sources may be present at the same time.

Because of the nature of crystal lattices, there are certain points in the lattice at which a point defect is at its minimum potential. To move from one possible low-potential site to another the point defect must traneverse an energy hump. It follows that point defects are inherently fixed. They may become mobile under three conditions:

(1) Thermal agitation.

(2) The influence of a dislocation stress field.

(3) A combination of a dislocation field and thermal agitation.

Several specific cases of interaction will now be discussed.

3.1.1 Interaction between fixed point defects and mobile dislocations

3.1.1.1 In the absence of thermal agitation

It is assumed that the dislocation has a general friction characteristic of the form

$$f = A + B v^n \quad \text{where} \qquad \ldots\ldots (3.1)$$

f = friction force per unit length

A is a constant

B is a constant

v is dislocation velocity and

n is a constant

The values of the various constants are not stipulated so that f= 0 may be seen as a special case.

Beginning with a dislocation loop which is not in the immediate neighbourhood of point defects, It will expand with application of stress. The point defects (of both signs) are taken to be distributed in a random way.

Interactions will be either repulsive or attractive. In the absence of the "B v^{j}" term in equation (:), an attractive interaction can not retard the dislocation. The dislocation will tend to accelerate as long as the attractive point defect is ahead of its centre and slow down when the attractive point defect is behind its centre. However if the inherent friction in the dislocation is velocity dependent, the dislocation would tend to dissipate the interaction energy by vibrating like a string and finally coming to rest with the interacting defect in its least potential position if the overall dislocation velocity is small. If the dislocation has a greater overall velocity the attractive point defect will cause additional energy dissipation by accelerating a segment of the dislocation line.

A repulsive interaction on the other hand, will tend to stop a dislocation until sections of dislocation line on either side of the interacting defect have moved forward sufficiently to pull the line past the repulsive

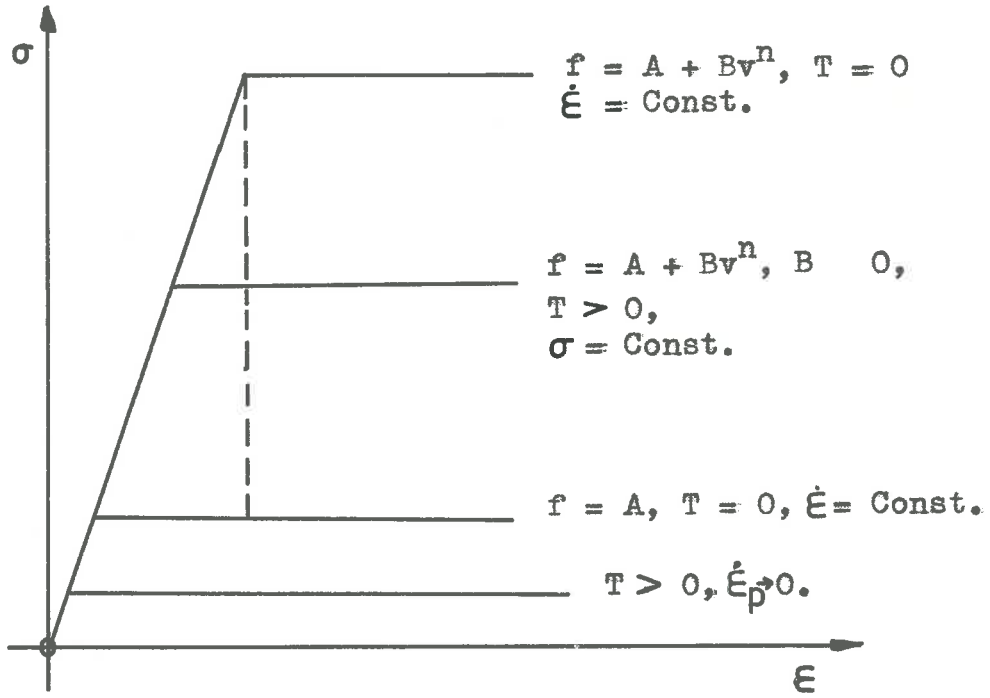

FIG. 3.1 Stress-Strain Curves for a Dislocation in a Crystal containing Fixed Point Defects.

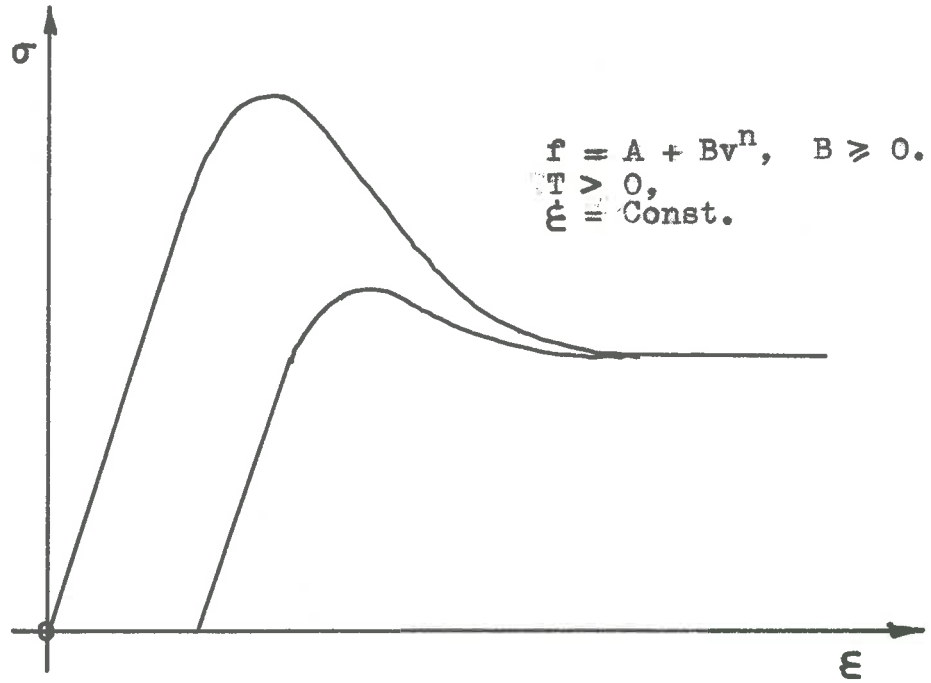

FIG. 3.2 The Variation of the Sress and the Plastic Strain Rate when a Crystal containing Fixed Point Defects is strained at a constant Rate.

field. In this process extra length of dislocation line is first produced and then the additional line energy is dissipated as the dislocation line returns to its previous length.

The "stress-strain" curves that are to be expected when a dislocation is started and forced through a lattice containing point defects is shown in Figure 3.1.

If the friction function is of the form $f = A$ then the stress will increase along OQ to Q and on breaking through the barrier of point defects the dislocation line will acquire enough momentum to traverse others and the stress will fall along QR to R and remain at this level.

However, with the velocity dependent form, $f = A + B\,v^n$ the momentum of the dislocation can not be maintained and the stress remains high. In the former case yielding once started is very sudden, in the latter case it is slow for the dislocations are also slow moving.

On the macroscopic scale, the dependence of flow stress on strain rate can only be found when it is known how the rate of dislocation generation varies with stress. This subject will be left until later.

3.1.1.2 In the presence of thermal agitation

It is assumed that the point defects are essentially fixed, but thermal agitation is sufficient to give some assistance to the dislocation in overcoming the resistance of the point defects.

If the stress is raised to σ_p and held there, the dislocation will commence to move slowly through the lattice, being dependent on thermal assistance in overcoming the point defects. Thermal activation assists the dislocation in overcoming point defects as well as its inherent friction.

If the stress is raised suddenly to σ_{ϵ_p} and held there plastic strain does not follow immediately but builds up in a short period to a steady value. This delay period indicates the time taken by the random thermal processes to release a dislocation line from a point defect obstacle at that applied stress.

With the introduction of this thermal effect, the distinction between dislocations of the type

$$f = A \qquad \ldots\ldots (3.2)$$

$$f = A + B\,v^n \qquad \ldots\ldots (3.3)$$

is greatly reduced because in the case $f = A$, the momentum

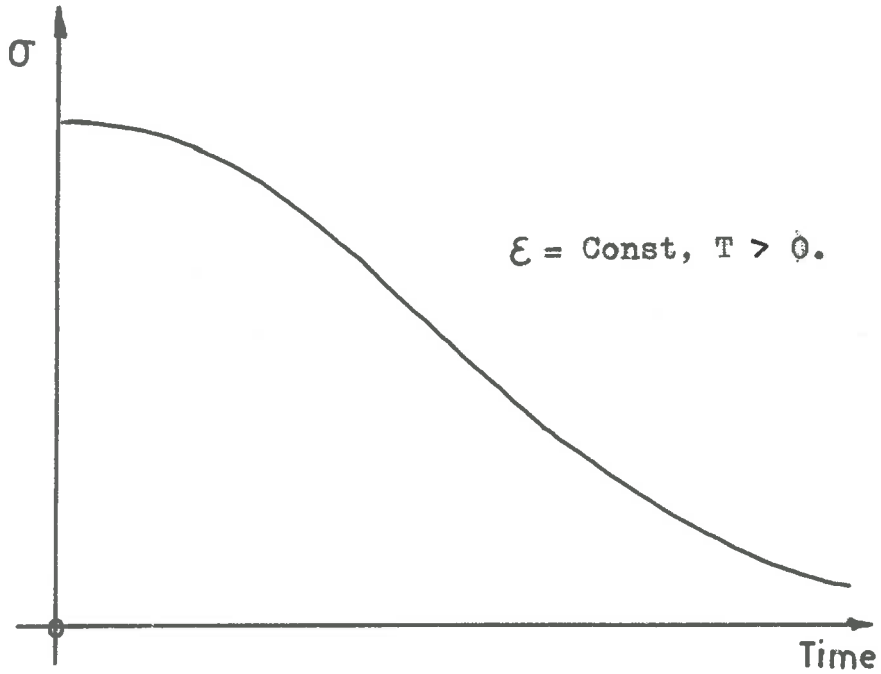

FIG. 3.3 The Variation of Stress with Time when a Cryatal containing Dislocations and Fixed Point Defects is suddenly subjected to a constant Strain.

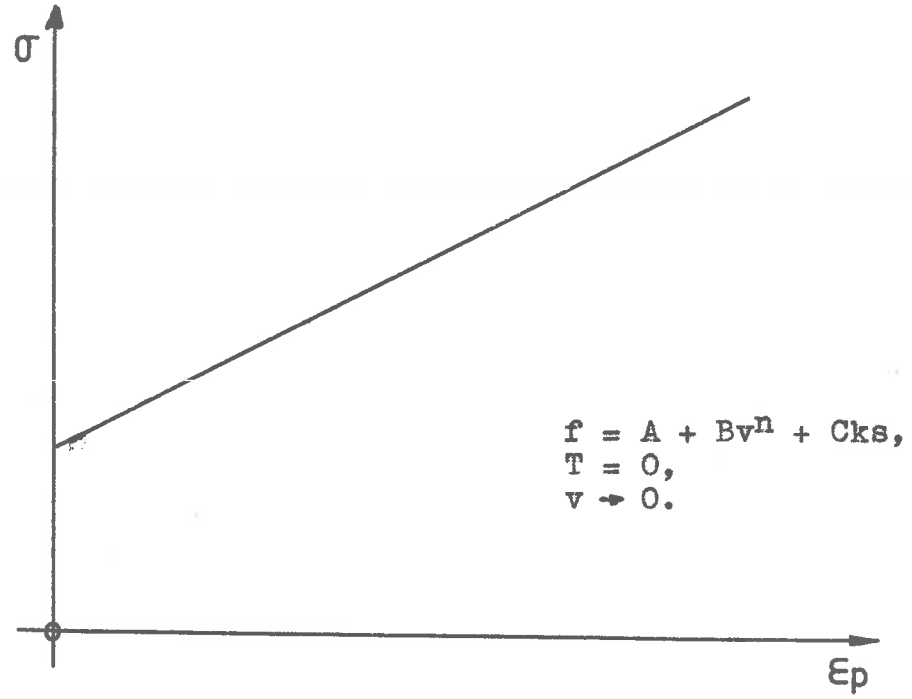

FIG. 3.4 Stress Vs. Strain for a single Dislocation in a Lattice containing Mobile Point Defects.

of the dislocation is dissipated by vibrations of a released segment of dislocation line between other segments which are not yet released. However, the momentum may not be completely dissipated so that the thermal process can be assisted somewhat by the kinetic energy of the dislocation, which increases the rate of strain.

If, instead of a constant stress, a constant strain rate is applied, the rate of plastic strain increases from zero to a peak then falls off to a steady value.

Stress behaves in a similar manner, when a constant strain rate is applied, and is illustrated in Figure 3.2.

If an elastic strain is suddenly applied and held the stress will diminish at an accelerated rate until it falls to zero. This process is illustrated in Figure 3.3.

This process is very similar to delayed yielding but there is the significant difference that yielding is not sudden but commences at an accelerating pace from the moment of loading.

3.1.2 Interaction between mobile point defects and mobile dislocations

3.1.2.1 In the absence of thermal agitation

The interaction between point defects and dislocations may be so strong that the defect is dragged along with the dislocation. This increases the resistance of the dislocation to motion and the equation for friction takes the form

$$f = A + B v^{n} + Cm \quad \text{where} \qquad \ldots\ldots (3.4)$$

C is a constant depending on the mobile point defect

m is the linear density of mobile point defects along the dislocation line.

A dislocation is assumed to begin in a zone of crystal free from point defects. Mobile point defects are scattered in a random manner throughout the lattice. As the dislocation moves it will pick up more and more of these point defects and the frictional resistance increases. If the distribution of point defects is random and uniform,

$$m = k s \qquad \ldots\ldots (3.5)$$

where k is a constant and

s is the distance travelled by the dislocation line.

n has a limiting value n_L, when the dislocation is saturated.

Whence

$$f = A + B v^n + C k s \qquad \ldots\ldots (3.6)$$

The stress required to move such a dislocation will increase linearly with the distance travelled by the dislocation, and with the plastic strain ϵ_p. This is represented in Figure 3.4.

If a series of dislocations are generated on the same slip plane the first dislocation will tend to collect all the mobile point defects. Subsequent dislocations will move rapidly until they intersect with the first dislocation where a pile-up of dislocations results. The first dislocation is therefore assisted by dislocations behind it.

If such a "loaded" dislocation succeeds in emerging from the crystal, the mobile point defects will have been swept from this slip plane, and subsequent slip will take place far more readily on that plane than on other parallel slip planes.

3.1.2.1.1 <u>In the presence of fixed point defects</u>

Initially the effect of fixed point defects may

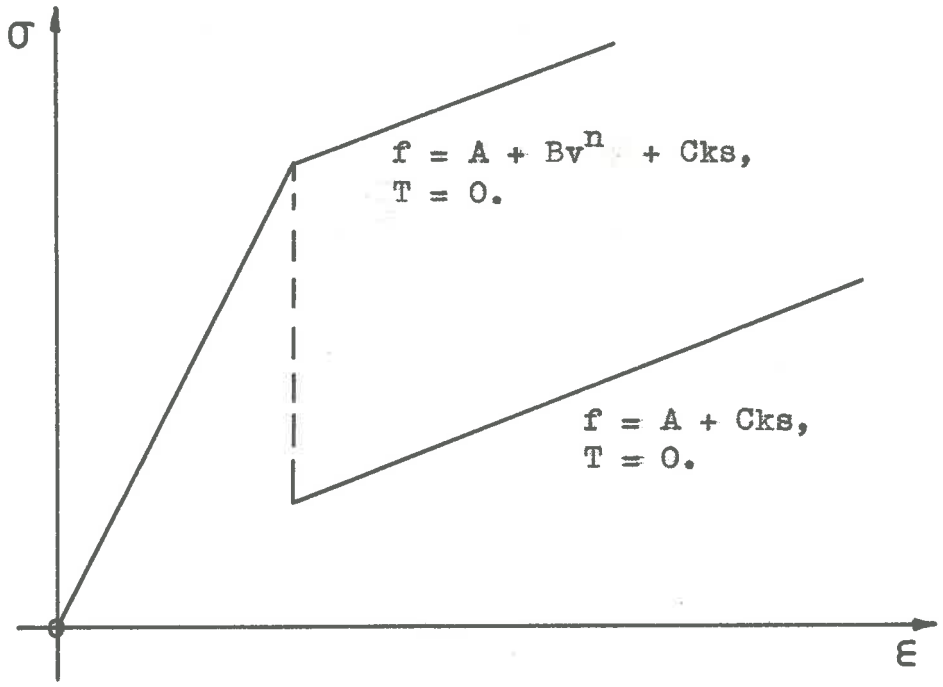

FIG. 3.5 Stress-Srain Curves for types of Dislocation in a Lattice containing Fixed and Mobile Point Defects.

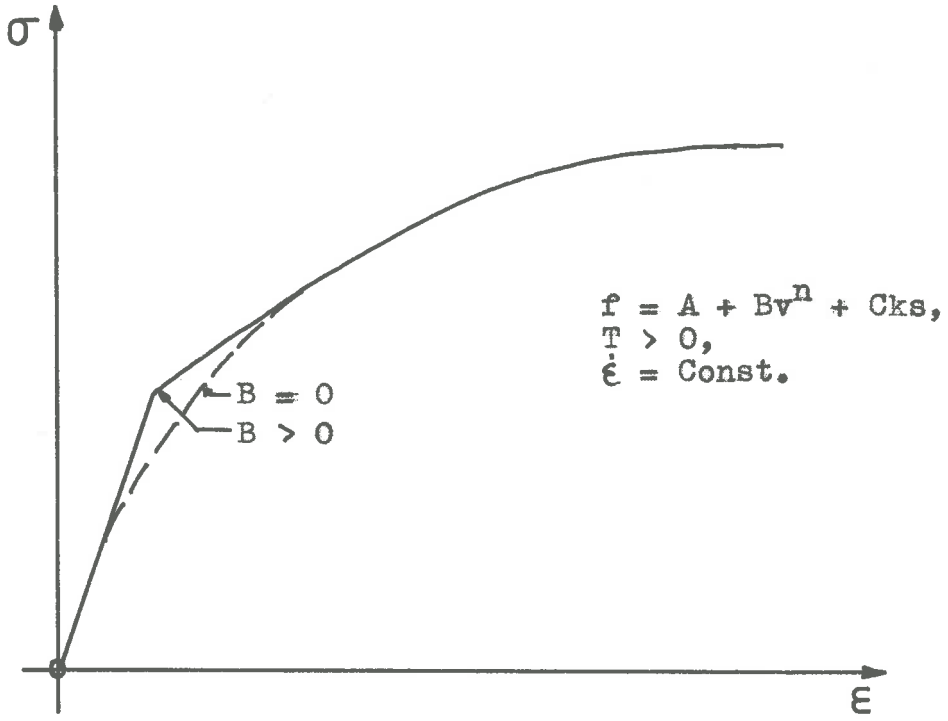

FIG. 3.6 Stress-Strain Curves for two types of Dislocation in a Lattice containing Fixed and Mobile Point Defects, subjected to Thermal Agitation.

be far more important than the effect of mobile defects. If the velocity dependence of dislocation friction is small, momentum may assist in overcoming fixed defects but this effect will gradually diminish in comparison to the stress required to overcome friction due to mobile point defects. The stress-strain curve for such a dislocation is presented in Figure 3.5. To maintain the momentum of the dislocation, the applied stress must be increased to compensate for the increasing point defect drag.

If the momentum effect does not operate, the stress-strain curve for a dislocation has the general form of Figure 3.4, with the difference that the yield stress is higher than in the absence of fixed point defects, as can be seen from Figure 3.5.

3.1.2.2 In the presence of thermal agitation

Thermal agitation assists the applied stress in moving the dislocation. An edge dislocation is at its lowest potential when it is symmetrical about the half plane. Hence, the smallest jump for a segment of edge dislocation is from one half plane to the next. At each stress, a minimum length of dislocation line segment will remain one half plane forward of the segments on either side

of it. Using this jump length, the energy involved and the temperature, one can compute the rate at which the dislocation will move under thermal assistance.

Mobile point defects tend to hold the dislocation line back. Segments of dislocation line between those point defects will tend to curve outwards, ending to a cusp at each point defect. Some of the energy required to move the point defect is now supplied to the dislocation line, the distribution being such that both point defects and dislocation line move at the same rate. The computation of the dislocation velocity is again a straightforward process.

When the spacing of point defects is equal to or less than the minimum dislocation line segment for forward jump, the point defect and half the dislocation segment on either side may be taken to jump as an integral unit and the velocity-stress-temperature relationship found.

As the dislocation moves through the lattice its density of mobile point defects will increase until a thermal equilibrium is reached.

For a constant strain rate (or dislocation velocity) the stress to move a single dislocation will vary as shown in Figure 3.6. At the beginning the dislocation

is relatively free of point defects and the stress is low. As the concentration of point defects increases, the stress also increases tending to a constant value when the concentration of mobile point defects in the dislocation has reached its equilibrium value.

With thermal agitation, the mobile point defects are still swept out of the slipplane, but a greater number of dislocations will be required. Also, as there will be a diffusion of point defects into the swept zone a continuous supply of dislocations is required to sweep out the point defects.

3.1.2.3 In the presence of thermal agitation and fixed point defects

The situation envisaged in this case is mobile dislocation, mobile point defects, and other point defects which diffuse so slowly that their mobility only becomes significant with stationary dislocations.

The analysis for a dislocation with a low density of mobile defects will also apply here with the difference that the energy values will be somewhat greater.

If a constant strain rate is applied to a crystal containing a dislocation the resulting stress-strain plot will be one of two kinds. If the rate of thermal release

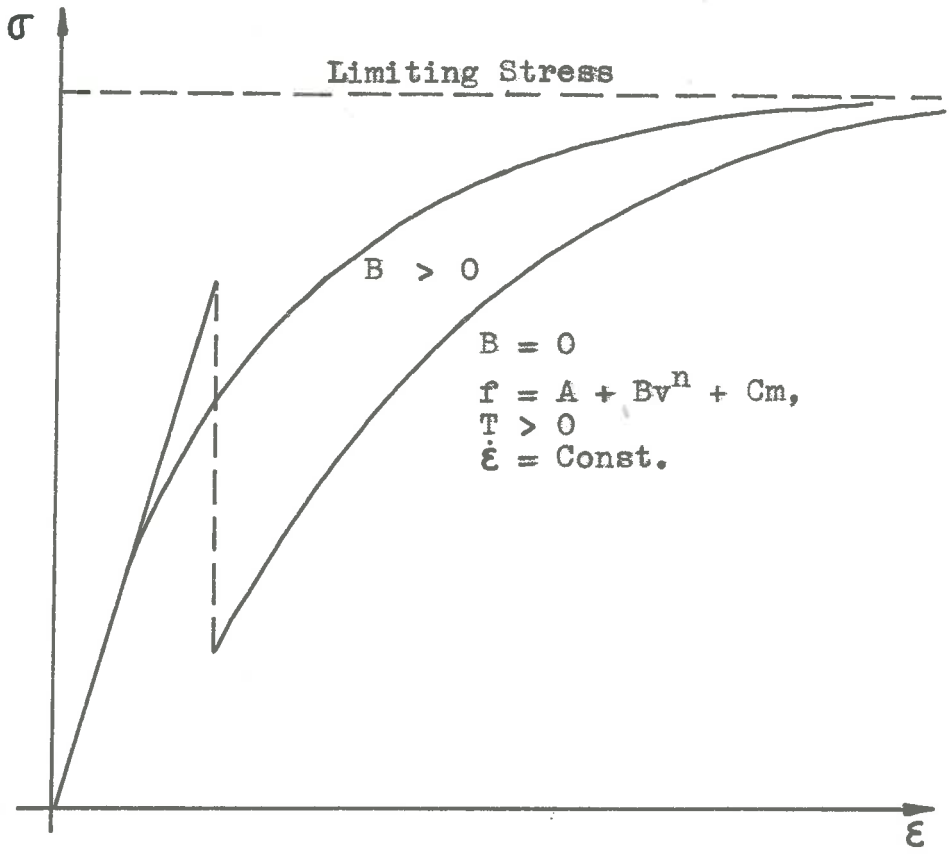

FIG. 3.7 The Stress required to move a Dislocation in a lattice containing Fixed and Mobile Point Defects, and subjected to Thermal Agitation.

from fixed point defects is low enough and the dislocation friction is velocity independent, the dislocation may build up enough momentum to travel some distance without requiring thermal assistance to pass fixed point defects. As the density of mobile point defects increases, however the dislocation will eventually slow down to a thermally controlled rate.

Without the momentum effect the strain will increase and the dislocation will accelerate to a velocity peak before falling back to a steady value. The two stress plots are illustrated in Figure 3.7.

It is seen that the curve for mobile point defects but no fixed point defects is very similar to the case with fixed point defects but no momentum effect, the difference being that to maintain the same strain rate the yield point in Figure 3.7, as well as the limiting stress are higher than the corresponding quantities for the case of Figure 3.6.

If the temperature is elevated, the point defects which have been treated as fixed above become more mobile. They may then be treated in the same way as the mobile dislocations were treated above. The difference is that the equilibrium concentration for these point defects will be much lower.

3.2 APPLICATION OF THE POINT DEFECT-DISLOCATION INTERACTION PHENOMENA IN THE LITERATURE

Having discussed the interaction of dislocations and point defects, the use made of these phenomena will now be reviewed.

The classic paper on the effect of impurity atoms on the mechanical properties of a metal is doubtless that of Cottrell and Bilby[17]. They assume that yielding (in iron) takes place as soon as dislocations existing in the crystals have broken away from their atmospheres of impurity atoms which have accumulated in them.

This theory has several major faults. Firstly an activation process involves the duration of loading prior to yielding as well as the magnitude of the applied stress. There is a stress in iron below which yielding never takes place. Above that stress however, a delayed yielding phenomenon is noted.

The presence of a yield stress below which a crystal remains elastic indefinitely implies a process which is either of a kind not influenced by thermal activation or one in which the activation energy is so large that activation is highly unlikely.

This yield point varies with temperature, decreasing as the temperature increases and although Cottrell and Bilby are able to fit their activation function to the experimental variation of the yield point with temperature, the problem posed above remains and only becomes the more intriguing.

Fisher[18] applied Cottrell's theory to delayed yielding. He obtains an expression for delayed time which has the form

$$\ln(\text{delay time}) = -A + BG^2/\tau T \quad \ldots\ldots (3.7)$$

where A and B are constants

G is shear modulus

τ applied shear stress and

T the absolute temperature

This equation fits experimental points reasonably well. The constants A and B are selected for a particular kind of steel with a given preparation. The temperature and stress values are inserted, being experimental conditions.

The fit however, is not completely satisfactory. While the curves are in approximately the right place (the agreement being worst at low temperature) with the

right slope, they appear to have the wrong shape. It can be seen by inspection that straight lines would fit the experimental points far better. This is confirmed by Wood and Clark who drew straight lines through their points (which were also used by Fisher).

Pfeiffer[43] employs the observation that prior to delayed yielding a small amount of plastic deformation occurs. During this pre-yield interval N dislocation segments have moved.

Now the frequency of a particular random event at a particular place is given by the expression

$$\nu = \gamma_0 \, e^{-E/kT} \quad \text{where} \qquad \ldots\ldots (3.8)$$

ν is the frequency of the event

γ_0 the Debeye frequency

E the energy associated with the event

k Boltzman's constant and

T the absolute temperature.

The frequency of N events happening in succession is

$$\gamma' = \frac{\gamma_0}{N} \, e^{-E/kT} \qquad \ldots\ldots (3.9)$$

and if the period for this sequence of events is τ ,

$$\tau = \frac{N}{\gamma_0} e^{E/kT} \quad \ldots\ldots (3.10)$$

and $$\ln \tau = \ln \frac{N}{\gamma_0} + E/kT \quad \ldots\ldots (3.11)$$

Now Pfeiffer obtains an expression for E

$$E = E_0 - \sigma b s l \quad \ldots\ldots (3.12)$$

where E_0 is the activation energy in the absence of stress.

σ is applied stress

b is Burgher's vector

s is length of dislocation segment affected by σ

l is distance segment displaced by σ

whence

$$\ln \tau = \ln \frac{N}{\gamma_0} + \frac{E - vT}{kT} \quad \ldots\ldots (3.13)$$

where $v = b s l$ $\ldots\ldots (3.14)$

This equation may be contrasted to that of Fisher who has the stress in the denominator. Pfeiffer obtains straight lines and is able to obtain estimates for E_0 and v which are quite reasonable.

Pfeiffer does not explain and it is not obvious why N events with activation energy E should have to occur in succession especially since N is obtained by counting the number of dislocation segments which have moved before sudden yielding takes place.

Fisher's estimate for the activation energy is based on the assumption that a segment of dislocation loop breaks away from its "Cottrell atmosphere" under thermal activation and applied stress. The length of segment which can be kept away from the solute atom by the applied stress has a critical minimum value below which the loop returns to its previous position while above this dimension the dislocation segment free of the locking atmosphere enlarges under the applied stress. Fisher's method contains the assumption that the energy associated with impurity locking is distributed uniformly along the dislocation line.

Fisher's analysis has another deficiency when compared to experiment. According to the analysis, each dislocation loop is released by one activation process. Consider a single dislocation. The probability that under applied stress this dislocation will be released from its locking atmosphere is zero at the moment stress

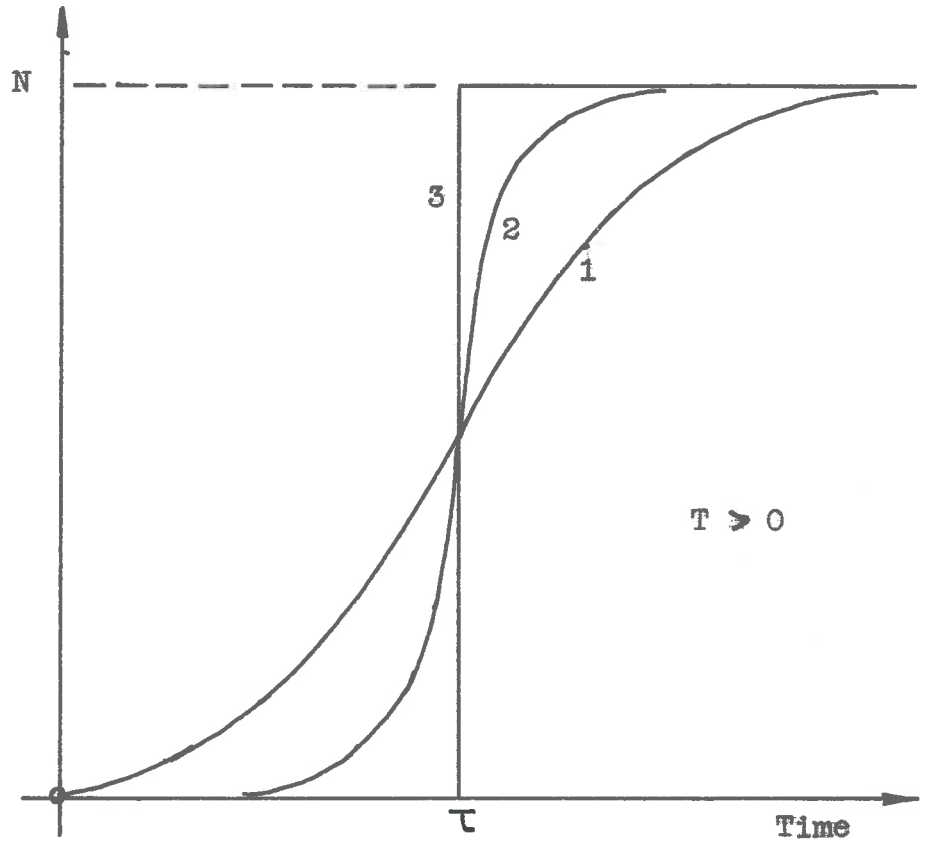

FIG. 3. 8 The Number of Dislocation out of a total of N released by Thermal Agitation, vs. the Duration of the applied Stress.

1. If the Dislocation is released by a single Activation Process of frequency $1/\tau$.
2. If the Dislocation is released by a series of Activation Processes of total period τ.
3. The Ideal variation for Sudden Yielding.

is applied and increases continuously from that point onwards tending to unity. If there are N dislocations which may be freed by Fisher's activation process then the number of dislocations which have been freed at any moment may be plotted against the loading interval as shown in Figure 38. It follows that a single random activation process will not release the dislocations suddenly. However if several activation processes must take place before the dislocation is released, the change-over from the condition where very few dislocations are released to the condition where nearly all are released can happen in a time interval much smaller than the loading interval resulting in "sudden" yielding.

Pfeiffer's analysis not only agrees better with experimental results but is consistent with the very sudden yielding process. He himself offers no mechanism which would relate the series of activation processes his analysis requires, with the phenomenon of sudden yielding. A possible explanation is offered later when a new nucleation process is introduced.

Conclusion

The use of point defects and thermal activation concepts in explaining the yield point and delayed yielding in iron has met with only partial success.

Delayed yielding phenomena are described well by a function which involves applied stress, activation energy and a series of activation processes. A physical dislocation mechanism which would fit in with these conditions is, however, not apparent.

While Pfeiffer's analysis describes delayed yielding well, Fisher's analysis has more relevance to the static yield point (i.e. the stress below which the metal will carry an elastic load indefinitely). If a constant delay time is chosen, one obtains a variation of the yield stress with temperature which may be fitted to experimental points. The discrepancy here is that the theory predicts finite delay times which are no longer relevant because experimental delay times for stresses below the yield point are infinite.

Again a mechanism which would explain why delay times are as predicted in one stress range and are no longer relevant in a lower stress range, is needed.

3.3 DIRECT OBSERVATION OF DISLOCATIONS UNDER HIGH MAGNIFICATION

Thin metal foils transmit electrons, but not without diffracting and reflecting them. Hence transmission electron microscopy has become a powerful tool in examining albeit thinned down sections of metal specimens.

Prior to the development of electron microscopy, the dislocation theory had already been brought to a high level of development. The interaction of dislocations with point defects, grain and twin boundaries, with each other; the generation of dislocations and the dependence of the nature of the dislocation on the structure and energy properties of the lattice being the main divisions of the dislocation theory.

The techniques for the direct observation of dislocations would naturally be employed to verify these theoretical structures. To date many metals and alloys have been investigated. While many of the properties of dislocation have been verified, evidence for a dislocation generating mechanism is unexpectedly scarce. Whelan[44] for example, in carrying out a comprehensive examination of stainless steel which revealed dislocation networks,

pile-ups against grain boundaries and even a pile-up of very closely spaced dislocations terminating in a crack failed to reveal a source which could have generated the dislocation. One micrograph, Figure 20[44], shows dislocation being nucleated at an edge of the foil, and travelling a short distance ~1μ into the foil. Another interesting feature of this micrograph is that near the edge of the foil there are greatly extended dislocations (the stacking fault standing out quite distinctly), while further inwards the dislocations are not significantly extended.

Whelan also notes that when a dislocation splits into a pair of partials, the process appears to take place very suddenly. Another process which also implies dislocation nucleation is shown in Figure 17[44]. The split dislocation 'B' expands producing a relatively long stacking fault band. Subsequently a pair of partial dislocations appear on the plane previously swept over by one partial of dislocation 'B'. The second pair of partials is of opposite sign and annihilates dislocation 'B'. In the writer's view the second pair of partials were nucleated on this slipplane. The possibility of a generating mechanism can be discounted because the glide plane on which this mechanism would have to operate had just been swept over by a partial dislocation. The

possibility that a dislocation entered this plane by climb can also be discounted. Very regular dislocation arrays are shown in Figure 9[44]. If dislocations in stainless steel were prone to climb at the temperature of the observations made by Whelan, this would be revealed by dislocation arrays.

Further evidence that dislocations may be nucleated in metals is provided by the experiments of Price[45,46] on zinc. He prepared whiskers and platelets with a range in thickness of 0.05μ to .5μ which had an (0001) orientation and appeared to be dislocation free. These specimens were able to sustain an elastic strain of $2\text{-}10 \times 10^{-3}$. At the elastic limit the flow stress fell suddenly to about 2/3 of the yield stress.

Because of the orientation of the specimens, the resolved shear stress on the basal plane was zero, and deformation was by pyramidal slip. Plastic deformation was always found to begin at a stress concentration, in a narrow zone which traversed the whole cross-section of the specimen. As this zone hardened slip would continue to spread into undeformed parts of the crystal.

That deformation always began at the most highly stressed point, and that it spreads to the remainder

of the crystal from that point implies either that there is a prolific supply of dislocation generators which all have nearly the same activation stress or that the initiation of deformation and probably the propagation of deformation through the crystal has nothing to do with dislocation generating mechanisms of the Frank-Read type.

For a crystal of such small dimensions (the smallest about 2 mm. x 10μ x .05μ) the first alternative is highly unlikely and the apparent perfection of the crystals adds further weight to the second alternative, namely that some kind of dislocation nucleation at the stresses measured is involved.

The possibility that dislocations may be nucleated at ordinary stress levels does not invalidate dislocation generating mechanisms such as the Frank-Read source. It is likely however, that in crystals which possess a low dislocation density, the role of such generating mechanisms is secondary.

Conclusion

The notable absence or scarcity of dislocation generators amongst the many dislocations revealed by the electron microscope, together with evidence favouring the hypothesis of dislocation nucleation, justifies the search for a mechanism by which dislocations may be nucleated in a dislocation-free crystal at normal stress levels.

3.4 MICROSCOPIC EXAMINATION OF DISLOCATION PROPERTIES

Before the classic work of Price[45,46] crystals of other substances had already been made, which by all the evidence appeared to be dislocation free. Dash[33] in 1958 presented evidence that he had grown silicon crystals which were free of dislocation. Yet he reports no unusual properties of these dislocation-free crystals. In an earlier paper[47] in which he presents some excellent Frank Read sources, Dash also presents micrographs of other half loops of dislocation which begin and end on a surface and have no apparent source.

Gilman and Johnston[29] made a study of dislocation nucleation in lithium fluoride. After proving that their etching technique revealed all dislocations, they introduced dislocation into the crystals by pressing steel balls against the surface and also by inducing thermal stresses. Their calculations showed that these dislocations had been nucleated in the lithium fluoride crystals at stress levels which were of the same magnitude as the yield point of the crystals. Dislocations were also introduced by bending a crystal specimen at -196°C. On subsequent etching numerous glide bands were revealed. In addition, groups of two, four or six etch pits were found, indicating that one, two or three dislocation loops

were present. These loops could be "popped out" of the crystal by applying a reversed stress or etched out. In either case the ready escape of the dislocation from the crystal and the absence of any further evidence of dislocation strongly suggests that these dislocations were introduced into the crystal by a process of nucleation.

Gilman and Johnston also noted that if a single dislocation half loop is expanded by the application of stress, other half loops form in the wake of the first half loop though generally not on the same plane. As this process continues, a narrow slip band is formed which has a constant dislocation density and continues to expand with further straining. This behaviour is strongly reminiscient of Price's zinc crystals which also exhibited a widening zone of deformation.

When moving dislocations are viewed under the electron microscope they are seen to leave a trace in their wake which gradually fades. This phenomenon may have some connection with the observations by Gilman and Johnston, that new dislocation half loops appear in the wake of a moving dislocation half loop.

Neglecting for the present the problem of how dislocations are nucleated at ordinary stress levels, it can still be argued that dislocation nucleation will occur

preferentially near a crystal surface, and also that if there are any dislocations already existing on the surface, a new dislocation will be nucleated in their vicinity.

To nucleate a given length of dislocation line, the nucleating process must provide the energy that is associated with it. If the dislocation line is nucleated in the body of the crystal, it will be a more or less circular dislocation loop. If the radius of this loop is greater than a critical value, the existing stress will expand it and if the radius is below that value, the loop will collapse.

The same length of dislocation line nucleated near a crystal surface will take the form of a half loop which therefore has twice the radius of the corresponding full loop formed inside the crystal. Consequently such a half loop will expand at a stress level only half that at which a full loop expands.

If such a half loop is nucleated in the vicinity of an existing dislocation, the line energy associated with some of the nucleated loop is reduced. If further, the dislocation near which the new half loop is nucleated is not pinned, it can accomodate itself to the shape of the new half loop and so decrease further the energy required to form a new half loop.

The argument may now be summarized:

1. Dislocation lines are nucleated on crystallographic planes on which stable loops form first.
2. Provided that the nucleation energy is made available as readily near the surface as in the bulk of the crystals, the nucleation of half loops is preferred.
3. Dislocations are nucleated preferentially in the vicinity of existing dislocations which are not pinned down in the lattice.

In terms of this nucleation hypothesis many of the results obtained by Gilman and Johnston become explicable.

For example, they measured the velocity of dislocation in the range 10^{-7} cm/sec and 10^{3} cm/sec. For velocities below about 10^{2} cm/sec, the dependence on stress may be expressed in the form[48]

$$V = (\tau/\tau_o)^n \qquad \ldots\ldots (3.15)$$

where τ = applied stress

τ_o = stress at which V = 1 cm/sec

$n = 34$

for a given crystal at a given temperature.

The quantity τ_o depends on the prior treatment of the crystal (e.g. impurities, neutron bombardment etc. as well as the temperature).

This relationship clearly implies that V=0 when τ=0. But this is not so. For all stresses below the yield stress τ_y there is no deformation, which means also that there is no dislocation motion. It appears then that at the yield stress dislocations undergo a sudden change in mobility which is related to dislocation nucleation.

Their[5] observation of the formation of loops in the wake of existing dislocations is explained readily. If the dislocation is propagated slowly, no loops form. However, a 30% overstress results in profuse dislocation formation. The new dislocation must form on glide planes adjacent to the plane on which the existing dislocation moves, the distance between these planes would have to be about $10^{-2}\mu$ for an effective interaction to be powerful enough. In this way a slip band grows in width as deformation continues, exhibiting a definite boundary on its edges.

Gilman and Johnston[29] also found that surface preparation had a noticable effect on the shape of the

stress-strain curve for the crystal. For as-cleaved specimens, the yield point and subsequent flow stress are about the same. If the surfaces of the crystal are electrolytically polished however, yielding takes place above the flow stress, exhibiting a stress peak. If the polished surface is sprinkled with carborundum, which introduces fresh dislocations into the crystal the stress peak is removed. It may be concluded that a small amount of surface damage assists deformation by providing sites on which dislocations may be nucleated more readily.

Another deformation phenomenon to which the nucleation hypothesis can be applied is the regularity of the spacing of slip bands. That slip bands in lithium fluoride possess a regular spacing can be seen for example from Figure 19[30]. It is clear that the nucleation energy is provided by the applied stress. When a dislocation is nucleated at any point in the crystal, the nucleation process somehow concentrates elastic energy in the surrounding lattice to nucleate a dislocation. The boundaries of slip bands are zones of dislocation nucleation and if they are too close together the ratio of nucleation points to crystal volume becomes too high and a higher stress is then required to operate the slip systems. Consequently the slip band spacing in a crystal tends to be uniform.

An anomaly very similar to that presented by delayed yielding phenomena appears also when results of dislocation velocity measurements are taken into account.

From their measurements, Gilman and Johnston[30] formulated an expression

$$v_s = f(\sigma)\, e^{-E/kT} \quad (+25^{\circ}C > T > -50^{\circ}C) \qquad \ldots\ldots (3.16)$$

Stein and Low[46] working with silica iron obtained an expression

$V = (\tau/\tau_o)^n$ where τ is applied stress and τ_o the stress at which V = 1 cm/sec. Their results were obtained in the velocity range 10^{-8} to 10^{-2} cm/s. A similar expression could be applied to the results of Gilman and Johnston which would be valid over the range 10^{-7} to 10^{2} cm/sec. The work of Ericson[49], which extends that of Stein and Low confirms this dislocation behaviour.

Stein and Low[46] tested their specimens over the range 78°K to 373°K. They find (Figure 9) that at low stress and high temperature the plot of ln V vs $\frac{1}{T}$ is a straight line but as stress increases and temperature decreases the deviation from a straight line increases.

Straight line graphs imply a pure thermal activation process which ceases at 0°K and consequently

the dislocations would also cease moving regardless of what stress is applied. Materials do deform at even the lowest temperature and the deviation from a pure activation process is to be expected.

This must be taken together with another observation by Gilman and Johnston[29] who find that in the temperature range 78°K to 500°K the yield point is described well by the function

$$\tau_y = 5.75\, e^{\frac{-5.5T}{1000}} \quad \text{kgm/mm} \qquad \ldots\ldots (3.17)$$

This expression is bounded at 0°K and probably predicts the yield stress at this temperature.

Thus the expression for the yield stress which is hardly an activation process (for below the yield stress the crystal resists flow indefinitely), an activation type expression is found to be suitable, while for dislocation motion, which could well be dependent on an activation process, a more complicated process is involved.

If the activation energy for dislocation motion were of the form $E = E_0 - a\tau$ where τ is the applied stress the ln V vs $1/T$ plots would be a series of straight lines which tend to the horizontal as $\tau \to 0$.

The shape of the experimental curves suggests rather that E is dependent on the dislocation velocity as

well as either stress or temperature or both.

The nature of the nucleation process which is to be developed in the following pages may resolve these anomalies. If the nucleation hypothesis is indeed relevant then one may well require that it should throw much light on problems of this kind.

4.0 A PROPOSED HYPOTHESIS OF DISLOCATION MULTIPLICATION

In the previous section some of the deficiencies of the theory of deformation in its present form were discussed.

Experimental work was cited, which is of such a nature as to suggest the existence of a dislocation multiplying mechanism capable of producing dislocations at measured stress levels.

Such a mechanism must not depend on crystal imperfections. Consequently, this mechanism, if there is one, will be a property of the perfect real crystal, which means that it must be inherent in the nature of the interatomic bond.

4.1 SOME NECESSARY CHARACTERISTICS OF A NUCLEATION MECHANISM

While a nucleating mechanism is sought chiefly to provide an explanation for low-stress nucleation of dislocation, such a mechanism, if it exists, will have other effects as well. A suitable mechanism must perform the following functions:

(1) Relate the stress required to nucleate a dislocation to the dimensions of the crystal so that large crystals which fail at stress levels below E/1000 as well as small ones (whiskers) which are elastic up to E/30 are equally included.

(2) Relate the nucleation stress to the temperature of the crystal, and so, incidentally provide an explanation for melting and the liquid state.

(3) Relate the nucleating stress to the duration of the stress, which provides an explanation for such phenomena as delayed yielding and creep.

(4) Relate the nucleating stress to any imperfections that may be present in the real crystal. Under this heading is included every factor that causes the real crystal to deviate from its regular crystalline nature.

The flow stress of a crystal may be the stress at which dislocations will move or the stress at which they are nucleated, depending on which is the larger. These two states of shear deformation, which may be described as mobility controlled or nucleation controlled may be distinguished from each other in that in the former case the density of mobile dislocations will be high, while in the latter case it will be much lower.

If the resistance to the motion of dislocations is caused by point defects, then dislocation arrays will be favoured, as was shown in the previous section 3.1. In this case mobility controlled flow will take place preferentially in narrow glide bands.

In comparing the predictions of a nucleation hypothesis with experimental results it is necessary to be able to distinguish the two modes of flow.

A similar argument applies to fracture. It is likely that a mechanism that nucleates dislocations will also nucleate cracks. It may seem at first sight that once a stable crack is nucleated it will be propagated in an uncontrolled manner so that the fracture stress is nucleation controlled. It will be seen in section 5 that a crack may also be impeded such that it is in effect "mobility" controlled.

4.2 POSSIBLE NUCLEATION MODELS BASED ON VARIOUS SURFACE ENERGY HYPOTHESES

These models are derived without taking any account of the nature of the inter-atomic bonding in crystals.

4.2.1 The Variable Surface Energy Hypothesis

Each isolated crystal is bounded by a closed surface. A crystal in a polycrystalline solid may be enclosed partly by a crystalline surface and partly by an inter-crystalline boundary.

Suppose that inside this closed surface, a new, smaller closed surface forms. According to this hypothesis, the surface energy of the new surface is smaller than that of the enclosing surface. There is assumed to be a definite relationship of the form

$$\frac{s}{S_o} = f\left(\frac{a}{A}\right) \qquad \ldots\ldots 4.1$$

where 's' is the surface energy of the new surface of area 'a', and S_o the surface energy of the enclosing surface of area 'A'.

There are assumed to be two kinds of surface. The total surface is the boundary between the crystal and

vacuum or air. When a surface is within the zone of influence of another surface it is defined to be a partial surface.

A partial surface of special importance is that which results when two layers of atoms are displaced by relative shear. This kind of boundary may arise inside a crystal, but is taken to be of the same nature as inter-crystalline boundaries.

The surface energy of a sub-surface within the crystal boundaries may be so low that a total or partial surface may result when stress is applied. The surface may develop into a dislocation or a crack and become self-sustaining.

To make the hypothesis explicit it must be added that if more than one sub-surface is nucleated, their surface energy is equal and is determined by inserting the sum of their areas in equation 4.1.

Equation 4.1 has introduced the effect of size. A crack or dislocation becomes self-sustaining at a stress level determined by the dimension of the void and the associated surface energy. The void is the space enclosed by the new surface.

The effect of temperature may also be introduced.

It is apparent that if the total area 'a' is concentrated in one void, the deformation mechanism (crack or dislocation) becomes self-sustaining at a lower stress than would be the case if the same area was distributed over a number of voids. The effect of thermal agitation is to enlarge and diminish existing voids in a random manner. Small voids may be annihilated completely. The surface energy of the remaining voids is decreased, and they are enlarged. In this way thermal activation favours the development of a limited number of voids, and so reduces the stress at which the crystal will deform.

Thermal agitation can also produce temporary voids. At temperatures approaching the melting point of the crystal, the thermally activated voids are so large, that stable dislocations can be introduced at very low stress levels.

Melting is explained as follows: when thermal activation is sufficient, the thermal nucleation of surfaces may allow small fragments of crystal to be momentarily disconnected from the main crystal on all sides. This allows the fragment to rotate and move out of alignment with the main crystal. Should this happen on the surface of the main crystal, the fragment may remain misaligned for a considerable time interval. Another phase consisting of such fragments if possible. This is the liquid state.

The melting point is the temperature at which the rate of condensation of these fragments and their rate of reformation is equal both in the liquid and at the solid-liquid interface. This defines a unique temperature.

The effect of imperfections in the real crystal is to harden it. These imperfections will often encourage the formation of voids in their vicinity. The greater the density of imperfections, the greater the number of these induced voids, and the higher the failure stress. Imperfections can also make a crystal more resitant to thermal softening by making these induced voids more stable against thermal annihilation than they would be otherwise. Imperfections which are capable of inducing voids into the crystal in their vicinity may also be able to induce melting in the same locations at elevated temperatures, thereby producing soft spots at these temperatures.

4.2.2 The Partial Surface Hypothesis

The concept of a partial surface was already introduced. In this section a particular kind of partial surface is taken into consideration.

If a surface is formed by the gradual separation of two adjacent atom planes in a crystal, then the zone between these two layers of atoms, described as the void,

passes through a stage intermediate to the undisturbed lattice and the fully developed surface.

In this intermediate stage, the two layers of atoms are still able to exert forces upon each other. The energy associated with the partial surface may have any value less than the full surface energy of the crystal. The void associated with a partial surface is defined to be a partial void.

According to the partial surface hypothesis, when a crystal is stressed, some of the elastic energy is converted to surface energy by the formation of partial voids. The following energy relationship is assumed to be valid

$$\sigma V_p = \bar{\gamma}_p s_p \qquad \text{..... 4.2}$$

where σ is the applied stress, V_p the partial void volume, s_p the total partial surface area and $\bar{\gamma}_p$ the average partial surface energy.

The second assumption of this hypothesis is that small partial voids may be annihilated with the accompanying growth of one or more larger voids, and that a large void will also contain a proportion of its surface that is either fully developed (so that stress is no longer transmitted across that portion of the void) or developed to such a degree that dislocations may readily form. The

one is a tensile stress nucleated void and the other a shear stress nucleated void.

The application of this hypothesis to obtain a dimension, temperature and imperfection dependence of the failure stress is analogous to the application of the variable surface energy hypothesis, and will not be repeated here.

4.3 A HYPOTHESIS BASED ON THE METALLIC BOND

In the previous section hypotheses were suggested which might correlate a diversity of experimental data. In this section the same thing will be attempted, but from a different point of view; namely on the basis of a particular theory of bonding.

4.3.1 The Metallic Bond

A simplified version of the free-electron theory of metals will be employed here. An analysis is presented in Appendix 9.3. In section 9.3.1 it is shown that if the containing walls of the model are moved relative to each other, the quantum state of the particle is undisturbed.

For a crystal this means that elastic deformation does not disturb the quantum state of the free electrons.

If a crystal is divided into smaller fragments, the potential energy of the fragments is increased because the total surface energy has been increased.

Surface energy may be interpreted by the use of the model of Appendix 9.3. According to this model, a crystal can have surface energy only if the formation

of the new surface confines the free electrons to a smaller volume. Not all the electrons are equally effected - the low energy electrons may be confined to a smaller volume than electrons of higher energy. One may define an average volume reduction for the electrons as a whole by the equation

$$S = \bar{P} \cdot \Delta\bar{x} \qquad \ldots\ldots 4.3$$

where S is the surface energy,

$\bar{P}$ is the kinetic electron pressure, and

$\Delta\bar{x}$ is the effective distance through which the electron gas is displaced inwards as the surface forms.

In the sections that follow, a hypothesis involving the appearance of new electron states in the crystal, will be developed.

4.3.2 The Effect of a Strain Gradient on the Metallic Crystal

Consider a crystal in which there are two regions, A and B under different strains E_A and E_B. In the other region, C, the strain varies from E_A to E_B. In this region, therefore, a strain gradient must exist.

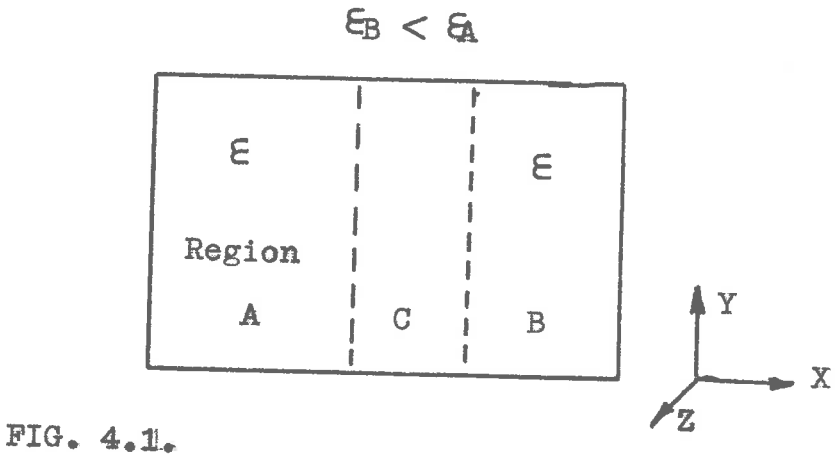

FIG. 4.1.

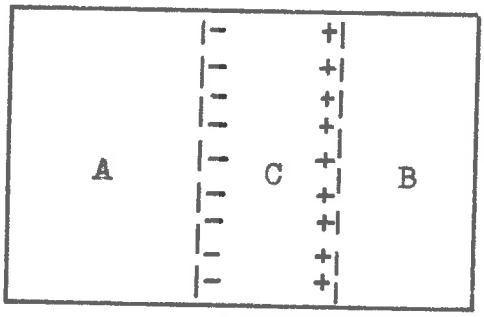

FIG. 4.2.

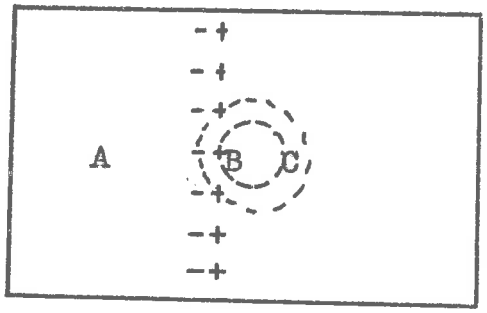

FIG. 4.3.

If $E_A > E_B$, then electrons entering the region B have been accelerated, for the potential of the electrons in this region is more positive (due to the closer spacing of the ions) and the change in potential appears as increased kinetic energy.

In Figure 4.1 the region C where the strain varies has been presented as having plane boundaries. This means that all electrons with their quantum numbers $n_x = 0$ can take up positions dictated by the strain potential gradient - as illustrated by Figure 4.2. The electrons which have no velocity in the X direction ($n_x = 0$), have a reduced density on the left side of region C and an increased density on the right side. The associated electrostatic potential gradient is opposite in direction to the strain potential gradient. If enough electrons are displaced, the strain potential gradient is cancelled out completely.

Now consider a spherical region in which the strain has the value E_B. The region C has now become a shell, Figure 4.3. The surfaces of constant strain are now curved and any electron with the quantum number n_x equal to zero (but n_y, $n_z \neq 0$) would enter and leave region C and can no longer follow a surface of constant strain. This means that the kind of charge separation that can take place when the surfaces of constant strain are

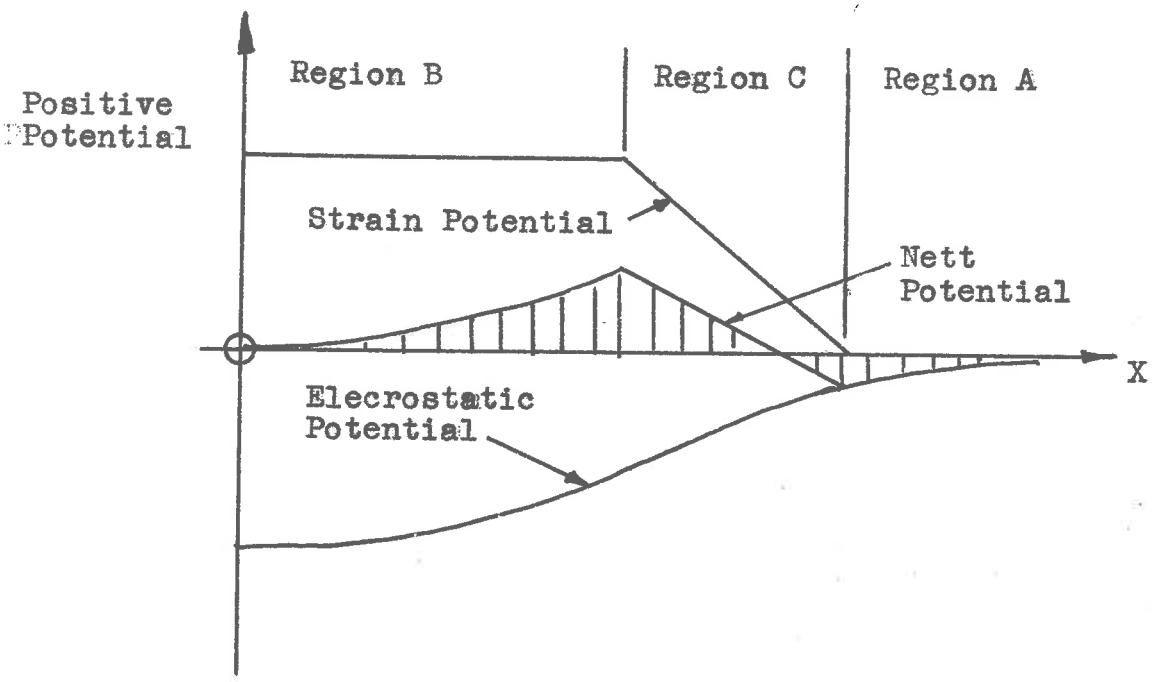

FIG. 4.4 The Potential Field that is capable of Isolating Electrons in Region B

plane is no longer possible. Any electron which passes through region C periodically will be subjected to a periodic motion in the X direction. This is not possible since $k_x = 0$, and the electrons will pass through this region in a non-periodic (i.e. random) manner.

Thus, for a curved zone of strain gradient, the strain potential gradient can no longer be cancelled by an equal and opposite electrostatic potential gradient.

The strain potential gradient will tend to reflect electrons moving out of the region B back into this region. This builds up an excess negative charge which tends to be distributed evenly throughout region B. Figure 4.4 illustrates the net potential variation due to a combination of elastic strain potential and electrostatic potential due to moving charges. It is apparent that electrons approaching region B are reflected by the initial potential rise outside region C, and electrons moving through region C from B are also reflected. When the two effects are the same, the overall potential of the region B has a stationary value.

4.3.3 Isolated Electron States

In the previous section it was shown that a certain kind of potential variation is associated with a

a curved zone in which there is a strain gradient.

Suppose that the spherical shell presented in Figure 4.3 were to expand. The associated potential pattern would then expand also. Now, there are low energy electrons in zone A whose total kinetic energy is so small that they are highly reflected when approaching the region C. These electrons are therefore "compressed" into a smaller volume by the expanding potential pattern.

The low energy electrons of region B are able to fill an increasing volume. These electrons are isolated from the remainder of the crystal by the potential barrier which confines them. Those electrons in region B which have a kinetic energy of the same order as or greater than the peak of the potential barrier are not isolated.

Those electrons which are strongly reflected by the potential barrier suffer a change in kinetic energy because the potential barrier is in motion. The effect of the potential barrier may be likened to the action of a piston in compressing or expanding a gas. The kinetic energy of the electrons is changed, although their quantum states remain unaltered.

Those electrons which are only partially reflected tend to be unaffected because they will be in zones A and B, so that there is no overall change in their kinetic energy.

The isolating of electrons in the region B means that the quantum states which these electrons filled in the undisturbed crystal are now unfilled in region A. One would therefore expect electrons in the higher quantum states to give up some energy and occupy these unfilled levels.

The number of electrons isolated in zone B is determined by the requirements of electrical neutrality. It was noted earlier that electrons are accelerated on entering zone B. The duration of their stay is therefore reduced. This would reduce the negative space charge. When these electrons leave the zone, they may be reflected at the potential gradient surrounding it. This tends to increase the space charge.

If the balance is toward a net negative charge, the potential gradient is such as to remove the potential gradient that accelerates the electrons. The isolated energy levels are diminished also. Both of these changes act so as to reduce the unbalance.

If the balance is towards a net positive charge, the potential in region B is made more positive and more isolated electron states are made available. As these states are filled, the positive potential diminishes until a point of balance is reached.

The number of electrons that may occupy isolated energy states is thus a function of the volume available, and the highest energy that an electron may have and remain in an isolated level. The maximum energy is a function of the potential hump which contains these electrons.

If it is assumed that the requirements of neutrality have a negligible effect on the number isolated energy states available, then the depth of the potential well that contains these electrons will be proportional to the difference of the strain of regions A and B.

From Equation 9.28, the number of available electron states is

$$N = V_1 (\Delta E)^{3/2} \qquad \ldots\ldots 4.4$$

where V is the volume of region B

and $\Delta E = E_A - E_B$.

As the volume of region B increases, the curvature

of region C diminishes. Electrons with one of the quantum numbers (n_x, n_y or n_z) = 0 are concentrated in parts of the lattice as shown in Figure 4.3 so that the electrical potential difference exists in regions C and A. This potential difference is induced by the strain potential gradient. If the electric field in a particular crystallographic plane passing through region C is E_o and the equivalent field due to the potential gradient is E_p then

$$\frac{E_p}{E_o} = \frac{l_p}{l} \qquad \text{..... 4.5}$$

where l_p and l are the distances travelled by an electron through region C, and the whole crystal respectively. This relationship shows that the strain gradient is completely counteracted when the zone C has traversed the entire crystal. The effective potential gradient is therefore $(E_p - E_o)$ and

$$(E_p - E_o) = E_p \left(1 - \frac{l_p}{l}\right) \qquad \text{..... 4.6}$$

As the effective potential decreases, the maximum energy of the isolated energy levels is decreased also. This reduces the number of isolated electron states available.

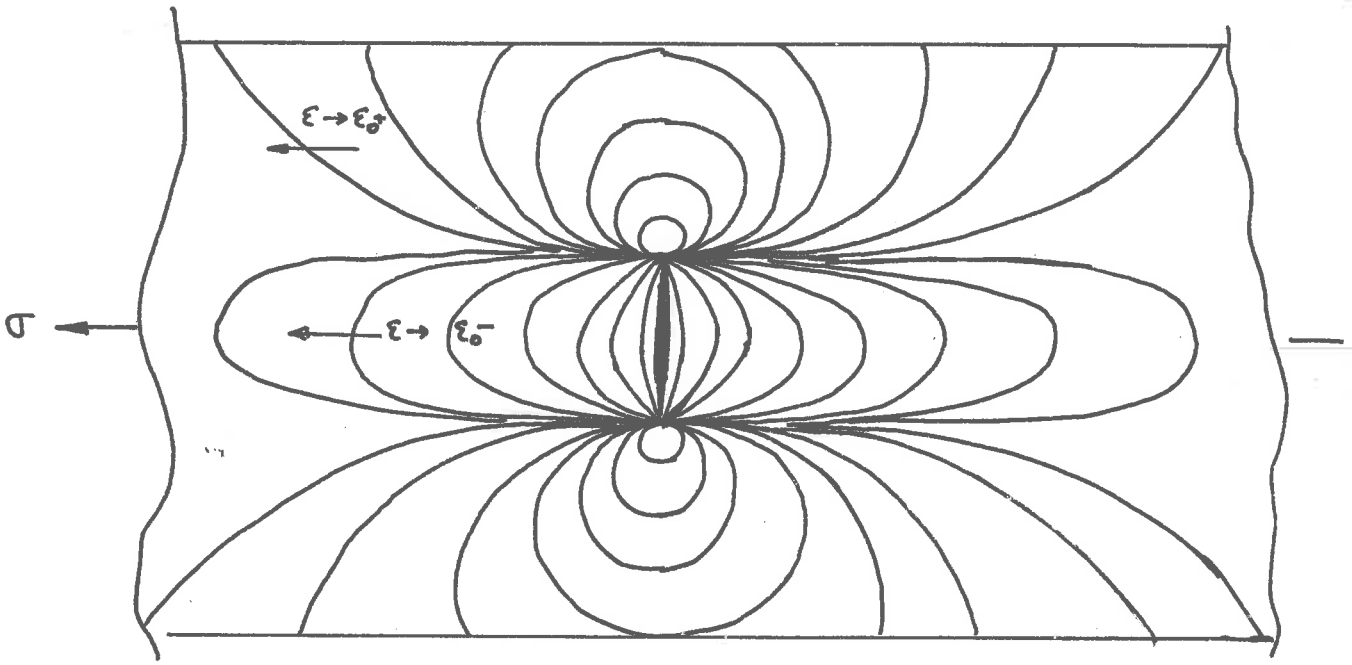

FIG. 4.5 Lines of constant Principal Strain in a Crystal under stress, containing a Void. The Strain is assumed to be zero in Regions immediately adjacent to the Void.

4.3.4 The Effect of a Void on the Metallic Crystal

When two adjacent layers of atoms in a crystal move apart, a space forms between them. This space is a void.

If a void is formed in a crystal under tensile strain, the portions of crystal adjacent to the void have their strain reduced. This is illustrated in Figure 4.5. It is seen that there is a region where the strain is smaller than the average strain, and another region where the strain is greater.

Two regions in which electron states of low energy may be isolated, are associated with the void. These regions are bounded by the void, the transition surface between the high-strain and low strain zones (which are cylindrical surfaces for a round void), and the strain potential gradient. The latter forms the boundary directly opposite to the void.

The strain potential gradient in the direction normal to the void surface is much smaller than any of the other gradients. Let the X direction be normal to the surface of the void.

To be isolated, an electron must have quantum numbers defined by

$$E_x \geq \frac{n_x^2 h^2}{8a'^2 m}$$

$$E_y \geq \frac{n_y^2 h^2}{8b'^2 m} \qquad \ldots\ldots 4.7$$

$$E_z \geq \frac{n_z^2 h^2}{8c'^2 m}$$

which yield maximum values n_x', n_y' and n_z'. The void and its associated strain pattern are symmetrical about an axis in the X direction, whence

$$E_y = E_z = E' \qquad \ldots\ldots 4.8$$

The total number of electron states possible may be found by using the method of Appendix 9.3.2, which gives

$$\frac{E'}{2} = \frac{2\pi m_e' h'^2}{h^3} (8a'^3 b'^2 c'^2 n_x)^{\frac{1}{2}} \ldots\ldots 4.9$$

It is assumed that $E_x \ll E'$. The quantity $a'b'c'$ defines the volume occupied by the isolated electrons.

The ratio of the isolated states to the total number of electron states in the undisturbed crystal is

$$\frac{N'}{N} = \frac{1}{2} V' \left(\frac{E'^2 E_m}{\pi^3}\right)^{\frac{1}{2}} \qquad \ldots\ldots 4.10$$

where $V' = a'b'c'$ and E_m is the maximum kinetic energy of electrons in the crystal.

While electrons moving in the YZ plane may be contained in the isolated state if their energy in this plane is equal to or less than E', it does not follow that quantum states which satisfy this condition will be found. For example, an electron in the state n_x^0, n_y^0, n_z^0 may fall to another available level $(n_x^0 + 1)$, 0, 0, which is not isolated because $n_x > n_x^0$. If this limitation is taken into account, the ratio of electron states becomes

$$\frac{N'}{N} = V' \left(\frac{E_x^3}{\pi^3 E_m}\right)^{\frac{1}{2}} \qquad \ldots\ldots 4.11$$

4.3.3 The Transformation of the Energy Associated with the Isolated Electrons into Thermal Energy

In previous sections, the situations that could lead to the generation of isolated electron states were considered.

When an isolated energy state becomes available, electrons in the higher energy levels can give up some of their kinetic energy and occupy these new states. This may happen in several ways.

The process of greatest interest here is that in which an electron only slightly above the new level falls into this level. The level vacated is similarly filled by an electron in a slightly higher level and so on.

Each new electron state can thus involve the transfer of a large number of electrons from one level to a slightly lower level. The energy made available need not be released immediately. The permissible time delay is given by the Heisenberg uncertainty relationship

$$\Delta E \cdot \Delta t \geq h \qquad \ldots\ldots 4.12$$

where ΔE is the energy that must eventually be emitted and Δt the allowed delay.

When a new surface develops, the electrons are confined to a smaller volume. The work done against the electron kinetic pressure appears as an increase in the kinetic energy of the electrons. The change in velocity of an electron whose X component of velocity is v_x is, from equation 9.22

$$\Delta v_x = v_x \frac{\Delta x}{a} \qquad \text{..... 4.13}$$

where Δx is the distance by which the effective x-dimension, a, of the crystal is shortened by the appearance of a new surface.

The associated change in kinetic energy is

$$\Delta \varepsilon_x = m v_x \Delta v_x = m v_x^2 \frac{\Delta x}{a} \qquad \text{..... 4.14}$$

$$\Delta \varepsilon_x = \frac{n_x^2 h^2}{4a^3 m} \cdot \frac{\Delta x}{a} \qquad \text{..... 4.15}$$

which shows that provided Δx is the same for all n_x, the change in kinetic energy associated with the formation of a surface is proportional to n_x^2.

The energy made available when an electron goes from n_x to (n_x-1) is

$$\Delta \varepsilon'_x = \frac{h^2}{8a^2 m}(n_x^2 - (n_x-1)^2)$$

$$= \frac{2h^2 n_x}{8a^2 m} \qquad \text{..... 4.16}$$

or

$$\Delta \varepsilon'_x = \frac{n_x^2 h^2}{4a^2 m} \cdot \frac{1}{n_x} \qquad \text{..... 4.17}$$

It is apparent that the energy increment gained by electrons when a surface is formed would be equal to the energy made available by an electron that goes from one energy level to the adjacent lower level if

$$\frac{\Delta x}{a} = \frac{1}{n_x} \qquad \text{..... 4.18}$$

which implies that Δx should not be the same for all values of n_x.

Sufficient energy will be available for the formation of a surface if

$$\frac{1}{n_x} \geq \frac{\Delta x}{a} \qquad \text{.....4.19}$$

for all n_x.

Voids do not generally cover the entire cross section of a crystal. The increase in the kinetic energy of the electrons when a void forms is given by

$$\Delta E_x = \frac{n_x^2 h^2}{4 a^2 m} \cdot \frac{\Delta x}{a} \cdot \frac{A}{bc} \qquad \text{..... 4.20}$$

where A is the area of the void, and 'bc' the sectional area of the crystal. It is assumed that energy may be exchanged by electrons with the same X quantum number.

The transfer of electrons to lower levels will furnish sufficient energy for the surface energy of a void if

$$\frac{1}{n_x} > \frac{\Delta K}{a} \cdot \frac{A}{bc} \qquad \text{..... 4.21}$$

for all n_x.

Now n_x and ΔK are both characteristics of the crystal so that

$$\frac{1}{\Delta K n_x} > \frac{A}{abc} \qquad \text{..... 4.22}$$

Thus, if a surface is forming at the same time that electrons are transferring from one level to a lower level, the excess energy may be retained as surface energy.

4.3.6 Nucleation of a Void in a Metallic Crystal

The possibility of new energy states in crystals containing voids has been considered. The conditions for the transformation of energy released, when electrons go to lower energy states, into surface energy has also been derived.

Consider a crystal placed under a tensile stress.

If a partial void appears in this crystal, new energy states will be associated with it. The energy made available through the appearance of the new energy states furnishes surface energy for the developing void.

Equation 4.11 shows that the ratio of the new electron states to those of the whole crystal is a function of both the volume occupied by these states and the maximum allowed energy of the confined electrons.

The allowed energy E_z will be a function of the applied strain E_x and the diameter of the void. The volume of the space into which the new electron states are confined is assumed to be proportional to the third power of the diameter of the void.

Thus assume

$$E_x = f(E_x, D) \qquad \ldots\ldots 4.23$$

$$V' = K.D^3 \qquad \ldots\ldots 4.24$$

The diameter of the void influences the allowed energy in that the curvature of the lines of constant strain determine the degree to which an electrostatic potential gradient can neutralize the strain potential gradient.

If the void is so small that this effect is negligible the relationship

$$E_x = Ex \text{ or } \sigma_x \qquad \text{..... 4.25}$$

can be assumed. A void for which this relationship holds is defined as a small void.

The development of small voids will now be considered.

The surface energy associated with a small void is proportional to its area.

Thus

$$E_s = s. \pi D^2 \qquad \text{..... 4.26}$$

where s is the surface energy per unit area.

N' new energy states are associated with this void so that the available energy

$$E_e = N' E_s \qquad \text{..... 4.27}$$

$$\text{If } E_x = K_1 Ex \text{ and} \qquad \text{..... 4.28}$$
$$V' = K_2 D^3$$

$$E_e = N \frac{K_2 D^3}{V} \left(\frac{K_1^3 E_x^3}{E_m^3} \right)^{\frac{1}{2}} R_m \quad \ldots\ldots (4.29)$$

Put $N = \rho V$ where ρ is the number of electrons per unit volume (a property of the crystal), then

$$E_e = \rho K_2 D^3 \left(\frac{K_1^3 E_x^3}{E_m^3} \right)^{\frac{1}{2}} R_m \quad \ldots\ldots (4.30)$$

It is considered that

$$K_2 \approx 1$$

$$\frac{K_1 E_x}{E_m} \approx E_x, \text{ so that}$$

$$E_e \approx \rho D^3 R_m (E_x)^{3/2} \quad \ldots\ldots (4.31)$$

Also, if α is the separation of atoms in a crystal, then

$$S \approx E_m / \alpha^2 \quad \ldots\ldots (4.32)$$

A void is possible if

$$E_e \approx E_s \quad \ldots\ldots (4.33)$$

i.e. $$E_x \approx \left(\frac{\alpha}{D} \right)^{2/3} \quad \ldots\ldots (4.34)$$

using $$\rho \approx \frac{1}{\alpha^3}$$

According to equation 4.34, the slightest applied strain will lead to the formation of a void of unlimited extent. Very small crystals in which even the largest possible void satisfies the requirements for a "small" void, would therefore have no strength at all.

The relationship 4.22 is based on the more restricted assumption that if one electron of X quantum number n_x has acquired excess energy, only those electrons with the same X quantum number may share this energy.

The area of a small void will always be less than the total sectional area of the crystal if

$$\Delta n_x > a \qquad \text{..... 4.35}$$

whence from 4.22

$$\frac{A}{bc} < \frac{a}{\Delta n_x} \qquad \text{..... 4.36}$$

$$\frac{A}{bc} < 1 \qquad \text{..... 4.37}$$

The following conclusions can be drawn from this:

For small crystals the void is limited in size by the requirement 4.22. The void area will always be a certain fraction of the sectional area of the crystal.

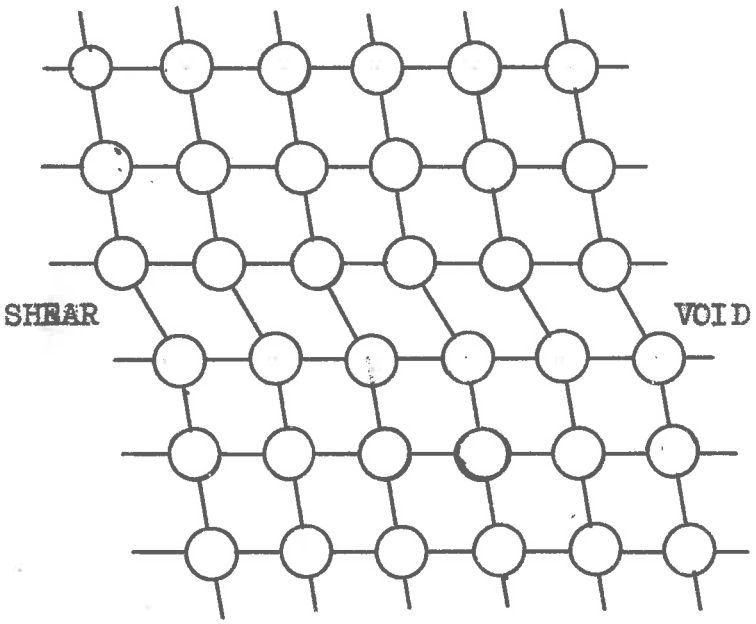

FIG. 4.6 Illustrating the Atomic Arrangement that Constitutes a Shear Void.

For large crystals, the void is limited by the neutralization of the strain potential gradient by the electrostatic potential gradient. The size of such a void will be independent of the size of the crystal.

Under stress, these voids can become cracks which can traverse the whole section of the crystal. As the void grows, under the influence of the applied stress, the electrons in the isolated states are returned to the remainder of the crystal, and the "borrowed" energy associated with the isolated energy states is returned to the system.

4.3.7 The Shear Void in a Metallic Crystal

So far only tensile voids have been considered. The shear void is defined as the region between two adjacent planes of atoms which have undergone a relative shear motion much larger than other pairs of atom planes in the neighbourhood.

A shear void can be expected to obstruct the passage of electrons with a velocity component in a direction normal to the surface of the void. Figure 4.6 shows a shear void. It is apparent that the path of electrons will be obstructed. A definite surface energy will be associated with a shear void.

The difference between a tensile and a shear void is that the surface energy associated with a tensile void increases linearly with the separation of the atom planes at first, and levels off to a constant value. The shear void exhibits the same initial increase, but the surface energy attains a maximum and begins to diminish, coming to zero when the two atom planes are in step again.

Consider the behaviour of small crystals (where the void area is limited according to equation 4.22). When the void has attained its limiting size, it resists the effects of increasing stress until the stress is large enough to furnish the necessary surface energy. As the void diameter increases with increasing stress, the surface energy at the centre will reach the maximum. The surface energy will now diminish so that a ring of void is produced which may become an ordinary dislocation.

If the crystal is large the limiting void dimension may be so great that a series of rings at which the surface energy is a maximum are formed. Such a void can generate an indefinite number of dislocations when sufficient stress is applied.

It is noteworthy that if the crystalline plane is rough on the atomic scale, the relative shear of two such planes will also involve a separation of the planes

from each other. This will encourage the formation of a tensile void, which may open up into a crack if a suitable stress is present. The stress at which the void develops into dislocations is also increased.

4.3.8 The Application of the Temporary Electron State Hypothesis to Non-metallic Materials

According to this hypothesis, an aggregate of atoms behaves in such a way when placed under stress, that new electron states of low energy are introduced into the crystal. The energy associated with these new states becomes available for nucleating a void. If a sufficiently high stress is applied, the void may develop, restoring the energy released by the electrons which have entered the new states, and resulting in a crack or a dislocation.

Covalent bonds are similar to the metallic bond in that the electron orbitals of adjacent atoms overlap. The result is a single electron system in which each electron must have a different set of quantum numbers. It is conceivable that under strain a covalently bonded material will also produce new electron states.

If the electrons in ionic crystals were totally confined to the negative ions, a connected system would not be possible. This is not the case however, and the

application of this hypothesis to ionic bonds is also possible.

Similar arguments apply to molecular chains such as those found in plastics and near crystalline groups of molecules such as those found in glass.

The special conditions associated with each of these materials will modify the application of the hypothesis. It is suggested that the hypothesis is likely to find a very general application, and so serve to explain the properties of, it is hoped, all kinds of solids.

4.3.9 The Interpretation of Various Solid State Phenomena by Means of the Permissible Electron State Hypothesis

The treatment of the various properties of solids will be undertaken in a qualitative way only. It is intended to show the application of the hypothesis. A quantitative interpretation would doubtless be a better proof of the validity of this hypothesis, but that is also a task of considerable magnitude.

4.3.9.1 The Yield Point

According to the hypothesis, a void of significant dimension is nucleated. The limits of this void are determined by the size of the crystal or the size

of the void. The void exists on "borrowed" energy, in the sense that if it is extended to cover the entire crystal section, the energy associated with its nucleation must be supplied to the crystal in addition to the surface energy associated with its extension.

For a given crystal, the size of the nucleated void is determined. The stress that must be applied to develop this void into a dislocation is determined also. The crystal therefore has a definite yield point. Above the yield point, dislocations are multiplied. Below this point the generation of dislocations ceases altogether.

A void may also be associated with a moving dislocation. If the resistance to the motion of a dislocation of the classical kind is higher than the stress at which the dislocations are generated, the dislocation may widen by the formation of a void if a widened dislocation is likely to encounter less resistance. Thus the propagation as well as the generation of dislocations may be nucleation controlled, and the effect of imperfections such as impurity atoms is diminished.

The activation energy made available by thermal fluctuations can assist an applied stress in producing a dislocation. Such a process is time dependent, and explains the creep process.

Thermal agitation can have another effect by disturbint the homogenity of the crystal. The process by which an electrostatic potential gradient counteracts a strain potential gradient is thereby modified. As a result, larger voids are possible, and the yield point is reduced. This temperature dependence is not a true activation process for it is only the disrupting effect associated with thermal fluctuations not the energy as such, that is involved.

The yield point at each temperature will have a definite value. Thermal fluctuations will nevertheless have a small effect on the generation of dislocations. As the applied stress approaches the yield stress some of the more favourably activated voids will develop, making the transition from elastic to plastic behaviour more gradual. Crystal imperfections can have a similar effect.

4.3.9.2 Delayed Yielding and the Yield Point

Although temperature is involved in determining the yield point it is not an activation process and a very slight time dependence only is to be expected.

It seems that delayed yielding is associated with impurity atoms that form strong bonds with the crystal

atoms. When a shear void forms, these atom bonds remain and constrain the two atom planes forming the void. The void can develop when sufficient of these atoms have diffused away from the void. The greater the applied stress, the greater the energy supplied to the impurity atom bonds, and the lower the activation energy required.

The analysis of Pfeiffer[43], described in section 3.2, which employs a large number of activation processes that occur in parallel, and an activation energy that decreases with increasing applied stress applies readily to the above hypothesis. This is also the analysis which fits experimental results best.

Sudden yielding is characteristic of the delayed yielding process. It also occurs if the specimen is loaded very slowly. In this case the impurity atoms on the void are able to remain in near-equilibrium with the surrounding crystal. As the stress increases the impurity atoms in the void diminish in number until the void is released and develops rapidly. This becomes evident macroscopically if the nucleating stress is greater than the flow stress - also a necessary condition for delayed yielding.

Dislocation arrays produced by the first generators can produce favourable stress fields for subsequent generators. The result is a widening

deformation band such as the Neumann bands. In this way the overall stress can be lower than the stress at which dislocations are actually being generated.

4.3.9.3 Strain Hardening

Price[45], testing zinc crystals found his specimens (which were of high perfection) yielded first where the stress could be expected to be highest. After the onset of deformation, the stress fell to about two thirds of the peak value. As deformation continued the region at which yielding took place widened into a deformation band that eventually included the whole crystal. When this had happened, the flow stress began to rise.

Apparently in Price's specimens, the stress for nucleation exceeded the stress at which the dislocations are mobile. Once a single source is active, the dislocation generated by it may pile up in such a way as to increase the stress in small portions of the crystal. New generators would be activated in such regions and the deformation band would continue to expand.

The second stage of the deformation process begins when the entire crystal is included in the deformation band. During this stage, the density of dislocations throughout the crystal increases. The

interaction between dislocations continues to raise the flow stress.

The third deformation stage begins with the onset of tensile voids. These do not generally result in a cleavage failure for the specimen contains so many dislocations that a crack is readily arrested. The stress concentrations associated with these voids maintain deformation for a time until the specimen fails by fracturing.

Bridgeman[37] has shown that if the specimen is placed under hydrostatic pressure, the second stage (which is linear) can be extended far beyond the usual failure strain. A high hydrostatic pressure would be expected to do that, for it prevents the development of cracks (as he himself writes).

Crystals in which several intersecting glide systems can be activated will be expected to strain harden more rapidly.

4.3.9.4 Grain Size

It has already been shown that for small crystals, the size of the nucleated voids is limited by the dimensions of the crystal.

According to Fujita[56] the Griffith crack becomes mobile when

$$\sigma = (2E\gamma/\pi L)^{\frac{1}{2}} \qquad \text{..... 4.38}$$

where E is the Young's Modulus, γ the surface energy and L the half length of the crack. According to equation 4.37, the half length L may be defined as

$$L = k \sqrt{\text{sectional area of crystal}} \qquad \text{..... 4.39}$$

$$= kd$$

where $k < 1$, d is the square root of the crystal area.

Inserting in equation 4.38

$$\sigma = \left(\frac{2E\gamma}{\pi kd}\right)^{\frac{1}{2}} \qquad \text{..... 4.40}$$

$$\text{i.e.} \quad \sigma \propto d^{-\frac{1}{2}} \qquad \text{..... 4.41}$$

Such a relationship is indeed found to apply[58]. Although the above analysis applies strictly to a crack, it will serve equally for determining the stress at which dislocations will be generated.

As the size of the crystals increases, the strength does not fall indefinitely but tends towards a constant value, for the size of a void is self-limited.

4.3.9.5 Impurities and Imperfections

The effect of impurity atoms on moving dislocations, and in causing delayed yielding has already been discussed in section 3.1 and 4.3.9.2.

Imperfections can encourage the nucleation of a void in their vicinity. For example, if a series of vacancy sites condense into a disk, a void nucleated in that region will require less energy to be developed. If a large number of such vacancy disks are present, many voids appear, and they influence each other such that the stress required to activate them increases.

The behaviour of quenched-in vacancies follows this pattern. Meshii and Kaufmann[59] quenched pure gold and measured the yield point after various ageing intervals. The specimens were quenched from just below the melting point. They found that the yield stress increased linearly with increasing quenching rate between 10^4 and 10^5 °C per second. On subsequent ageing at 100°C the yield stress increased further, tending towards a steady value. If the specimen is annealed at higher temperature, it softens again.

This may be interpreted as follows: the heated specimen contains many vacancies. If it were quenched suddenly (i.e. at an infinite rate) to a low temperature, these vacancies would be frozen in just as they were at elevated temperature. However the quench extends over a finite temperature so that some of the vacancies will have diffused out of the crystals and others will have condensed into larger vacancy groups.

The larger of these vacancy groups can attract a void, and the specimen is hardened by the presence of many voids. With further ageing, more of the vacancies condense onto the existing groups, as well as forming new ones. The number of voids is increased further, and the specimen becomes harder still. As the vacancy concentration reaches it equilibrium value, the yield stress also levels off to a steady value.

If the specimen is aged at higher temperature, the vacancy groups gradually vanish by the diffusion of vacancies out of the crystals. The yield properties of the specimen approach those of a furnace-cooled specimen.

It is observed also that the specimens with a high yield stress have a low strain hardening rate. The high stress is determined by the requirements of dislocation

nucleation. Once a dislocation is formed it will propagate rapidly. This keeps the dislocation density at a lower level and thereby reduces the number of dislocation intersections and the consequent strain hardening.

Dissolved impurities can act in the same way as vacancies. They are soluble in the crystal at high temperature but precipitate out on cooling.

The precipitation of such solutions on many sites is encouraged by introducing dislocation into the crystals, which may then act as nucleation sites for precipitation. This strain ageing treatment is used to improve the properties of a material.

4.3.9.6 Alloys

The effect of mixing various elements in the molten state on the subsequent solid is varied.

If a solid solution is formed, the effect of the alloying element is to increase the flow stress of the crystals.

It was pointed out previously that during the formation of a shear void relative sliding takes place. If the atom planes contain solute atoms of different size,

the surface energy associated with a shear void is increased. This will appear as a higher dislocation generating stress. The progress of dislocations will be similarly affected so that the flow stress is also increased.

If the alloying elements introduce two or more phases into the final solid, solution hardening will still occur (for the various phases are usually solutions), but a new control over the grain size of the solid is made available. Transformation temperatures in the solid state make it possible to reduce the crystal dimensions of a solid specimen.

Phases may be precipitated out as lamellae, spheroids, needles, etc. These precipitates can act as numerous nucleation sites, thereby hardening the crystal, or they can isolate various portions of the crystal from each other, with the same result.

Non-metallic solute atoms such as oxygen introduce isolated bonds into the crystal which resist the development of voids, and so increase the yield stress.

4.3.9.7 Fatigue

Under repeated loading voids will appear and vanish with each load cycle. If the crystal contains

impurities that can diffuse, they will tend to accumulate at places where voids regularly appear, and precipitate out. With every loading cycle a small amount of energy is added to the void and it continues to grow.

Up till now the location of the void in the crystal has been ignored. It can easily be shown that if the void forms at the surface of the crystal it will develop with a smaller applied stress than a void in the body of a crystal.

Fatigue voids that have developed at the crystal surface are therefore open to the atmosphere. At the stress peak, atmospheric molecules or ions may enter the void and become attached to void surfaces. When the load is removed, the void does not collapse completely. Some of the elastic energy has been converted into surface energy. On the next loading cycle, the void is slightly greater and the adsorbed molecules penetrate more deeply and so on.

The existence of an endurance limit suggests that below a certain applied stress level, impurity atom bonds can prevent the void from opening sufficiently for foreign molecules to penetrate. It is significant that the materials that exhibit an endurance limit also exhibit delayed yielding and a sudden yield point.

According to this interpretation, surface treatment and protection as well as the medium surrounding the specimen should all affect the fatigue life of the specimen. It is well known that this is the case.

4.3.9.8. Surface Effects

Andrade[60] discusses the effect of an oxide layer on the mechanical properties of single crystals. The effect of an oxide layer (as little as 20 atoms thick) on cadmium is to increase the critical shear stress by 50%. This increase in stress remains constant for glides of up to 600%.

The interpretation of this phenomenon is as follows: the oxide layer represents a source of oxygen ions. When the crystal is strained, voids form preferentially at the surface. Before these voids are fully developed, oxygen ions have penetrated them and spanned the void with isolated bonds. As long as the deformation stress is nucleation controlled, the increase in flow stress due to the oxide layer remains constant and independent of the amount of glide.

If surface voids are inhibited altogether, internal voids are activated. Internal voids are not affected by surface deposits.

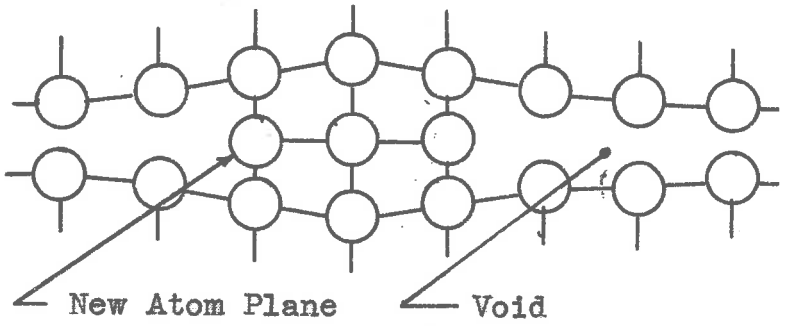

Vacancies are generated at the Void by Thermal Agitation, and diffused away, leaving Interstitial Atoms in the Void. These Atoms aggregate to form a new Atom Plane.

As the new Atom Plane grows, the Void releases a Dislocation Loop. The Atom Plane may be looked upon as a Prismatic Dislocation Loop.

FIG. 4.7 Thermally Assisted Developement of a Void.

The behaviour of silver, also reported by Andrade, is unusual in that the oxide layer actually causes an increasing strength of the crystal with increasing temperature above about 180°C, when tested in air.

The affinity of silver for oxygen is relatively small - the oxide layer is so thin as to be invisible, possibly a monatomic layer.

If two similar crystals are tested in air and argon at room temperature, both yield at the same stress but the specimen exposed to air strain hardens at a much greater rate so that at 20% glide, the difference is a factor of 10.

The oxygen ion being only lightly attached to the silver surface is more mobile than on other metals. The ion does not constrain the void, but tends to be carried away by the dislocations generated by the void. The impurity atoms so distributed throughout the glide plane increase the back stress, causing other glide systems to be activated. By the time the stress has reached the level where internal voids can become active, the impurity is distributed so evenly that internal dislocations are impeded as much as those from surface voids. Surface voids can therefore continue to generate dislocations and the hardening continues.

4.3.9.9 Twinning

On certain atomic planes in a crystal a shear displacement of one plane relative to the next does not bring the two planes into alignment as a dislocation normally does. A dislocation that produces such a misfit must be driven by a stress large enough to supply the misfit surface energy. Another dislocation on the adjacent plane deepens this misfit zone. The energy associated with the misfit will not increase if these dislocations produce a new crystal which has the same structure as the parent crystal but with a different orientation.

Consequently, such planes of misfit will tend to widen into crystals, and deformation will be concentrated into this system in preference to the nucleation of many individual dislocations on isolated glide planes.

A nucleation mechanism which can generate a series of dislocations in places dictated by minimum energy requirements is needed to sustain the twinning process. The proposed nucleation hypothesis meets this requirement, and so provides an explanation for the twinning process.

4.3.9.10 The Effect of an Ultrasonic Sound Field

An ultrasonic sound field of small wavelength can have the same effect on a void as a thermal disturbance. This is one way in which the nucleation hypothesis has been tested. Blaha and Langenecker[61] found that a crystal subjected to an ultrasonic sound field had its flow stress decreased, and increased again as soon as the field is switched off.

4.3.9.11 Green

The energy associated with a dislocation loop that is stable even at high stress amounts to many hundreds of electron volts. The average thermal energy associated with any mode of vibration is about $\frac{1}{10}$ e.v. at 1000°C. Clearly the generation of a stable dislocation loop by a single stage activation process is unlikely.

The energy required to nucleate a point defect pair - an interstitial and a vacancy, in the crystal lattice will be high. If the vacancy is formed on the crystal surface the activation energy required will be less because the atom must not be wedged into the lattice. The formation of a vacancy at the surface of a void can be expected to require even less energy because an atom will require less energy to enter a partial void than it requires to transfer onto a full surface.

Voids will therefore be intense sources of vacancies. The atoms released when the vacancies are formed accumulating in the void. This plane of atoms in effect converts the void into a ring. This is illustrated in Figure 4.7. While the atoms on either side of the void are in line the two zones have been

relatively displaced by one or more interatomic diameters. When the dislocation is finally released, a disk-like layer of atoms remains.

The rate at which the dislocations are generated depends on the applied stress and the temperature. Temperature determines the rate at which vacancies are generated at the void and the applied stress determines the size which the void ring must acquire before the dislocation loop can be released.

The atom disk may be seen as a prismatic dislocation loop.

The propagation of the released dislocation loop will also depend on activation.

4.3.9.12 The Melting Point and the Nature of the Liquid State

In large crystals the size of voids is limited by the ability of a potential gradient to isolate new electron states. The larger the void, the greater the extent to which an electrostatic potential gradient can build up to neutralise the strain potential gradient.

Thermal agitation distorts the strain pattern around a void and disturbs the electrons that produce the electrostatic potential gradient. The consequent reduction in the electrostatic neutralisation allows the void to

grow larger. A larger void can be developed by a lower stress, so that the strength of the crystal is reduced.

As the temperature is increased, thermal activation assists the applies stress in generating and propagating dislocations, but activation alone will not generate dislocations.

Voids will not only form when a stress is applied to a crystal but may also be formed by thermal agitation. Such voids are temporary. Nevertheless, the generation of vacancies can be achieved in two stages with the assistance of temporary voids. This will approximately square the rate of vacancy generation.

If the voids are below the surface, the result is a mixture of vacancies and interstitials. At the surface of the crystal, atoms released into temporary surface voids can diffuse onto the surface. This reduces the density of interstitial atoms and the concentration of vacancies will be higher.

A new phase is possible, for if the crystal were to disintegrate into a large number of small crystallites, the boundaries between these crystallites will act as surfaces. No part of the crystallite is far removed from the surface and the large vacancy concentration can be maintained.

The crystallites may be formed at the surface of a crystal by the condensation of vacancies into disks. The crystallites in the liquid phase will break up by a similar process. The melting temperature is the temperature at which the rate of condensation and the rate of generation of crystallites at the crystal surface are equal and similarly for the liquid phase.

A definite temperature is defined by this, which is consistent with the observation that solids have a definite melting point, and liquids a definite freezing point.

Crystallites will be small, so that liquids have no long range order. The presence of a high concentration of vacancies combined with thermal agitation will disrupt the short-range order also.

Liquids will conduct heat and electricity but these properties while analogous in some respects to those of a polycrystalline solid, will differ from the solid state properties of the same material.

4.3.9.13 Conclusion

Although derived from different points of view, the variable surface energy hypothesis and the temporary electron state hypothesis have some resemblance to each other.

The temporary electron state hypothesis is one that should be applicable to all solids. It may be used to interpret the behaviour of solids along the lines indicated in this section.

The usefulness of this hypothesis in explaining the process of melting and the molten state is no small triumph.

A quantitative application of this hypothesis awaits a rigorous development of the theory.

5.0 EXPERIMENTAL WORK

During the course of this investigation several avenues of experimental research were undertaken. These were:

(1) Shear Deformation Tests.

(2) Crack Propagation Tests.

(3) Micro-Indentation Tests.

5.1 Shear Deformation Tests

The general aim in performing this series of experiments was to deform specimens in shear over a wide range of deformation rates, and temperatures, obtain data on the deformation stress pattern, flow lines and obtain a correlation between these results and deformation theory.

Experiments involving various shear rates and test temperatures are described in the literature. Tests in which several kinds of information are taken from the specimen simultaneously are less frequent. This series was intended to investigate the problem by correlating the maximum information with a deformation theory simultaneously.

Low shear rate tests (shear rates 10-1000 per sec.) were carried out in a shaper, the forces being recorded on film via a cathode ray oscillograph. Steps

were taken to increase the range to 10^5 per second by building a special testing rig. This device was also to be adapted to very low strain rate tests, i.e. strain rates below 10 per second.

At the time the writer's intention had been to follow up a series of experiments which would be as severe a test as possible of the current deformation theory as well as any theory that he might propose. He eventually decided that while the shear testing approach might yield a considerable amount of significant data its application in criticising a deformation theory would be no more effective than a large amount of experimental data already available in the literature. Further work was therefore suspended for the time being. At this point the low shear rate method had been well tested and the high rate rig had been finished and tested but without obtaining force readings. The shear test apparatus is described in Appendix 9.4.

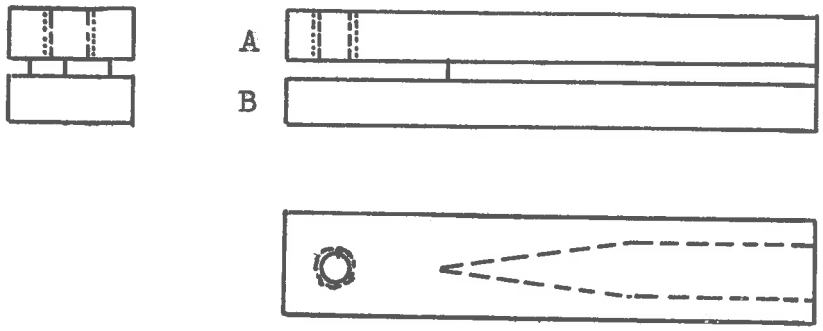

FIG. 5 .1 Illustrating the Fracture Specimen of the first Kind (Type 1).

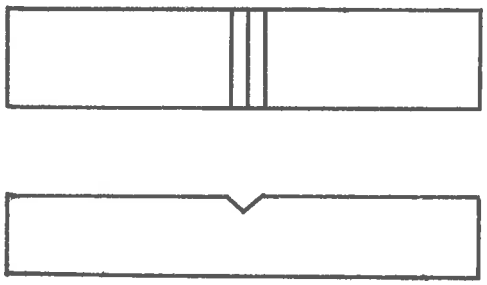

FIG. 5.2 Illustrating the Fracture Specimen of the second Kind (Type).

5.2 Crack Propagation Tests

Several materials were subjected to this test, cast iron, a high grade steel (quenched and tempered), mild steel, zinc, bismuth and cadmium. Cadmium could not be made to propagate a crack and no results were obtained for this metal. Tests were carried out at room, dry ice and liquid nitrogen temperatures.

5.2.1 Specimen Geometry

Two testing arrangements were used. To obtain a measure of the energy absorbed by the propagating crack a specimen preparation of type 1 was employed. The second preparation was intended also to permit a microscopic study of the crack during propagation which was carried out only at room temperature on bismuth. The two preparations are shown in Figures 5.1 and 5.2.

It was found that specimens machined according to Figure 5.1 propagated a crack readily in the plane of the reduced section. The specimens were loaded by inserting a screw into the tapped hole (1) Figure 5.1 and forcing the two beams A and B apart.

5.2.2 The Force Cell

To measure the energy absorbed by the specimen during the propagation of the crack, the magnitude of the

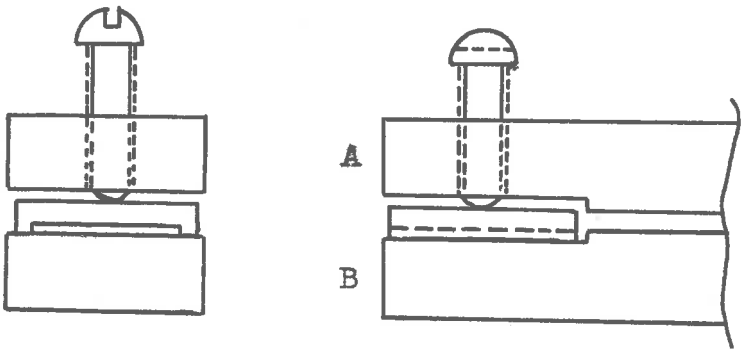

FIG. 5.3 Showing the Location of the Force Cell on Specimens of Type 1.

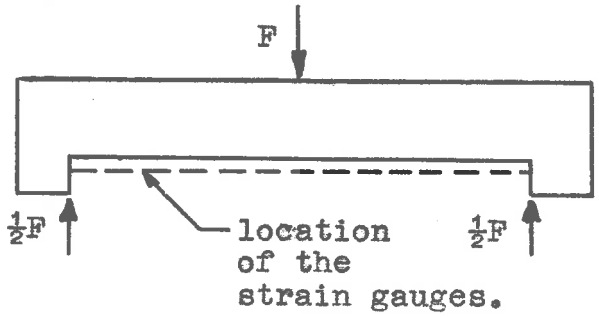

FIG. 5.4 Details of the Force Cell.

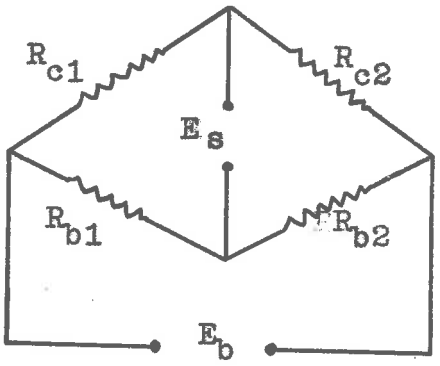

FIG. 5.5 The Strain Gauge Circuit.

loading force and the distance through which this force acts were obtained. A force cell, Figure 5.4 was designed and made so that it could be inserted into the space between the cantilevers A and B, Figure 5.3.

The separation of the two cantilevers can be obtained simply by measuring the angular rotation of the loading screw.

The bridge circuit for the force cell is shown in Figure 5.5. R_{G_1} and R_{G_2} are strain gauge resistances and are attached to the force cell and arranged to be parallel and perpendicular to the strain in the force cell respectively. It follows that R_{G_1} is sensitive to the load acting on the force cell, while R_{G_2} is not and serves as a temperature compensating resistance. R_{B_1} and R_{B_2} are built into the Philips Strain Bridge used in these experiments. R_{B_1} is varied manually to bring the signal E_s to zero. The bridge voltage E_b is high frequency AC to facilitate the amplification of E_s and so increase the sensitivity of the measuring instrument. The scale for R_{B_1} is calibrated directly in microstrain.

5.2.3 Calibration of the Force Cell

To calibrate the force cell, a steel calibrator was made, which would fit into the testing rig in the same

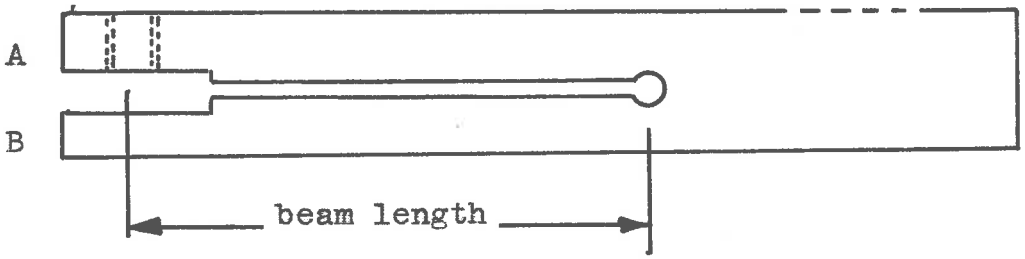

FIG. 5.6 The Force Cell Calibrator.

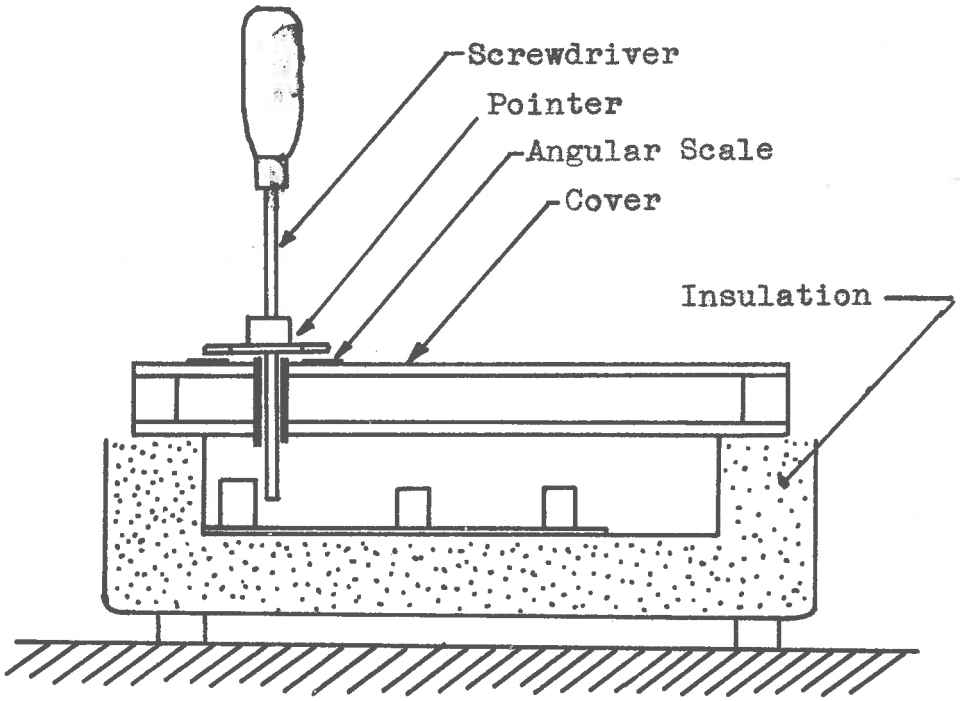

FIG. 5.7 Controlled Temperature Testing Rig.

way as the specimens and so made it possible to calibrate the force cell at room temperature as well as the liquid nitrogen temperature (-196°C). The calibrator is shown in Figure 5.6.

The calibrator may be assumed to be linear so long as the steel (tough high quality steel, quenched and tempered) is below the elastic limit, so that the stiffness of the two cantilevers with forces applied at the centre line of the hole, can be calculated and measured. The measured stiffness was obtained by pulling the two levers apart at the centre line of the hole with a known force, and measuring the relative displacement of the two cantilevers with a micrometer. Readings obtained by reversing the direction of the force (pushing the two cantilevers together) gave the same stiffness and the computed stiffness agreed well with the measured values.

5.2.4 The Specimen Testing Rig for specimens of type I

The overall dimensions of specimens of type I are 5" x $\frac{1}{2}$" x $\frac{1}{4}$". The testing rig, Figure 5.7, consists of an insulated container in which the specimen can be located and covered by liquid nitrogen. The container is covered by a glass cover with a suitably located hole to

allow a screw-driver to be inserted to rotate the loading screw. The rotation of the screw-driver is used to measure the rotation of the loading screw and hence the separation of the two cantilevers on the specimen. The specimen is located in such a way that it will not rotate when the loading torque from the screw-driver is applied to it.

5.2.5 Procedure for calibrating the force cell

The calibrator with the force cell is inserted into the rig in the same way as the specimen. If room temperature calibration is required, the cover is replaced and the system is permitted to reach a temperature equilibrium. The loading screw is turned through about one turn (pitch $^1/_{32}$ inch) in about 15 steps and unloaded again in an equal number of steps. For each angular setting the bridge is balanced and the reading recorded.

With a knowledge of the stiffness of the calibrator a calibration curve, force vs. bridge reading can be plotted. The points on this plot are found to lie on a straight line with small scatter only, indicating that the force cell arrangement is both precise and reliable.

To calibrate the force cell at liquid nitrogen temperature, the container is filled with the liquid after

inserting the calibrator and replenished until boiling ceases, indicating that the calibrator has been brought to the temperature of liquid nitrogen. The cover is now replaced and the calibration carried out as previously. When reducing the data obtained for plotting allowance must be made for the slight increase in the elastic modulus of the calibrator material.

5.2.6 Procedure for testing the specimens

The procedure outlined above for calibrating the load cell also applies when the specimens are actually subjected to the splitting test which destroys the specimen

The results are reduced and plotted. A typical plot is shown in Figure 5.8. This plot will be analysed in the next section.

The load which will propagate a crack is generally slightly dependent on the loading rate. The loading rate was not controlled precisely the interval between successive loadings being about 10 seconds. No high speed plotting tests were carried out, so that the dependence of the applied load on loading rate could not be determined. It is likely, however that the dependence on loading rate will not be very significant. This can be said because

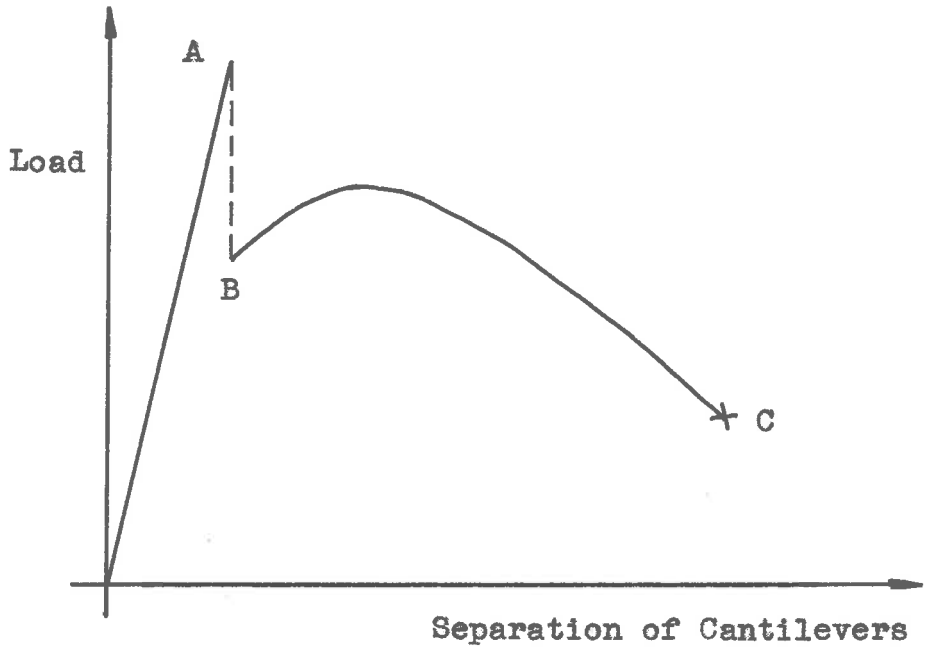

FIG. 5.8 Typical Controlled Fracture Plot.

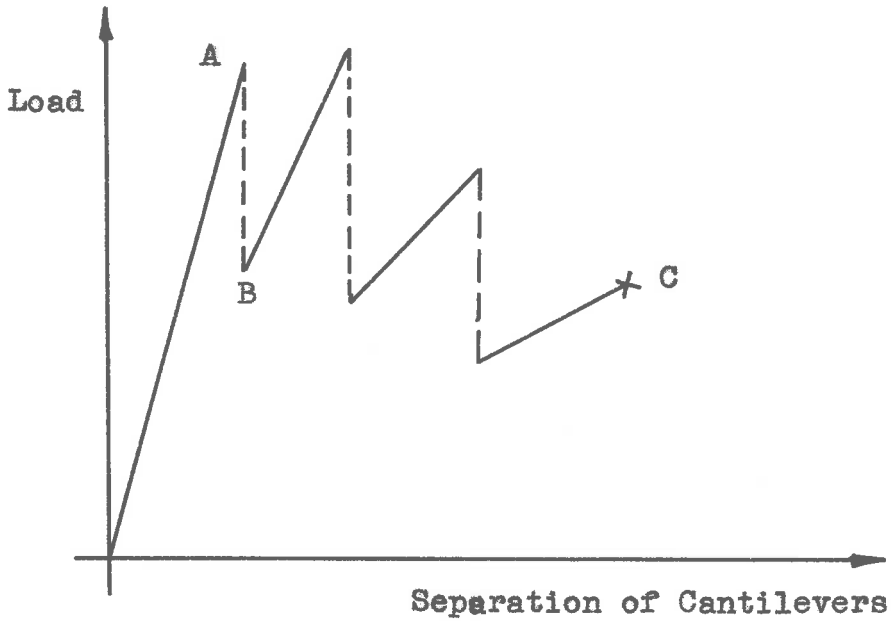

FIG. 5.9 Typical Semi-Controlled Fracture Plot.

of the general characteristics of brittle fracture and because of some experimental evidence which was obtained from the steel specimens.

5.2.7 Analysis of the Splitting Test Force-Distance Plots

When plotted, the graphs of loading force vs. displacement of the cantilever arms usually appear as shown in Figure 5.8 or 5.9. The plot shown in Figure 5.8 may be described as a controlled crack propagation, i.e. the crack moves in response to loading. The plot in Figure 5.9 however is better described as a semi-controlled propagation. When the crack moves it does so at an uncontrolled rate but the specimen does not break through.

Consider first the propagation characteristic of Figure 5.8. From the origin to A, the specimen is loaded elastically. A crack is formed at the apex of the narrowed section (Figure 5.1) and propagates in an uncontrolled manner for some distance. During this instant, a snap is heard and the load reading falls suddenly. This event is expressed by the vertical line AB on the plot (Figure 5.8).

From this point on, continued loading causes the crack to move continuously towards the other end of the specimen. As the crack moves back, the leverage of

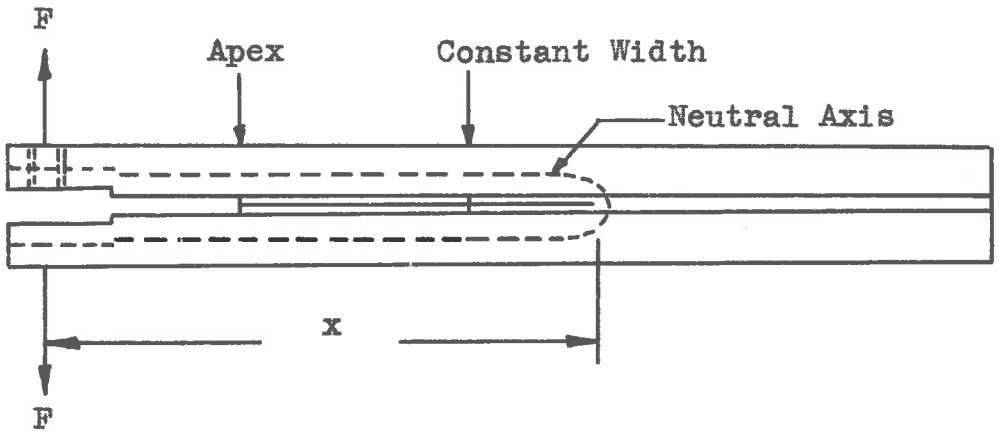

Moment of Force at Crack = F.x

FIG. 5.10 The Specimen may be looked upon as a Curved Beam.

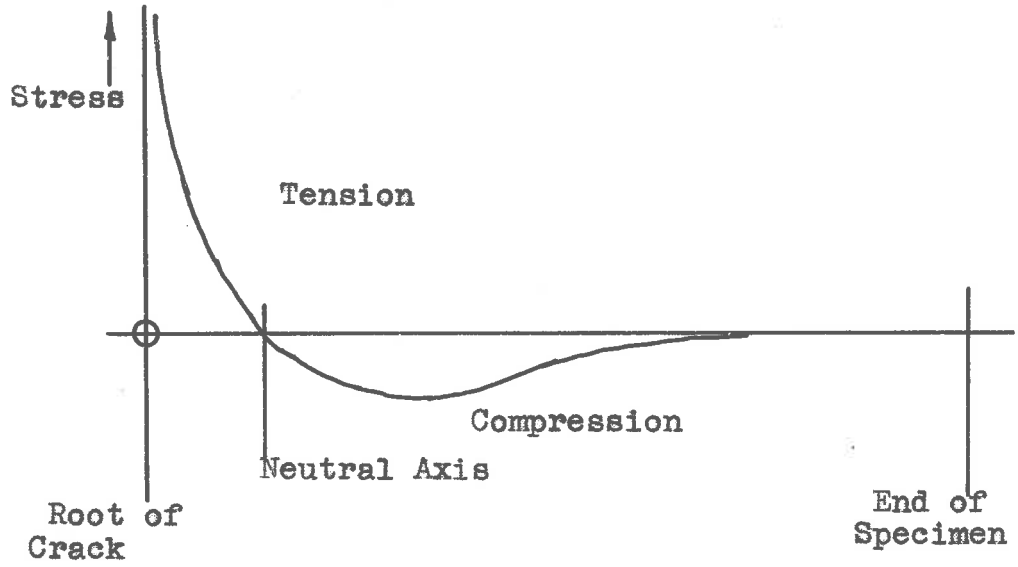

FIG. 5.11 The Stress Pattern in the Vacinity of the Crack.

the force applied with the loading screw increases. However the two cantilevers become longer in the process and if the load screw is not advanced, an advance of the crack causes the applied load to fall by reducing the stiffness of the two beams.

Figure 5.10 shows that the specimen may be likened to a curved beam with a very small internal radius (the radius of the root of the crack) and the stresses near the crack are shown in Figure 5.11. It can be said without entering a lengthy proof that the stresses due to the bending moment of the loading force predominate at the crack.

The approximate condition of equilibrium may be expressed in the form

$$M = k\,l \qquad \text{.... 5.1}$$

where $M = Fx$ the moment at the crack due to the loading force

l = length of crack and

k = constant

At those points on the specimen where the width of the reduced section is constant, l is taken to be constant and so

M = constant

i.e. Fx = constant = K 5.2

For a cantilever the deflection δ is related to its other properties by the expression

$$\delta = \frac{Fx^3}{3EI}$$

where E = Youngs Modulus

I = Modulus of section

When a crack propagates in a controlled manner, the required force F_1 ($\frac{K}{x}$) is equal to the applied force F_2 ($\frac{3EI\delta}{x^3}$). Suppose that δ is held constant and the crack is propagated slightly.

If $\frac{\partial F_1}{\partial x} > \frac{\partial F_2}{\partial x}$ then the crack will stop, i.e. the propagation is controlled. Now, from 5.2

$$\frac{\partial F_1}{\partial x} = -\frac{K}{x^2} \quad \text{..... 5.4}$$

and from 5.3

$$\frac{\partial F_2}{\partial x} = -\frac{2EI\delta}{x^4} = -\frac{3K}{x^2} \quad \text{..... 5.5}$$

Whence it follows that

$$\frac{\partial F_1}{\partial x} > \frac{\partial F_2}{\partial x} \quad \text{..... 5.6}$$

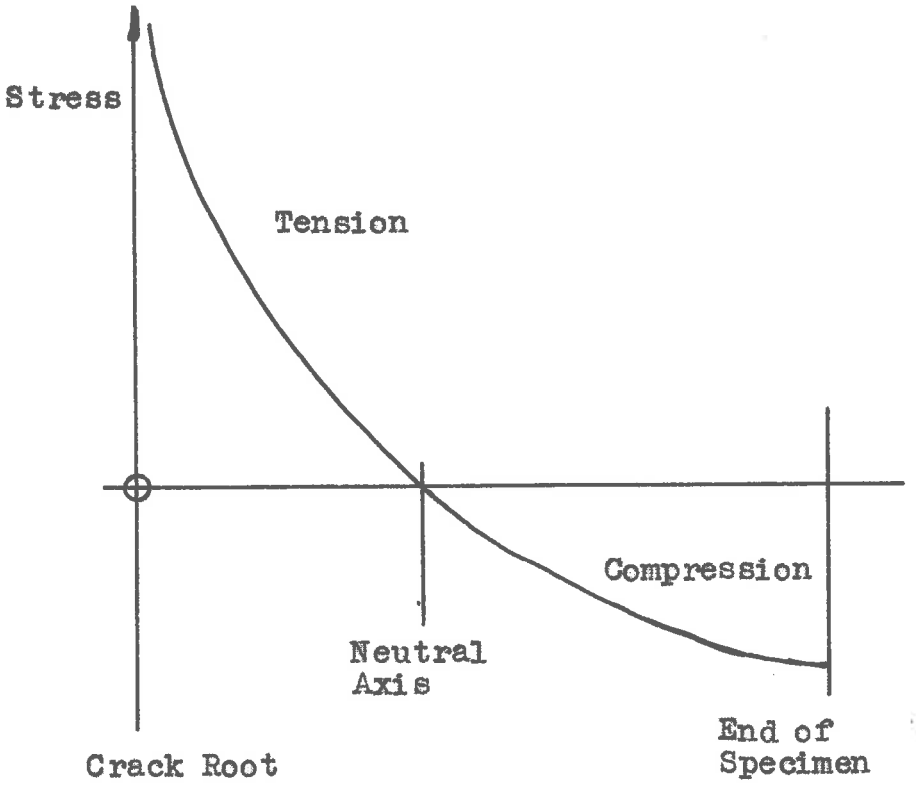

FIG. 5.12 The Effect of the End of the Specimen on the Stress Pattern near the Crack.

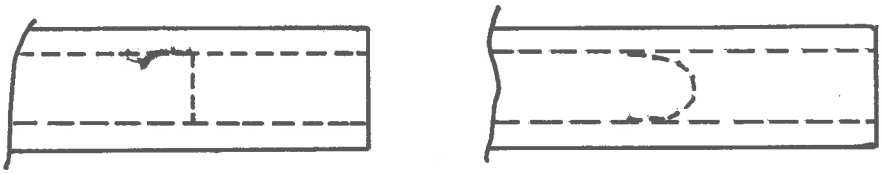

a) Straight Crack b) Curved Crack

FIG. 5.13 If the Crack is Curved, a greater Proportion of its Length is near the Boundary of the Fracture Zone where the Stress is not tri-axial.

As long as the equations 5.1 and 5.3 are satisfied propagation is controlled.

As the crack approaches the end of the specimen, the assumptions which lead to equation 5.1 are not applicable and the crack becomes uncontrolled again. It can be seen from Figure 5.12 that the stress pattern in the specimen alters markedly as the crack approaches the end of the specimen.

Two causes can be offered for the semi-controlled propagation shown in Figure 5.9. Firstly, if a crack can be propagated more easily at high speed then a discontinuous plot of the kind shown in Figure 5.9 can be expected. The load must be built up to move the crack at low speed initially. However as it accelerates, the moment which will maintain it falls and the crack is uncontrolled until the applied load falls below the value required to maintain the dynamic propagation.

The second cause of semi-controlled crack propagation is due to the tendency of the length of the crack to vary. The section through which it is intended that the crack should travel is less than the overall width of the specimen. If the crack leaves this narrowed section its length must increase. As the length of the crack increases, the load to propagate it also

increases. Eventually the crack returns to the narrower section. The length of the crack now decreases as it progresses and propagation may be uncontrolled until the crack has again entered the narrower section. The specimen retains a record of the meanderings of the crack and the periodic variation of the width of the fractured or cleaved surface can be compared to the periodic variation of the load.

A third factor must also be taken into account. Cracks were propagated in materials which are normally ductile, as for example mild steel. The success of this method depended on generating a triaxial stress situation. Where the crack emerges from the bulk of the specimen, the stress situation is not, however, triaxial. The significance of these end effects depends on the shape of the crack. Figure 5.13 shows a straight and a curved crack. For case (a) the proportion of the crack in the non-triaxial stress field is much less than for case (b). If the shape of the crack varies between these two extremes, the consequent variation in F may be quite large. For case (b) there are strips of specimen at the sides which are essentially under a pure tensile stress and yield in the usual way before tensile failure takes place.

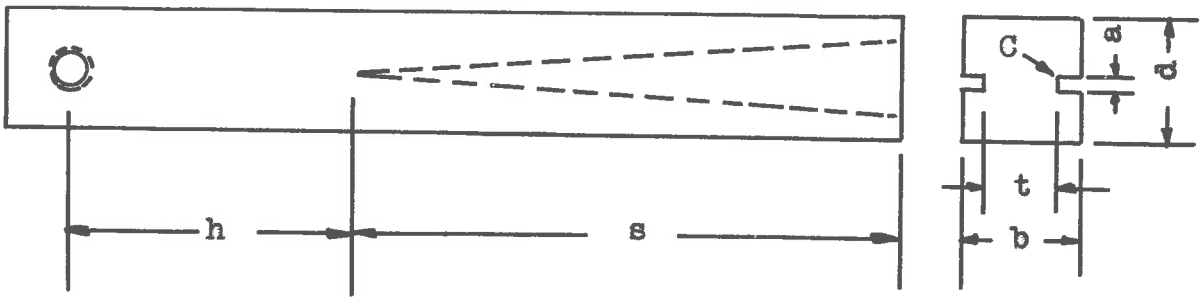

FIG. 5.14 The Cast Iron Specimens.

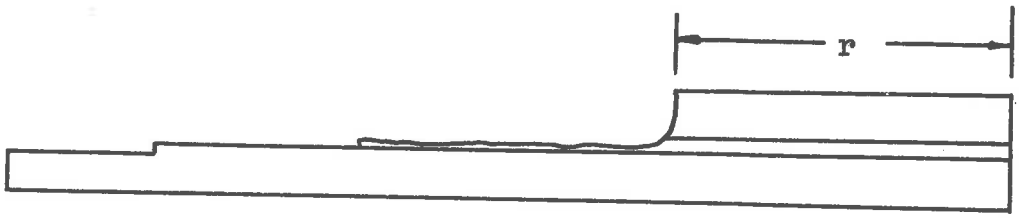

FIG. 5.15 Mode of Failure of the Trial Cast Iron Specimens.

5.2.8 Results of Splitting Tests

The materials tested were:

(1) Cast iron (commercial grade)

(2) Mild steel (commercial grade)

(3) High tensile tool steel (T.C.H.)

(4) Zinc

(5) Bismuth.

5.2.8.1 Cast Iron

Preliminary tests were carried out with cast iron. The purpose in this instance was not so much to obtain results of significance to deformation theory as to test the usefulness of specimens of the kind described in Figure 5.1.

Four specimens of the kind shown in Figure 5.14 were prepared and tested to destruction. The various dimensions are tabulated in Table 5.1 together with the mode of failure which is illustrated in Figure 5.15. All four specimens failed in this manner, as may be seen from Figure 5.16.

The mode in which these specimens failed is anomalous. The crack, in turning from the narrowed section, which it was intended to follow into the wider lever arm (which in all cases is more than three times as wide)

TABLE 5.1 Details of Trial Specimens

Dimension / Specimen	h	s	t	a	b/	d	r
1	1.17"	1.85"	0.12"	0.06"	.48"	.32"	.50"
2	1.18"	1.86	0.23	0.055	.48	.32	.96
3	0.63	2.16	0.28	.055	.53	.42	.95
4	1.05	2.23	0.28	.059	.48	.53	1.18

appeared to take the course of highest rather than lowest energy.

It is also apparent from examination that the cracks prefer to come to the surface at the corners 'c' in Figure 5.14. This is to be expected as there is an additional stress concentrating effect in that locality.

It is tempting to propose the hypothesis that the crack turns into the beam section when the bending stress reaches a certain value. From a measure of the width (w) of the reduced section at the point where the crack turns and equation 5.1, the bending moment M is given by

$$M = kw$$

The beam stress σ is given by the usual expression

$$\sigma = \frac{M}{t} = \frac{6kw}{b[r(d-a)]^2} = \frac{6kw}{b\,i^2} \qquad \ldots\ldots 5.7$$

If the hypothesis is valid, the quantity $\frac{W}{b\,l^2}$ will be the same for each specimen. The various quantities are set out in Table 5.2.

TABLE 5.2 Analysis of trial results.

Specimen \ Dimension	w	b	l	$\frac{W}{b\,l^2}$	$\frac{W}{bl}$
1	0.10	0.46	0.12	14.5	1.76
2	0.12	0.40	0.12	17.4	2.08
3	0.17	0.33	0.18	9.2	1.76
4	0.15	0.48	0.23	5.2	1.36

It is seen that the expression for stress $\left(\frac{W}{b\,l^2}\right)$ is not constant but indicates a definite trend - diminishing with increasing beam stiffness. On the other hand, $\frac{W}{bl}$ which is equivalent to (1σ) does not show any significant trend although the scatter is considerable.

This can be explained as follows. To establish itself in the beam, a crack must penetrate to a considerable depth away from the reduced section. The greater the depth of the beam, the more slowly will the available stress diminish as the crack approaches the neutral axis, allowing the crack to penetrate further into the beam and so preparing the way for the ends of the crack

to move away from the corners 'C' shown in Figure 5.14.

To conclude then, the results seemed to indicate that the crack will follow its intended course as long as the quantity $\frac{W}{bl}$ (or $\frac{W}{l}$ since the results do not permit a test for the significance of 'b' to be made as this quantity was kept almost constant) is less than some maximum.

The value of this maximum can be expected to depend on the kind of material used but the above results indicate that for each material a suitable shape can be found.

Cast iron is more brittle under normal circumstances than the other materials used (except the as-quenched steel specimen) and also very poor in homogeniety. The usefulness of the results obtained had to be estimated with some reservations. Nevertheless it indicated the feasibility of this approach and the experiment was embarked upon in earnest.

5.2.6.2 High Tensile Steel

A commercial, high quality tool steel was used in this experiment. Two trial specimens were prepared first, to gain some preliminary information about the behaviour of the specimen. The specimens were machined in the annealed state, and subsequently quenched in oil from

the prescribed temperature. They were tested in the as-quenched state.

The composition and other information supplied by the manufacturer is presented below:

Composition: C (.90%), Si (.20%), Mn (1.20%), Cr (.40%), V (.50%).

The Rockwell Hardness and tensile strength vary with tempering temperature and are presented in Table 5.3.

TABLE 5.3

T°C	0	50	100	200	300	400	500
R4	65	62.5	61.5	60	57	54.5	-
T.S	140	-	-	125	115	-	70

The tensile strength figures were obtained indirectly from data supplied by the same manufacturer about another tool steel of somewhat different composition but almost identical hardness-tempering temperature characteristic.

Details of the trial specimens are set out in Table 5.4.

TABLE 5.4

Dimension / Specimen	h	s	t	a	b	d	r
1	1.10	1.75	.21	.065	.50	.493	0
2	1.19	2.24	.22	.065	.46	.579	0

Both specimens broke through leaving two halves, and exhibiting a fine and homogeneous surface texture where the crack was propagated. The fracturing process was controlled throughout except at the end where (as expected) the propagation became suddenly rapid and resulted in the complete separation of the two halves. The latter stage of rapid propagation did not result in a noticeably different surface texture.

If the two halves of the specimen are placed against each other back to back, a rapid and reasonably sensitive test for bending of the cantilever arms is made. It appears that bending while slight was present (resulting in a gap of about .005 inch max.) and seemed to be confined to the end where the width to be fractured was greatest.

The two halves when placed together in their relative position prior to fracture are found to mate well, the crack becoming almost invisible. If the fracturing process had been accompanied by plastic deformation, such a close fit would not be possible.

Four additional specimens were now prepared for a fully instrumented test. Two of the specimens were used in the as-quenched state, and the other two were tempered in boiling water (100°C) for two hours.

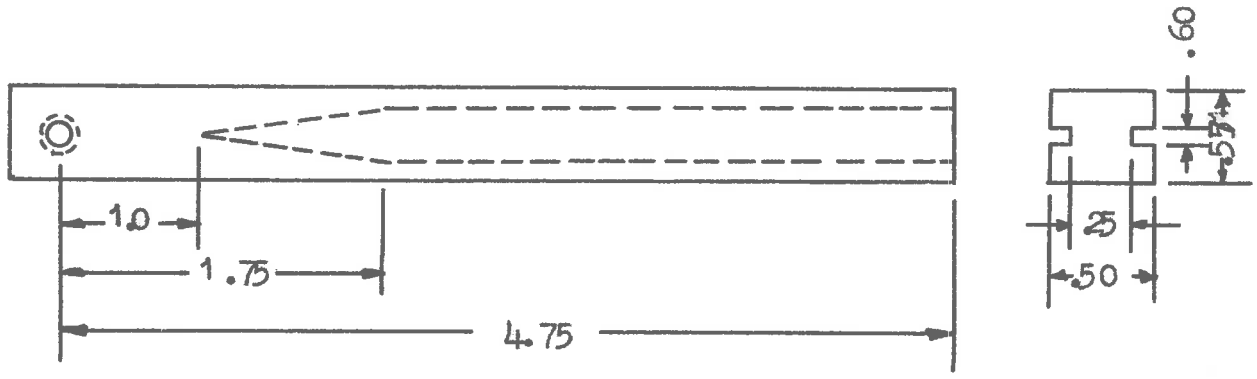

FIG. 5.17 Dimensions of the Steel Specimens (inches).

One each of the as-quenched and tempered specimens were tested at room temperature (15°C) and the other two at the temperature of dry ice (-76°C). To be certain that the specimen actually settled down to that temperature, a stabilising period of more than an hour was allowed before a calibration or test, the dry ice chips being heaped over the specimen or calibrator.

The results in reduced form are presented in Table 5.5.

The geometry of the specimens (which is the same for each of them) is shown in Figure 5.17. The detailed results of the four splitting tests are presented in graphical form in Figures 5.19 to 5.22. A photograph of the specimens is shown in Figure 5.18.

5.2.6.2.1 Specimen I

Figure 5.19 shows the results for specimen I whose new surfaces may be seen in Figure 5.18. These results could have been almost predicted. The splitting process may be broken up into four stages, A, B, C and D. Stage A is the loading stage during which deformation is elastic. A crack which can be distinctly heard brings in stage B. During this stage the load increases as the length of the crack increases faster than the moment arm.

TABLE 5.5 Results of Tests on Steel.

Specimen	I	II	III	IV
Test temperature	15°C	15°C	-78°C	-78°C
State of steel	as-quenched	tempered 2 hrs. 100°C	tempered 2 hrs. 100°C	as-quenched
Atmosphere	air	air	CO_2	CO_2
Interval between quench and test	10 days	10 days	20 days	20 days
Texture of fractured surface	fine and homogeneous	as for I	as for I	as for I
Type of propagation of crack	controlled	semi-controlled (weak)	semi-controlled (strong)	semi-controlled (weak)
Bending of the two halves of specimen	Nil	Nil	Yes	Yes
Nominal Surface Energy (16 in/in^2)	1.95	2.66	3.99	3.32

The linearity of four points defining this part of the load curve is noteworthy. When the crack enters the parallel section, the load can be expected to fall as the moment arm increases. This is observed during stage C. The last stage is very brief - the uncontrolled propagation of the crack out of the specimen, leaving it in two pieces.

Two things may be pointed out concerning stage C. Firstly, while the load falls in a general way it is actually increasing at several points. This can be related to the meanderings of the crack into and out of the beam section. It is possible by this means to relate the position of the crack to the load at that point.

The second and more important phenomenon is that the load was observed to decrease while no additional rotation is applied to the loading screw. The usual procedure was to apply a rotation to the loading screw and record the immediate bridge reading and the new angular reading. After this, the bridge reading will have fallen and this process will eventually appear to cease. The second bridge reading was then recorded. This interval is of the order of one minute. The graph (Figure 5.19) shows two plots, the upper recording the bridge reading immediately after loading and the lower the load when motion of the crack apparently ceases. It is seen that the two

curves are related, for they vary together.

The movement of the crack during these intervals can be computed. Referring to equation 5.3

$$\delta = \frac{F x^3}{3EI}$$

then

$$\frac{F_1 x_1^3}{3EI} = \frac{F_2 x_2^3}{3EI}$$

$$\text{i.e.} \left[\frac{x_1}{x_2}\right]^3 = \frac{F_2}{F_1} \qquad \text{.... 5.8}$$

If the initial value of x is known, and the crack is assumed not to move during the relatively short loading period, then the distance travelled by the crack can be computed from the knowledge of the load values. Comparison with the actual travel should then test this hypothesis. The starting value x_o will be that corresponding to the point on stage B where the two plots meet. This value is estimated to be 1.19". From equation 5.8, at each screw setting,

$$\frac{x_2}{x_1} = \left(\frac{F_1}{F_2}\right)^{\frac{1}{3}} \qquad \text{.... 5.9}$$

and the cumulative product P is given by

$$P = \left[\frac{x_2}{x_1}\right]_1 \times \left[\frac{x_2}{x_1}\right]_2 \times \cdots \times \left[\frac{x_2}{x_1}\right]_n \quad \cdots (5.10)$$

where n is the number denoting the screw setting (in this case 17). The value of P is found to be 2.50, whence from

$$x_n = x_o P \quad \cdots (5.11)$$

the distance from the lead screw would be 3.00 inches. The actual value is 4.78 inches.

The loading time was 1-2 seconds while the period between the maximum and minimum readings was 50-100 seconds. Clearly the crack will travel somewhat before the first reading is taken (about 3 to 4 seconds after the loading is commenced) as the average velocity will be relatively high during this period.

It can be concluded then that to propagate a crack, a critical stress must be imposed on the specimen and the rate of propagation increases with the excess of stress above this critical value. The form of the relationship cannot be deduced from the data obtained from specimen I, but specimen II furnished some data on this matter.

Inspection of stage B shows that the two curves separate some time after the crack has been initiated. This can be explained as follows: when the crack has just begun, a small movement will increase its length by a considerable proportion of the initial length for

$$w = k(x - x') \qquad \text{.... 5.12}$$

where w is the width in the tapered segment of the reduced section and x' is the distance of the apex (where the crack begins) from the leading point

$$\frac{dw}{w} = \frac{k\,dx}{k(x - x')} = \frac{dx}{x - x'} \qquad \text{.... 5.13}$$

which $\to \infty$ when $x \to x'$.

This means that as the crack moves it widens rapidly, so that that portion of the applied moment which would cause the crack to move a measurable distance is used up in propagating an additional length of crack over a much smaller distance. The velocity effect will therefore become apparent only when the crack has moved some distance into the specimen.

The position of the crack when this separation first becomes apparent was estimated by using equation 5.9

with the difference that the force ratio is obtained by joining the point (on the graph) where the two traces meet to the origin. At a given loading screw angle this line and segment A will give two forces whose ratio is fixed.

A mathematical relationship between load and the beam deflection is cumbersome and so a theoretical load-deflection curve was computed using equations 5.7, 5.8 and 5.12, and data from Figure 5.17. This curve is presented in Figure 5.23 and may be compared with Figure 5.19. As expected, the load reaches a maximum at the point where the tapered segment ends (x = 1.75") and falls off after that.

The stages A and B correspond to that part of the curve from x = 1.0 to x = 1.75. No transition is, of course, apparent in the calculated curve. This difference implies that the stress required to introduce the crack is much larger than that required to propagate it. This is to be expected, for as long as the crack is absent the apex of the tapered section will tend to yield. When the crack finally forms (in each of the four specimens the crack began in the plane of the inner surface of one of the cantilever arms where the stress concentration effect is greatest) it is rapidly propelled away from its point of formation and from there on some correspondence between the calculated and experimental graphs is to be expected. The

linearity of stage B is therefore somewhat accidental and the points will generally be expected to lie on a curved line.

The previous estimate for x_o can now be revised and another value substituted. The point (on Figure 5.17) where the two curves begin is at 0.8 maximum load. On the calculated curve, the value of x at 0.8 maximum load is 1.52" (previous value 1.19"). Using the previous cumulative product P = 2.50, the value of $x_o P$ now becomes 3.80 (previous value 3.00) and is an improvement on the previous value, being closer to the hypothetical 4.78. Apart from the explanation already offered namely, that a significant interval elapsed between the application of load and obtaining the first reading, the distance covered by the crack when it is propagated out of the specimen in an uncontrolled manner, must also be taken into account. This distance can only be estimated.

It is interesting to note that if the position of the crack, when the last force reading was taken (just before uncontrolled failure) is computed by using equation 5.9, the result is 3.32". This means that the uncontrolled propagation took place over a distance of 1.5 inches, about six times the thickness of the loading arms. It must be

noted that this distance estimate is a maximum value. Any plastic bending in the loading arms will result in an estimate for the distance of the crack from the loading point that is too great.

5.2.8.2.2 Specimen II

The results obtained from splitting this specimen are shown graphically in Figure 5.20 and the surface formed in Figure 5.18. The load maximum is not where it should be. The crack has penetrated one of the loading arms and the width of the crack is still increasing in the parallel section. In this specimen the load maximum and crack maximum can be correlated with particular ease so that the quantities x = 2.07", screw rotation 325 degrees and bridge reading 1.47 occur together. Apart from this, the correspondence between the experimental and calculated curves is good.

For this specimen the estimate for x_o is 1.37 inches (using the calculated curve, Figure 5.22, as previously). The cumulative product was found to be 2.65 so that $x_o P$ came to 3.90 inches, which compares well with the value obtained for specimen I (3.80 inches) although the two graphs (Figures 5.19 and 5.20) are significantly different.

During this experiment information was obtained, which is not available from the previous run, namely values of the bridge reading at various time intervals after loading. From this data the velocity of propagation of the crack can be computed. This information shows how the velocity of propagation of the crack depends on the loading moment. In all about forty computed points are plotted in Figure 5.23.

To obtain the magnitude of the crack velocity at the various times (and loads), the value of x is required for each point. This can be found in two ways. One may use the cumulative product method already described or one may use another more accurate method which is described below.

It has already been pointed out that the curves of Figure 5.19 (and also Figure 5.20) begin with a straight line which has been labelled as stage A. During this interval there is not yet a crack in the specimen and the deflection is accommodated by bending of the loading arms. The deflection is given by the expression

$$\frac{1}{2}\delta_1 = \frac{P_1 x_1^3}{3EI} \quad \text{where} \qquad \ldots\ldots 5.14$$

x_1 is the distance between the loading point and the apex

of the tapered section (h = 1.0"). Later, when a crack has been formed and has penetrated into the specimen the relationship is

$$\frac{1}{2}\delta_x = \frac{P_2 x^3}{3EI} \qquad \text{..... 5.15}$$

If the crack is immobile, the loading arms act as cantilevers with a stiffness given by

$$\left[\frac{\partial P_1}{\partial \delta}\right]_{x=\text{const}} = \left[\frac{6EI}{2x_1^3}\right] \qquad \text{..... 5.16}$$

Thus if the slopes $\frac{\partial P}{\partial \delta}$ at x_1 and x are known then one can find x relative to x_1 according to

$$\frac{\partial P_1}{\partial \delta} \Big/ \frac{\partial P_2}{\partial \delta} = \frac{12EI}{2x_1^3} \Big/ \frac{12EI}{2x^3} = \left[\frac{x}{x_1}\right]^3$$

..... 5.17

If EI = constant

$$x = x_1 \left[\frac{\partial P_1}{\partial \delta} \Big/ \frac{\partial P_2}{\partial \delta}\right]^{\frac{1}{3}} \qquad \text{..... 5.18}$$

Now, if the crack is fixed, the load displacement curve is a straight line passing through the origin and the point representing the measured load at any displacement. (This assumes elastic bending and no plastic set in the loading

arms). Thus, through every point on the load-displacement plot of the kind shown in Figures 5.19 and 5.20, a line could be drawn passing through the origin and showing the variation of load with displacement for that value of x.

$\frac{\partial P_1}{\partial \delta}$ is already known and $\frac{\partial P_2}{\partial \delta}$ can be easily found. x_1 is known and x_2 can thus be computed.

One of the things consequent on this is that if the crack does not move during the loading then the point corresponding to a reading taken just before turning the loading screw and the point corresponding to the reading obtained just after, are collinear with the origin. Such lines are drawn in Figures 5.19 and 5.20. It will be noted that the line from the origin through a point on the lower curve does usually pass through a point on the upper curve but it sometimes passes to the left and sometimes to the right of the respective point on the upper curve.

If this loading line passes on the left side of the point on the upper curve one can say that the crack must have moved during the loading interval (provided that the discrepancy is not due to instrumental errors). However if the loading line passes to the right of the point on the upper curve, no explanation is forthcoming and one

can only assume that the discrepancy is due to some kind of experimental error. Possible sources of error are misreading the angle of rotation of the screw or of the strain bridge value, an unfavourable combination of random errors inherent in the apparatus and a zero shift in the strain bridge. The latter appears to be the most likely and may be due to temperature differentials in the force cell or the wiring, or it may also be due to the electronic equipment used.

By using equation 5.18 one can obtain another value of x at the loading screw angle at which failure eventually occurred. These values may be compared to the cumulative product method for it employs a different initial value for x. It is found that these values are 3.3¼ inches and 3.7½ inches for specimens I and II respectively and may be compared to the values 3.00 and 3.90 inches obtained with the cumulative product method, and using Figure 5.23 to determine the initial point.

All of these values fall short of the maximum possible value for x (4.00) and the values derived by using equation 5.18 are even lower. One obvious correction is that which accounts for the variation of the stiffness of the loading arms due to the reduced section which begins at the point where the crack also begins.

From equation 5.17 this correction factor is given by

$$x \text{ (corrected)} = x \sqrt[3]{\frac{I}{I_1}} \qquad \ldots\ldots 5.19$$

I_1 corresponds to x_1

since $I = \frac{b\,h^3}{12}$ where b = width,

h = depth of rectantular beam

$$\sqrt[3]{\frac{I}{I_1}} = \frac{h}{h_1}$$

$$= \frac{\frac{1}{2}d}{\frac{1}{2}(d-a)t/b} \quad \text{(see Figure 5.14)}$$

$$= \frac{d}{d - a\frac{t}{b}}$$

$$= 1.05 \quad \text{(Figure 5.16)}$$

If this factor is included, the values 3.71 and 3.74 become 3.52 and 3.95.

Another correction factor which is more difficult to estimate is that the apex of the tapered section yields during loading up so that the initial value x_{1_0} is in effect larger than 1.0 inch.

Figure 5.24 shows that the computed velocity values for the crack are subject to a considerable scatter. A straight line is drawn through the points. The velocity

of the crack clearly falls to zero at some critical load moment (loading force x x). The nature of the dependance of this velocity on the load moment as indicated by this graph is represented as well by a straight line as any other.

The readings obtained at the final load screw setting (shown as x) lie on an approximate parabolic curve. The velocity decreases as the load moment falls but eventually increases again as the actual stress rises because of the end effect. Because of the end effect, these readings were not taken into account when drawing in the straight line.

5.2.6.2.3 Specimen III

This specimen is markedly different from the previous two. The splitting test was carried out at the temperature of solid carbon dioxide ($-76^{\circ}C$). The tendency of the load reading to fall after the application of a rotation to the loading screw is noticeably absent. In its place is the semi-controlled splitting process (Figure 5.24) with the corresponding variation in the width of the cracked section (Figure 5.18).

In the course of this test, the loading screw ran out of thread, so that the specimen had to be unloaded.

a spacer inserted, and the specimen loaded again. The unloading and loading line should be straight but are seen to be subject to considerable scatter about a straight line.

The load required to start the crack up again and to propagate it is seen to be less after the unloading period (which is separated from the previous readings by an interval of about one hour). This result must be treated with some reservation in view of the scatter of points on the unloading and loading curve. The difference may be due to a zero shift, but it must be stated that the zero at the commencement of the test, during the insertion of the spacer and at failure of the specimen was noted to be the same in each case (0.02).

It may be said tentatively that unloading reduces the load required to maintain the crack.

It may also be said that at a reduced temperature the tendency of the crack to run into the loading arms is greater.

5.2.8.2.4 Specimen IV

This specimen is similar to No. III except that the perturbations of the crack are not so violent. A spacer had to be inserted again. The graph (Figure 5.22) shows that the points obtained after unloading appear to

be displaced for the loading and unloading curve should correspond much more closely.

No new phenomena were found in the results of this experiment. The load after unloading is again less than prior to it.

5.2.8.2.3 Discussion of all four specimens

Several comparisons between the four specimens can now be made.

Firstly there is an observable dependence on crack velocity on the loading moment at room temperature. At reduced temperature this vanishes.

Secondly, the energy consumed during the propagation of the crack is greater for the specimens tested at reduced temperature. This is clearly supported by Figures 5.25 and 5.26 which are plots of loading moment against the position of the crack. Ideally the loading moment rises from zero at x = 1.0" (the apex of the tapered section) to a definite value at x = 1.75" (where the section is parallel) and remains at this value until the crack approaches the end of the specimen when the moment begins to fall, reaching zero when the crack emerges from the specimen.

The real curves differ from the ideal ones in

several respects. Firstly the load moment at the value x = 1.0 (where the crack begins) is not zero. Secondly the part of the curve beyond x = 1.75" is not smooth but subject to periodic fluctuations which can be correlated to the variation of the width of the surface of fracture. Thirdly, the latter part of the curve where the loading moment falls again is not available because the crack becomes uncontrolled and no measurements can be taken.

With specimen III a comparison of the load moments and the width of the surface of fracture is possible. The moment peaks are at x = 1.75, 2.20, 2.7 and = 3.5. The width maxima are at x = 2.2, 2.9, 3.6 and a slight maximum at 4.2. It is doubtful whether the slight width maximum at x = 4.2 will give a noticeable load maximum. Also the first moment peak on the graph is supported by one point only (see Figure 3.26). If this peak is ignored, then the correspondence between the x values at moment and width maxima is much better, namely 2.2, 2.2; 2.7,2.9; 3.5, 3.6.

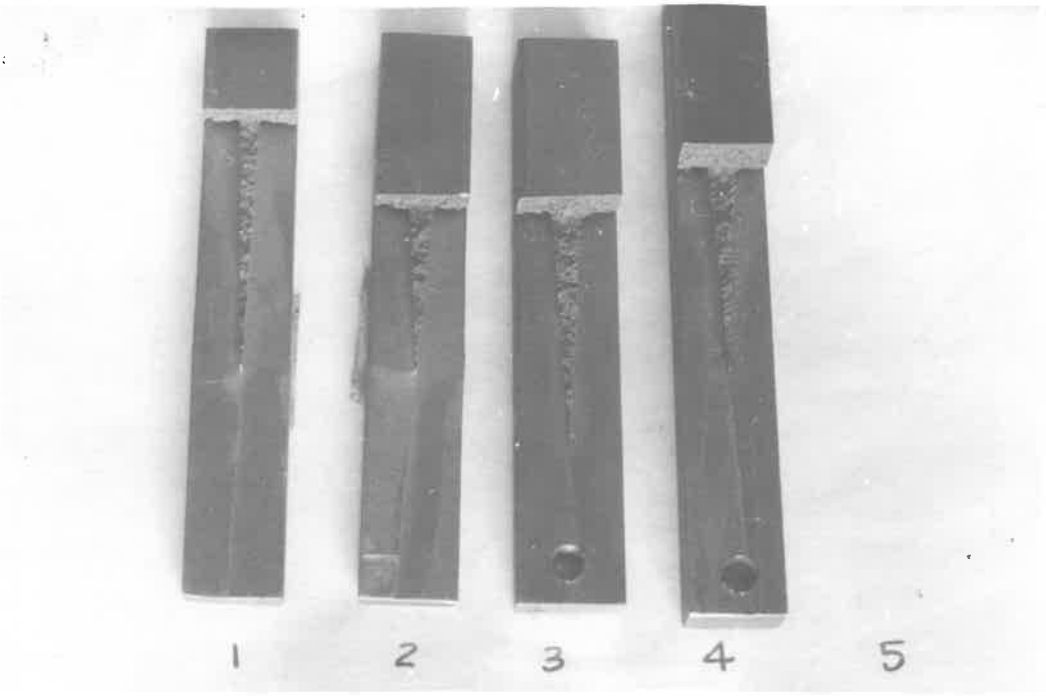

FIG. 5.16 THE FRACTURE SURFACES AND MODE OF FAILURE OF THE TRIAL CAST IRON SPECIMENS.

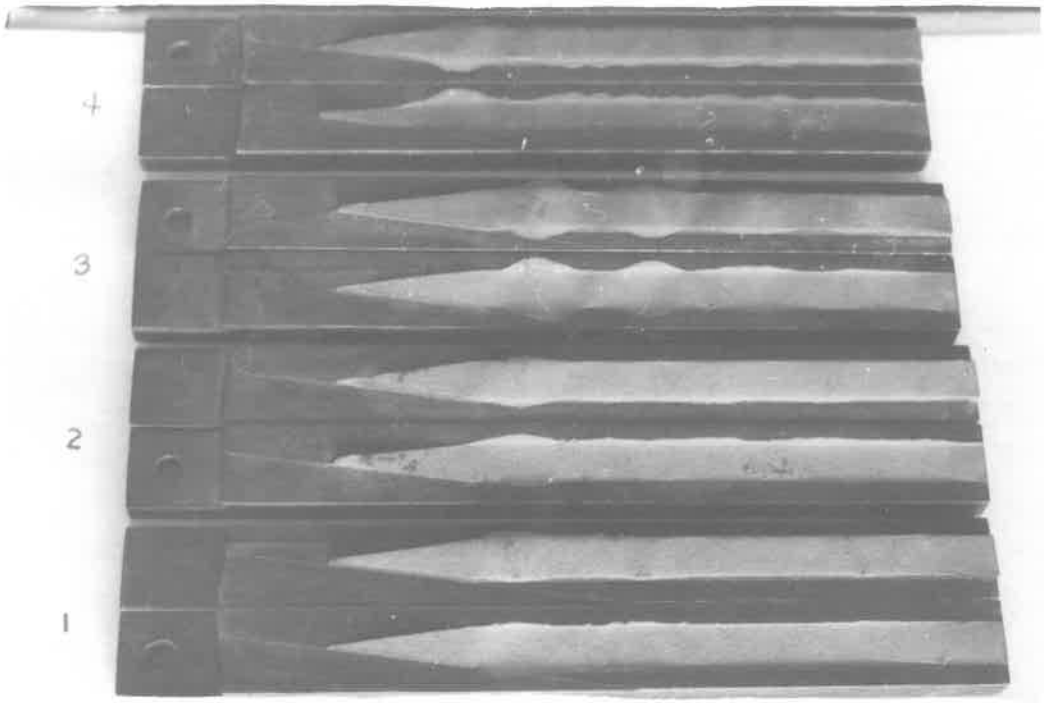

FIG. 5.18 THE FRACTURE SURFACES AND MODE OF FAILURE OF THE STEEL SPECIMENS.

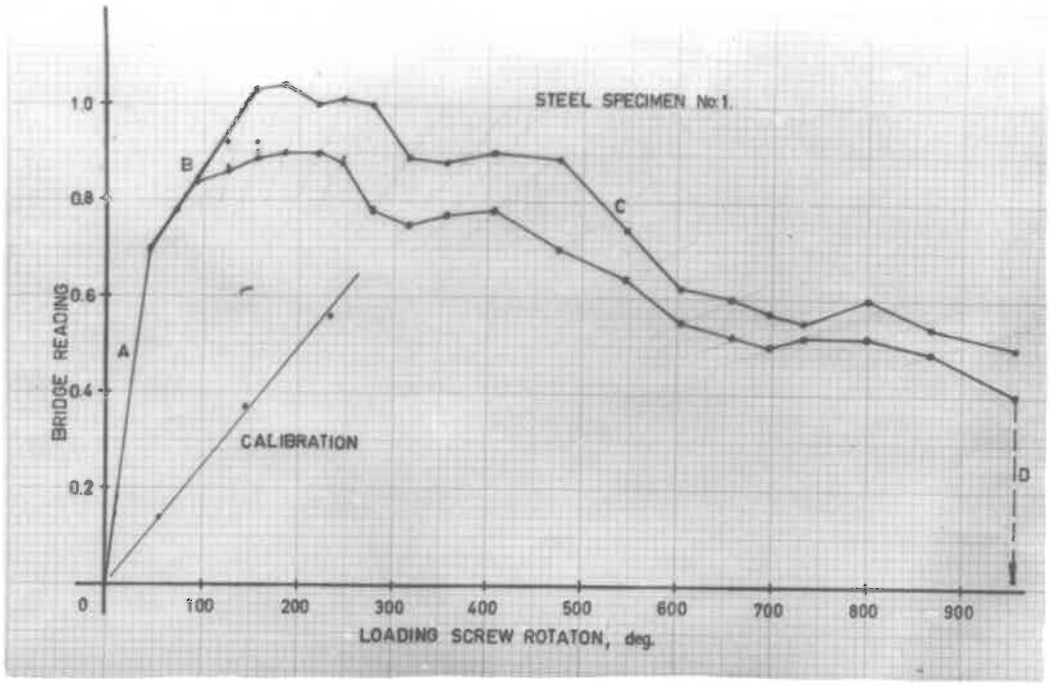

FIG. 5.19 THE LOAD DISPLACEMENT PLOT FOR SPECIMEN 1 FRACTURED AT ROOM TEMPERATURE.

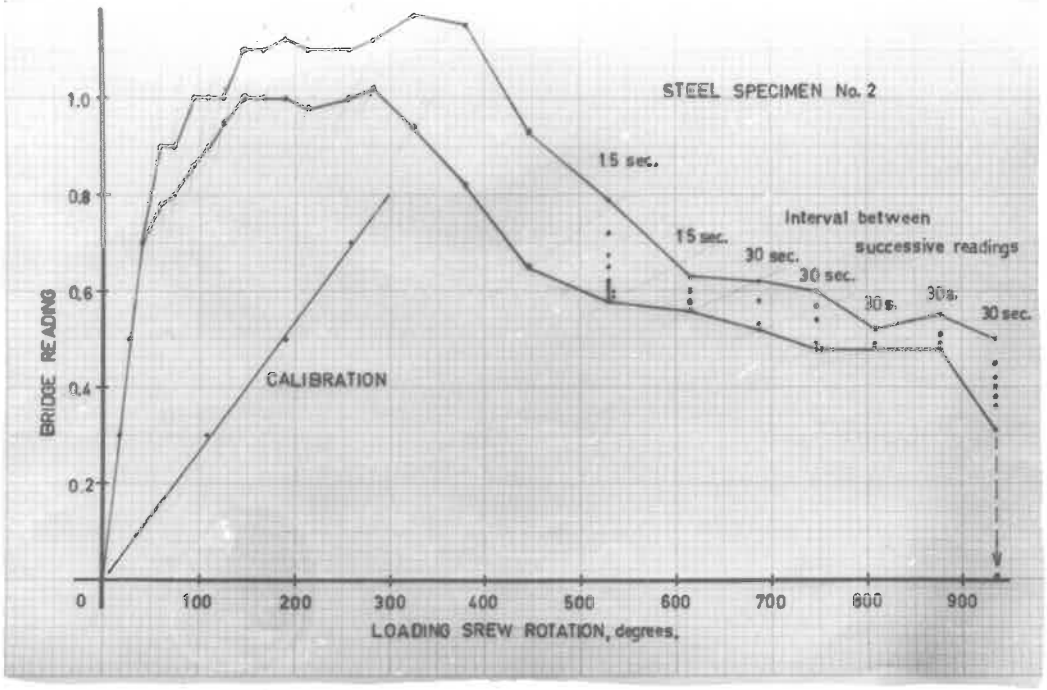

FIG. 5.20 THE LOAD DISPLACEMENT PLOT FOR SPECIMEN 2 FRACTURED AT ROOM TEMPERATURE.

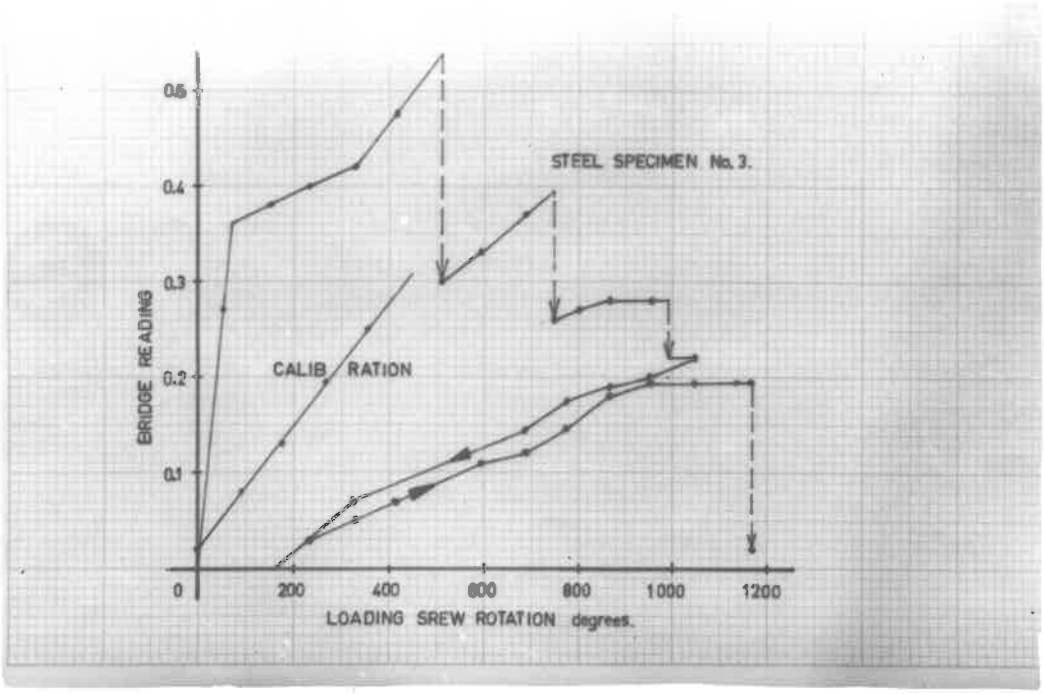

FIG. 5.21 THE LOAD DISPLACEMENT PLOT FOR STEEL SPECIMEN 3 FRACTURED AT -78°C.

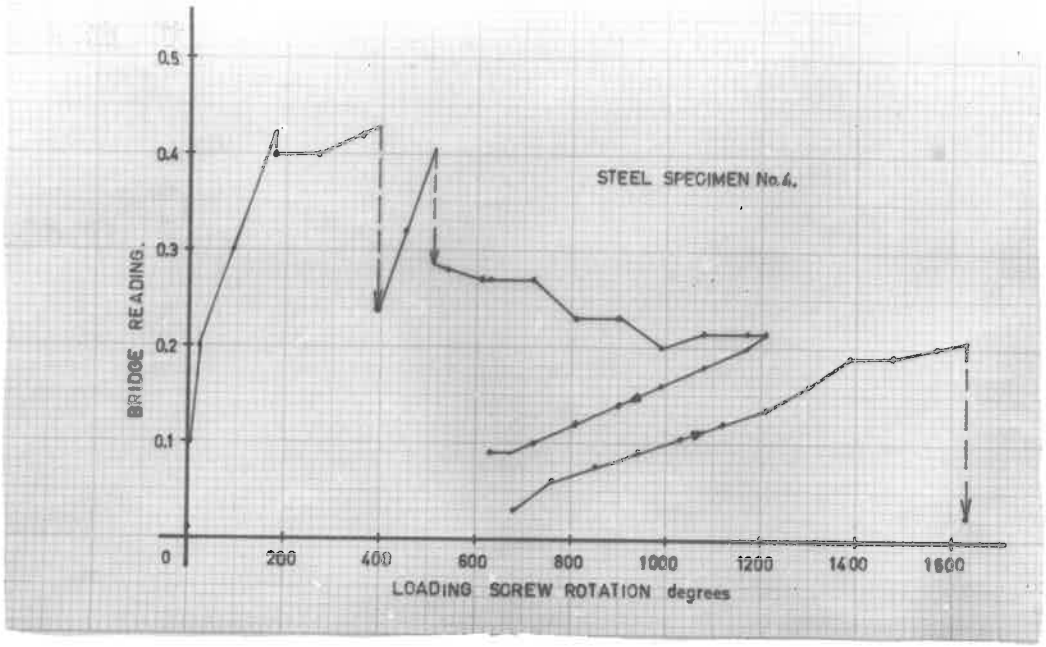

FIG. 5.22 THE LOAD DISPLACEMENT PLOT FOR STEEL SPECIMEN 4 FRACTURED AT -78°C.

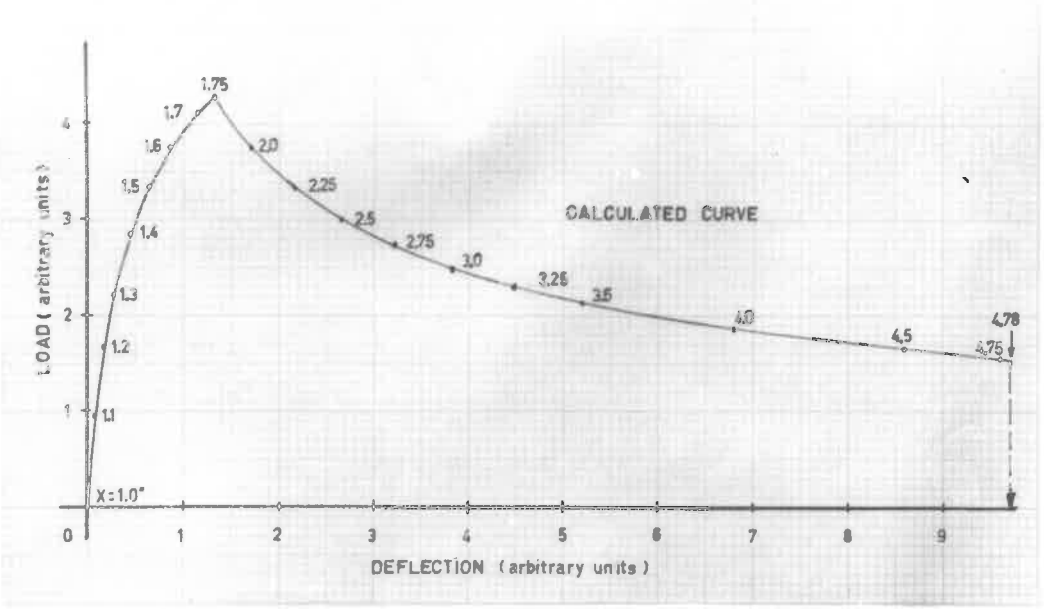

FIG. 5.23 A THEORETICAL LOAD-DEFLECTION PLOT BASED ON THE GEOMETRY OF THE STEEL SPECIMENS 1 TO 4.

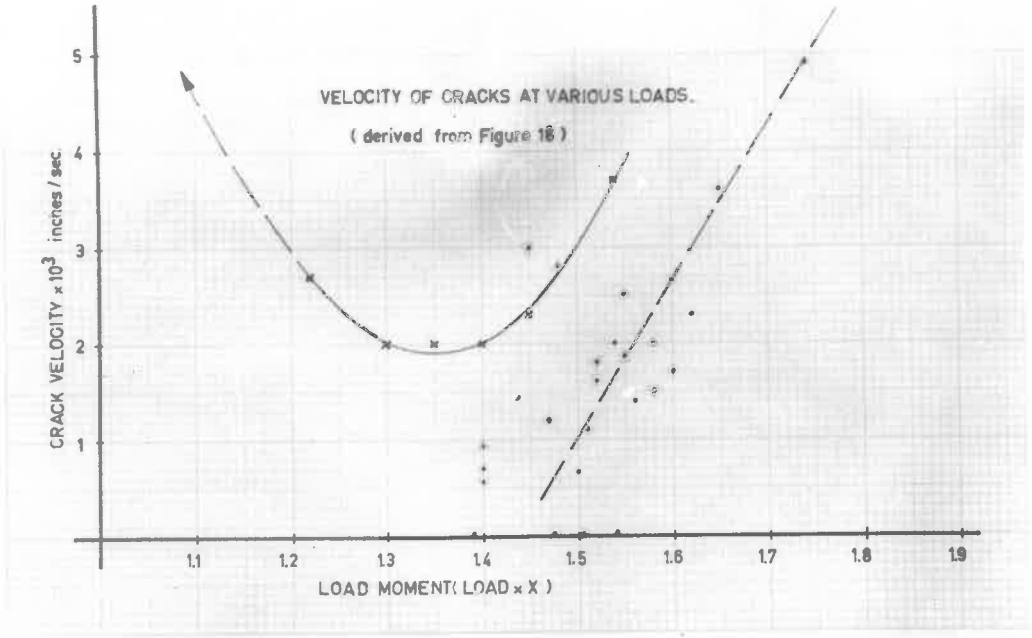

FIG. 5.24 THE VARIATION OF THE FRACTURE RATE WITH THE APPLIED LOAD FOR STEEL SPECIMENS AT ROOM TEMPERATURE.

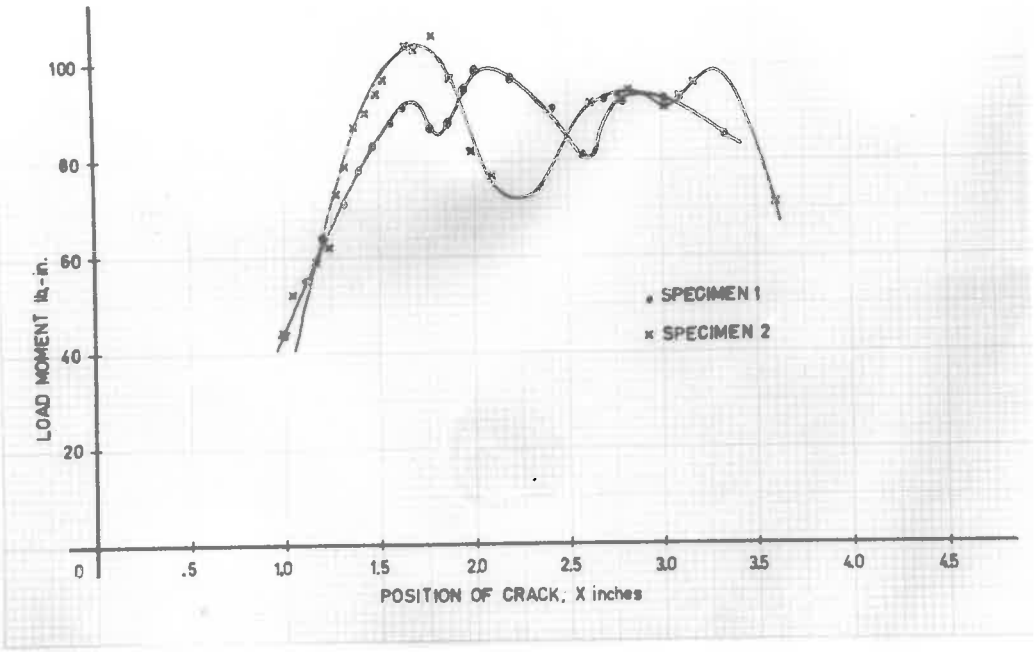

FIG. 5.25 THE VARIATION OF THE LOAD MOMENT WITH THE COMPUTED LOCATION OF THE FRACTURE FOR STEEL SPECIMENS 1 AND 2.

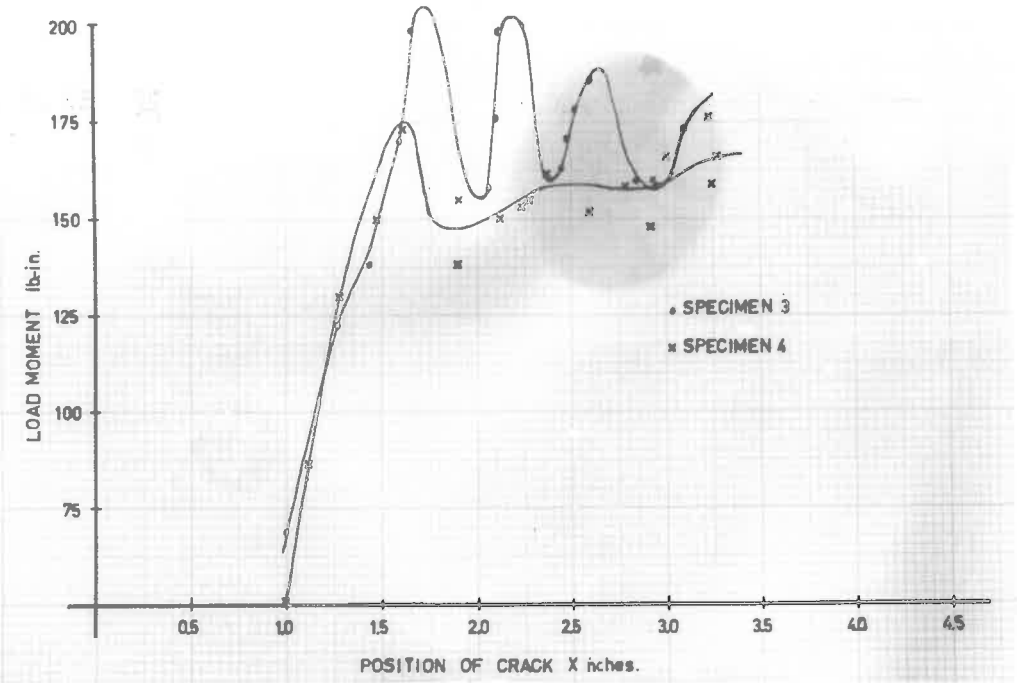

FIG. 5.26 THE VARIATION OF THE LOAD MOMANT WITH THE COMPUTED LOCATION OF THE FRACTURE FOR STEEL SPECIMENS 3 AND 4.

5.2.6.3 Mild Steel

It was considered that mild steel would flow too readily at room temperature and so all tests were carried out with the specimen under liquid nitrogen.

An initial test specimen machined to the same dimensions as the previous steel specimen did not propagate the crack in the desired zone but resulted instead in the failure of one of the loading arms. The fracture zone was therefore reduced from a width of about 0.25 inches to about 0.175 inches.

Three were soaked at 900°C (above the α-γ transition temperature) and quenched in water. Three were soaked at 900°C and furnace cooled to 200°C in 20 hours. The remaining three were held in reserve. It must be remarked that to protect the specimens against excessive corrosion they were sealed into a mild steel container. The water quench was therefore far less severe than it would have been had the specimens been brought into direct contact with the water.

In view of the anomalous behaviour of the steel specimens which absorbed more energy at the reduced temperature (when it would have been expected to be more brittle) room temperature tests on the mild steel were

later carried out as well using the three reserve specimens. One was used in the as-machined condition, the other soaked at 900°C and quenched in water and the third also soaked at 900° and slowly cooled in the furnace.

Only one of the three specimens, the one tested in the as-machined condition was split. However, in the process the two loading arms were severely bent and the fracture could be propagated only with the greatest difficulty. Several times the specimen was unloaded for fear of damaging the load cell, and loaded without the cell. The greater loading rate which is possible when readings are not taken appears to favour the propagation of the fracture for the crack did not appear to move when the load cell was inserted and the loading rate (because of delays in obtaining readings) was much lower.

The heated and quenched specimen (No. 12) began to fracture but eventually the loading arms simply bent outwards. Here again the loading run with the force cell was abandoned and the specimen was loaded again without the use of the force cell.

Specimen No. 14 which had been heated and furnace-cooled (about 18 hours) could not even be made to begin to fracture.

The results obtained are presented in Table 5.6.

TABLE 3.6 Dimensions of Mild Steel Specimens

Specimen No.	b	a	h	d	e	t	p	w	Remarks
1	0.75	4.0	0.5	0.5	.035	0.17	1.20	0.16	
2	.75	4.0	0.5	0.5	.035	.18	1.75	.14	
3	.75	4.0	0.5	0.5	.035	.19	1.8	.17	
4	.75	4.0	0.5	0.5	.035	.18	3.42	.09	
5	.75	4.0	0.5	0.5	.035	.20	2.93	.11	
6	.75	4.0	0.5	0.5	.035	.18	3.30	.09	
7	.75	4.0	0.5	0.5	.035	.24	0	.21	
8	.75	4.0	0.5	0.5	.035	.18	0	.16	
9	.75	4.0	0.5	0.5	.035	.18	0	.18	
10	.75	4.0	0.5	0.5	.035	.19	0	.19	unnearly limit
11	.75	4.0	0.5	0.5	.035				No crack formed
12	.75	4.0	0.5	0.5	.035				Crack propagated .4" and then broke.

* See Figures 14 and 15 for the significance of the various dimensions.

5.2.8.3.1 The furnace-cooled specimens

This group includes specimens 1 to 3. Specimen 2 failed by breaking one of the loading arms. Specimens 1 and 3 however failed by the breaking of both loading arms, Figure 5.27. The surfaces of fracture of the three specimens are very similar and are courser than those of the group 4-6 and the group 7-9. Bending of the loading arms was not noticeable.

The load displacement plots are characterised by an early peak where the crack is established and a series of minor peaks which are not readily correlated to the surface markings. The loading force remains substantially horizontal until one or both loading arms fail, Figures 5.28 to 5.30.

5.2.8.3.2 The water-quenched specimens, Nos. 4 to 6

The loading arms were found to break off earlier than in the previous group (the average values of r being 3.08 as against 1.62 for the previous group). The surface is courser, and crystal facets seem to be larger. Again, bending of the loading arms was absent, and two of the specimens, 5 and 6, had both loading arms broken off, Figure 5.31.

The introduction of the crack into specimen 6 is

accompanied by a very small load peak, Figure 5.34. The load is seen to increase continuously until both loading arms fail. After beginning at the apex of the tapered section, the fracture entered one of the loading arms and remained there until failure took place. Thus, the length of the crack was considerably greater than the width of the tapered section, as may be seen by inspecting Figure 5.3.

5.2.6.3.3 The as-machined specimens, Nos. 7-9

All of the specimens in this group broke in the desired manner - by propagating the fracture through the reduced region, Figure 5.35. A noticeable amount of bending of the loading arms accompanied the propagation of the crack.

The fracture surface is fine compared to that of the other two groups.

The load-deflection plots, Figures 5.37 to 5.39, exhibit a pronounced initial load peak followed by a considerable number of small minor peaks. The load tended to remain constant after the initial peak, a situation which is to be expected because the tapered zone continues almost to the end of the specimen, so that the quantity moment arm/width is almost constant.

An examination of the fracture surfaces will show

that no surface markings can be correlated with the series of minor peaks in the load displacement plots. It appears as if crack propagation at very low speed and very high speed takes place at a smaller stress than propagation at intermediate speeds.

5.2.6.3.4 The reserve specimens, Nos. 10-12

These specimens were tested at room temperature, No. 10 in the as-machined state, No. 11 in the slow-anneal and No. 12 in the quenched state.

Specimen 10 split through the reduced section (see Figure 5.39) but with great difficulty and was bent severely in the process. No readings could be taken. The fracture surface shows a tendency to be inclined to the plane of the reduced section at an angle of 45°, the axis of rotation being along the longitudinal axis of the specimen. A pattern of striations running along the fracture surface is also very obvious.

In specimen 12 a crack could be started with great difficulty only. This fracture became immobile after moving less than half an inch and the loading arms began to bend, Figure 5.40.

With specimen 11 a crack could not be commenced at all and the loading arms commenced to bend immediately, see also Figure 5.40.

5.2.8.3.3 Calibration

Calibration runs were performed at the beginning and at the end of the low temperature tests. These are shown in Figure 5.39.

It must be noted that the loading screw on the calibrator had a pitch of $^1/_{24}$ of one inch, while the mild steel specimens were loaded by means of screws with a $^1/_{32}$ inch pitch.

The points from the calibration run taken at the end of the experiment tended to wander from the linear relationship drawn through them. Such a variation is unusual however, as an inspection of the linear parts of the load-displacement plots, for example Figure 5.38 will show. It is possible that the supply of liquid nitrogen might have been running low. In addition, an angular reading error is possible if the angular scale is not centred precisely on the loading screw.

It is suggested that the deviation from linearity is far more likely to be due to a combination of these errors than to an inherent non-linearity in the load-reading system. The straight line drawn through these points is therefore the best estimate for the load cell characteristic, namely 0.49 bridge units per degree of

rotation and when the stiffness of the calibrator (1430 lb/in) is taken into account, the calibration factor is 0.33 lb/bridge unit.

5.2.8.3.6 Discussion of the Results of the Mild Steel specimens

The surface energy of fracture for the mild steel specimens is presented in Table VII. From the calibration runs presented in Figure 5.39, the scale factor for the bridge reading was found to be 0.33 lb/unit.

The pitch of the leading screw was $^1/_{32}$ inch and the scale factor for converting the area under the load-displacement plots to energy is thus readily found. For example, if the horizontal scale is 500 degrees of rotation per inch and the vertical scale 100 bridge units per inch, the energy represented by each square inch under the curve is

$$100 \times .33 \times \frac{500}{360} \times \frac{1}{32} \quad \text{lb/in}$$

$$= 1.43 \text{ lb/in.}$$

It is found that the energy consumed by the heat treated specimens is about 32 lb. in per square inch, while the as-machined specimens required only 17 lb in/in^2. Comparison with the steel specimens (Table V) the mild steel in the furnace treated state consumed ten times as much energy.

TABLE 5.7 Results from Mild Steel Tests

Specimen No.	Area under L-D plot	Fracture area in^2.	Conversion Factor	Energy Fract. surf. $lb\ in/in^2$.	Remarks
1	18.74	0.88	1.43	30.5	
2	19.66	0.79	1.43	35.2	33.7 average
3	18.54	0.83	1.43	32.1	
4	5.93	0.36	2.86	30.4	
5	7.65	0.69	2.86	32.6	30.3 average
6	6.34	0.67	2.86	27.9	
7	9.50	1.00	1.43	13.6	
8	13.53	0.92	1.43	20.8	16.9 average
9	10.76	0.93	1.43	16.2	
10	-	1.00	-	-	
11	-	-	-	-	
12	-	-	-	-	

Another interesting result is the tendency to a simultaneous failure of both loading arms. This happened to four of the specimens while two others had only one loading arm broken. There are several ways in which this may happen.

(1) A simultaneous failure due only to chance.

(2) Division of one crack into two which travel apart.

(3) The formation of a new crack ahead of the fracture with its plane normal to the longitudinal axis of the specimen.

(4) A metallurgical flaw in the specimens.

The first alternative may be ruled out because a simultaneous failure by random effects would occur very infrequently.

The second and third alternatives are more plausible and a mechanism for each may be sought.

It is conceivable that planes of weakness perpendicular to the direction of rolling may have been introduced into the specimen during its preparation. The appearance of the fracture surface does not indicate any visible trace of such a flaw however.

It is clear that the mild steel specimens absorbed much more energy than is needed merely to form the surface of fracture. Most of the energy absorbed will have been

expended in producing plastic deformation.

The stress dependence of the propagation of the fracture was again noticed. The two discontinuities prior to the fracture of the specimen No. 9 took place when no additional loading was being applied, the delay being about two seconds. Final failure occurred after a delay of three seconds after the last loading increment.

The furnace cooled and water quenched specimens absorbed about the same energy. The specimens were cooled in a mild steel container, so that the water quench took about one or two minutes (against 20 hours for the furnace cooled specimens). A direct quench would have resulted in a finer grain structure still. The indications of this experiment are that surface energy is not greatly dependent on the grain size of the mild steel.

The as-machined specimens differ from the other two groups in that the grains have been severely cold worked. They consumed about half as much energy as the other specimens did. A comparison of the as-machined specimens tested at room temperature and liquid nitrogen temperature is instructive.

The low temperature surface had a homogeneous, fine structure appearance, with a sprinkling of fine

bright spots that indicate flat crystalline surfaces. There is no pronounced orientation of the surface, for the surface appears equally bright when viewed from various angles. The irregularities are on a crystalline scale and variations on a larger scale are absent.

The room temperature specimen which absorbed many times as much energy (measurements had to be abandoned for fear of damaging the load cell, but the energy consumption would be in the vicinity of 100 to 200 lb in/in^2.) also had irregularities on the crystalline scale. The only large scale irregularity is the tendency of the fracture surface to be inclined at about 45° to the plane of the reduced section, the rotation being about the longitudinal axis of the specimen. The brightness of this surface is strongly dependent on the surface orientation, as may be seen from Figure 5.33 (specimen 10).

It is clear that specimen 10 is an example of shear fracture, and as a consequence, the other specimens which were tested at low temperature may be looked upon as having failed by brittle fracture, but with associated shear deformation.

The mild steel specimens present a body of evidence that suggests a process in which one fracture system can initiate a second fracture system. Certain

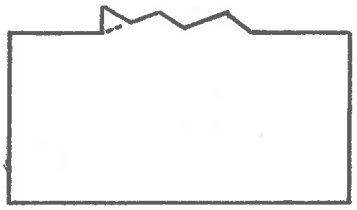

a) The as-machined Specimen (10) tested at Room Temperature.

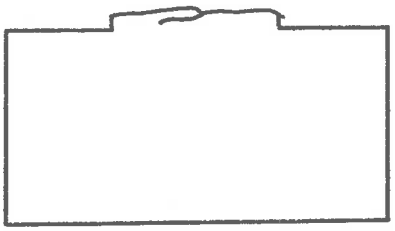

b) The as-machined Specimen (8) tested at -196°C.

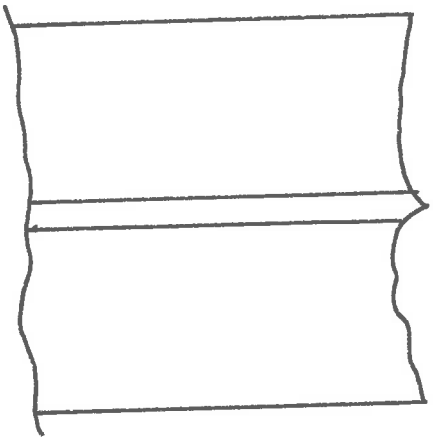

c) The Cusp on the Fracture Surface of those Specimens for which both Loading Arms broke off simultaneously.

FIG. 5.41 Various Fracture Characteristics of the Mild Steel Specimens.

details of this process are however peculiar to each specimen.

A cross-section of the as-machined specimen tested at room temperature is shown in Figure 5.41a. The ridges and valleys shown in this diagram run the full length of the fracture. The only variation is that at some points the fracture surface follows the dotted line. The change-over from one configuration to the other is quite sudden. Thus if the fracture emerges from the reduced section at the corner 'a', a new fracture might form from corner 'b' inwards along the dotted line. The two fracture systems might run together for a short distance but they are eventually joined by a fracture lying in the plane of the cross section and the new fracture becomes part of the main system. The resulting 'dashed line' effect may be seen on the photograph of specimen 40 in Figure 5.35.

Another phenomenon is observed on specimen 8, which was tested in the as-machined state at reduced temperature. This effect is noted near the end of the specimen where the fracture surface is widest, and is illustrated in Figure 5.41b. It appears as if a secondary crack had run through the material over a distance of about one half of an inch, producing a thin foil of metal about .010" thick (visual estimate). This foil appears to be about .030" wide and showed no 'lift'; i.e. it was not pulled away from the body of the specimen. With a razor

blade it could be readily lifted. It is conceivable that the foil was lifted during the propagation of the crack, but accidentally pushed back before being noticed.

The third phenomenon is observed on specimen 2. Here a fragment about 0.2 inch long and .1 inch wide and a thickness of .06 inch is partly torn from one loading arm, about one quarter of an inch before this arm broke from the remainder of the specimen. It seems that in this case the fracture took two different paths which met again, leaving the fragment.

The last phenomenon, exhibited by all four specimens, whose loading arms broke off simultaneously, is illustrated in Figure 9.4c. When the fracture divides into two fractures each entering one of the loading arms the resulting fracture surface shows a cusp at the point where the single fracture system divided.

It appears that some kind of mechanism by which a fracture system can divide is operative. It is suggested that if the two ends of the crack penetrate into the loading arms in opposite directions equally then two fracture systems will result. If one end of the crack deviates more than the other, its effect will predominate and a fragment of specimen will be partly torn from the fracture surface.

This is supported by two of the specimens (Nos. 1 and 3) in which the fracture width is the greatest. The cusp-line on these two specimens run diagonally from one corner of the reduced section to the other, an effect which is not readily apparent from Figure 5.27.

Microscopic examination of the fracture surfaces gave independent support to the previous conclusion that specimen 10 failed by ductile fracture while specimens 1 to 9 failed by brittle fracture. Under a metallurgical microscope specimens 1 to 9 were found to possess numerous crystalline fracture faces, very similar to those presented in the literature. While small reflective surfaces could also be found on specimen 10, these areas lacked the usual cleavage markings and were probably burnished during the shear fracture process.

The fracture faces of specimens 7-9 were the smallest, those of specimens 1-3 came next and the group 4-6 had the largest faces. The latter group of specimens also indicated the greatest density of cleavage steps. The expected trend would be cold worked, water quenched and furnace cooled, but the last two are reversed. It might be suspected that the wrong heat treatment might have been ascribed to the group 1-3 and 4-6. But the oxide layer on the group 1-3 is more developed than that on the group 4-6 indicating that the former specimens had been

at elevated temperature for the greatest period of time. This agrees with the heat treatment - furnace cooled - which is ascribed to this group.

Close examination of the specimens 1-9 shows that most of the surface is composed of cleavage facets. Most necessarily associated with some kind of shear deformation.

While each crystal will produce cleavage facets corresponding to its orientation, and some crystals probably have several, cleavage appears to have moved from one crystal to the next with only a change in direction.

5.2.6.3.7 Conclusion

Several significant phenomena have emerged from this series of experiments. Gilman[12] using single crystals propagated cleavage with negligible plastic deformation. The polycrystalline steel specimens of the previous section propagated a cleavage fracture with a significant amount of associated shear deformation. The cold worked mild steel specimens absorbed about ten times as much energy at reduced temperature and about one hundred times as much at room temperature. At this point fracture was no more by cleavage.

Another interesting phenomenon to emerge so far is the tendency of a fracture system to multiply.

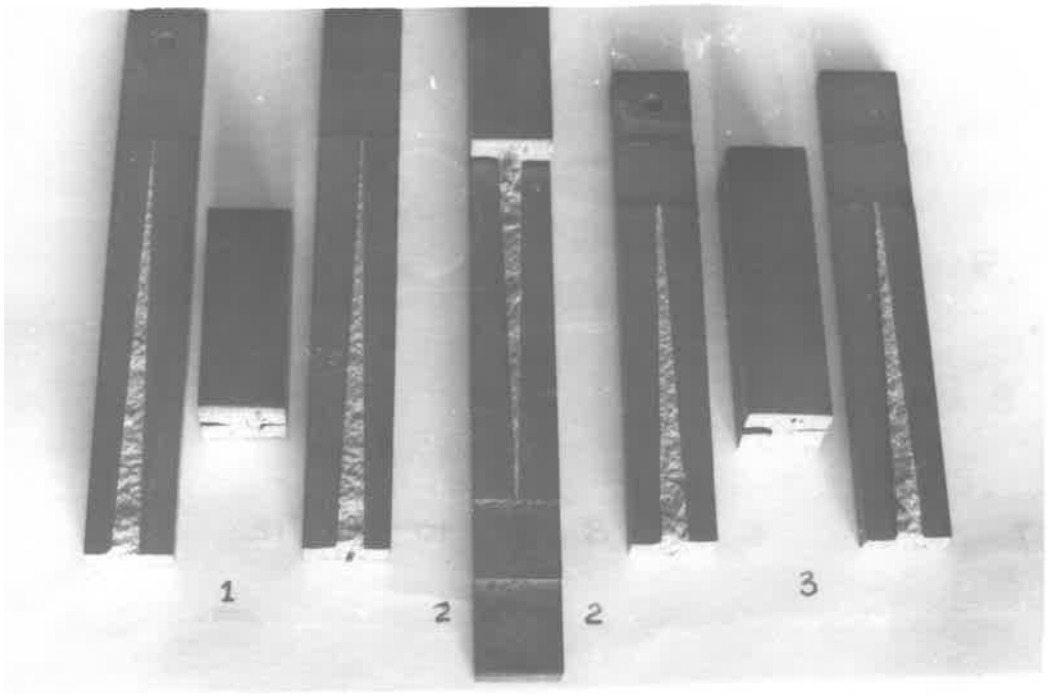

FIG. 5.27 THE RACTURE SURFACES AND MODE OF FAILURE OF THE FURNACE COOLED MILD STEEL SPECIMENS TESTED AT -196°C.

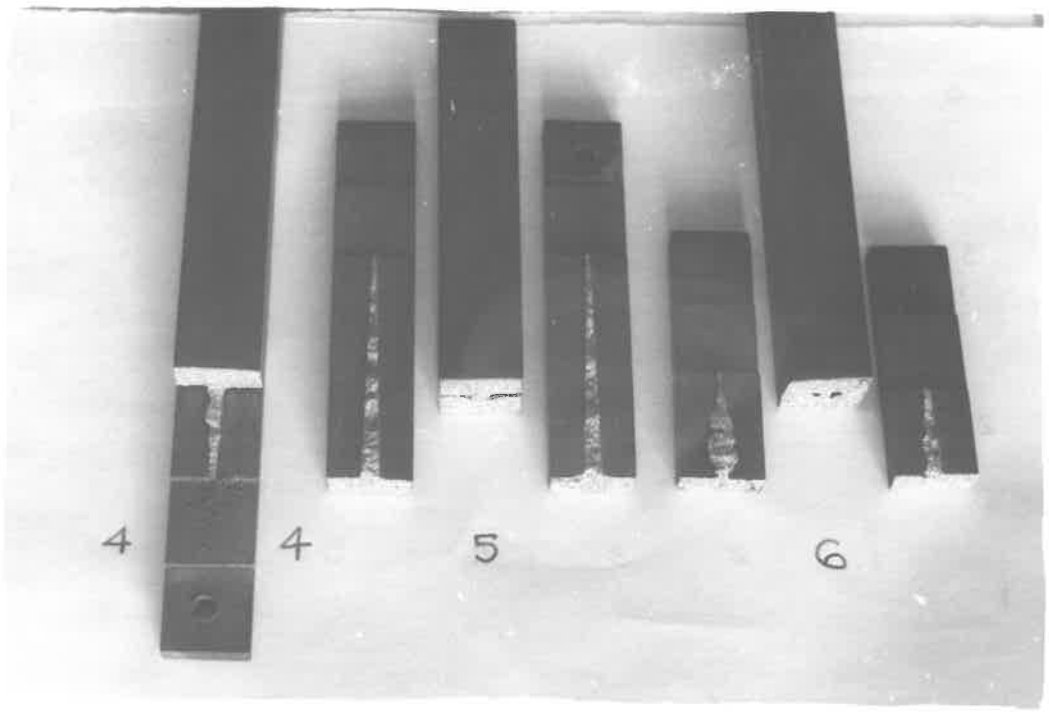

FIG. 5.31 THE FRACTURE SUFACES AND MODE OF FAILURE OF THE WATER-QUENCHED MILD STEEL SPECIMENS TESTED AT -196°C.

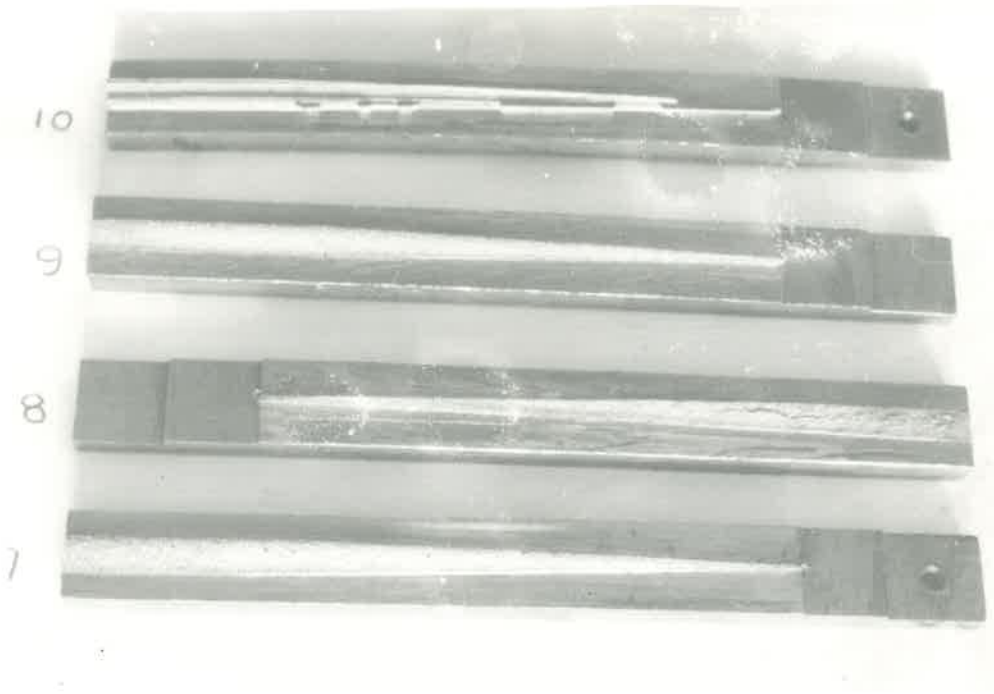

FIG. 5.35. THE FRACTURE SURFACES AND MODE OF FAILURE OF THE AS-MACHINED SPECIMENS (7-9), FRACTURED AT -196°C, AND THE SPECIMEN 10 FRACTURED IN THE AS-MACHINED STATE AT ROOM TEMPERATURE.

FIG. 5.40 THE MODE OF FAILURE OF THE FURNACE COOLED AND QUENCHED SPECIMENS (NOS. 11 AND 12), TESTED AT ROOM TEMPERATURE.

FIGS. 5.28, 5.29, 5.30, 5.32, 5.33, 5.34, 5.36, 5.37 AND 5.38.
THE LOAD-DISPLACEMENT PLOTS FOR THE MILD STEEL SPECIMENS 1-9, FRACTURED AT -196°C.

FIG. 5.39.
THE CALIBRATION PLOTS OBTAINED BEFORE AND AFTER THE FRACTURE TESTS.

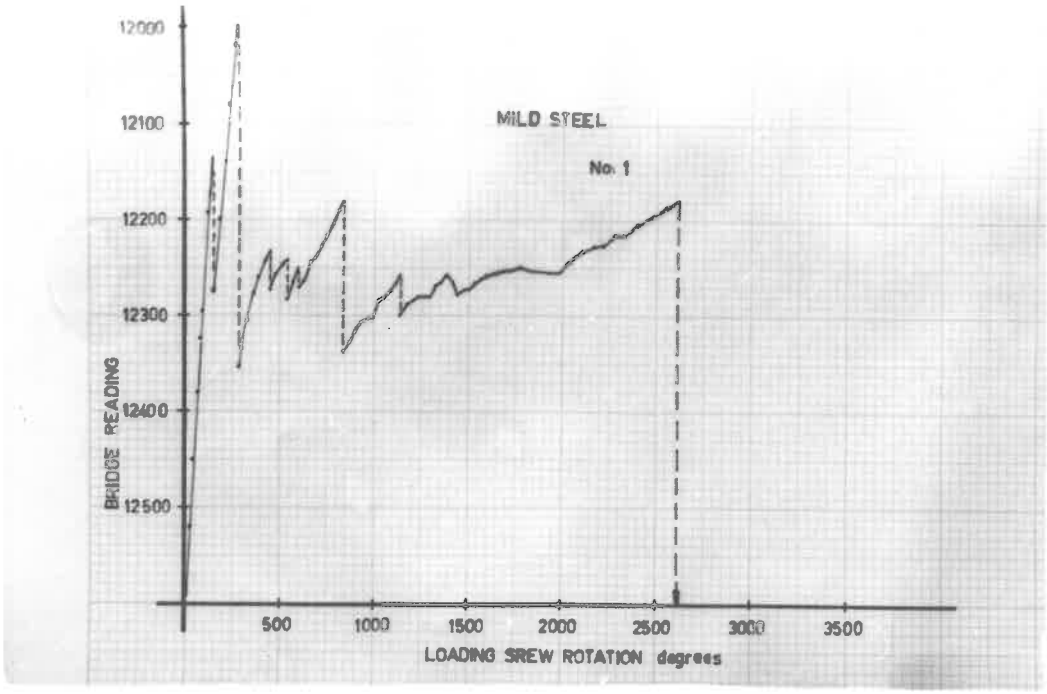

FIG. 5.28.

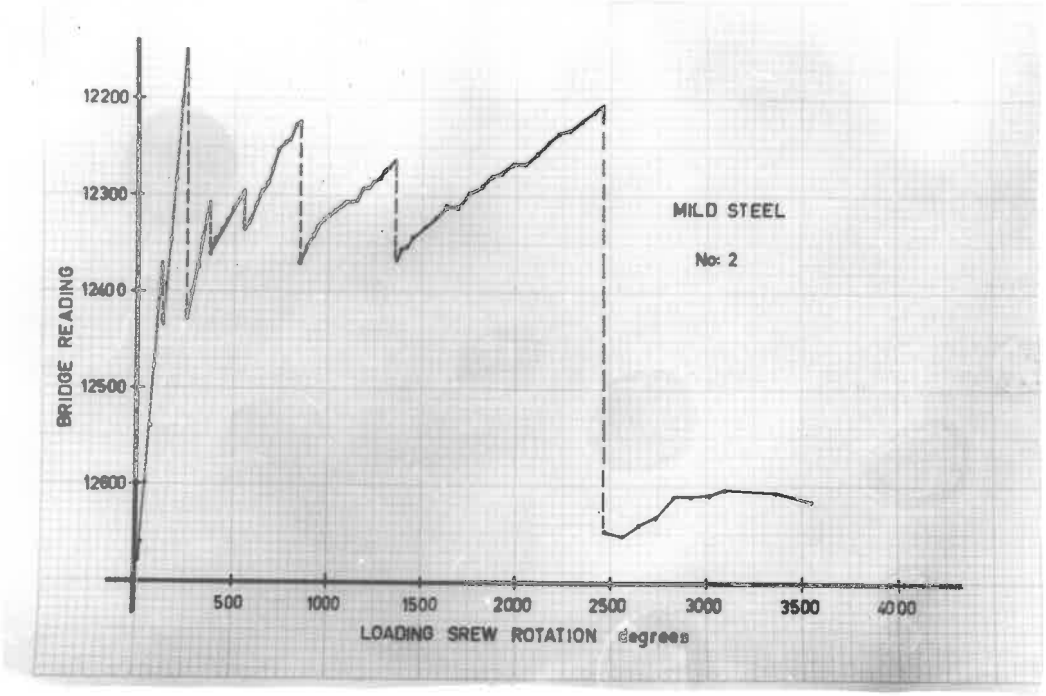

FIG. 5.29.

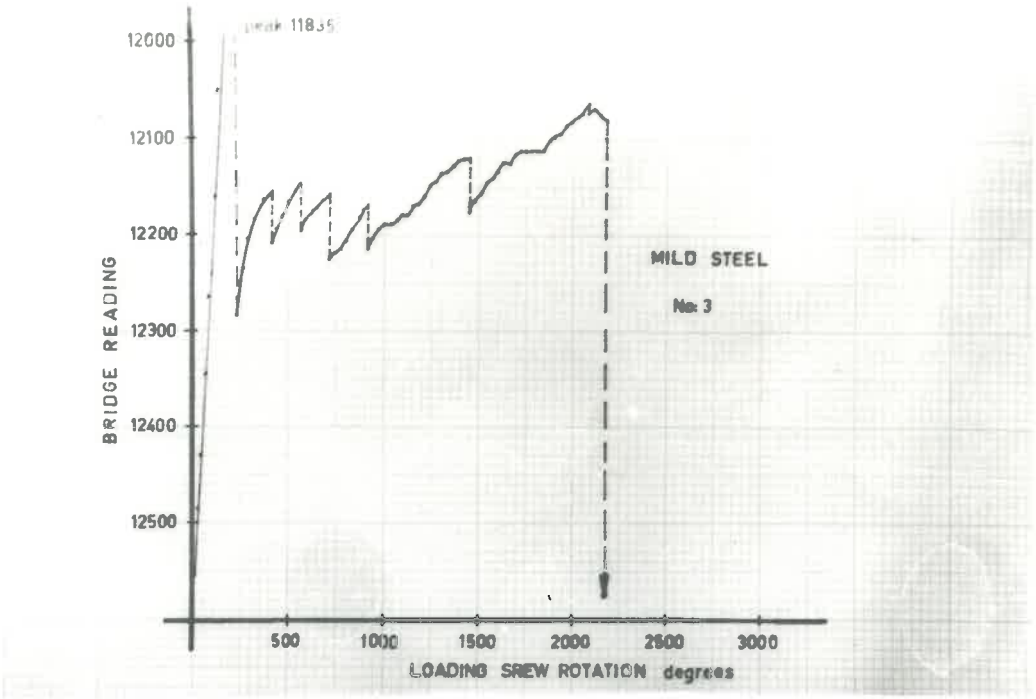

FIG. 5.30.

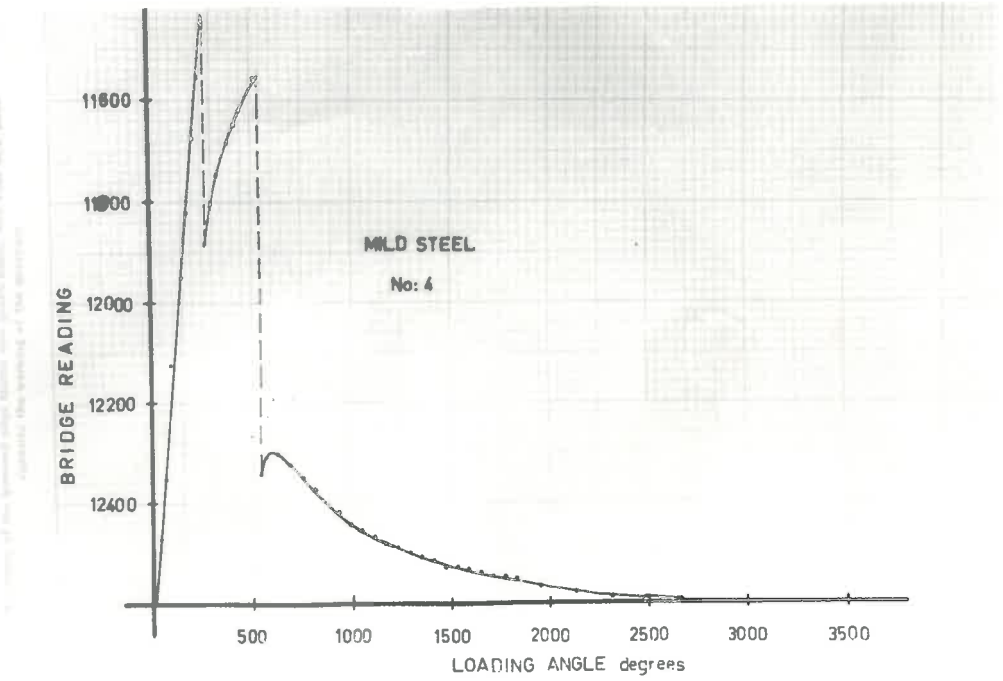

FIG. 5.32.

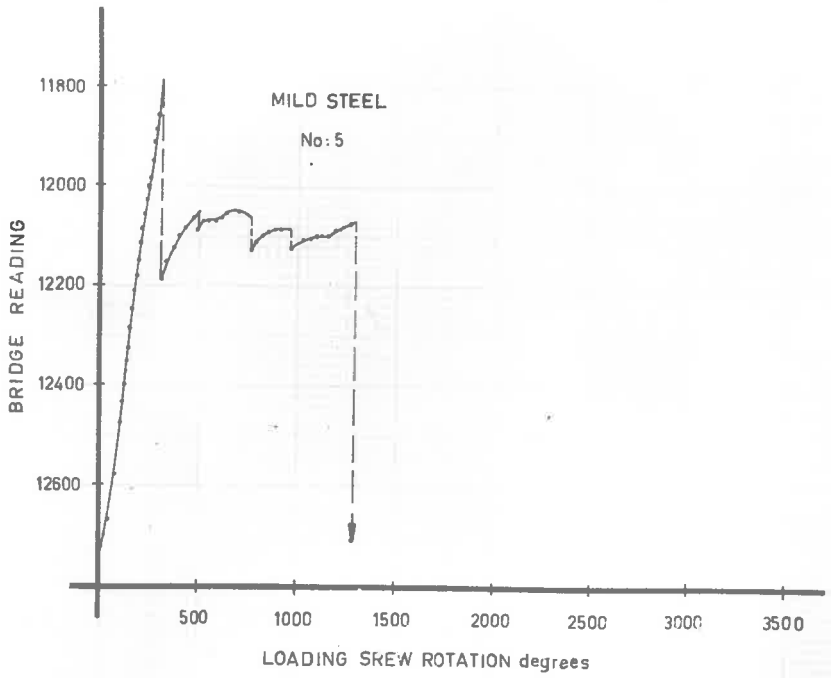

FIG. 5.33.

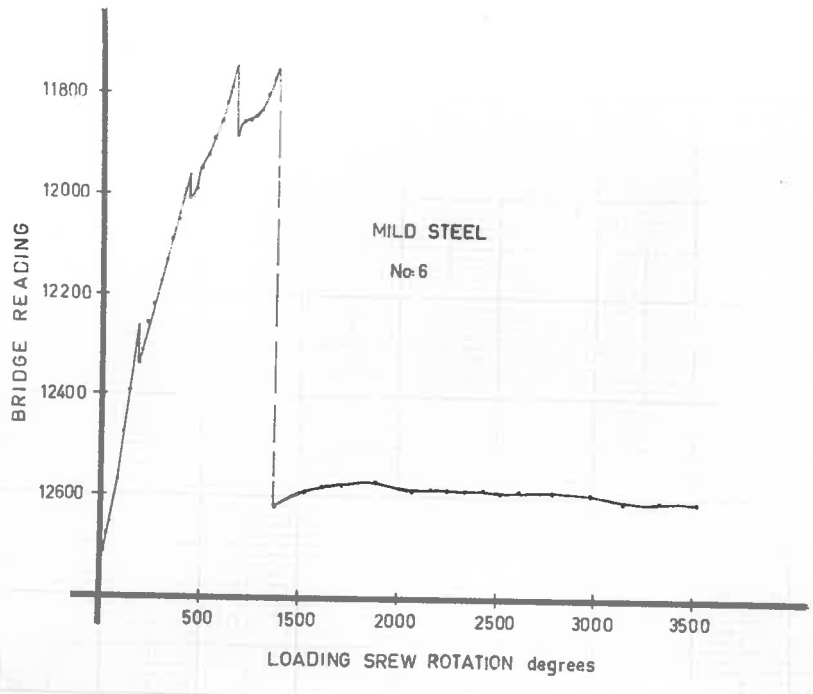

FIG. 5.34.

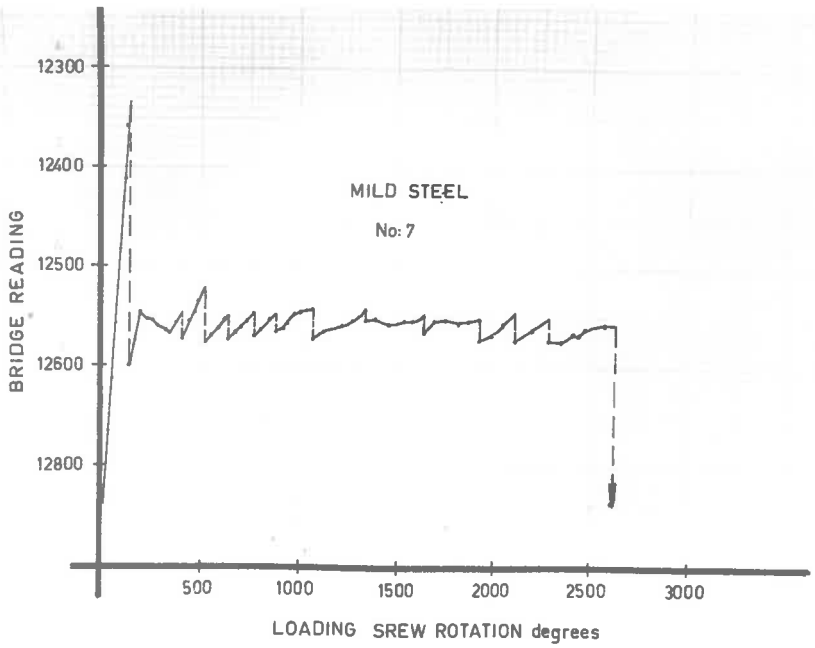

FIG. 5.36.

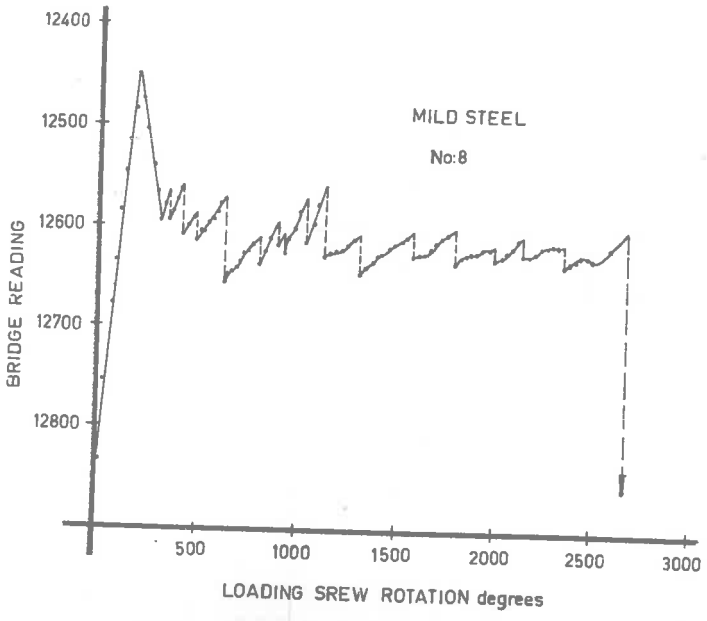

FIG. 5.37.

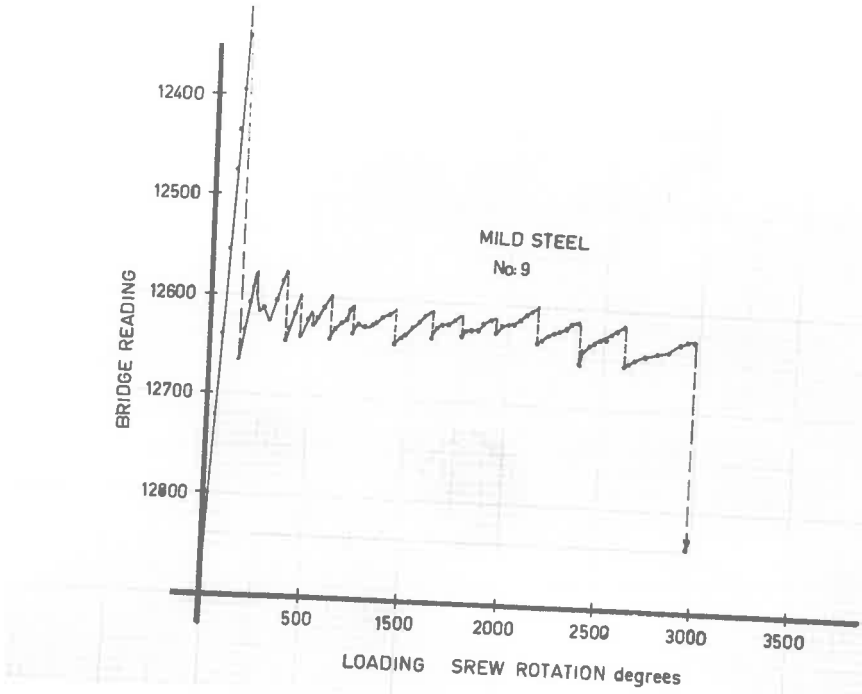

FIG. 5.38.

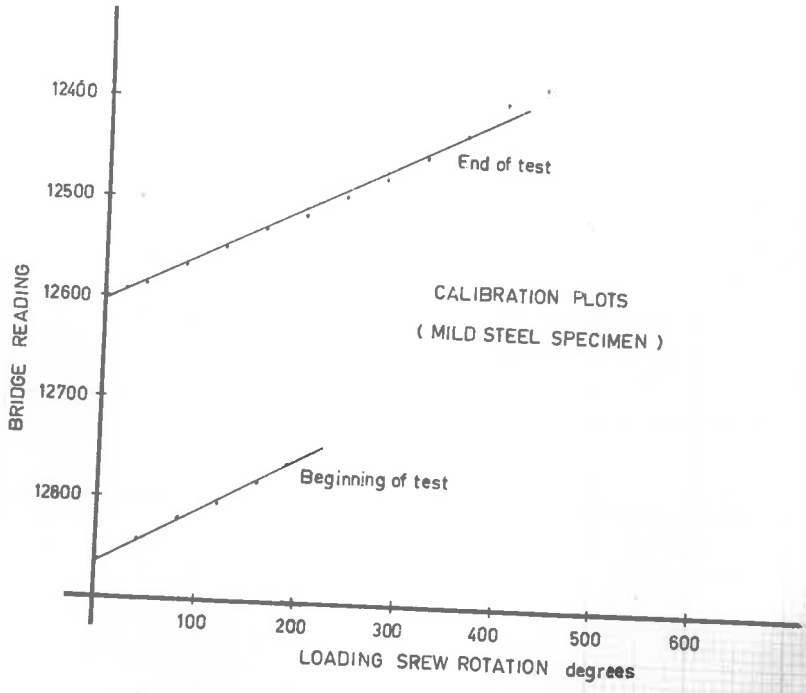

FIG. 5.39.

5.2.6.4. Zinc

At the time when this experiment was performed, the writer was unaware of the excellent work already done by Gilman[12] on the direct measurement of surface energies of crystals, including zinc.

Had he elected to perform his splitting tests on single crystals of zinc, the writer would have duplicated Gilman's work. Fortunately, he chose polycrystalline specimens, containing of the order of 10 or more crystals.

There were several reasons for this. Since this test was to be one of several experiments it was desirable to reduce the amount of equipment and preliminary preparation needed. The growing of single crystals with specific orientation would doubtless have been a more exacting and lengthy process than growing a specimen of the same shape but containing several large, randomly oriented crystals.

If the crystals are so large that the fracture could be expected to be contained in one of them at any time, then the information furnished by the single crystal specimens would be provided by the polycrystalline specimens also. This meant that a saving in time and equipment was possible at the expense perhaps of less tidy results.

However there was also a more positive reason. These large crystals could be expected to influence each other during the passage of the fracture and in addition, the behaviour of the crack at a grain boundary could be studied. Information from this source might not be obtained in any other way, so that the polycrystalline specimen presented a distinct advantage.

Accordingly polycrystalline specimens of a wide range of grain sizes were prepared and tested.

As there was no obvious reason for using zinc of superhigh purity, material available locally was used. A chemical analysis of the specimens is included in Table 5.9.

5.2.3.4.1 Preparation of the Zinc specimens

The zinc used in these experiments was purchased in the form of bars. These bars were melted in a mild steel crucible and poured into pre-heated test tubes. These test tubes were placed vertically onto a stand and inserted into a small furnace whose opening faced downwards.

The test-tube stand has the property that it moves downwards at a steady rate and so gradually withdraws the test tube from the furnace. The furnace is at a

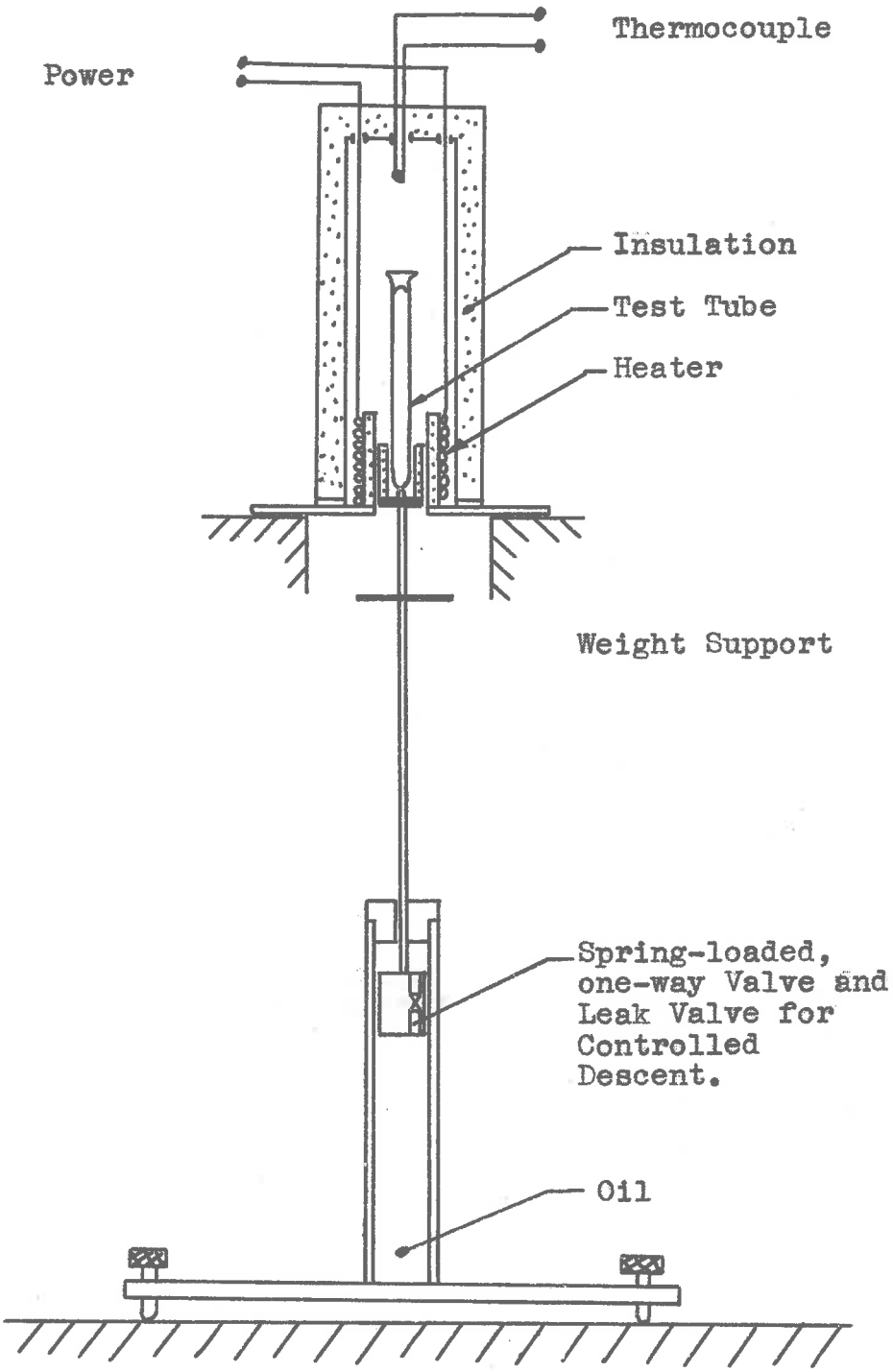

FIG. 5.43 The Apparatus used in preparing the Zinc Specimens from the Melt.

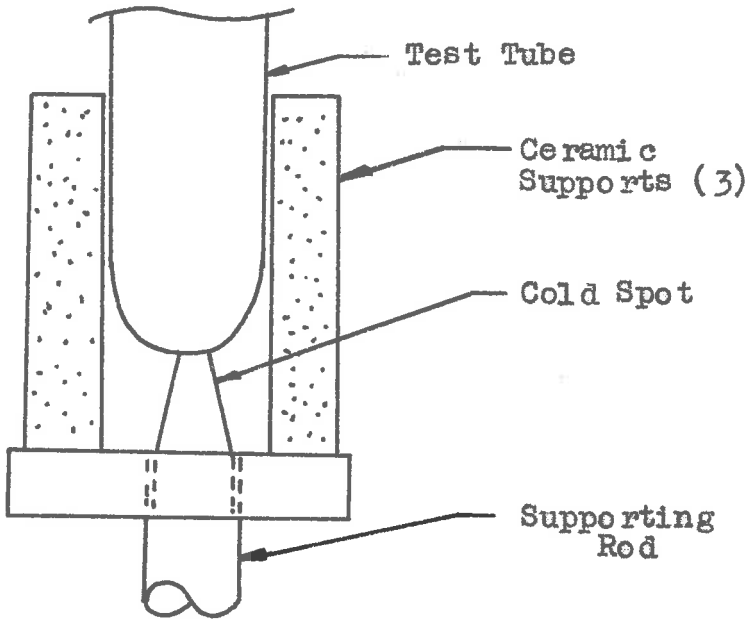

FIG. 5.44 The Provision of a Cold Spot to initiate Solidification.

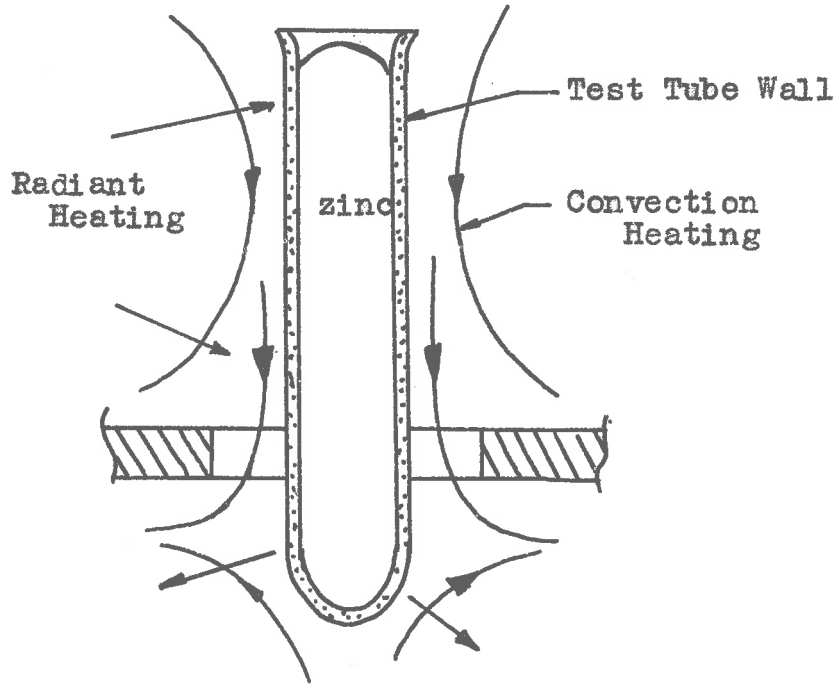

FIG 5. 45 The Heat Flux Pattern around the Test Tube that determines the Temperature Distribution in the Zinc.

temperature considerably greater than the melting point of zinc (419°C) so that as the bottom of the test tube emerges, a steady-state heat flow balance is set up in which the melting point temperature first appears on the bottom of the test tube and gradually moves upwards.

This apparatus is shown in Figure 5.43. The leak valve was adjusted so that the piston descended from the top to the bottom of the cylinder in about two days. If a more rapid descent was required weights placed on the heat baffle achieved the desired rate of fall.

To initiate crystallisation at the bottom of the test tube the mild steel supporting rod was extended so that it supported the weight of the test tube directly, as may be seen from Figure 5.44. This provided a cold spot at which crystallisation was to be initiated.

Figure 5.45 illustrates the factors involved in determining the temperature distribution in the zinc. It is immediately apparent that the temperature variation along the outside surface of the test tube is greater than the variation in the zinc. Initially, when the whole of the test tube is in the furnace, all of the zinc is above the melting point. Gradually, as the bottom emerges from the furnace, the heat loss from the zinc increases

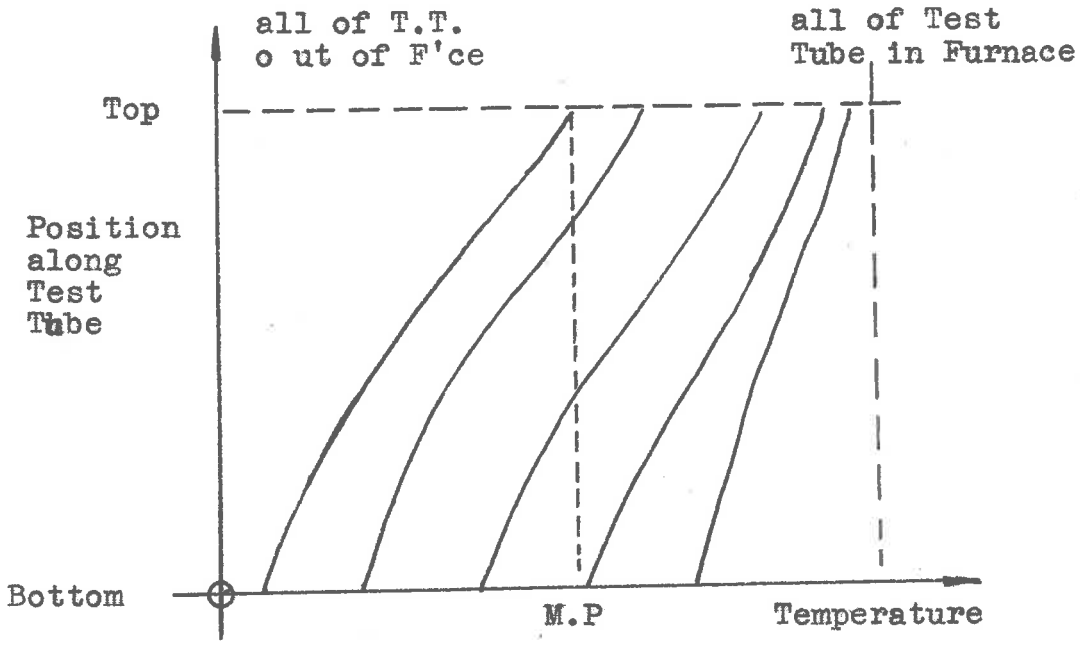

FIG. 5.46 The Distribution of Temperature in the Zinc for various Positions of the Test Tube in the Furnace.

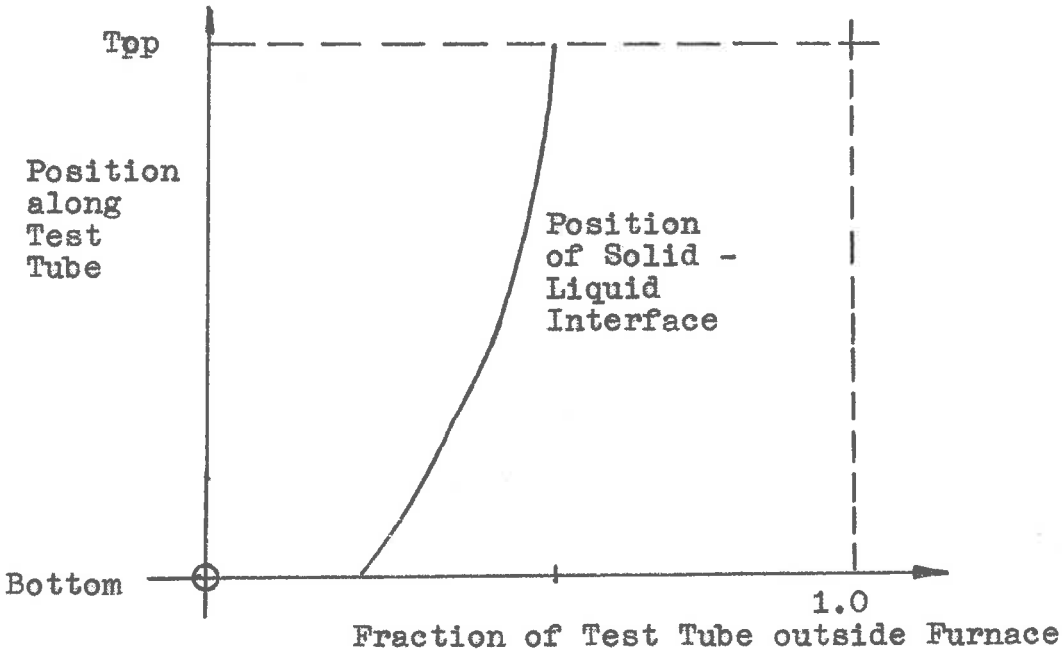

FIG. 5.47 The Interval during which the Zinc is undergoing a change of State.

and the temperature of the zinc falls; the fall being greatest at the bottom of the test tube. An estimate of the variation of the temperature of the zinc is presented graphically in Figure 5.46 for various positions of the test tube in the furnace, and Figure 5.47 shows the interval during which there is a solid-liquid interface. If the test tube is falling steadily then the slope of the curve in Figure 5.47 represents the velocity of the interface. This is only an estimate, but it illustrates that the rate of solidification is smallest at the beginning and greatest at the end of the freezing process. It also illustrates that crystal growth is taking place during a fraction only of the duration of the procedure.

Thus, if a 6" test tube is used, and the rate of descent is ½ inch per hour, then crystal growth will take place during perhaps 12 hours of the 48-hour run, and the solid-liquid interface has an average speed of ½ inch per hour.

One other aspect of the process of solidification must be considered. When the zinc was poured into the test tubes initially, its appearance through the glass was invariably silvery. After the solidification run, the surface generally appeared irregular and discoloured, as if covered by an oxide layer. This suggests that

it is in part at least an accumulation of impurities present in the zinc. Thus in the course of preparing the specimens, the zinc was also purified.

One may expect that the purest and largest crystals would be found at the bottom of the test tube where solidification took place at the lowest rate.

The segregation of impurities to the zinc-glass interface is assisted most by a solid-liquid interface that is convex upwards so that the solid is highest at the centre of the test tube. There appears to be no reason however for this situation, and the interface was probably plane, which still permits the transfer of impurities to the outer surface of the zinc.

The next step in the procedure was to remove the glass from the specimens. It was found that to remove the test tubes it was necessary to destroy them. This was done by carefully tapping the glass with a sharp instrument to produce small fragments which might fall off or might require another small blow to dislodge them.

This is one of the least controlled links in the procedure, for during the removal of the glass, the specimens could well be deformed. Deformation of the crystals was not expected to be an important parameter in

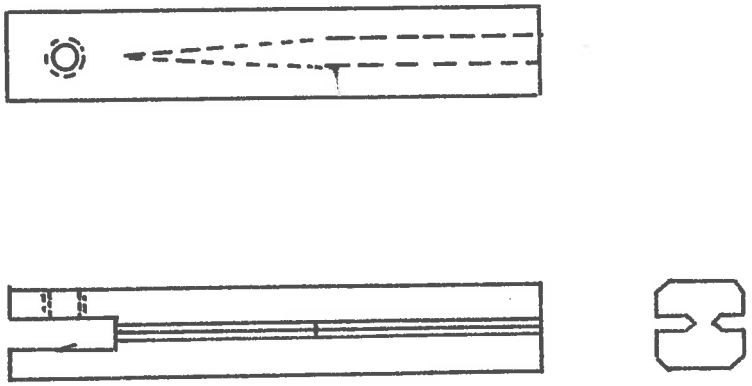

FIG. 5.48 Full Scale Drawing of the Zinc Specimens.

the splitting tests. Nevertheless, this deformation would be both random and unknown and was therefore minimised by exercising the utmost care.

In places, the glass was bonded to the specimens. At these points, the glass was carefully ground away. The writer assumed that any deformation of the specimens at this stage of their preparation was both minute and confined to the outermost layers of the specimens, which were subsequently machined away.

The zinc specimens were about 6 inches long and $\frac{1}{2}$ inch in diameter. The upper end gave the appearance of containing oxide and other impurities. This end was cut off and the remainder cut into two equal bars.

These bars were then machined to the shape indicated in Figure 3.4B. At this stage deformation due to the machining operation was inevitable. Very light cuts could be expected to produce a thin zone of deformation only and were therefore used.

It may be remarked that while zinc crystals are very directional in both flow and cleavage, the transition of the cut from one crystal to another was not accompanied by any visible markings on the machined surface.

Two batches of specimens were prepared. The first batch contained crystals of the order of 1 cm. diameter and the second crystals of the order of 0.2 cm. diameter.

5.2.6.4.2 Procedure

The specimens were tested at the temperature of liquid nitrogen. The test rig was the one employed in the steel and mild steel tests, and the procedure was essentially the same (see sections 5.2.5 and 5.2.6).

5.2.6.4.3 Results

The first batch, specimens 1-5, was tested before the second batch was machined. It was found that in all of the specimens in this batch the fracture soon left the narrowed region it was intended that it should follow, and entered one of the loading arms, causing it to break off, Figure 5.49.

In two of the specimens of the second batch, Nos. 7 and 8, the reduced section was made very narrow. Figure 5.50 shows that in only one of these specimens did the fracture remain in the reduced section. These specimens are interesting in that they permit one to study the changes that take place when the fracture passes from

a region in which the fracture width and the crystal size are of the same order to a region in which the fracture width is much greater.

The load-displacement plots for the twelve specimens tested are presented in Figures 5.91 to 5.92. Other data are given in Table 5.8, including the energy expended in the formation of unit projected area of fractured surface.

TABLE 5.8

Specimen No.	½ Nominal Area in^2	Graph Area in^2	Conversion Factor in lb/in^2	Nominal Specific Surface Energy in lb/in^2	Remarks
1	0.11	16.6	0.130	9.8	Batch 1 Average Value 4.94
2	0.08	9.1	0.130	7.4	
3	0.23	14.6	0.0326	1.0	
4	0.20	8.5	0.130	2.8	
5	0.06	13.7	0.0326	3.7	
6	0.09	9.7	0.0815	4.4	
7	0.05	2.2	0.0815	1.8	
8	0.11	11.2	0.0815	4.2	Batch 2 Average Value 3.80
9	0.39	16.8	0.165	5.5	
10	0.12	9.0	0.0815	3.1	
11	0.09	5.4	0.130	6.1	
12	0.06	5.4	0.0815	3.7	

Overall average = 4.28

TABLE 5.9

The Impurities present in Zinc.

Impurity	Fe	Pb	Bi	Cu
Specimen 4	trace	none	faint trace	trace
Specimen 6	trace	trace	faint trace	trace
Total Impurities by weight, 0.01% .				

Close-up photographs, with magnification of the order of 10x and some micrographs of these specimens are presented in Figures 5.63 to 5.105.

5.2.8.4.3.1 The First Mode of Fracture

An examination reveals that there are at least two modes of trans-crystalline fracture in these specimens. One mode suggests the ideal cleavage process. The fracture surface is flat and mirror-like, and crossed by occasional, irregular, cleavage steps. More frequent on these surfaces are more or less regular arrays of twin bands. Two groups of parallel twin bands are found and the directions of the twin bands are inclined at 60° to each other. Examples of such surfaces are presented in

Figures 5.71, 5.82, 5.83, 5.89, 5.90, 5.99 and 5.100. In Figures 5.83 and 5.99 the density of slip bands is seen to be relatively high near the boundary of the cleavage face (which also defines the extent of the crystal.) It seems that in these instances the cleaved crystal accommodated itself to the neighbouring crystals through shear deformation.

Specimen 4 contained a large crystal so oriented that a large cleavage surface of the first kind was formed. Figure 5.71, which is an enlarged photograph of this surface, provides an excellent macro-microscopic study. During the test on this specimen the fragments shown in Figure 5.49 were also formed. They were still attached to the main part of the specimen, and were broken away easily to illustrate the complex nature of the fracture. At least two cleavage processes on parallel planes about 1 mm. apart must have been active during the test on this specimen.

To obtain Figure 5.71, the specimen was photographed with a directional light source. Small angular changes on the cleavage surface are therefore revealed by intensity changes in the photograph. These defects were probably present in the crystal prior to the test as warping of the lattice and low angle boundaries. It is unlikely that they were formed during the test.

One of the more unusual phenomena found on these surfaces is presented in Figure 5.16b, which is a micrograph of a cleavage facet found on the polycrystalline specimen, No. 11. Here a cleavage step begins at the boundary of the facet and follows an interrupted course towards the centre where it divides into two cleavage steps which are continuous. The cleavage step lines are black initially but become white and continue to the boundary of the facet. The change-over from black to white is quite sudden and it is tempting to regard the dashed-line appearance of the single cleavage step as a sequence of black and light markings.

Unfortunately it was impossible to bring an objective of higher resolution within focusing distance of this facet. The following interpretation of this result is suggested: A cleavage step may be revealed in one of three ways; by the shadow cast by it, by its tendency to reflect incident light coming from the microscope in such a direction that the light does not enter the objective, and thirdly, by reflecting light back more strongly than their immediate surroundings. A fourth possibility not relevant here is the change in focal distance across the cleavage step.

Cleavage steps are generally inclined steeply to the plane in which they lie, in the specimens examined,

so that a change from dark to light suggests an angular change in the cleavage step which approaches 90°. If the dashed-line effect found in Figure 5.94 is due to such angular changes then the event is indeed unusual.

Another phenomenon associated with fractures of this kind may be noticed on examining Figure 5.89. Two fracture planes meet in a straight line and deviate from each other by about 30° (centre of specimen.) A similar arrangement is found on the middle left side of this specimen with the difference that the two planes form a depression.

Slip bands, also found on these surfaces, occur less frequently than twin bands and are usually found near the boundary of the surface where the crystal has probably deformed to accommodate neighbouring crystals during the fracture process. Slip bands may be distinguished from twin bands by being thinner (they appear as lines in these micrographs), straighter and are inclined, usually at 30° or 90° to one of the twin directions. They are present in Figures 5.82, 5.83, 5.86, 5.88, 5.89, 5.90, 5.91, 5.99 and 5.100.

5.2.8.4.3.2 The Second Mode of Fracture

The second kind of trans-crystalline fracture

may be distinguished from the first in two ways. In the same crystal, the two kinds of fracture surface are inclined at approximately 90 degrees to each other. Secondly, the fracture surface while plane on a macroscopic scale, is marked by a series of parallel lines. In all instances where the two kinds of fracture were found to occur together, these lines are also parallel to the lines of intersection with surfaces showing fracture of the first kind.

All of the specimens exhibit both kinds of fracture. Fracture of the second kind is especially prominent in specimens 1, 2 and 3, Figures 5.63, 5.64 and 5.72. The direction of these lines does not appear to depend on the direction in which the fracture traversed the crystal, compare Figures 5.64 and 5.72 for example. However, if the plane of fractures of the first kind lies approximately parallel to the plane in which it was intended that the fracture should be propagated, then some of the lines on fractures of the second kind are more strongly pronounced.

On closer examination, these lines turn out to be fractures of the first kind, as may be seen from Figure 5.93 on the lower right, or 5.63 at the lower right and left. These secondary fractures, as they may be called, are exceedingly penetrating. In the case of Specimen 4, the fragments shown in Figure 5.49 are the result of such secondary fracturing.

Closer examination of the specimen reveals many finer secondary fracture lines from a width of 10^{-4} in. upwards. The remaining line markings which appear to be a series of parallel cleavage steps could well mark the presence of smaller secondary fracture sites. The spacing between the line markings is regular at about 10^{-3} in.

The parallel line markings tend to dominate fracture surfaces of this kind. However some twin bands were found on the right of specimen No. 2 (Figure 5.63 and 5.65), which were normal to the probable direction of the fracture, i.e. inclined at about 45° to the line pattern.

It is relevant to ask how the density of the lines is related to their angular orientation. For this purpose the horizontal, i.e. the plane in which it was intended that the fracture should lie (Figure 5.48), will be used as reference, measuring the angle between the two planes in a vertical axially directed plane.

It was found that the width of cleavage facets was constant with respect to orientation at a value of about 0.001". The height of the cleavage steps is more variable. A fracture surface of this kind found on specimen No. 4, inclined at 135° to the horizontal plane exhibited cleavage steps whose height appeared to be $^{1}/_{5}$

to $^1/_{10}$ the distance between the cleavage steps, Figure 5.70. In other specimens the cleavage step height is of the order of the distance between the steps.

Two microscopes were found to be useful in examining the fracture surfaces. The one is a metallurgical microscope with globe illumination and a maximum object-objective distance in the vicinity of ½ inch. The second microscope intended more for use in a workshop has a constant magnification of 60x. The object-objective distance is about 4½ inches and in daylight one could readily distinguish cleavage steps and secondary fracture lines. On the surface of specimen 4 already referred to, unmistakable secondary fracture lines were found to be seperated by 3 to 7 cleavage steps.

5.2.6.4.3.3 Correlation between fracture energy and Mode of Fracture

The specimens for which the surface energy (Table 5.6) was found to be greatest, namely 1, 2 and 11, especially the first two, have a large proportion of fracture surface covered with the parallel line markings. The surface energy associated with Nos. 5 and 7 is exceptionally low. About half the fracture surface of No. 3 is not a fracture at all because the specimen contained a weakness there in the form of an oxide layer. Much of the remaining surface shows the line markings however.

At closer examination in daylight, the surfaces with line markings appear to be twisted.

The specimen No. 7 which also has a rather low surface energy value, differs from the other specimens in that fractures of the second kind show a less regular line pattern, and the density of irregular cleavage step markings on the cleavage facets is greater, Figure 5.76.

5.2.6.4.3.4 Comparison of Narrow and Wide Fracture Surfaces

Specimen No. 8 provides an opportunity for comparing the surface markings on the narrow and wide fracture surface. Several differences between the two regions are apparent. The wide zone contains a predominance of fractures of the first kind, as is apparent from Figure 5.80. On the other hand, the narrow zone is composed entirely of fracture surfaces of the second kind, not one surface of the first kind being apparent. Some of the inter-crystalline fracture surfaces are shown in Figures 5.65 to 5.67. It is obvious that the line markings are less regular than those of Figure 5.63, for example. Specimen No. 7 when examined also shows a complete absence of surfaces of the first kind. Some of the fracture surfaces, for example that shown in Figure 5.78, are highly reflective, but the line pattern

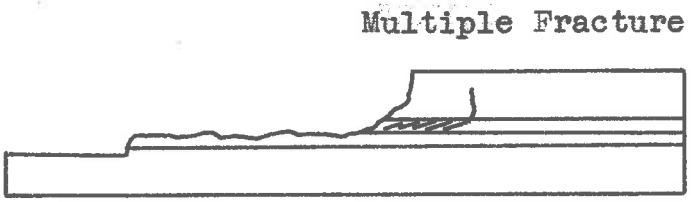

FIG. 5.104 The Appearance of the Multiple Fracture on Specimen 9.

is there. Another peculiarity of the narrow fracture zone in both Nos. 7 and 8 is that the deviation of individual inter-crystalline fracture surfaces from the mean surface is small. This is to be expected however, for in the wide fracture zones of all the specimens, fracture surfaces of the second kind are also less prone to deviation from the mean surface than fractures of the first kind.

5.2.6.4.3.5 Multiple Fracture Processes

Specimens 4 and 9 are good examples of more than one fracture process being active simultaneously. In the former this led to a number of fragments but for Specimen 9 the other fracture system is not apparent from the various photo- and micrographs. A sketch of the second fracture process found in this specimen is given in Figure 5.46.

The sketch shows a number of short, parallel fracture lines, one of which eventually turns up into the loading arm. Several of the other lines also extended some distance into the loading arm.

These parallel fractures must necessarily be progressing simultaneously wherever two or more of them overlap, for if one overtakes the others, the latter will not be under stress any more and cease to be propagated.

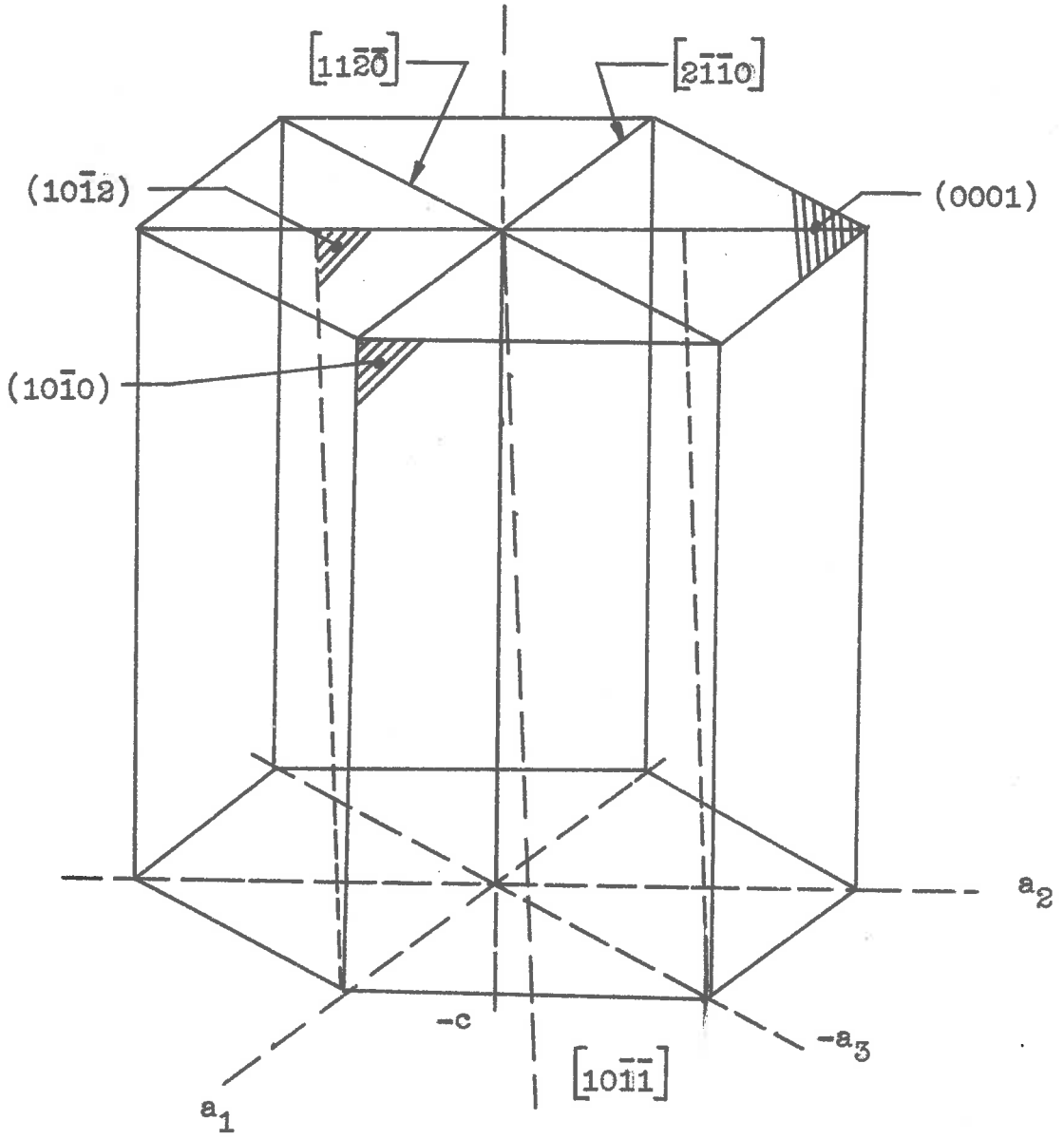
[11$\bar{2}\bar{0}$]
[2$\bar{1}\bar{1}$0]
(10$\bar{1}$2)
(0001)
(10$\bar{1}$0)
a_2
-c
-a_3
[10$\bar{1}\bar{1}$]
a_1

5.2.8.4.4 Discussion of Results

It is well to list briefly the most important mechanical properties of zinc crystals. For this purpose the unit cell of zinc is presented in Figure 5.105.

In zinc crystals, slip takes place in the basal (0001) plane in the $[2\bar{1}\bar{1}0]$ and $[11\bar{2}0]$ directions.

Twinning takes place on the $(10\bar{1}2)$ plane in the direction $[10\bar{1}\bar{1}]$.

Cleavage takes place on two planes (0001) and $(10\bar{1}0)$. It is interesting to note that the normal stress for cleavage on the two planes at -185^{0}C is 0.19 and 1.80 kg. per sq.mm. respectively, Table 28[51].

It follows from this that fracture surfaces of the first kind are cleavage surfaces parallel to the basal plane of the crystal. The cleavage facets on fractures of the second kind are cleavage surfaces on the $(10\bar{1}0)$ plane.

5.2.8.4.4.1 Basal Plane Fracture

The various markings found on basal plane surfaces will be discussed first. On several photomicrographs markings which are obviously twin bands are found. In zinc, twinning is the mode by which glide in a plane other than the basal plane can readily take place. Hence one would expect twin bands to be long in the [0100]

direction and narrow in the [$1\bar{1}00$] direction, as seen on the basal plane. Further, if twinning is confined to the ($10\bar{1}2$) plane one would expect only one set of parallel twin bands. In some instances, for example Figures 5.89 and 5.90 there appears to be only one set of twin bands. In Figures 5.82, 5.83 and 5.91, two sets of twin bands at a 60° relative orientation are clearly present.

Other markings which have the appearance of slip lines or slip bands may also be found in the photomicrographs referred to above. Two sets of parallel lines appear. One is at right angles to one of the twin band groups and the other inclined at 30° to the same twin bands.

Unlike slip, twinning is confined to a volume of crystal rather than to a set of glide planes. A twin zone grows if the deformation associated with this process makes available enough energy to maintain it. The growth of a twinned zone in directions lying in the twinning plane is likely to be the most favoured mode. But growth in directions which do not lie in the twinning plane is not excluded. It appears from the evidence presented above that growth in a direction inclined at 60° to the twinning plane is also possible though the critical resolved shear stress for this mode of growth is likely to be higher.

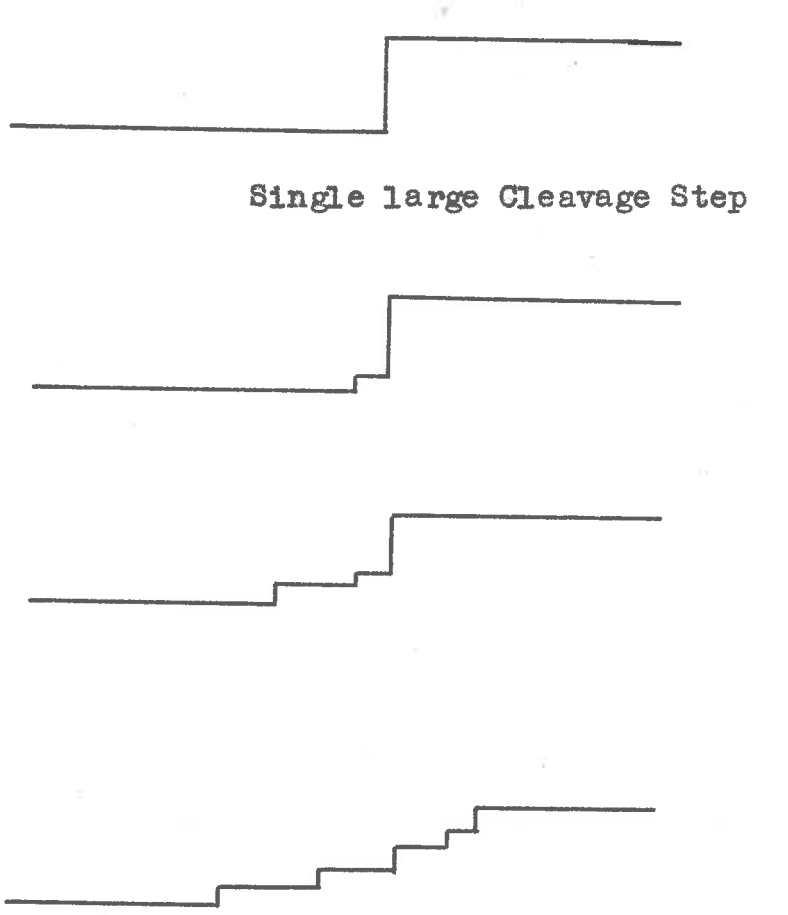

FIG. 5.106 Stages in Transformation of a large Cleavage Step into a number of smaller Steps.

The problem of the markings which appear to be slip bands remains however, and will be taken up again later.

Figures 5.88 to 5.90 present a rather striking pattern of cleavage lines. A total of about 100 cleavage step markings run together into four major cleavage steps. There is no reason to suppose that the small cleavage steps were formed first for it is difficult to find any reason for the way in which they join up.

It is almost certain that the large cleavage steps were formed first, and that the smaller cleavage steps are derived from them. If the process is viewed in section the phenomenon might appear somewhat as presented in Figure 5.106. The reason why a large cleavage step might transform into a series of smaller steps will be suggested after a consideration of fracture surfaces of the second kind.

5.2.8.4.4.2 Non Basal Fracture

The most striking feature of fracture surfaces of the second kind is the line markings found on them. These lines are found to be cleavage steps. Some of these steps have opened up into secondary fractures which are exceedingly penetrating. The secondary fracture surfaces are on the basal plane as are the cleavage step surfaces.

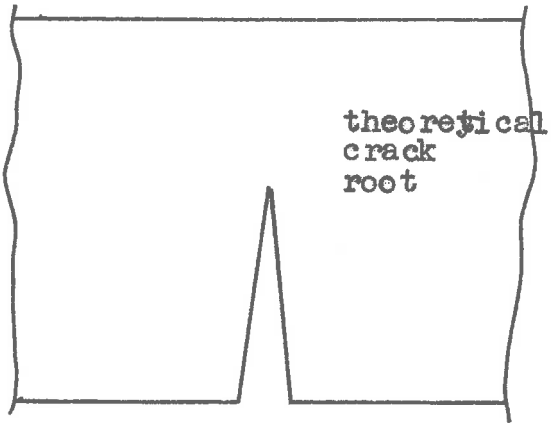

(a)

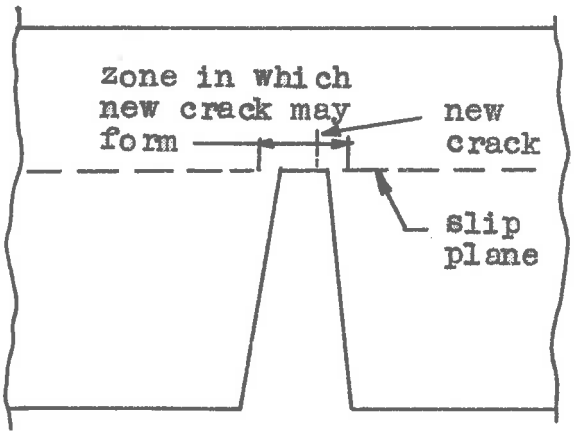

(b)

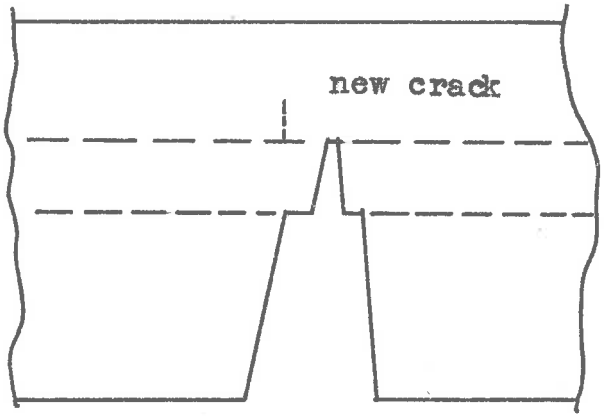

(c)

FIG. 5.107 Illustrating the Crack-Nucleated Glide Mechanism which may arrest a Crack.

From this fact emerges a very important anomaly. It was pointed out that cleavage on the basal plane can occur at a stress only one tenth the value required to maintain it on the other cleavage plane. The fracture surface on the $(10\bar{1}0)$ plane has many well developed secondary cracks yet the main fracture did not deviate from the surface on which the propagation of the fracture is more difficult.

There appears to be only one possible conclusion, namely that the secondary fractures were formed after the passage of the crack along the $(10\bar{1}0)$ plane. This does not explain the presence of the cleavage steps however.

5.2.8.b.4.3 A Fracture Mechanism for Zinc

To do this it is neccessary to assume that slip is nucleated in the vicinity of the crack root. This is presented in Figure 5.107. The effect of slip of this kind is to reduce the stress concentration factor at the crack root. This also means that if a crack of the type envisaged in part (a) of the Figure is to form, it must be nucleated anew.

If a crack of this kind is nucleated somewhere it will spread into the crystal and transversely. Its progress into the crystal will again be arrested by transverse slip and the process repeats itself, (a).

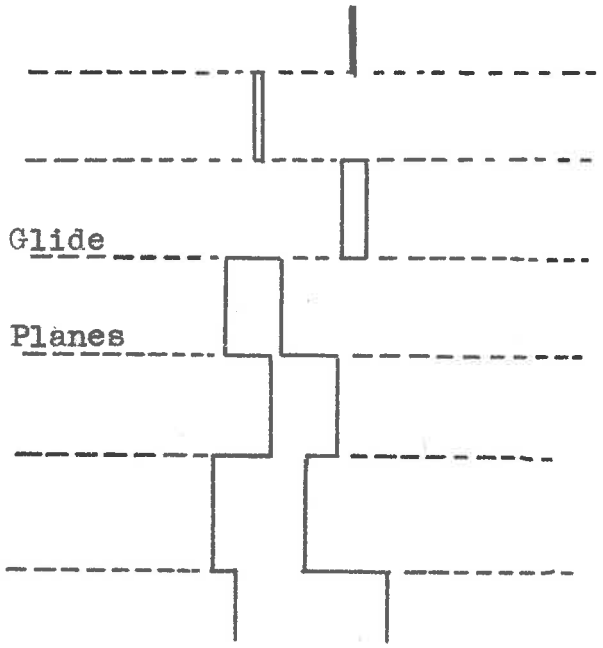

FIG. 5.10B A cross Sectional View of the Fracture Process predicted by the Crack-Nucleated Glide Hypothesis.

The slip plane produces a zone of crystal in which stress is tensile and varying only slowly. The point at which the new crack is formed is not well defined and cleavage steps of considerable height result.

It follows from this argument that the cleavage step surfaces form as a result of the sliding apart of the two crystal segments. This glide will of course take place on the slip planes activated by the fracture. The kind of situation which can be expected to develop from this is shown in Figure 5.10b.

In this Figure the cracks are presented as being well ahead of the point which the continuous fracture surface has actually attained. The sliding apart which results in the formation of the cleavage steps not only absorbs energy associated with the new surface formed, but energy is also required to maintain the shear deformation.

If the cleavage surface is along the $(10\bar{1}0)$ plane, the slip plane will be the basal plane. It is well known that cleavage along the $(10\bar{1}0)$ plane requires a higher normal stress than cleavage on the basal plane. It is hardly surprising, then, that some of the slip planes become secondary fractures, as the micrographs clearly show.

Further the most likely point for the appearance of a secondary fracture is a plane such as (c) of Figure 5.10B, which defines the "root" of the fracture. This plane is always well behind the leading crack on the $(10\bar{1}0)$ plane. This is in agreement with a conclusion reached earlier, that the secondary fractures must be formed at some distance behind the main fracture.

The hypothesis that at the crack root slip is nucleated, and the reasoning which follows this assumption is verified in a number of ways by the results of the experiments with zinc.

One of the results that this hypothesis explains is the discrepancy found to exist between value of the surface energy of zinc and the surface energy absorbed during the fracture tests. Gilman[12] who set out to measure the surface energy of zinc directly obtained a lowest value of 85 ergs per sq. cm. at liquid nitrogen temperature. This converts to 5.1×10^{-4} lb in. per sq. in. and may be compared to the average of 4.28 lb.in. per sq. in. for the zinc specimens.

According to the above hypothesis energy is absorbed not only by the main crack but by several other mechanisms. Taken in order of occurrence, the nucleation and propagation of slip which arrests the crack is the first mechanism of energy absorption that is activated.

After this there is the slip along the planes which eventually become cleavage step surfaces and finally the development of secondary fractures.

The secondary fractures are found to be very penetrating and this is probably true of the initial slip. These two mechanisms are therefore likely to be the main energy absorbers.

There is another mechanism of energy absorption not related to fracture phenomena as depicted above. This is large-scale shear deformation of the specimens. This deformation can be detected as a change in the shape of the specimens, and is noticeably present only in the fragment of No. 4. A study of the force-displacement plots for the various specimens, which will be undertaken later will add further weight to the claim that while some of the energy went into large scale deformation, most of the energy was indeed absorbed by the fracture.

The observation that the line markings lie in the basal plane when the main fracture is along the $(10\bar{1}0)$ plane, is quite consistent with this hypothesis for the basal plane is a plane of easy glide and the line markings will be the line of intersection of the two planes. These markings are therefore independent of the direction in

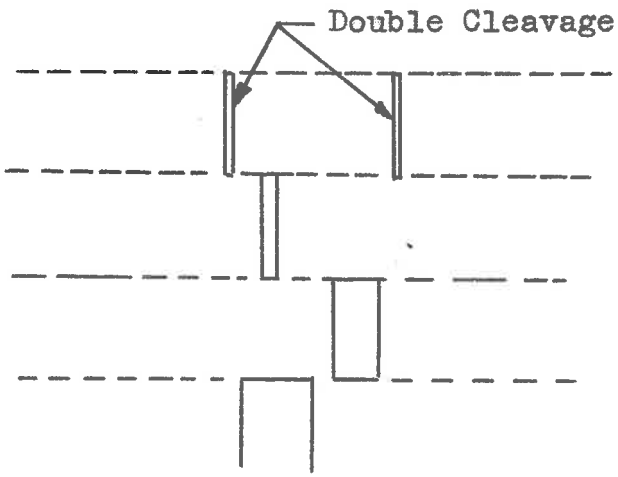

FIG. 5.109 Showing a Double Cleavage which can lead to the formation of a Filament.

which the fracture traverses the crystal. It follows from the nature of the experimental results that if the fracture moves in a direction normal to the line markings the crack is regularly arrested by slip. If the fracture then expands in a direction parallel to the line markings, the cleavage steps are propagated along their direction, and the cracks on the $(10\bar{1}0)$ plane are not arrested at regular intervals.

Explanation of other observations such as the great regularity of the line markings and the more variable nature of the cleavage step heights, require further additions to the above hypothesis as regards the nature of the mechanism by which the crack is arrested, which is left till later.

Figure 5.67 reveals a filament of crystal which was torn from the fracture surfaces. Its width is about 0.002 inch and its shape regular. These properties suggest that its sides are fracture facets and cleavage steps. It was pointed out earlier that according to the hypothesis put forward, cleavage is nucleated at regular intervals, and the location of the new cleavage is not well defined. Consequently cleavage may be nucleated at more than one point in the zone between two slip planes. If two such cleavages develop, as shown in Figure 5.109, a filament

may form and if it is attached to the different halves of the specimen at each end it will be pulled away from the surface, which then reveals its presence.

The presence of a series of parallel line markings on basal plane fracture surfaces other than twin bands may also be explained by using the proposed hypothesis. Zinc crystals do not exhibit slip in non-basal planes, but under the conditions associated with the root of a crack, non-basal slip may be nucleated. The propagation of such slip probably requires a high stress and it will therefore be less penetrating. The stress concentration at the "root" of a basal crack is not reduced to the same extent as for non-basal fracture and a new fracture will be nucleated in a plane closer to the plane of the previous crack. Line markings of this kind that are apparent on Figure 5.82 are spaced at approximately0.001 inch and are regularly spaced. Similar conclusions can be drawn from appropriate micrographs of specimens 8 and 11. Micrographs of specimen 8 also show two sets of parallel lines crossing.

According to the hypothesis, a fracture is impeded if it traverses possible glide planes. Thus if a crack is moving in a direction parallel to one set of glide planes it may still be arrested by another set of glide planes. The number of nucleation sites required in propagation of this kind is increased greatly as a consequence. Figure

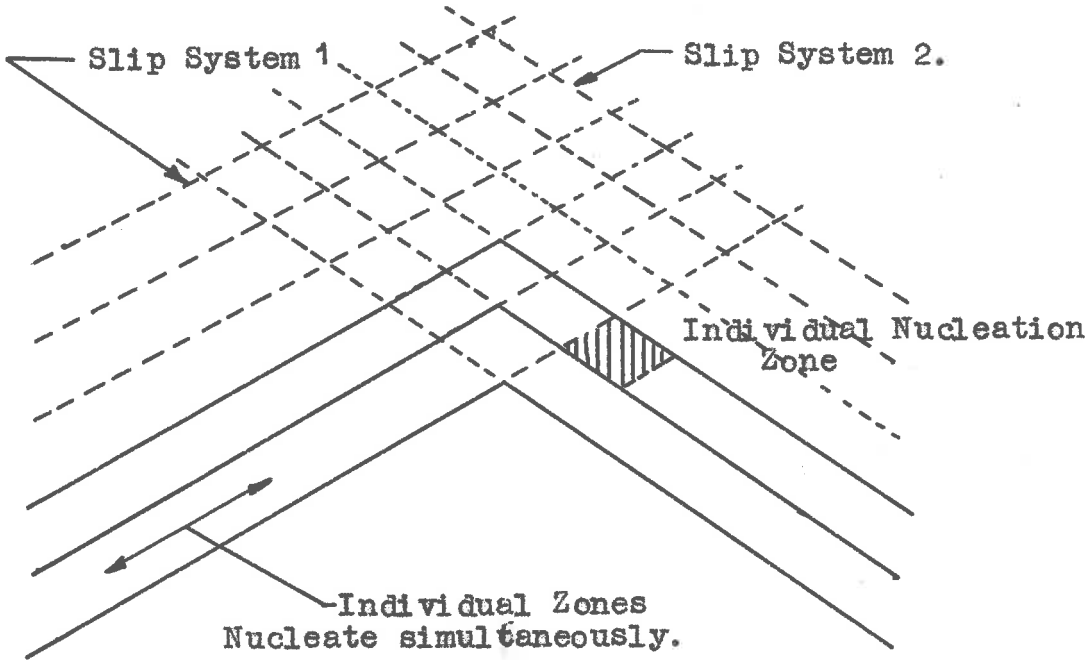

FIG. 5.110 The Fracture Process according to the Hypothesis when two Slip Systems are active.

5.110 shows how simultaneous nucleation by a series of adjacent nucleation zones, which makes available more energy for the slip system, results in a regular fracture front.

Figure 5.90 presents a complicated fracture surface the features of which can now be explained. The river-like irregular cleavage step markings may be explained by supposing that the large cleavage step from which the smaller cleavage steps radiate is really a fracture surface of the second kind whose line markings become the spreading cleavage steps.

The phenomenon of multiple fracturing noted on specimen 9 which implied that several closely spaced (about 0.010 inch apart) fractures were propagated simultaneously becomes intelligible when it is considered in the light of the above hypothesis.

Two fracture systems on parallel planes can share the same slip systems that are associated with arresting a crack if they are abreast of each other. Slip in the portion of crystal between the two fractures is reduced because the dislocation from the two sources can annihilate each other, and simultaneous fracturing will be favoured especially when basal plane fractures are propagated (as is the case for specimen 9), for the slip system in this case is non-basal and a high stress is required to maintain shear flow.

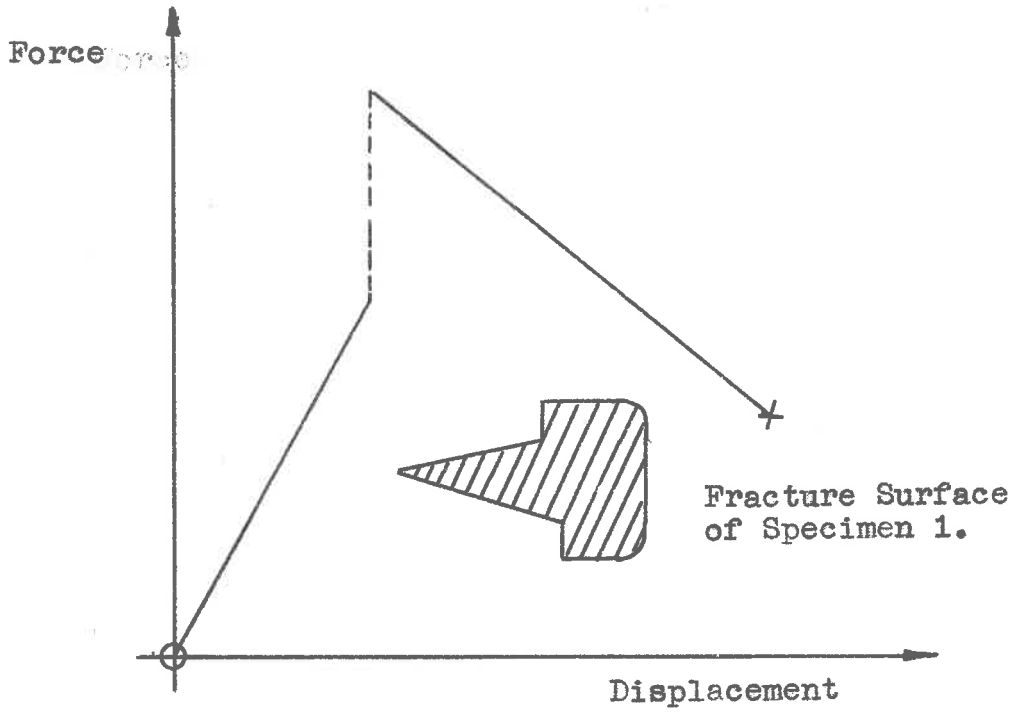

FIG. 5.111 The expected Shape of the Force-Displacement Plot for Specimen 1.

Micrographs 5.83 and 5.99 show slip lines or bands concentrated near the crystal boundary suggesting that the crystal deformed to accommodate neighbouring crystals. The fracture surface is a basal plane. The slip systems associated with these lines are non-basal and according to the hypothesis they are nucleated by the passage of the fracture. The more prominent appearance of these lines in a portion of the cleavage face can be explained by a higher local shear stress due to neighbouring crystals and a consequently greater penetration of the slip systems.

5.2.8.4.4.4 The Force Displacement Plots

The relationship between the loading force and the progress of a fracture was discussed in detail in section 5.2.7. From this, one may derive the kind of plot one could expect from the various zinc specimens. The zinc specimens are relatively inhomogeneous and force variations not predicted by the simplified theory referred to above must also be expected. By way of example, the expected plot for specimen 1 is presented in Figure 5.111 which also shows a lay-out of the fracture surface.

The actual plot, as may be seen from Figure 5.51, differs in that the initial build-up of force is rather rapid at first, then increases more slowly only to increase

at a rapid rate again. The fracture from the apex of the reduced section to the point where the fracture enters the loading arm, is of the first kind.

This suggests the following sequence of events. The initial steady and rapid rise of the loading force is due to elastic loading of the system. This stage is terminated by the appearance of a fracture of the first kind which is propagated while the force increases slowly. This fracture is terminated, apparently by unfavourably oriented crystals and the load increases again at a rapid rate. At the higher load, a new fracture system of the second kind appears and is propagated into one of the loading arms. This event is accompanied by a rapid fall in load. Thereafter the force remains rather constant and after some distance falls suddenly to a low value. One would expect the load to fall to zero as the fracture passes through the loading arm. Instead, the load remains constant. One concludes that much of the energy absorbed at constant load goes into bending the specimen.

Specimen No. 7 is also of interest in this respect for in this case bending can be checked readily. It is found that bending will account for a displacement equivalent to about 300 degrees of rotation of the loading screw. It was also ascertained that this bending was concentrated into the centre of the specimen.

If it is assumed that Specimen 8 behaved in a similar manner until the fracture turned into the loading arm, then the narrow fracture extends over about 400 degrees of loading screw rotation. The load minimum at 450 degrees in Figure 5.58 tends to support this. If it is assumed that during propagation in the narrow zone, about half of the energy was absorbed by bending the loading arms, then since the area to the left of the 450 degree ordinate bears the same ratio to the remaining area of the plot as the narrow fracture area bears to the loading arm fracture area, the proportion of energy absorbed in large scale deformation in the wide fracture is the same, namely about 50% goes into large scale bending, and the remainder is associated with the fracture mechanism.

The force-displacement plot that corresponds most closely to the "ideal" plot of Figure 5.410 is that of Specimen 12. As may be seen from Figure 5.50, the fracture entered the loading arm immediately at a sharp corner. The initial load increase corresponds probably to a widening of the fracture. The load reaches a peak and falls off smoothly to a steady, non-zero value. It is tempting to ascribe the shape of the plot between angles 300 and 700 degrees to bending although no evidence of such bending can be detected.

5.2.8.4.4.5 Transition of Fracture from a Narrow to a Wide Zone

It was pointed out previously that the narrow fracture was devoid of surfaces similar to fractures of the first kind.

Examination of the polycrystalline specimens of Batch 2 especially shows that basal fracture surfaces are always elongated towards the centre of the specimen.

Under the relatively rapid cooling during which these specimens were formed crystals can be expected to grow from the outside towards the centre. It appears that maximum rate of growth for zinc crystals is in a direction lying in the basal plane, so that the narrow fracture zones of Specimens 7 and 8 were simply devoid of suitably oriented basal planes. This also explains why the fracture turned so readily into the loading arms.

The specimens of Batch 1 however were grown more slowly and the direction of growth would be along the axes of the specimens. Consequently one would expect suitably oriented basal planes in the intended fracture plane. This is indeed so, as an examination of specimens of coarse grain structure such as Nos. 1, 2 and 4 shows. Yet the fracture still turned into the loading arms from basal to non-basal fracture.

This indicates that the fracture is propagated

more readily in a zone whose dimensions exceed those of the crystal (an argument that can not apply to Specimen 4, however.).

It is suggested that when a fracture passes through a crystal in the leading arm, the crystals adjacent to it limit its deformation and so reduce the energy absorbed. Also, crystals which fracture with difficulty tend to be isolated so that they carry an increasing share of the load and finally fail.

Because of this isolating process crystals which require a higher stress to fracture can be subjected to a higher stress without subjecting the remainder of the specimen to higher stress, which might lead to large-scale deformation. This mechanism also reduces the energy associated with wide fractures.

The marked tendency of the fracture to turn into the leading arms is therefore explained.

5.2.3.4.4.6 The Transfer of Fracture from one Crystal to Another

When the fracture passes from one crystal to another the surface markings and the inclination of the fracture surface change abruptly. This behaviour is consistent with the idea, implied by the hypothesis, that

fracture is a function of the relative orientation of the applied stress and the crystal lattice. There is nothing in the appearance of the photographs or of the specimens under the microscope to suggest that fracture mechanisms such as cracks cross the intercrystalline boundary.

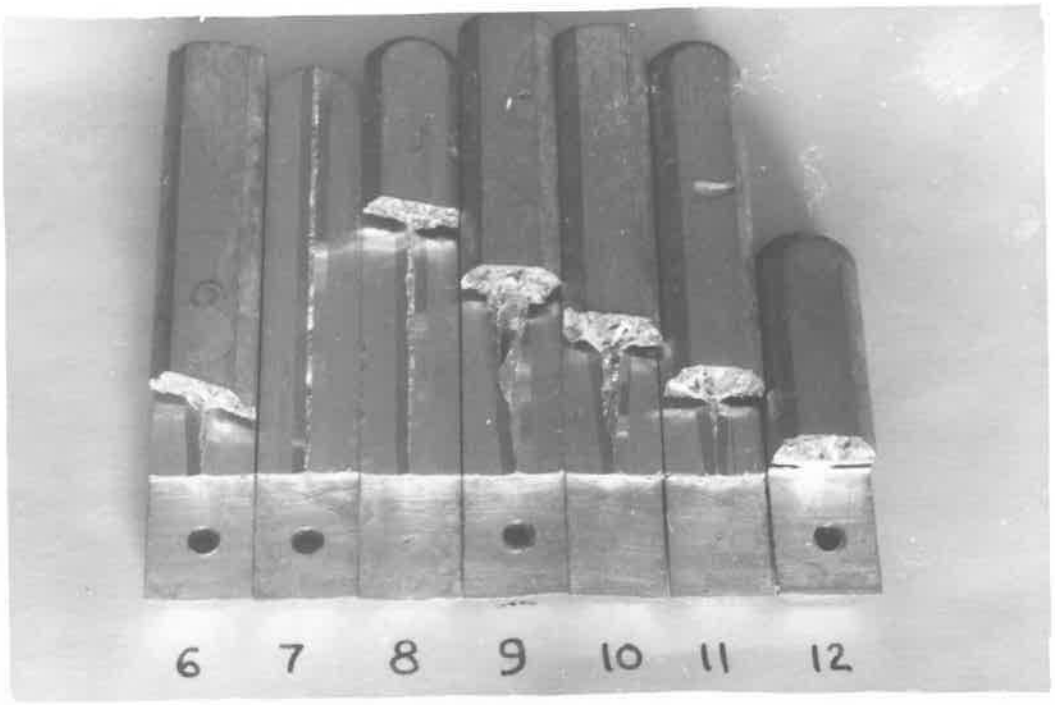

FIG. 5.50 THE FRACTURE SURFACES AND MODE OF FAILURE OF THE ZINC SPECIMENS, BATCH 2.

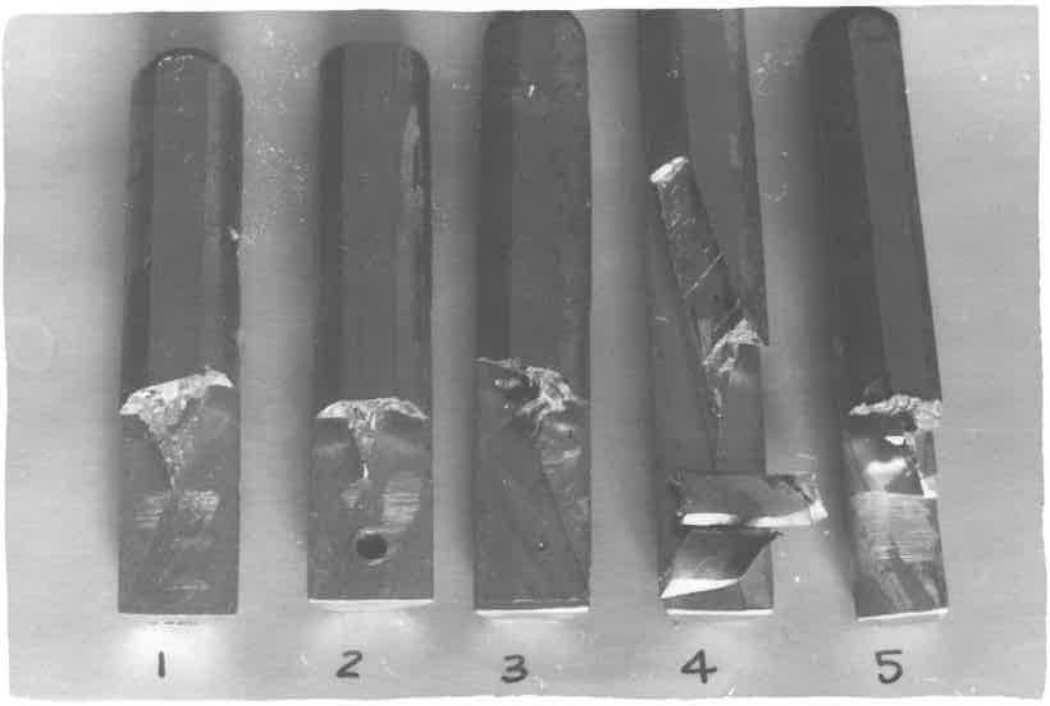

FIG. 5.49 THE FRACTURE SURFACE AND MODE OF FAILURE OF THE ZINC SPECIMENS, BATCH 1.

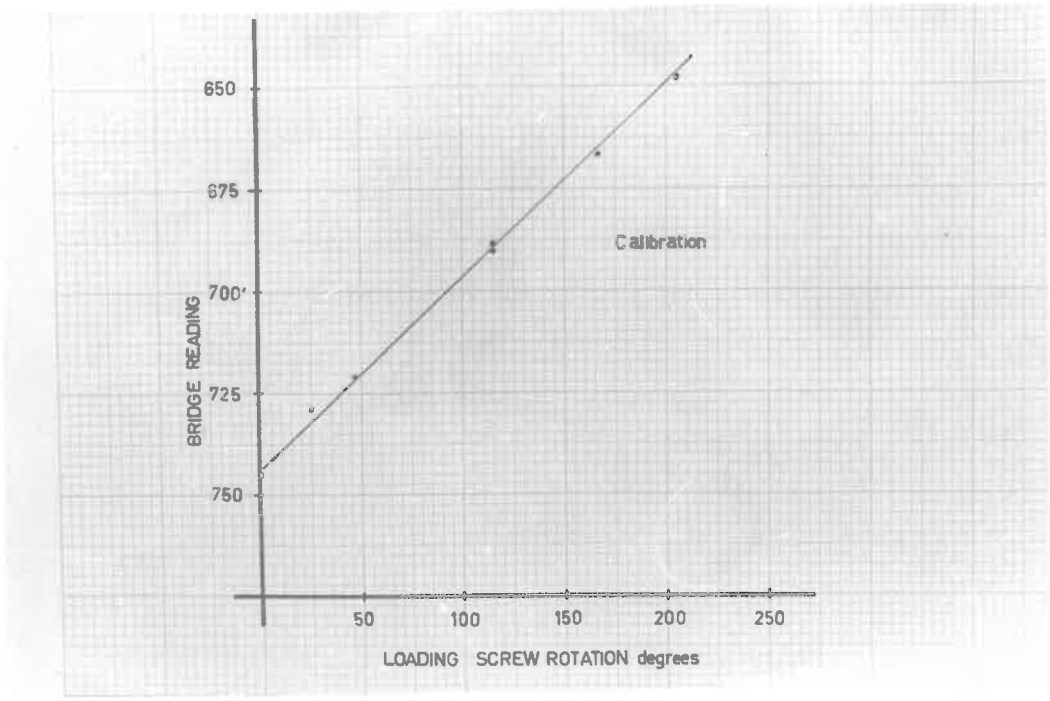

CALIBRATION PERFORMED DURING TESTS ON ZINC.

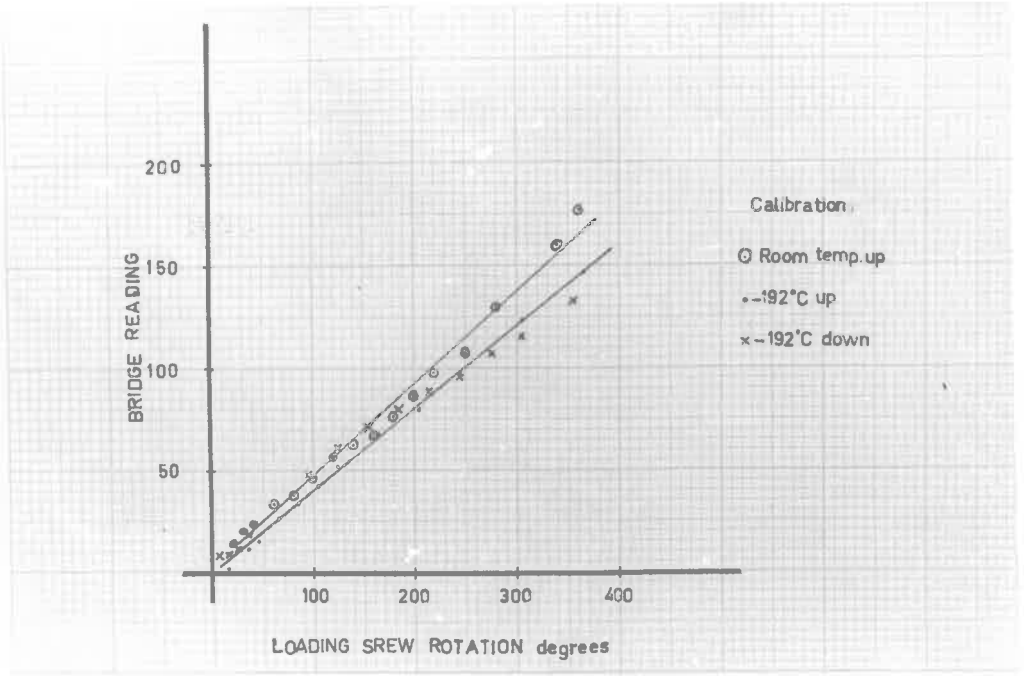

COMPARISON OF ROOM TEMPERATURE AND LOW TEMPERATURE CURVES.

FIG. 5.42 CALIBRATION CURVES.

FIGURES 5.51 TO 5.62

THE LOAD-DISPLACEMENT PLOTS FOR THE ZINC SPECIMENS 1-12, TESTED AT -196°C.

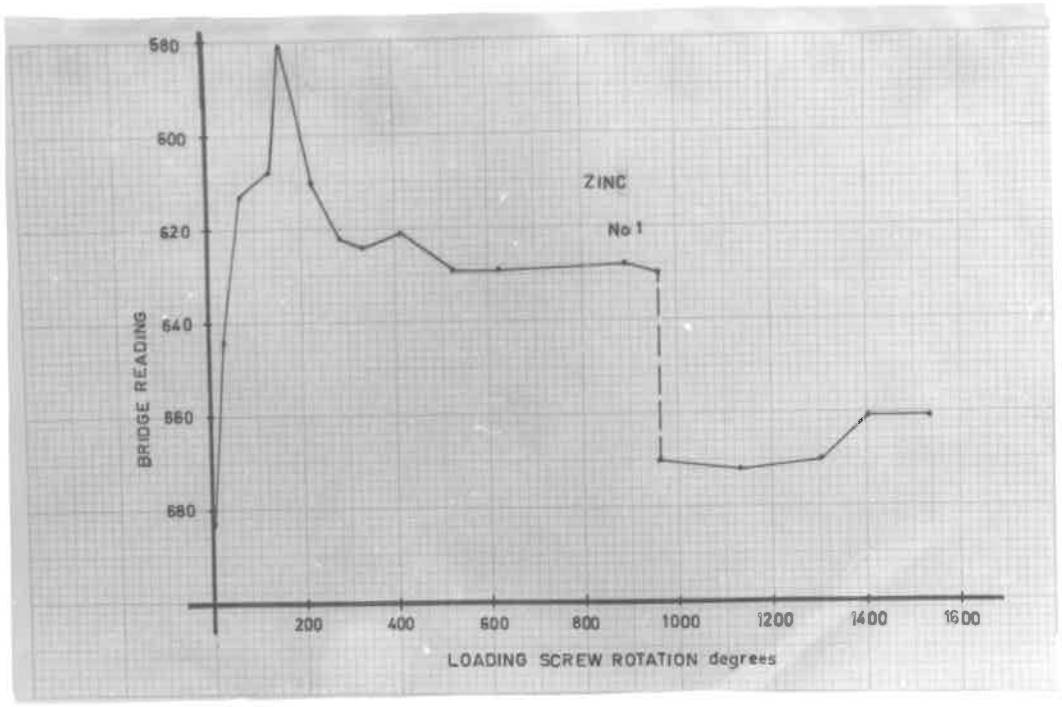

FIGURE 5.51.

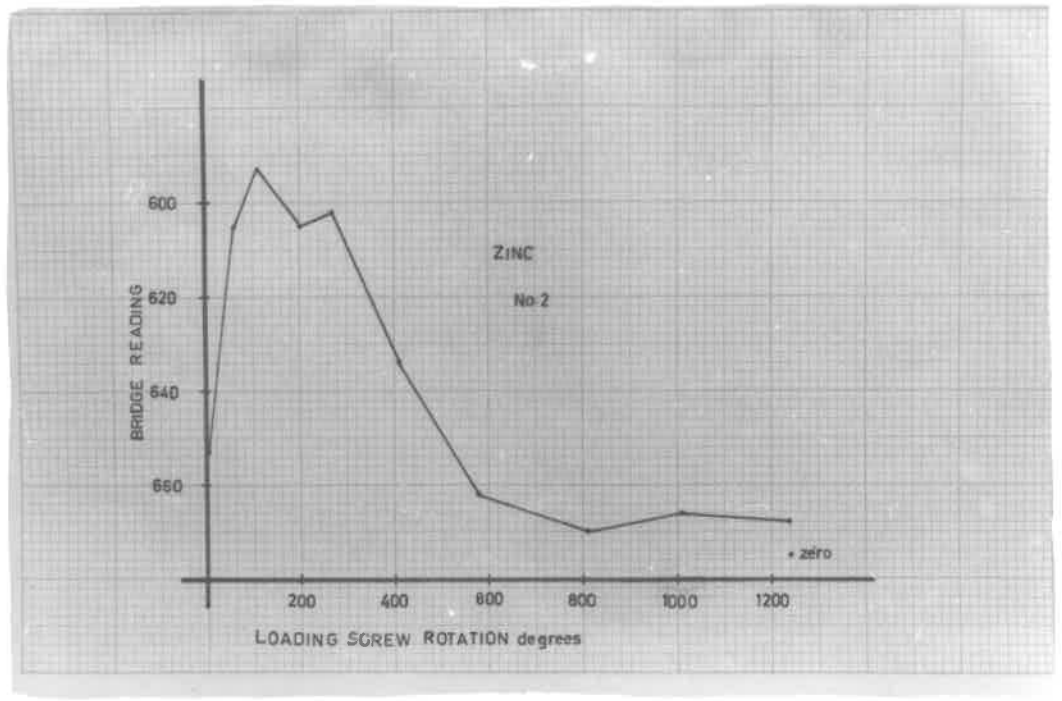

FIGURE 5.52.

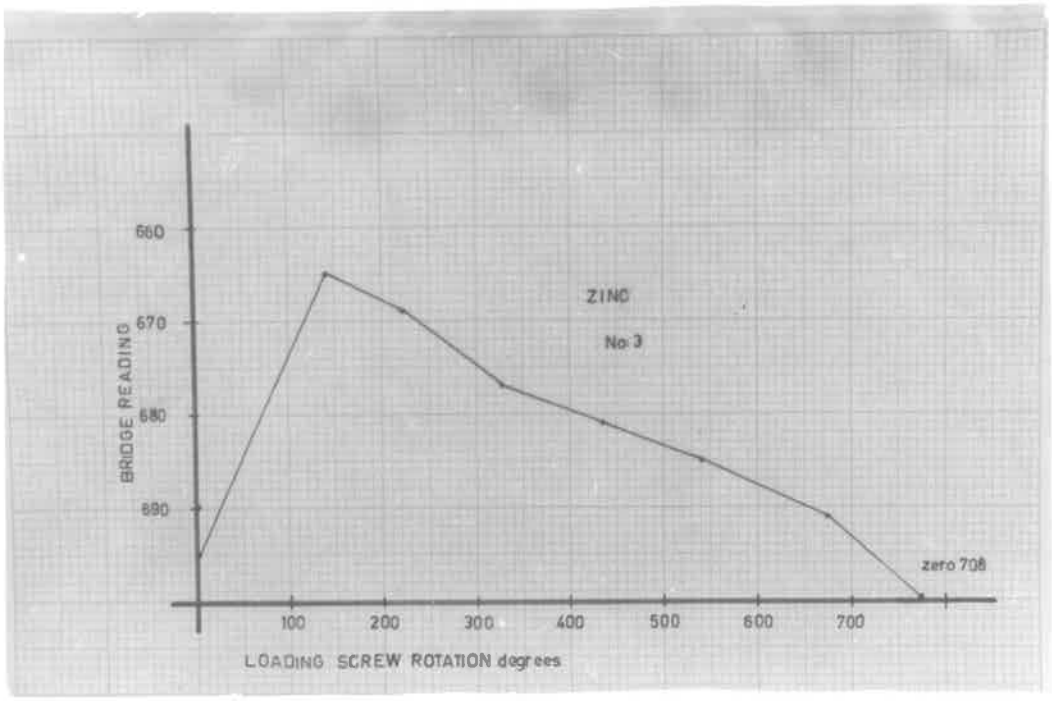

FIGURE 5.53.

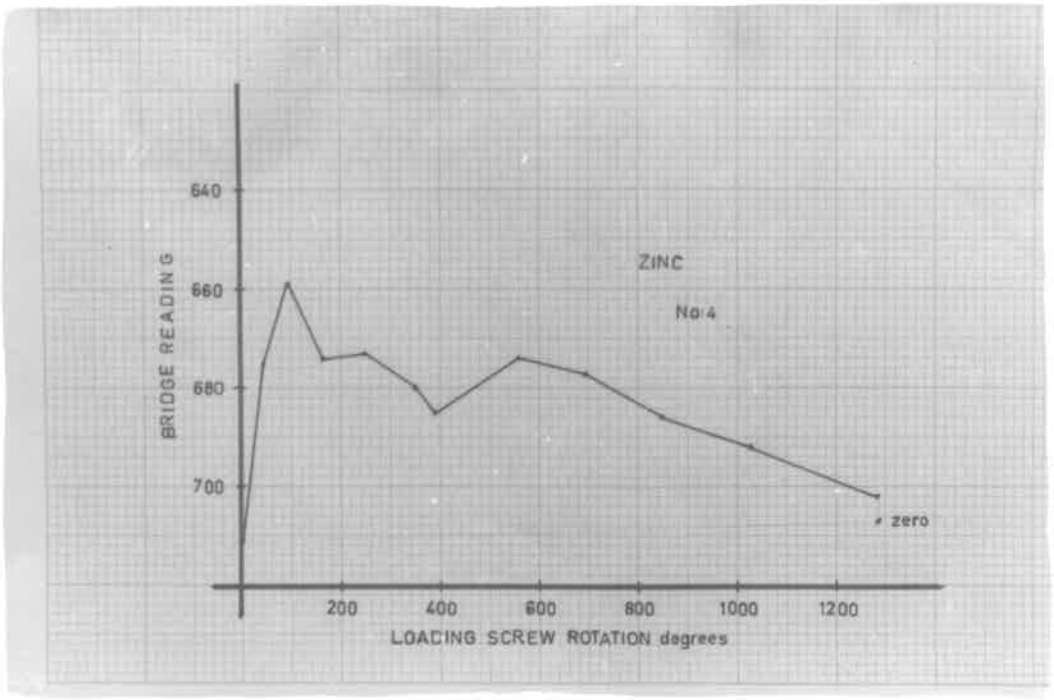

FIGURE 5.54.

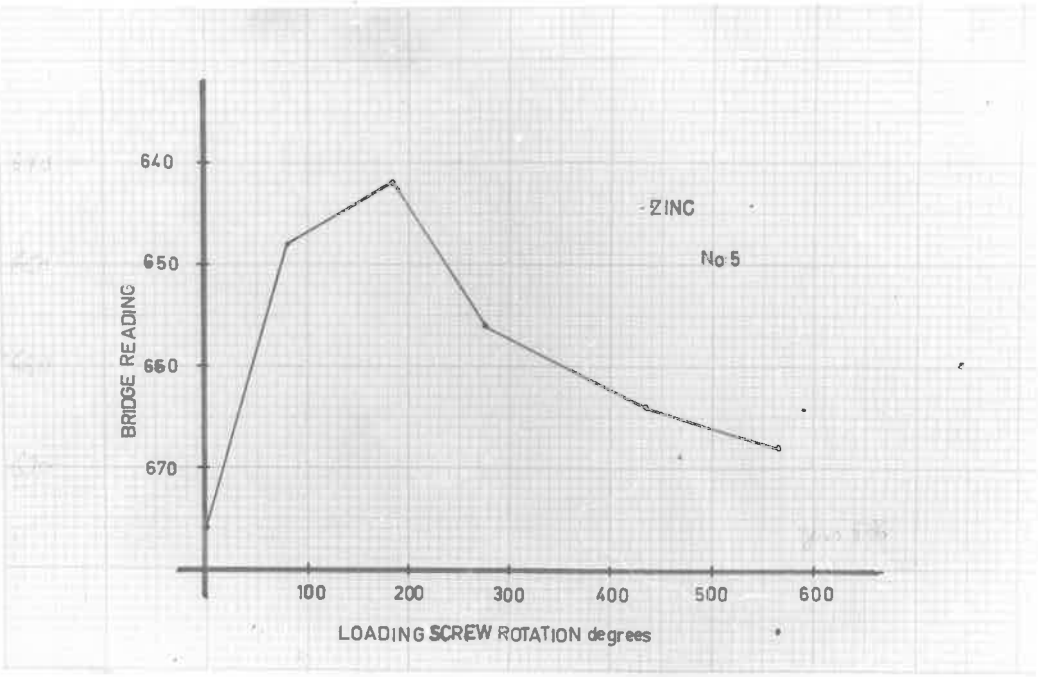

FIGURE 5.55.

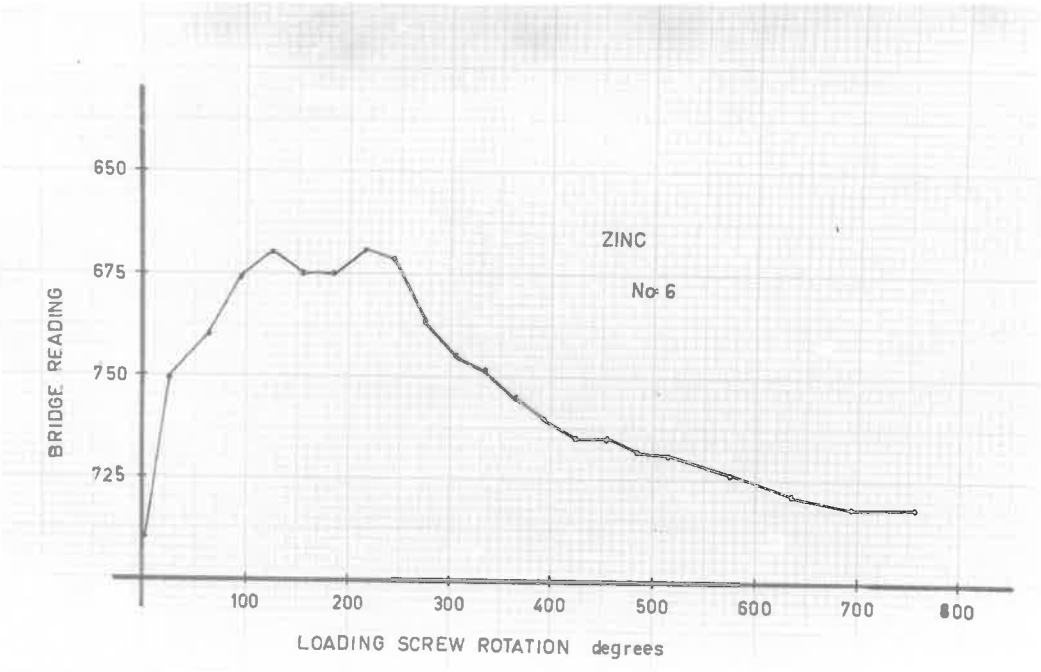

FIGURE 5.56.

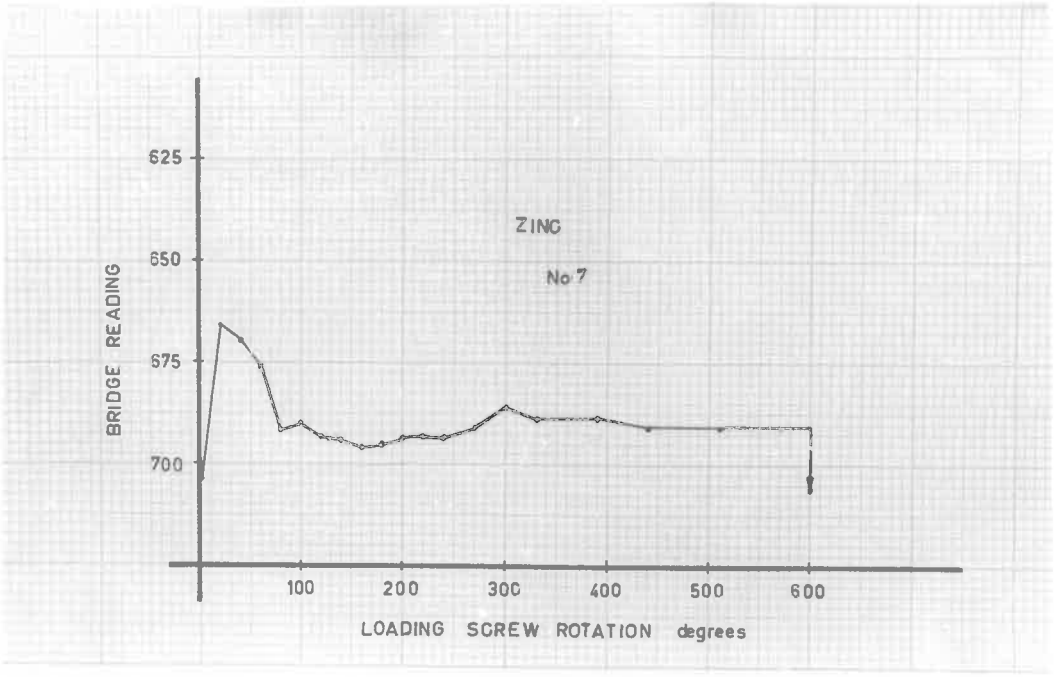

FIGURE 5.57.

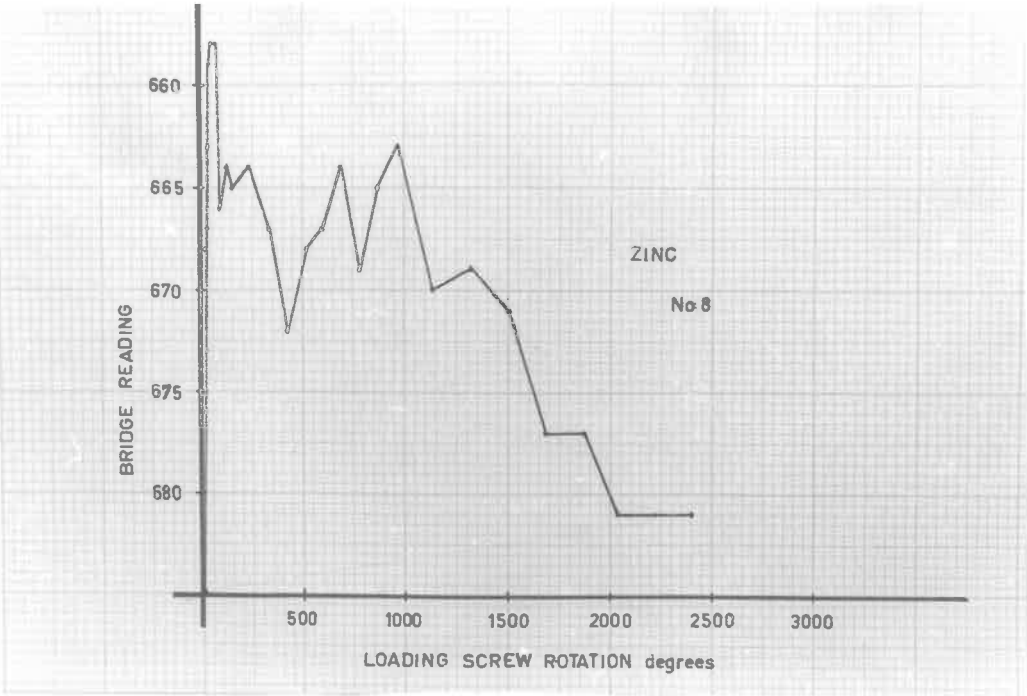

FIGURE 5.58.

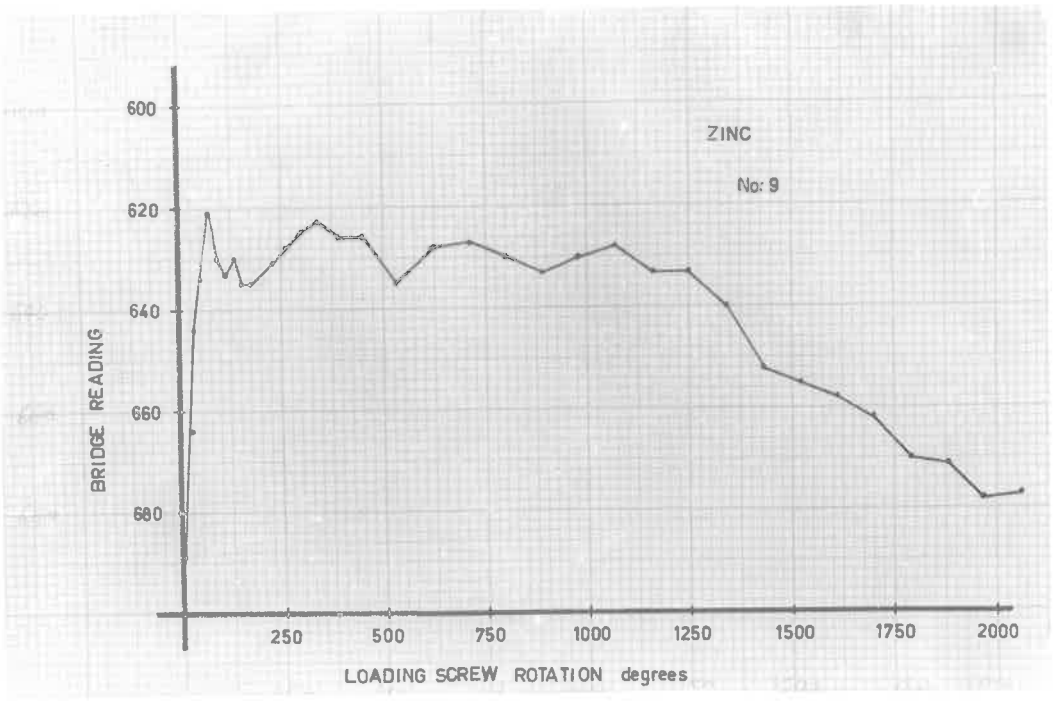

FIGURE 5.59.

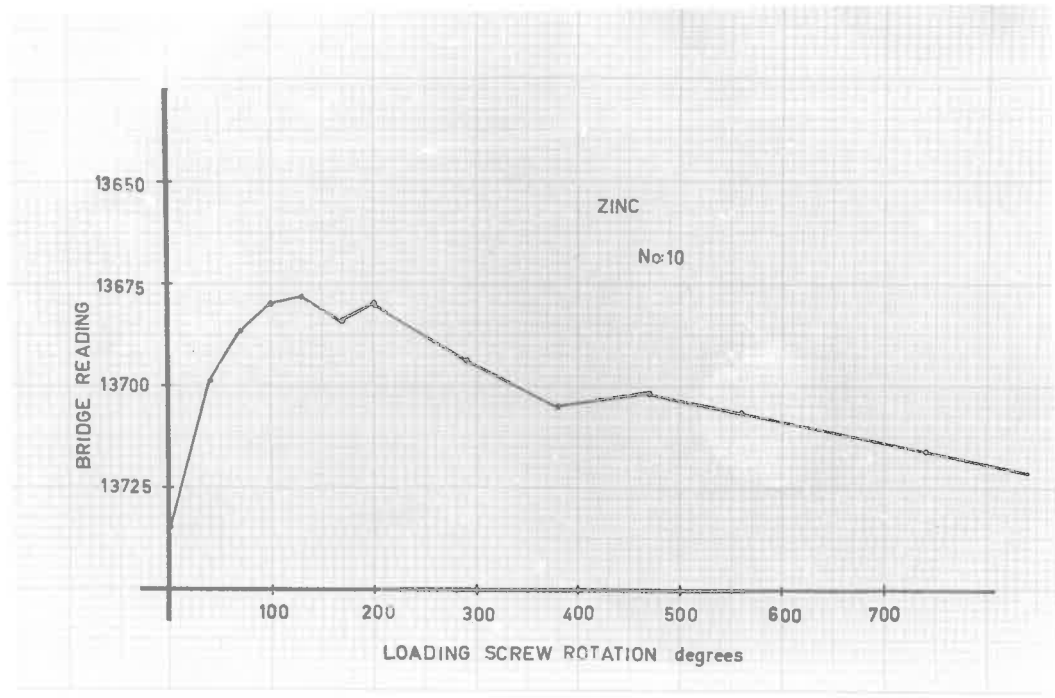

FIGURE 5.60.

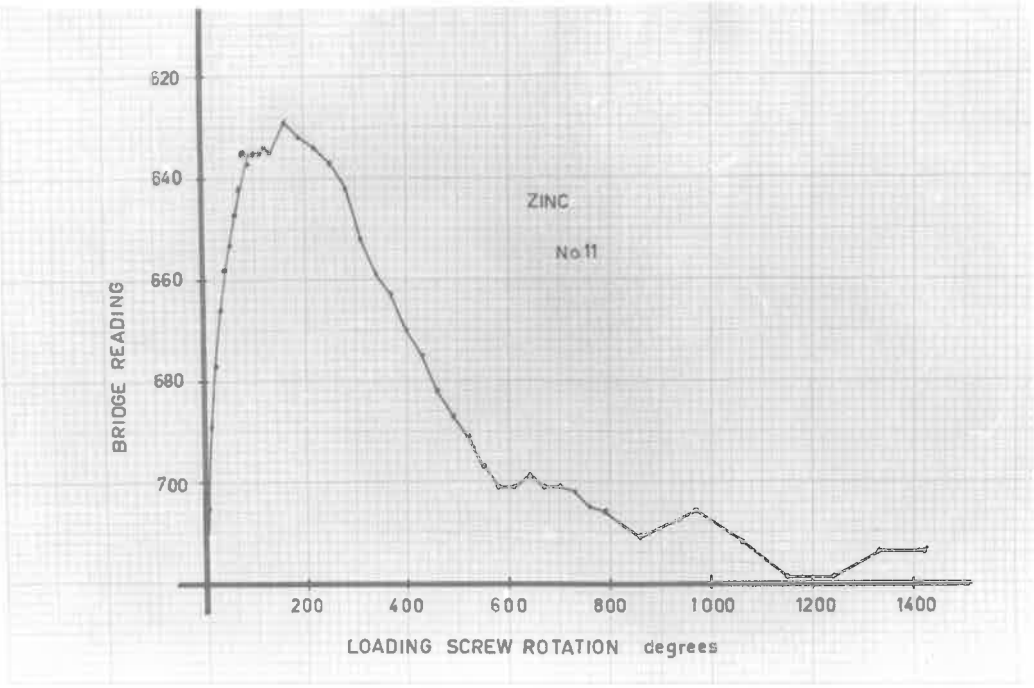

FIGURE 5.61.

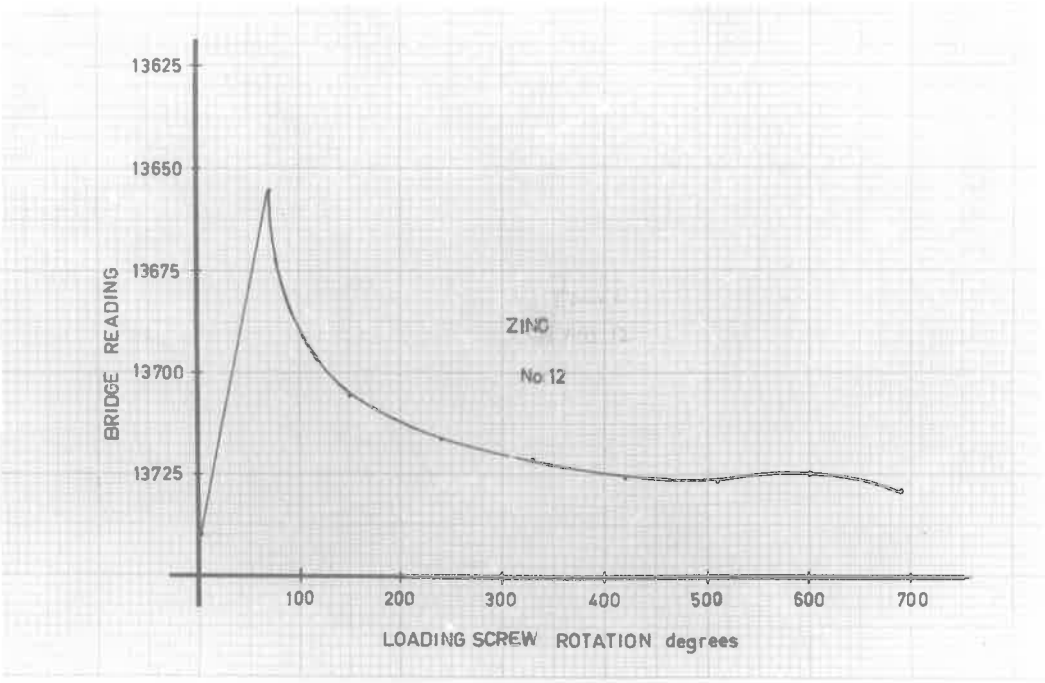

FIGURE 5.62.

FIG. 5.63 PHOTOGRAPH, FRACTURE SURFACE OF SPECIMEN 1 TAKEN IN DAYLIGHT (8X).

FIG. 5.64 PHOTOGRAPH, FRACTURE SURFACE OF SPECIMEN 2 TAKEN IN DAYLIGHT (8x).

FIG. 5.65 MICROGRAPH, UPPER LEFT OF FRACTURE OF SPECIMEN 2. (75x)

FIG. 5.66 PHOTOGRAPH, FRACTURE SURFACE OF SPECIMEN 3 TAKEN IN DAYLIGHT (8x).

FIGURE 6.63.

FIGURE 5.64.

FIGURE 5.65.

FIGURE 5.66.

FIG. 5.67 MICROGRAPH. A FILAMENT FROM A FRACTURE SURFACE OF THE SECOND KIND, SPECIMEN 3 (75x).

FIG. 5.68 PHOTOGRAPH. PORTION OF THE MAIN FRACTURE SURFACE OF SPECIMEN4, TAKEN IN DAYLIGHT (8x).

FIG. 5.69 PORTION OF THE MAIN FRACTURE SURFACE OF SPECIMEN 4, TAKEN IN DAYLIGHT (8x).

FIG. 5.70 MICROGRAPH. FRACTURE OF THE SECOND KIND FROM A FRAGMENT OF SPECIMEN 4 (75x).

FIGURE 5.67.

FIGURE 5.68.

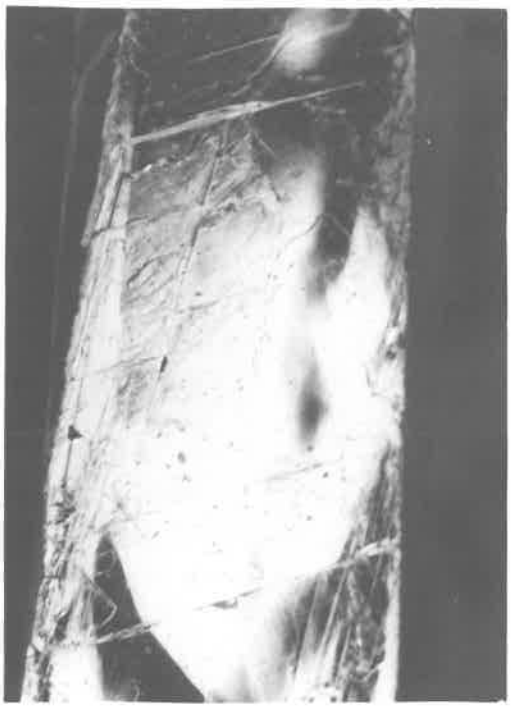

FIGURE 5.69.

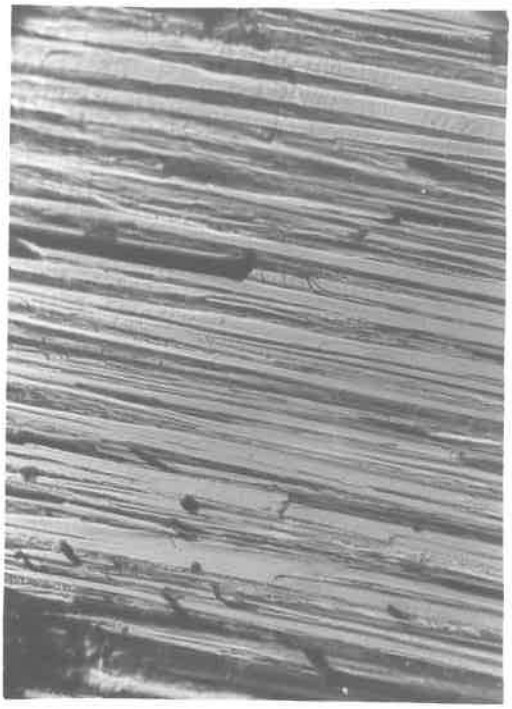

FIGURE 5.70.

FIG. 5.71 PHOTOGRAPH. THE WHOLE OF THE BASAL FRACTURE SURFACE ON SPECIMEN 4, AS SEEN UNDER HIGHLY DIRECTIONAL LIGHT (8x).

FIGURE 5.71.

FIG 5.72 PHOTOGRAPH. FRACTURE SURFACE OF SPECIMEN 5 TAKEN IN DAYLIGHT (8x).
NOTE SECONDARY FRACTURES.

FIG 5.73 PHOTOGRAPH. ANOTHER VIEW OF THE FRACTURE SURFACE OF SPECIMEN 5. Single LAMP ILLUMINATION (8x).
NOTE BASAL CLEAVAGE IN NARROW SECTION.

FIG. 5.74 PHOTOGRAPH. FRACTURE SURFACE OF SPECIMEN 6, TAKEN IN DAYLIGHT (8x).

FIG. 5.75 PHOTOGRAPH. NARROW FRACTURE ZONE OF SPECIMEN 6. SINGLE LAMP ILLUMINATION (8x).

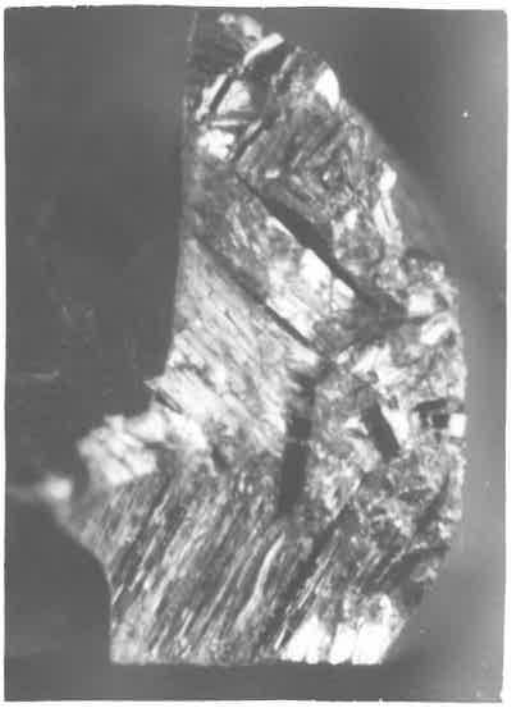

FIGURE 5.72.

FIGURE 5.73.

FIGURE 5.74.

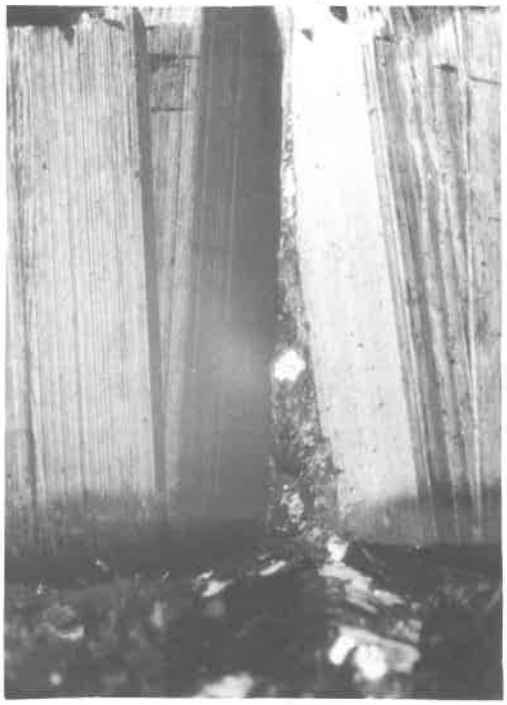

FIGURE 5.75.

FIG. 5.76 PHOTOGRAPH. PORTION OF FRACTURE SURFACE OF SPECIMEN 7 (8x).

FIG. 5.77 PHOTOGRAPH. PORTION OF FRACTURE SURFACE OF SPECIMEN 7, (8x).

FIG. 5.78 MICROGRAPH. FRACTURE SURFACE OF SPECIMEN 7 SHOWING FRACTURE OF THE SECOND KIND, (75x).

FIG. 5.79 MICROGRAPH. FRACTURE SURFACE OF SPECIMEN 7 SHOWING A FRACTURE SURFACE OF THE SECOND KIND, (80x).

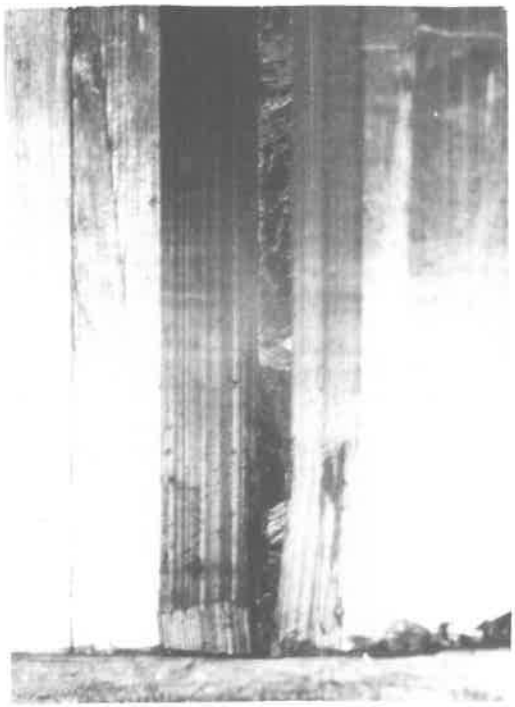

FIGURE 5.76.

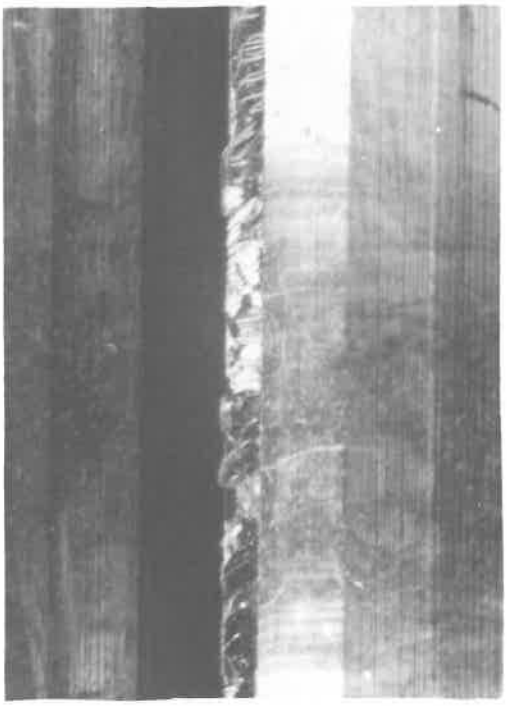

FIGURE 5.77.

FIGURE 5.78.

FIGURE 5.79.

FIG. 5.80 PHOTOGRAPH. FRACTURE SURFACE OF SPECIMEN 8, TAKEN IN DAYLIGHT (8x).

FIG. 5.81 PHOTOGRAPH. NARROW FRACTURE SURFACE ON SPECIMEN 8. ILLUMINATED WITH A SINGLE LAMP (8x).

FIG. 5.82 MICROGRAPH. FRACTURE SURFACE OF THE FIRST KIND, SPECIMEN 8, (75x).

FIG. 5.83 MICROGRAPH. FRACTURE SURFACE OF THE FIRST KIND. PORTION OF THE CLEAVAGE SURFACE PRESENTED IN FIGURE 5.82 (75x).

FIGURE 5.80.

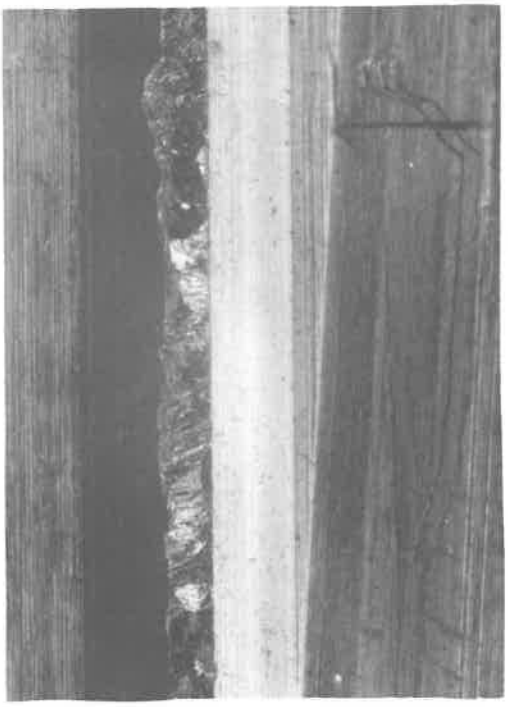

FIGURE 5.81.

FIGURE 5.82.

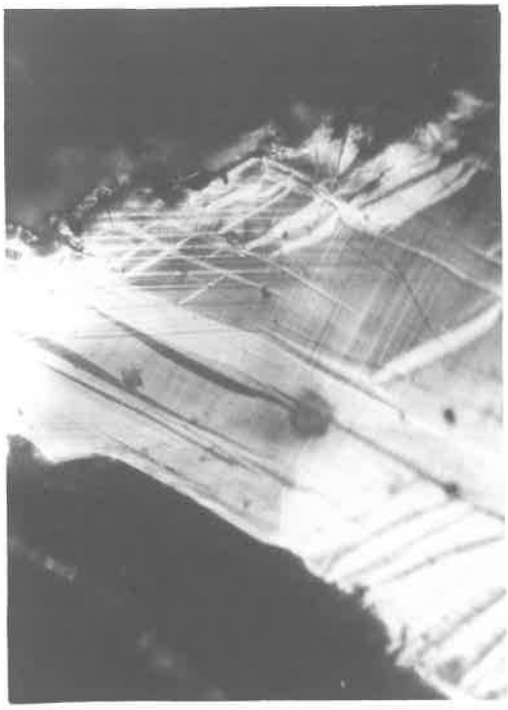

FIGURE 5.83.

FIG. 5.84 MICROGRAPH. FRACTURE OF THE SECOND KIND FROM THE FRAGMENT OF SPECIMEN 8 (75x).

FIG. 5.85 MICROGRAPH. FRACTURE SURFACE OF THE SECOND KIND FROM THE NARROW FRACTURE ON THE FRAGMENT OF SPECIMEN 8 (75x).

FIG. 5.86 MICROGRAPH. FRACTURE OF THE SECOND KIND FROM THE NARROW FRACTURE SURFACE ON THE FRAGMENT OF SPECIMEN 8 (75x).

FIG. 5.87 MICROGRAPH. FRACTURE OF THE SECOND KIND FROM THE NARROW FRACTURE SURFACE ON THE FRAGMENT OF SPECIMEN 8 (75x).

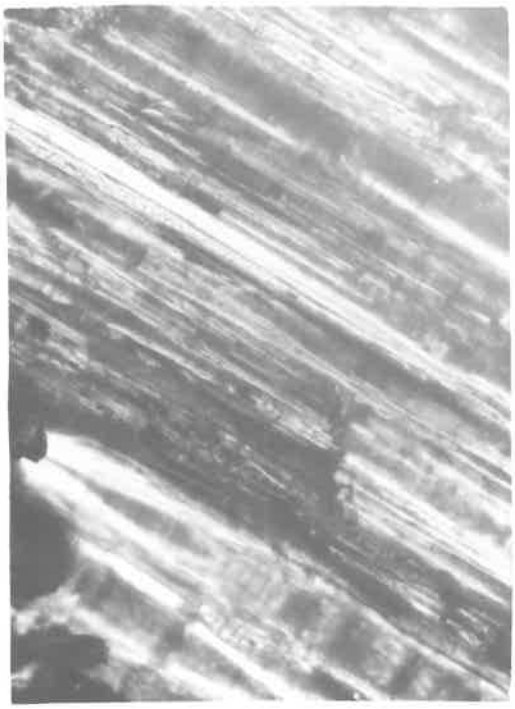

FIGURE 5.84.

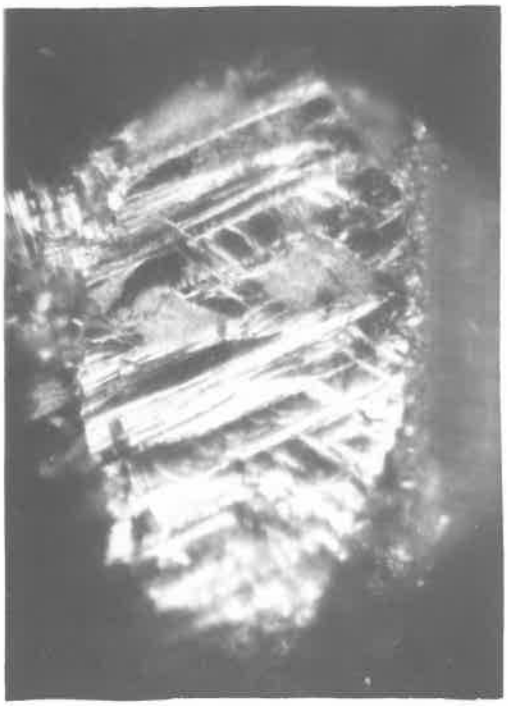

FIGURE 5.85.

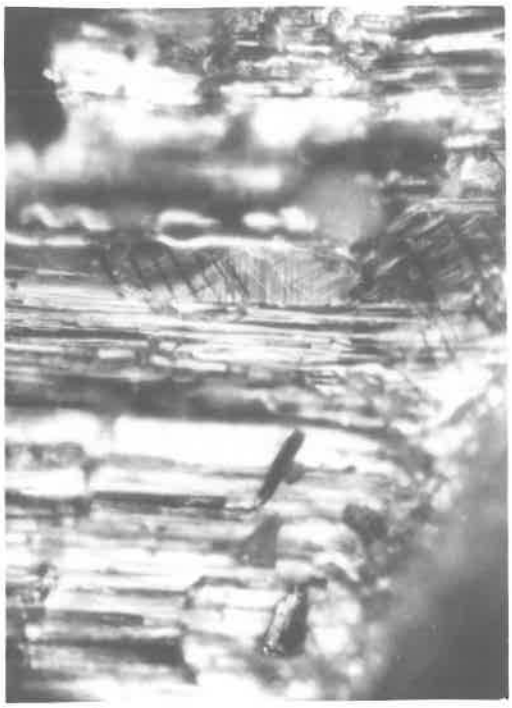

FIGURE 5.86.

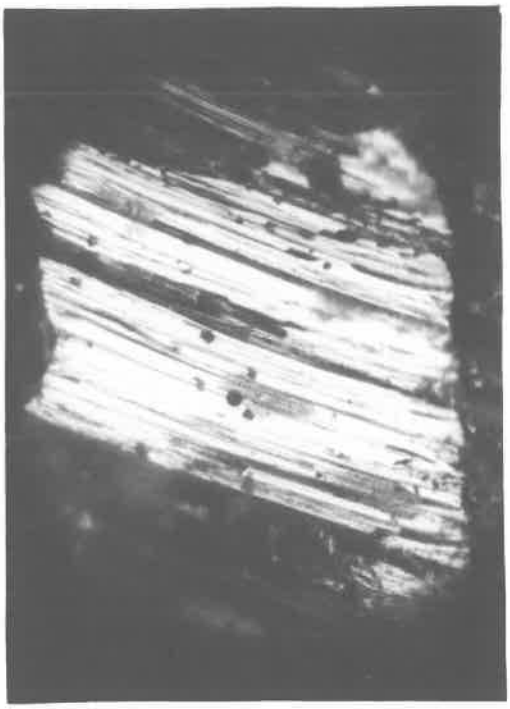

FIGURE 5.87.

FIG. 5.88 MICROGRAPH, FRACTURE OF THE FIRST KIND. LOADING ARM FRACTURE SURFACE ON THE MAGNET OF SPECIMEN 8 (75x).

FIG. 5.89 MICROGRAPH. ANOTHER VIEW OF THE AREA SHOWN IN FIGURE 5.88. (75x).

FIG. 5.90 MICROGRAPH. ANOTHER PORTION OF THE FRACTURE SURFACE SHOWN IN FIGURE 5.88, (75x).

FIG. 5.91 MICROGRAPH. FRACTURE OF THE FIRST KIND. LOADING ARM FRACTURE SURFACE OF SPECIMEN 8, (75x).

FIGURE 5.88

FIGURE 5.89.

FIGURE 5.90.

FIGURE 5.91.

FIG. 5.92 MICROGRAPH. SECONDARY FRACTURE OPENING. LOADING ARM FRACTURE SURFACE ON THE FRAGMENT OF SPECIMEN 8, (75x).

FIG. 5.93 PHOTOGRAPH. FRACTURE SURFACE OF SPECIMEN 9, TAKEN IN DAYLIGHT, (8x).

FIG. 5.94 PHOTOGRAPH. NARROW FRACTURE SURFACE ON SPECIMEN 10, (8x).

FIG. 5.95 PHOTOGRAPH. LOADING ARM FRACTURE SURFACE ON SPECIMEN 10, (8x).

FIGURE 5.92.

FIGURE 5.93.

FIGURE 5.96.

FIGURE 5.95.

FIG. 5.94 PHOTOGRAPH. NARROW FRACTURE SURFACE ON SPECIMEN 9. NOTE PREDOMINANCE OF BASAL FRACTURE SURFACES. (8x).

FIG. 5.97 PHOTOGRAPH. LOADING ARM FRACTURE SURFACE ON SPECIMEN 11, (8x).

FIG. 5.98 PHOTOGRAPH. NARROW FRACTURE SURFACE ON SPECIMEN 11, (8x).

FIG. 5.99 MICROGRAPH. BASAL PLANE FRACTURE SURFACE ON SPECIMEN 11. NOTE CONCENTRATION OF SLIP LINE MARKINGS NEAR GRAIN BOUNDARY. (75x).

FIGURE 5.94.

FIGURE 5.97.

FIGURE 5.98.

FIGURE 5.99.

FIG. 5.100 MICROGRAPH. BASAL PLANE FRACTURE ON SPECIMEN 11. NOTE DISCONTINUOUS CLEAVAGE STEP MARKING. (75x).

FIG. 5.101 PHOTOGRAPH. FRACTURE SURFACE OF SPECIMEN 12. (8x).

FIG. 5.102 MICROGRAPH. FRACTURE OF THE FIRST KIND ON THE FRAGMENT OF SPECIMEN 12, (75x).

FIG. 5.103 MICROGRAPH. FRACTURE OF THE SECOND KIND ON THE FRAGMENT OF SPECIMEN 12, (75x).

FIGURE 5.100.

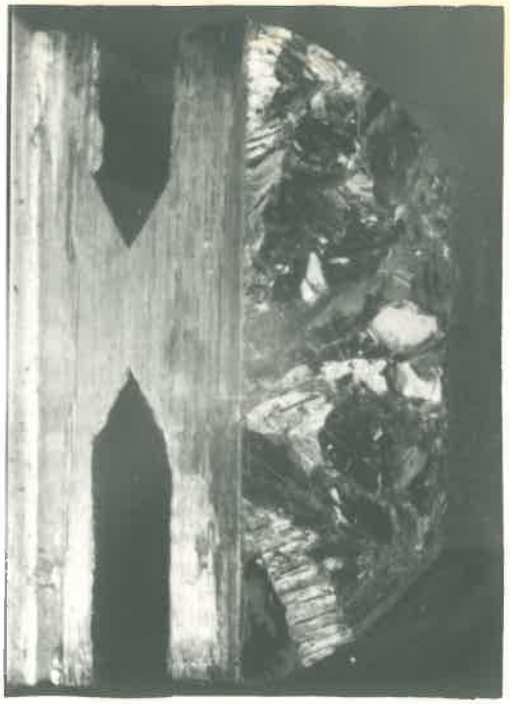

FIGURE 5.101.

FIGURE 5.102.

FIGURE 5.103.

5.2.6.3 Bismuth

Experience with zinc has shown that the technique which works well for steel is less suitable for a material such as zinc. All but one of the zinc specimens fractured through one of the loading arms.

The bismuth specimens were shaped and loaded in such a way as to encourage fracture through the body of the specimens in a direction normal to the longitudinal axis.

An ideally brittle material would fracture in a single uncontrolled process if prepared and loaded in this way. The steel specimens would have behaved similarly, but bismuth was expected to exhibit a controlled fracture process under these circumstances.

The fracture was expected to emerge at the sides of the specimens so that observation of the progress of the fracture would be possible. Some of the specimens were therefore prepared for visual observation of the fracture process.

5.2.6.3.1 Preparation of the Specimens

The bismuth was obtained from a chemical supplier

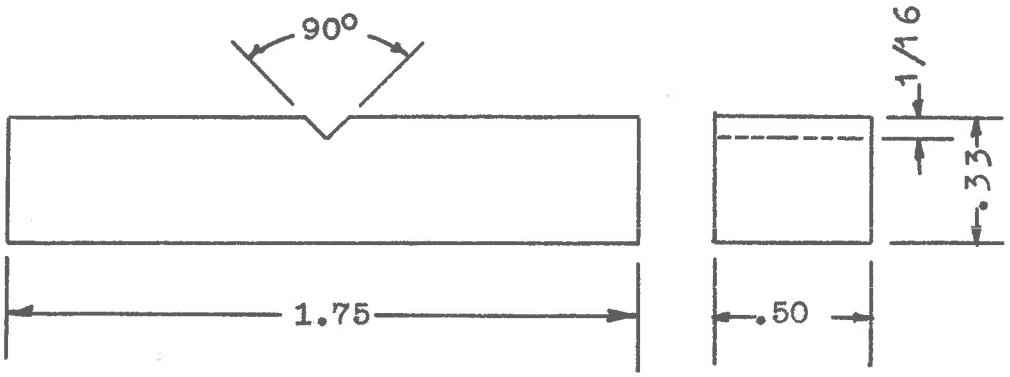

FIG. 5.112 The Dimensions of the Bismuth Specimens.

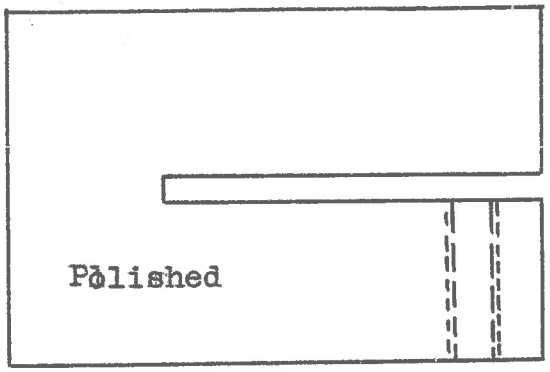

FIG. 5.114 The Preparation of the Specimens 6_a and 6_b for viual Observation of the Fracture Process.

in granulated form, but with unknown impurity content. The results of a subsequent chemical analysis are given in Table 5.10.

The metal was melted down in a mild steel crucible and cast into a rectangular mild steel mould. No effort was made to obtain single crystals. Some degree of control over the cooling rate and therefore the crystal size could be exercised by varying the degree of preheat given to the mould. This preheat was varied from full, i.e. above the melting point of bismuth (269°C), which gave the lowest cooling rate, to lesser values.

Ten specimens in all were cut. Of these specimens 1-5 were to be tested under liquid nitrogen. For them only one stage of preparation remained, which was the machining of a 90° groove across a wide face at the middle of the specimen. A fully prepared specimen of this kind is presented in Figure 5.11a.

Specimen 6 was cut into two equal parts and prepared as shown in Figure 5.11b. These were labelled specimens 6a and 6b. They were polished on each side, so as to reveal the surface events associated with the fracture most readily.

Specimens 7, 9 and 10 were prepared in the same

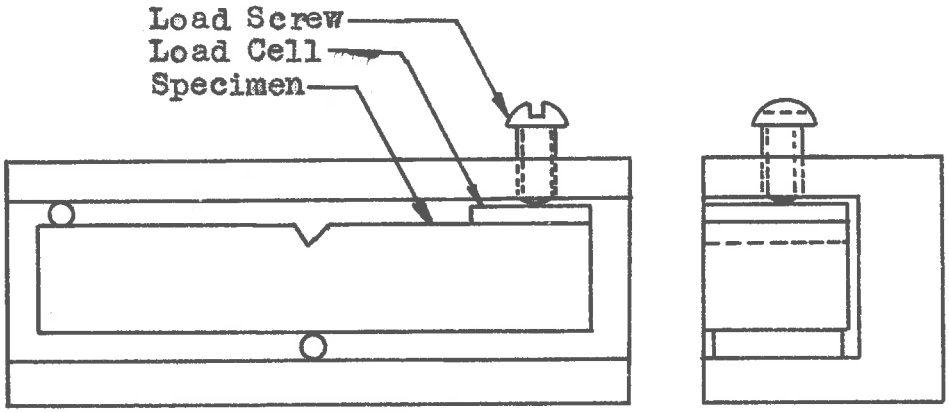

FIG. 5.113 The Loading Rig for the Bismuth Specimens.

manner as specimens 1-5, and were polished on each side.

Specimen 8 was to be tested at room temperature and was prepared in the same way as Nos. 1-5.

5.2.8.5.8 Procedure

A special loading rig was prepared and is presented in Figure 5.113. It is apparent that the maximum bending moment is applied at the centre of the specimen, and the maximum tensile stress at the notch root.

The loading force is applied by the loading screw, the force being transmitted through a force cell which supplies the force measurement. The distance measurement appears as a reading of the loading screw rotation.

The stiffness of the rig, which can be ascertained readily is much greater than that of the specimens, but is not negligible. However if, as is the case here, the load falls steadily towards zero, the stored-up elastic energy in the rig as well as the specimen being tested becomes negligibly small.

Specimens 1-5 were tested under liquid nitrogen in this loading rig.

Specimen 8 was tested at room temperature, and the readings recorded.

Specimens 6a and 6b were fastened onto a metallurgical microscope, and the surface events associated with the fracture process were observed. Specimen 6b was subsequently etched on one side.

Specimen 7, 9 and 10 were mounted in the loading rig, which was then fastened onto the object table of a metallurgical microscope. The surface events associated with the fracturing of these specimens was also observed. No readings of loading force and loading screw rotation were taken.

5.2.8.3.3 Results

These are presented under three headings in accordance with the threefold purpose of this series of tests.

5.2.8.3.3.1 The Surface Energy and Load-displacement Plots

The load and angle measurements were reduced and plotted. The plots so obtained are presented in Figures 5.115 to 5.120. From these the behaviour of specimens 1-5 can be compared with each other and with specimen 8, which was tested at room temperature.

The load displacement plots for the specimens fractured at low temperature show no discontinuities. The room temperature specimen, however, shows several small and one large discontinuity.

TABLE 5.10 Chemical Analysis of Bismuth

Impurity	Fe	Ag	Pb	Cu
Specimen 1	trace	small trace	small trace	less than 10p.p.m.
Specimen 9	trace	small trace	none	less than 10 p.p.m.
Total Impurities by weight less than 0.01%.				

TABLE 5.11 Surface Energy Associated with Bismuth Fracture

Specimen No.	Area of Load Plot $in.^2$	Energy absorbed by Fracture lb.in.	Area of Fracture Surfaces $in.^2$	Nominal Surface Energy $lb.in/in.^2$	Peak load units	Total loading screw rotation degrees	No. of crystal on fract. face
1	6.63	.428	0.28	1.53	80	500	4
2	3.17	.229	0.29	0.78	58	225	22
3	4.66	.335	0.29	1.15 (.86)	60	320 (500)	16
4	2.88	.207	0.29	0.72	58	340	18
5	5.00	.360	0.28	1.29	66	440	11
8	5.43	1.956	0.28	7.00	155	860	20

The factor for converting the area under the load-distance plots for specimens 1-5 is 0.072 lb.in. per sq.in. and for No. 8 0.36 lb.in. per sq.in. They are derived as previously.

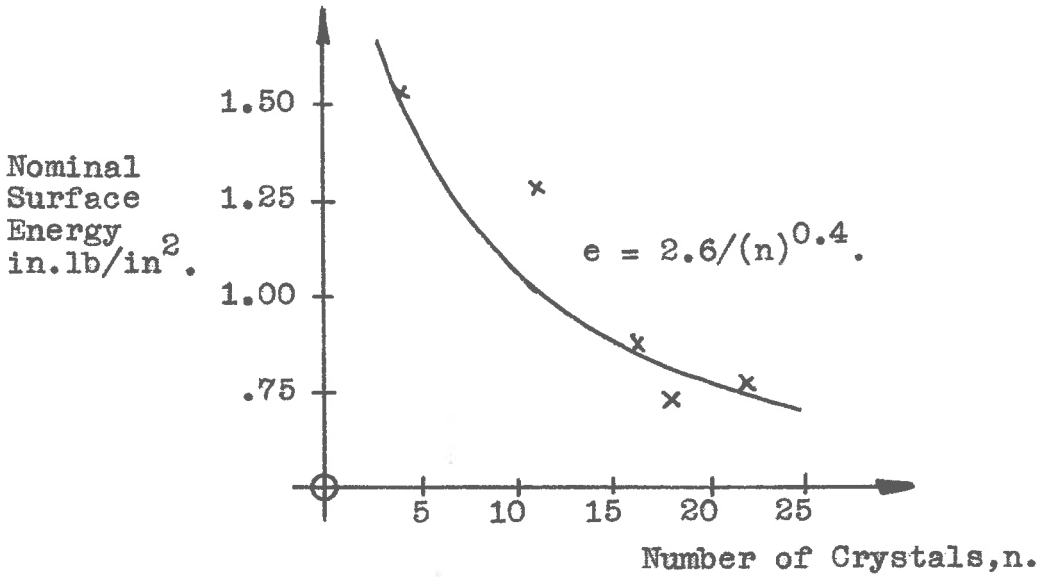

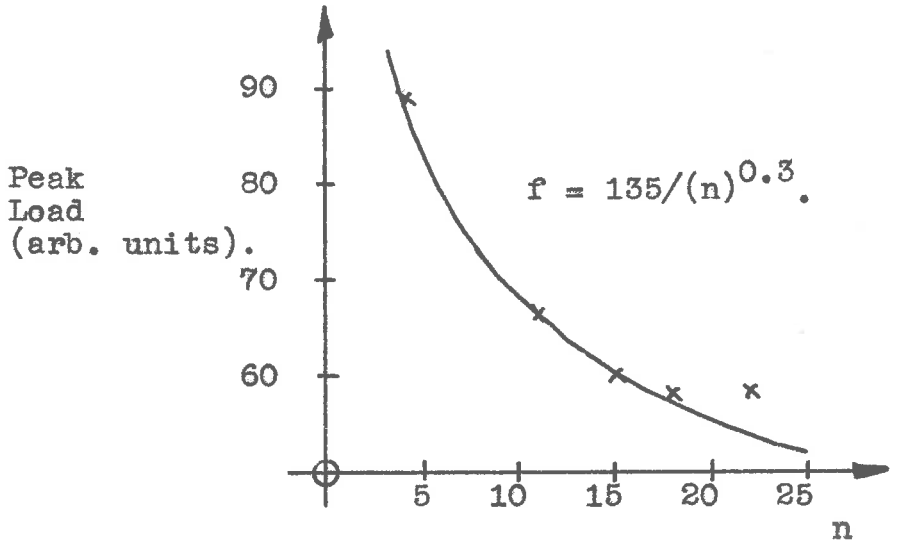

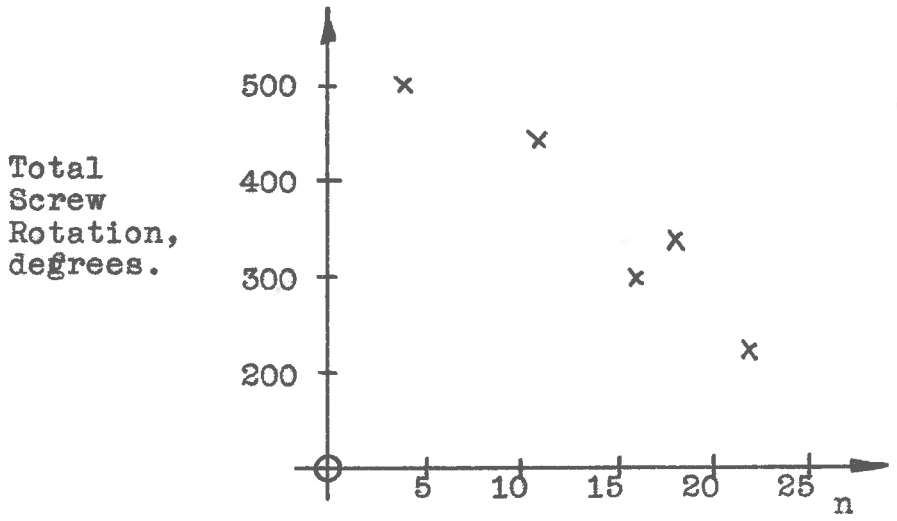

FIG. 5.121 The Variation of Surface Energy, Peak Load and total Screw Rotation with the Crystal Number.

In addition to the surface energy values, Table 5.11 also gives peak loads, total loading screw rotation and a crystal count on the fracture surface.

Inspection of Figure 5.117 shows that there was obviously a zero drift. If it is assumed that the plot should terminate at 300 degrees loading screw rotation, a 25% reduction in the plot area results and this would bring the surface energy value to 0.06 lb.in. per sq. in., which is comparable to Nos. 2 and 4. The corrected value is indicated in brackets in Table 5.11.

For specimens 1 to 5, the peak load and the nominal surface energy vary together and the crystal number varies in an inverse manner. In fact, if the peak loading force, and the surface energy are plotted against the crystal number, then, as may be seen from Figure 5.124 the surface energy varies approximately as $(n)^{-0.4}$ and the peak load as $(n)^{-0.5}$, where n is the number of crystals on the fracture surface. If the mean crystal dimension is defined by the expression

$$d = \left(\frac{A}{n}\right)^{\frac{1}{2}} \qquad \ldots\ldots 5.20$$

and since the specimens are similar,

$d \propto (n)^{-\frac{1}{2}}$, then 5.21

surface energy, $e \propto (d)^{+0.6}$, ... 5.22

peak load, $r \propto (d)^{+0.6}$ and 5.23

~~total screw rotation, $\theta \propto (d)^{+1.4}$ ..... 5.24~~

The specimens are geometrically similar and are loaded in the same manner. It may therefore be assumed that the peak load represents the normal stress that is required to propagate the fracture initially. As the fracture penetrates the specimen, the beam depth diminishes, and a diminishing load is able to maintain the required normal stress.

5.2.6.3.3.2 The Appearance of the Fracture Surface

Photographs and photomicrographs relating to the various specimens are presented in Figures 5.132 to 5.184.

Specimen 2

One of the most interesting fracture surfaces is that of specimen 2. There appear to be only two crystals and they are so oriented that they fractured in a plane nearly perpendicular to the longitudinal axis of the specimen.

The one crystal exhibits a plane, mirror-like surface on which the various markings are barely discerned with the unaided eye.

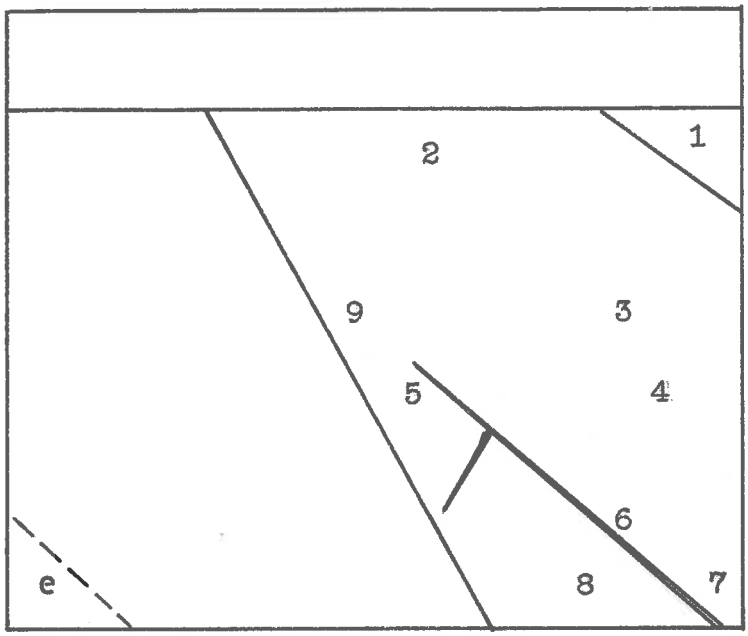

FIG. 5. 122 A Sketch showing the relative Location of the various Surface Features on the Fracture Surface of Specimen 9.

The surface exhibited by the other crystal shows a series of parallel line markings. The surfaces between these markings are plane and mirror-like. These lines are found to be steps or secondary fractures or both.

The polished sides of the specimen show sets of parallel bands and cracks which are also parallel to each other. These cracks correspond to the line markings on the fracture surface, and give some idea of the penetration of the secondary fractures.

Photographs of the whole fracture surface of this specimen are presented in Figure 5.149 showing clearly the two kinds of fracture surface. The fracture began at the top of this surface and terminated at the bottom.

In order to facilitate the presentation of various line markings and their location a sketch of this fracture surface is presented in Figure 5.122 with the various surface features marked in and numbered.

Region 1 is small and triangular, and the only place where twin bands were found, Figure 5.150. It is located at one corner of the fracture surface.

Region 2 is marked by two kinds of line markings. The one set of lines suggest contours on a map, but show no sudden changes in direction and begin and end at the boundary of the crystal. A portion of this region is

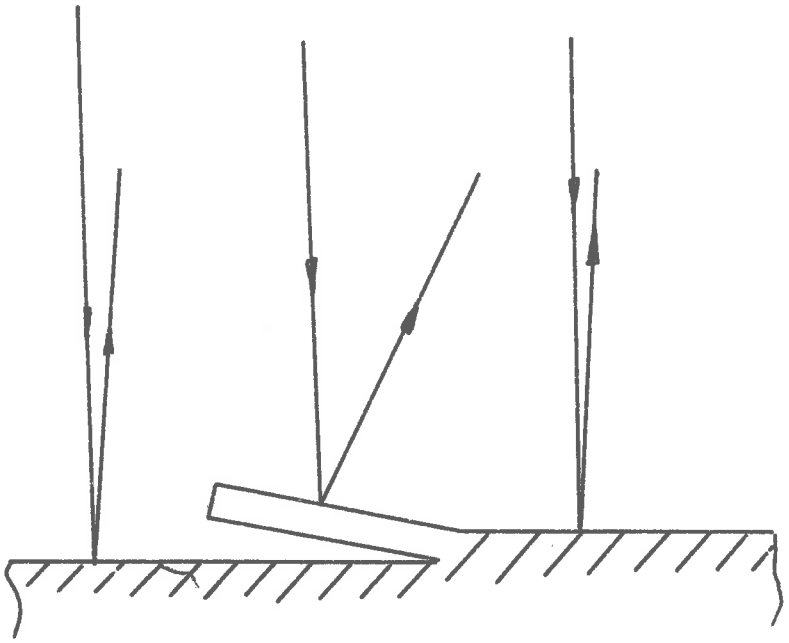

FIG. 5.123 An elongated Leaf of Crystal associated with a Cleavage Step reflects Light away from the Microscope Objective and appears as a dark Band, so revealing the Presence of the Cleavage Step which might othewise be invisible.

shown in Figure 5.151. Examination of the polished side does not reveal any direct correspondence between these lines and those on the polished surface.

The second set of lines are more irregular and may change direction suddenly. They are always approximately normal to the contour lines referred to above. They are seen clearly in Figure 5.153 for example in which three of the contour lines can also be discerned. That these lines are cleavage steps can be shown conclusively by reference to their occasional sudden widening into bands. These wide bands, when examined, turn out to be bismuth leaf that have been lifted away from the body of the crystal on one side. This rotation causes them to reflect light away from the microscope objective and so appear as dark bands, Figure 5.123.

Where the contour lines encounter a free boundary of the crystal, the situation is rather confused, as may be seen from Figure 5.152.

Regions 4, 5 and 9 are also characterised by the presence of contour lines. From these regions, other characteristics of the contour lines become apparent. Figure 5.154 shows that the contour lines are neither sinusoidal, and that adjacent lines are always out of

phase by half the wavelength. It may also be noted that some of these lines regularly curve more sharply on one side of the "moon" than on the other. The enlargement, Figure 5.157 in which the contour lines are approximately horizontal, shows that at points of great curvature, the line widens into a band.

Figure 5.155 shows another phenomenon connected with the contour lines. The band marking that crosses the path of the contour lines causes the lines to change direction until they are parallel to this band. Examined under high magnification, the band is seen to contain a crack, which is somewhat more apparent from Figure 5.156. The black band on the left of this figure is not a continuation of the line but a cleavage step where a thin strip of the crystal has been pulled away on one side, as explained previously.

Another somewhat similar situation is presented by Figure 5.156 where the contour lines are again obstructed by what appears to be a crack. This region is unusual in that the crack is surrounded on each side by a surface, possessing the usual kinds of line markings which are however not related to the larger systems on either side.

The metallurgical microscope used furnished illumination through the objective. The greatest angle

of incidence of the incident light is thus approximately equal to half the angle subtended by the objective aperture at the specimen surface. The greatest angle of reflection of light that appears in the image is similarly defined. It follows that the objectives of lowest power, which are further removed from the object, operate with the lowest angles of incidence and reflection.

Figure 5.158 presents a pattern that appears only when the 5x objective is used. The contour lines gradually become wider and their sinusoidal shape is lost. With a 10x objective, these bands remain, but are barely visible. The band on the extreme right of this figure forms the boundary between regions 4 and 5.

Region 5 is unusual in that the contour lines are absent. The cleavage step lines are present however. These cleavage step markings frequently form closed loops that are elongated in the left to right direction. Figure 5.122. One such loop whose boundaries are made particularly noticeable by dark bands already described, and sketched in Figure 5.123 is shown by Figure 5.167. A photomicrograph of this kind of surface is Figure 5.168 which also shows a sudden change in the density of the cleavage steps.

Regions 7 and 8 do not present any new phenomena. They are surfaces with a low density of cleavage step lines.

A crack and its associated markings found in region 8 is shown in Figure 5.159.

Both parts of this specimen could be readily examined. The two fragments can therefore be compared. The second fragment has the same general features as its counterpart. The cracks are wider and unmistakeable, region 9 has been rotated so that it appears black even under the 40x objective, and the band-like appearance of Figure 5.158 is absent. One new marking not found on the first fragment is presented by Figures 5.171 and 5.172, a series of straight parallel bands constant width cross the fracture surface.

The second crystal on the fracture surface of specimen 9 is characterized by the parallel secondary fractures that cover the entire fracture surface of this crystal. The appearance of the fracture surface between two of these secondary fractures is usually as shown by Figure 5.162, which is very similar to regions 2, 4, 5 and 9 on the other crystal fracture surface.

The surface between the cracks may be devoid of contour lines as Figures 5.163, 5.164 and 5.165 show. Bands such as those of Figure 5.163 which were found to be associated with fractures on the other crystal surface, usually reveal a crack on this surface also.

The development of bands on parts of the contour lines is also observed on this crystal as Figure 5.167 shows.

The secondary fractures in this crystal are usually straight. Occasionally a straight line is interrupted by a kink such as that shown in Figure 5.166. Such kinks are particularly frequent in region 'c' of the crystal surface, ~~Figure 5.165~~.

Bands in which the markings have a different direction also appear, Figure 5.168. These bands are parallel, straight and traverse secondary fractures without being affected. They are readily identified as twin bands formed before the fracture passed through them.

The secondary fracture lines are spaced more regularly on the right side of Figure 5.122 and the contour lines are absent.

There are no noticeable differences between the surfaces on the two fragments of the specimen.

Photographs of the polished sides of the fragments are shown in Figures 5.173 and 5.174. The correspondence of the secondary fractures with each other is notable. The upper fragment of Figure 5.174 shows a series of parallel bands. This fragment is also the one with the parallel bands on the fracture surface presented in Figures 5.169 and 5.172.

Specimen 10

As may be seen from Figure 5.175 there are two large fractured crystals. The one at the bottom of this figure is very similar to the fracture surface of specimen 9 which is marked by a series of parallel secondary fractures. These secondary fractures are closer together on this specimen, and the contour lines which run from one secondary fracture to the next are usually more closely spaced as well.

This is apparent from Figures 5.176 and 5.177. The spacing of the contour lines does not seem to depend on the width of the fracture surface which they span. Their spacing is variable, and the density of cleavage step lines seems to follow the density of these lines. The denser cleavage step lines are much more difficult to detect, however, indicating that the steps are probably smaller.

The diagonal lines in the lower right of Figure 5.175 turn out to be twin bands with their own secondary fracture systems and line markings. The interaction between these twin bands and the main crystal is sometimes complicated as the Figure 5.178 shows. While the twin band remains attached to the crystal on one side, on the other side, secondary fractures in both the twin and the main crystal have formed.

The crystal whose fracture appears on the top of Figure 5.178 consists of a series of plane fracture areas at different heights. As a consequence the most powerful objective cannot be brought within focusing distance of most areas of interest.

The various fracture planes differ from one another, as Figures 5.179 to 5.182 show. In Figure 5.179 the surface is crossed by a series of parallel twin bands without line structure and another, wider band with a line pattern of its own. It is possible that the unmarked twin bands appeared after the fracture.

The zig-zag pattern in Figure 5.180 is produced by a series of parallel and relatively wide twin bands in which the surface markings are inclined at 60° to the corresponding markings in the untwinned crystal.

The contour lines, when they are found are less regular than in other instances as Figures 5.181 and 5.182 show.

No new markings are found on the other fragment of this specimen.

Specimen 1

This specimen together with the other four which were submerged in liquid nitrogen have rounded markings on the fracture surface, which are probably caused by either,

chemicals in this liquid or the moisture which was deposited on the specimen after removal from the testing rig, despite the precaution taken against this.

The most noticeable difference between this specimen and the ones studied previously is that the contour lines are completely absent. In other respects the surfaces are essentially the same. There are large flat mirror-like surfaces marked by cleavage step lines, and twin bands whose surface is not marked by lines, Figure 5.135.

Twin bands with dense line markings are also frequent, as are surfaces marked by a series of parallel straight lines that represent secondary fractures. The spacing of these lines is quite variable and may be much closer than in specimens formerly studied, Figure 5.133.

Lines running across several secondary fracture lines have also been found. They are infrequent and do not appear to be influenced by the presence of the secondary fracture lines, Figure 5.132. The secondary fracture lines are also steps of considerable height, for the fracture surface on both sides of such lines cannot usually be held in focus at the same time.

Specimens 2 to 5

The remaining specimens tested under liquid

nitrogen provide very little information not already noted on specimen 1. Some of the effects are present in a more striking form. For example, cleavage step lines are often rather regular in shape, and may exhibit a series of steps or even be straight for some distance, as Figure 5.140 shows. The lines of Figure 5.134 are found on specimen 5 also, and with an objective of lower power these lines are also seen to be the boundaries between regions of different shading, Figure 5.141.

Specimens 7 and 8

These specimens were fractured at room temperature, and, as expected, exhibit the contour lines in profusion. A particularly interesting example from specimen 7, Figure 5.147 shows these lines curving through 180°.

On specimen 8 twin bands without line markings are found, but they are smaller and far less frequent than those found on the specimens tested at low temperature.

5.2.2.5.3.3 Visual Observation during Fracturing

This phase of the experiment was not particularly fruitful. The writer was concerned to observe the "root" of the fracture while it was moving. It is apparent, now that the fracture surfaces have been carefully studied, that a series of photographic records taken at various

stages in the progress of the fracture might have furnished additional information of some consequence.

It was noted, however, that the markings on the polished sides of the specimens - twin bands and secondary fractures developed gradually as the loading screw was rotated, although the interval over which a particular marking appeared to be developing was generally only a fraction of the total loading interval. The region in which twin bands developed generally followed and preceded the fracture.

Twin bands in particular were seen to grow when the loading screw was rotated, and continue for a small interval after the rotation of the loading screw had ceased.

Photographic records of the surface markings are presented in Figures 5.173, 5.174, 5.183, 5.184, 5.142, 5.143, 5.144 and 5.145.

It is apparent that the twin bands extend well back into the crystal, most of them terminating on the fracture surface.

The etched surface of specimen 6b shows twin bands in crystals far removed from the fracture. These were most probably introduced during the preparation of the specimen. The polished surface provides a better indication of deformation events that occurred during the fracturing process.

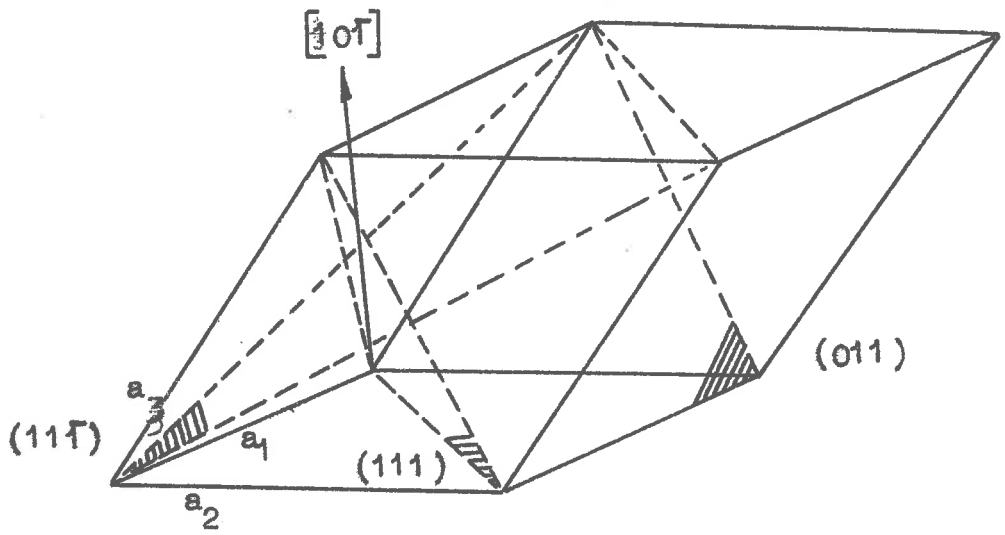

FIG. 5.124 The Unit Cell for a Rhombohedral Crystal.

5.2.3.5.4 Discussion of Results

Bismuth has a rhombohedral crystal structure. A unit cell of this kind is presented in Figure 5.13d, the various planes of interest in deformation being marked in.

Slip in bismuth occurs on the (111) plane in the [10$\bar{1}$] direction at a stress of about 0.2 kgm. per sq.mm. Twinning occurs on the (011) plane and cleavage on the (111) and (11$\bar{1}$) planes respectively. The normal stress for cleavage on these planes is 0.32 and 0.69 kgm. per sq.mm. respectively.

It is noteworthy that the twinning plane intersects both of the cleavage planes so that twin bands can be expected to appear on both cleavage planes.

1. The Cleavage Step Lines

That cleavage step lines are in fact what their name implies can be asserted with considerable confidence. Several observations support this.

These lines are irregular and angular, sometimes exhibiting a step-like appearance, Figure 5.13b. One would not expect a phenomenon which changes direction frequently to have a penetration into the crystal that is greater than the distance between successive changes in direction.

They frequently form closed loops, a phenomenon

consistent with the hypothesis that they are cleavage steps.

They exhibit relatively wide, dark bands which are also consistent with the hypothesis as Figure 5.123 shows.

No other explanation can be shown to be consistent with these properties of cleavage step lines.

Cleavage step lines, while they are irregular on a small scale do have an orientation on a larger scale as many of the photomicrographs show.

Cleavage step lines that do not form closed loops may fade out at one end but not at both ends. One end may be terminated at a boundary of a fracture surface such as a secondary fracture line or it may terminate at the junction of two or more similar lines.

This behaviour suggests that cleavage steps are formed in the following way:

When a fracture is propagated along a particular crystallographic plane, a similar fracture process may begin on a parallel plane slightly displaced from the first plane.

The stress situation requires that two such fractures can only be propagated if they are abreast of each other. The fracture that lags behind is no longer activated.

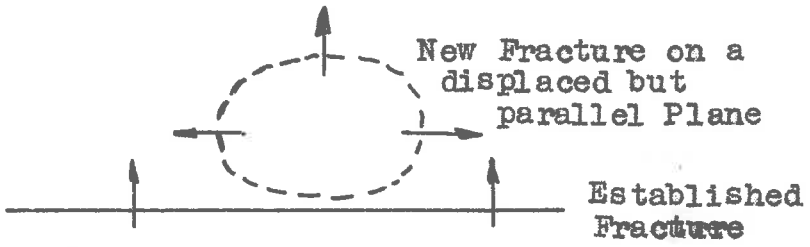

The Appearance of a new Fracture System in front of an established Fracture System.

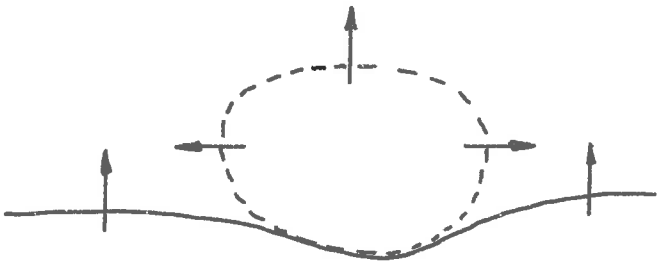

Interaction of the two Fracture Systems.

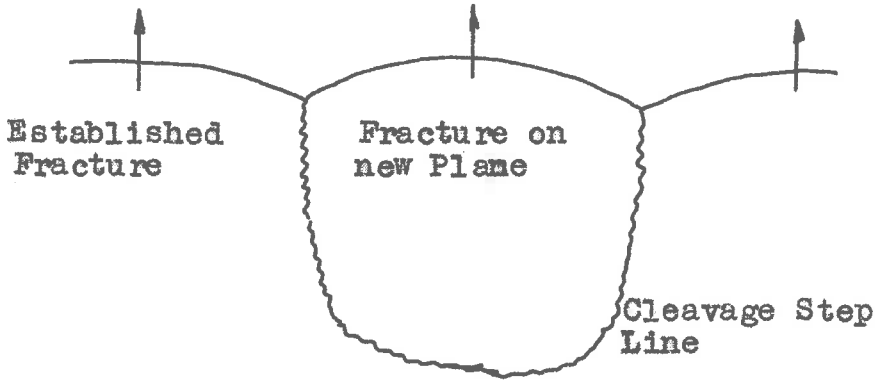

The Boundary between the two Fracture Systems becomes a Cleavage Step Line.

FIG. 5.125 A Mechanism for the Initiation of Cleavage Step Lines.

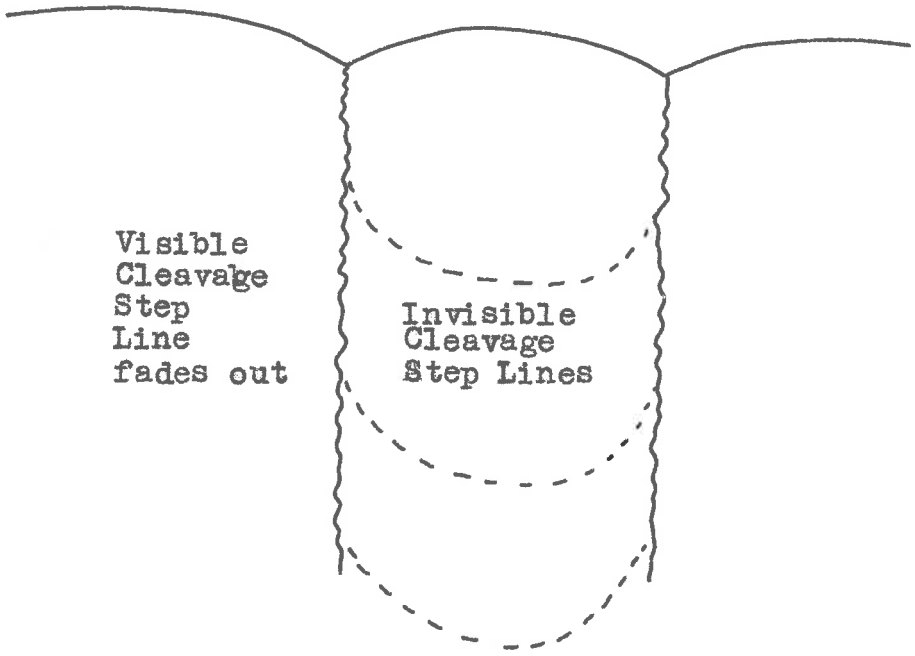

FIG. 5.126 A Mechanism to explain the fading out of Cleavage Step Lines.

The stress in front of an established fracture is high, and if a second fracture system is activated by this stress, it must form ahead of the fracture that activates it.

The new fracture process is therefore inevitably in front of the established fracture and active fracturing continues on the new plane as well as the plane on which the fracture is established, the boundary between the two being marked by a cleavage step, which becomes a line as the process continues. This sequence of events is presented in Figure 5.12b.

According to this model the cleavage step will be generally directed in the direction of motion of the fracture process.

If the new fracture process diminishes in length it may vanish, leaving a cleavage step loop.

Whenever fracture is transferred from one plane to another, a cleavage step loop, which often appears as two lines with a common origin, is formed. If the cleavage step is small it may be invisible. Thus a visible cleavage step line may appear to fade out as illustrated in Figure 5.12c.

The separation of the two surfaces along the cleavage step may take place by relative shear. The

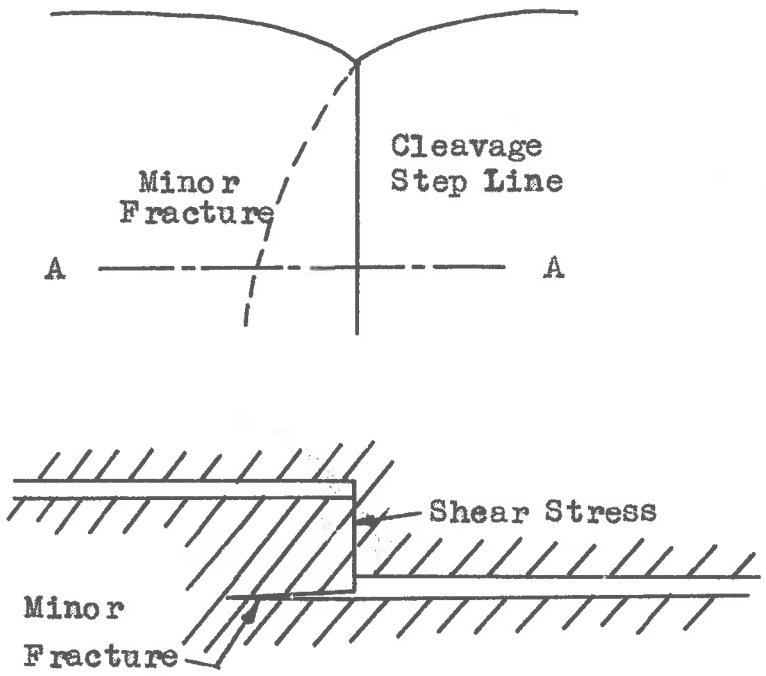

FIG. 5.127 A Mechanism for the Formation of the elongated Crystal Leaf at Cleavage Step Lines.

shear stress that opposes this motion may cause a minor crack as Figure 5.127 illustrates. The film of crystal so formed will be turned up in the manner of Figure 5.125 and give rise to the appearance of dark bands along the cleavage step lines.

Because the separation along the cleavage step will be by shear or fracture (depending on the inclination of the cleavage step to the main fracture surface), certain directions will be preferred and the cleavage step line may be straight or have the appearance of a stairway.

2. The Contour Lines

These lines, noticed only on specimens fractured at room temperature are always normal to the cleavage step lines, which means that they will be parallel to the lines traced out by the "root" of the fracture at various points in the process.

It is suggested that these contour lines are indeed formed at the "root" of a fracture when it becomes stationary. On the basis of results obtained from the experiments performed with zinc it was suggested that at the root of an ideal crack glide is nucleated which reduces the stress concentration in this region and so arrests the crack. This requires the periodic nucleation of cracks, the whole process being described by the term "fracture".

This hypothesis may also be applied to bismuth. It is suggested in addition, that due to thermal assistance at room temperature, the crack nucleated shear is made more penetrating, causing the stress concentration factor at the root of the crack to be reduced to a greater extent. This tends to make the movement of the fracture discontinuous when loading is applied continuously. At points where the fracture is moving slowly the fracture is "anchored" so that the process stops until the applied stress has built up sufficiently. The fracture then accelerates and "overshoots" the position dictated by the existing stress, and so comes to rest again.

The fact that these lines always begin and end at the boundaries of the fracture area on which they are found suggests strongly that they are formed at the root of the fracture. The root of the fracture is the only known phenomenon which must terminate at the boundaries of the crystal being fractured.

The continuity of the lines suggests that one line presents the location of the fracture root at a particular time.

The phase relationship of undulations on successive contour lines suggests a discontinuity process.

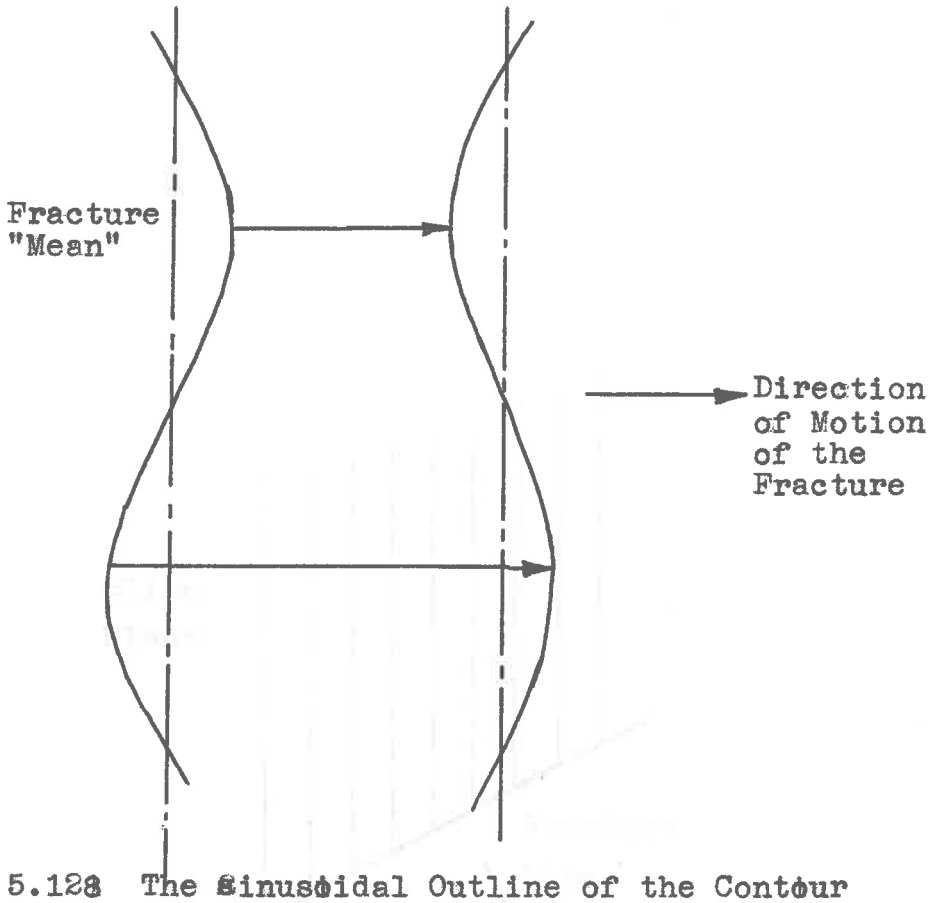

FIG. 5.128 The sinusoidal Outline of the Contour Lines is self-propagating.

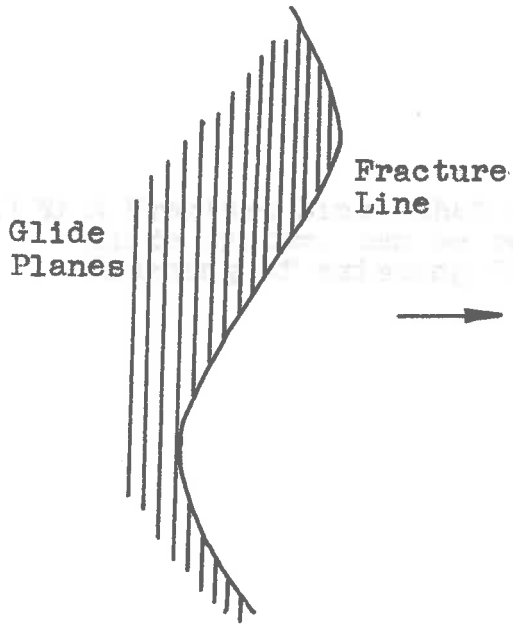

FIG. 5.129 The leading parts of the Fracture are resisted more than the trailing parts, making the sinusoidal Outline of the Contour Lines stable.

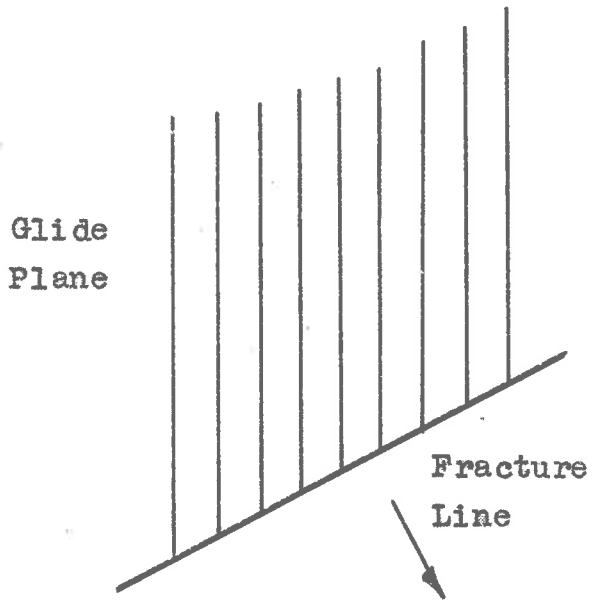

FIG. 5.130 A Fracture Line that is inclined to a Glide System, can be retarded by the Widening of existing Glide Systems.

This is illustrated in Figure 5.128. Suppose that the root of the fracture was located on one of these contour lines. Whereever the fracture "root" is behind the mean line, the acting stress is higher than in places where it is ahead of the mean line. When the fracture is released, those parts under high stress accelerate more rapidly and travel a greater distance. Thus the anti-phase relationship of Figure 5.128 results.

Contour lines are observed to be devoid of sharp changes in direction. If a fracture line is inclined to a glide system, then the fracture can propagate glide by widening existing dislocation loops, Figure 5.130. Since dislocations need not be nucleated, glide can occur at stresses below the stress at which the dislocations are nucleated. At the trailing portions of the contour line (which represents a fracture line), dislocations of opposite sign can meet, Figure 5.129. Twice the number of dislocations are available for glide in this region and the stress de-concentration due to glide is greatest here, allowing the fracture to sustain a greater applied stress. The trailing portions of the fracture are necessarily under a greater applied stress and the stability of the undulations is thereby explained.

At the more highly curved points, the contour lines are observed to open up into a band, suggesting

that the fracture was progressing slowly at these points while the remainder was stationary.

The widening of contour lines into bands as Figure 5.158 shows remains to be explained. This is most marked immediately after an interval in which no contour lines are apparent, and gradually merges with the usual line marking. This band is made apparent by the change in surface inclination in a manner very similar to twins. These bands are also parallel to twin lines found on the other fragment of this specimen. It is conceivable that in place of glide, the fracture nucleated a twinning process. Thus, instead of the periodic arrest of the fracture as suggested for contour lines, these contour bands led to the fracture being propagated at two different velocities. The absence of undulations on these bands which soon develop when the lines appear is significant in this respect.

The absence of the contour lines on the low temperature specimens is explained by saying that without thermal assistance to glide, the fracture is not arrested periodically.

3. Secondary Fracture Lines

In specimen 9 these lines are directed almost horizontally across the specimen.

The passage of the fracture as indicated by cleavage step and contour lines is in a direction parallel to the secondary fracture lines, from the boundary between the two crystals towards the side of the specimen.

The explanation put forward for the secondary fracture lines in zinc can be applied here.

A fracture that moves vertically as it did in the other crystal would be arrested by glide on the (111) plane (if the fracture surface is $(11\bar{1})$, and the secondary fractures on (111)). A fracture moving in a direction parallel to the glide plane does not encounter easy glide systems and is propagated more readily.

It is suggested that the process was as follows: Both the $(11\bar{1})$ and the secondary (111) fracture began at the intercrystalline boundary, and moved horizontally towards the side of the specimen. They were initiated successively so that the secondary fractures formed effective boundaries to fracture processes on the $(11\bar{1})$ plane.

The contour lines clearly indicate that the fracture processes between the secondary fractures occurred independently of each other.

At the boundaries of the fracture, the contour lines tend to get left behind and crowded together indicating that the fracture process progresses more slowly in these

regions. On the mirror-like surface of specimen 9 there are several bands near which the contour lines behave in a similar manner, as Figure 5.155 illustrates. On closer examination fracture lines are found to be in the centre of these bands. The line markings in these bands are not related to those outside them, Figure 5.156.

It appears that these fractures were formed before the fracture which produced the mirror-like surface appeared. The band of line markings is then the surface of a fracture secondary to the fracture that is represented by the black line in the centre of the band.

4. The Force-displacement Plots

It is apparent from the results presented in Table 5.11 that the nominal surface energy associated with the fracture is much greater than the surface energy of a bismuth crystal.

As before, this energy must somehow be associated with the fracture process for the specimens were not bent significantly, and the load was clearly controlled by the fracture process.

A discussion of the surface features of these specimens has already shown that the hypothesis put forward to explain certain features of the zinc specimens can also be applied here.

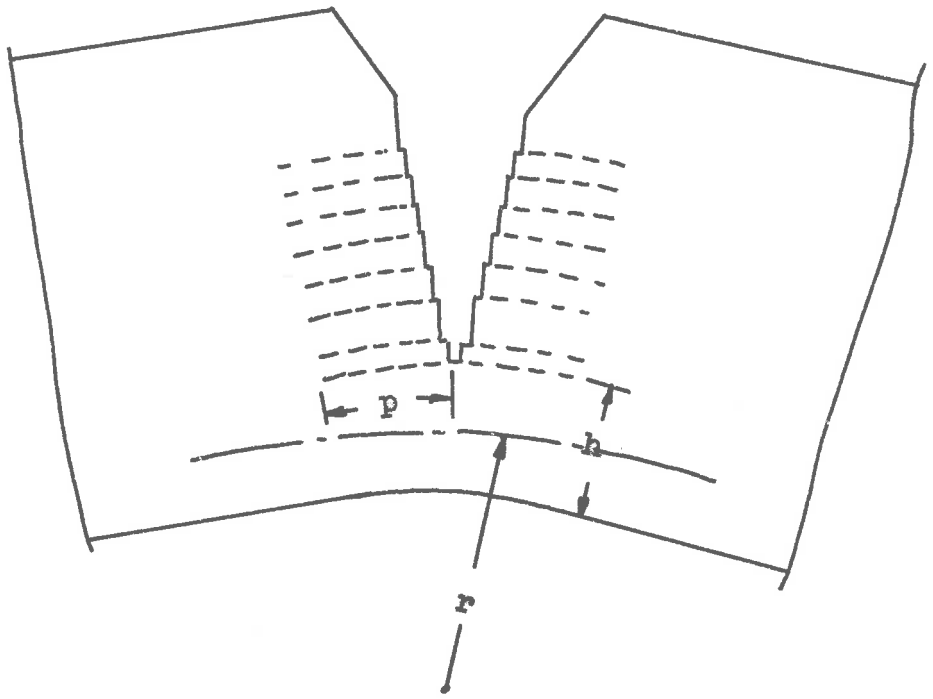

FIG. 5.13 The Fracture Process in the Bismuth Specimens according to the Nucleated Glide Hypothesis.

The appearance of contour lines has added almost direct support to the concept of crack-nucleated glide.

In a large crystal the penetration of the crack-nucleated glide is not influenced by the crystal boundaries. Small crystals, if they occur in a polycrystalline specimen, present an effective obstruction to such glide at the intercrystalline boundary. If this happens, the energy absorbed by a glide system is reduced, and the surface energy associated with the fracture is reduced.

It was found that the surface energy was indeed less for specimens containing smaller crystals.

Figure 5.(3) shows schematically the way in which the specimens are expected to fracture according to the glide nucleation hypothesis.

When the fracture has penetrated some distance into the specimen, the beam depth is 'h'. If glide has an effective penetration 'p' then the as yet undisturbed portion of crystal may be treated as a beam of length '2p', depth 'h', and width equal to the width of the specimen.

It is assumed that fracture is propagated when the outermost fibre stress of the beam has attained a certain value, i.e. the outermost fibre strain ' ϵ_o ' is constant for all 'h'. The curvature of this beam is therefore defined by the expression

$$\frac{1}{\rho} = \frac{\epsilon_0}{yh} \qquad \ldots\ldots 5.25$$

As the fracture penetrates the specimen, the curvature of the undisturbed crystal ahead of the fracture increases. The earliest glide planes have the smallest curvature, and as fracturing continues, these glide planes will either accommodate themselves to the new curvature with additional glide, or, alternatively they are isolated from further changes of curvature by the formation of secondary fractures.

Secondary fractures are found regularly on some fracture surfaces, suggesting that the accommodation of glide planes to changing curvature is limited to a redistribution and perhaps a somewhat increased penetration of existing dislocations. If this is the case, then the spacing of secondary fracture lines became closer as the value of 'h' diminishes, as is indeed the case for specimen 9.

The angular inclination of the two fragments to each other, $\Delta\theta$ is given by

$$\Delta\theta = \frac{2p}{\rho} = \frac{4\,p\,\epsilon_0}{h} \qquad \ldots\ldots 5.26$$

The moment carrying capacity of the beam of this model is proportional to the square of the beam depth.

The loading force is proportional to this moment and the loading screw rotation is proportional to $\Delta\theta$ so that

$$\theta \propto \Delta\theta \propto \frac{1}{\sqrt{f}} \qquad \ldots\ldots 5.27$$

where f is the loading force

$$\text{i.e. } f \propto \frac{1}{\theta^2}$$

The general appearance of the load displacement plots after the peak load conforms to this.

More precisely

$$f = \frac{E\, c_0^2\, p^2}{\theta^2} \qquad \ldots\ldots 5.28$$

where c is the Elastic Modulus of bismuth.

This relationship shows in addition the powerful effect of penetration and the normal stress required to propagate the fracture. Penetration is, of course, assumed to be constant throughout.

The surface energy e is

$$e \propto \left[\frac{E\, c_0^2\, p^2}{\theta}\right]_{\theta_1} = \frac{E\, c_0^2\, p^2}{\theta_1} \qquad \ldots\ldots 5.29$$

where θ_1 is the value at peak load.

$$\text{Now } \theta_1 = \frac{p\, c_0}{k_1} \qquad \ldots\ldots 5.30$$

where h_1 is the initial value of h so that

$$e \propto \epsilon_0^2 p \qquad \ldots\ldots 5.31$$

since h_1 is the same for all the specimens.

From the empyrical relationship between surface energy and crystal dimension, namely equations 5.22 and 5.23

$$e \propto (d)^{0.8}, \qquad \ldots\ldots 5.32$$

$$(d)^{0.8} \propto \epsilon_0^2 p \qquad \ldots\ldots 5.33$$

Now

$$\epsilon_0 \propto \text{peak force} \propto (d)^{0.6} \qquad \ldots\ldots 5.34$$

Whence

$$p \propto d^2 \qquad \ldots\ldots 5.35$$

This is a relationship of great significance for the glide nucleation hypothesis. It is based on measurements from relatively few specimens and must not be treated as a confident assertion. Nevertheless it is an interesting result, which may be used in examining brittle behaviour.

FIGURES 5.115 TO 5.119,

THE LOAD-DISPLACEMENT PLOTS FOR THE BISMUTH SPECIMENS 1 TO 5, FRACTURED AT -196°C.

FIGURE 5.120,

THE LOAD-DISPLACEMENT PLOT FOR SPECIMEN 8 FRACTURED AT ROOM TEMPERATURE.

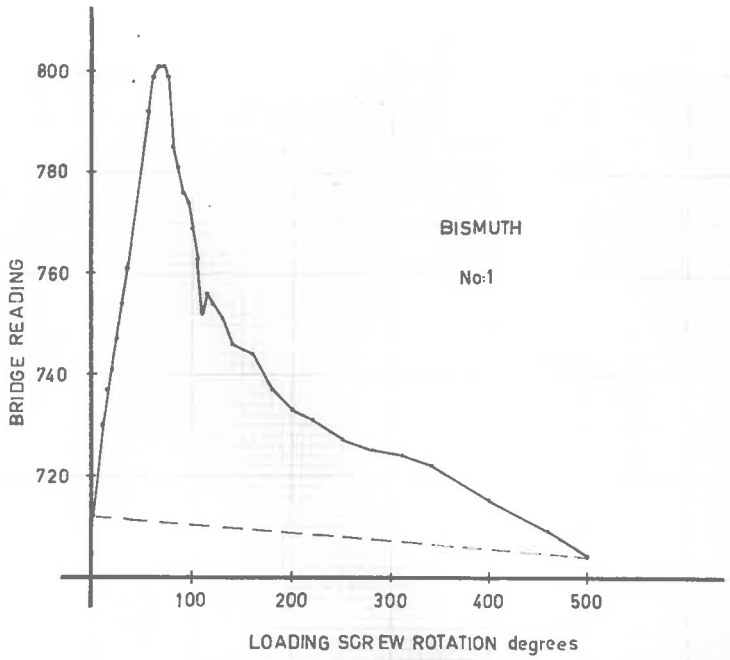

FIGURE 5.115.

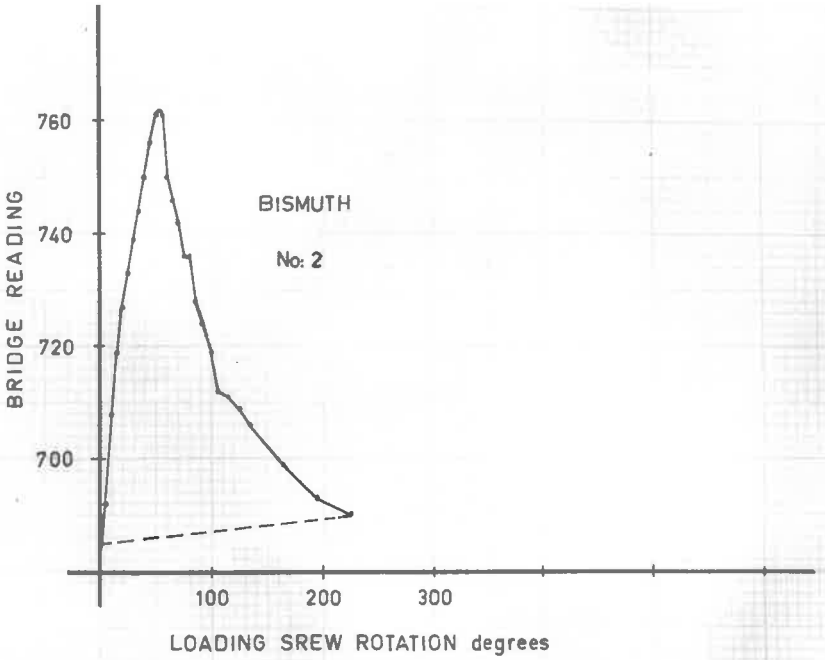

FIGURE 5.116.

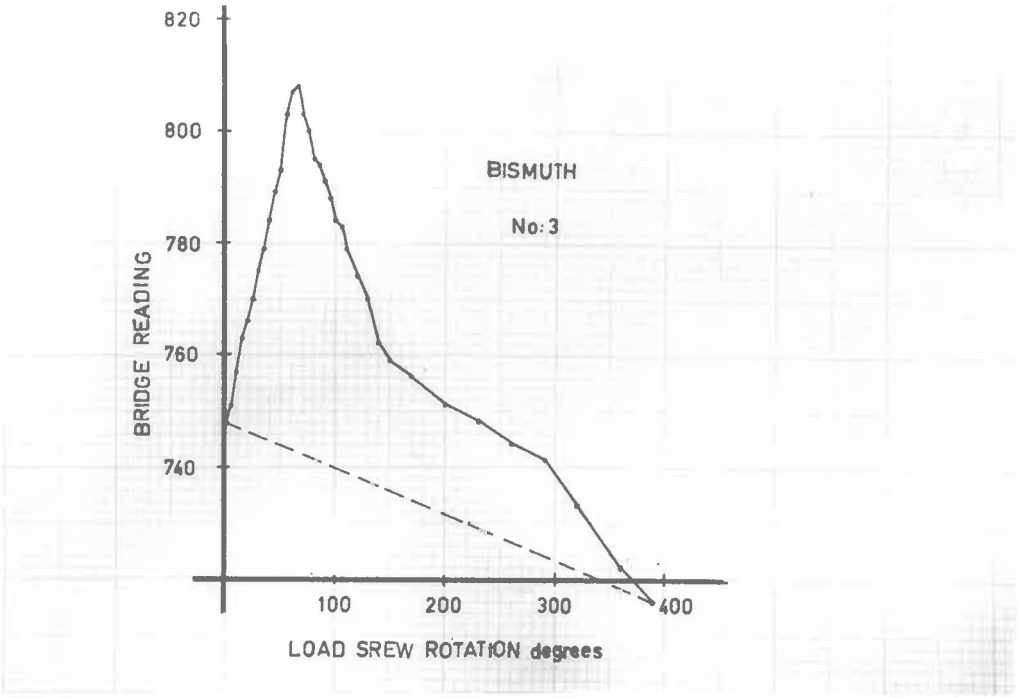

FIGURE 5.117.

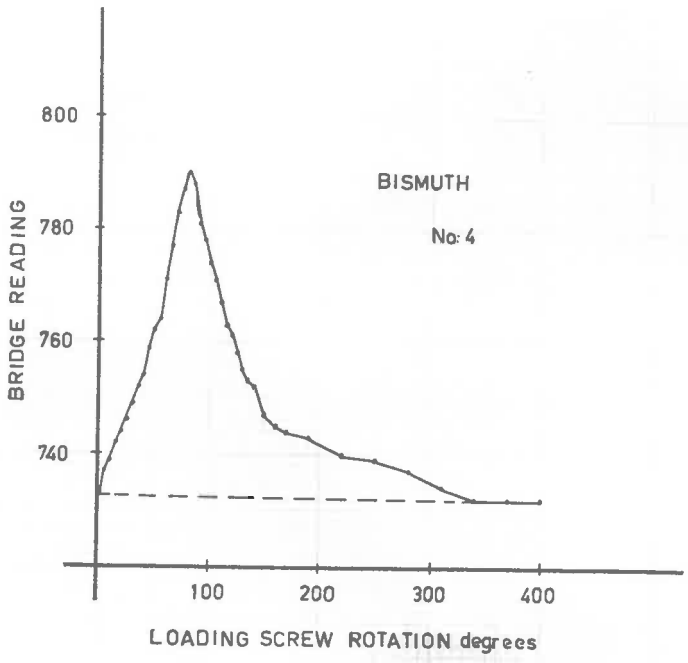

FIGURE 5.118.

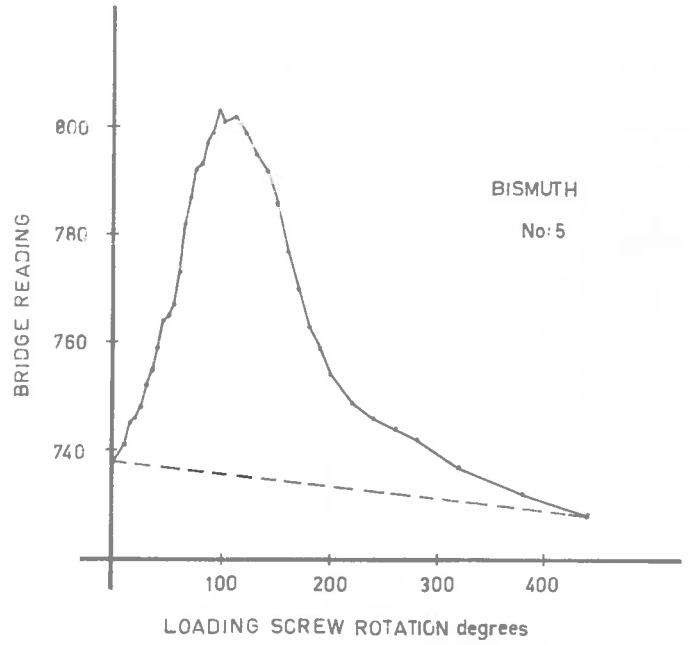

FIGURE 5.119.

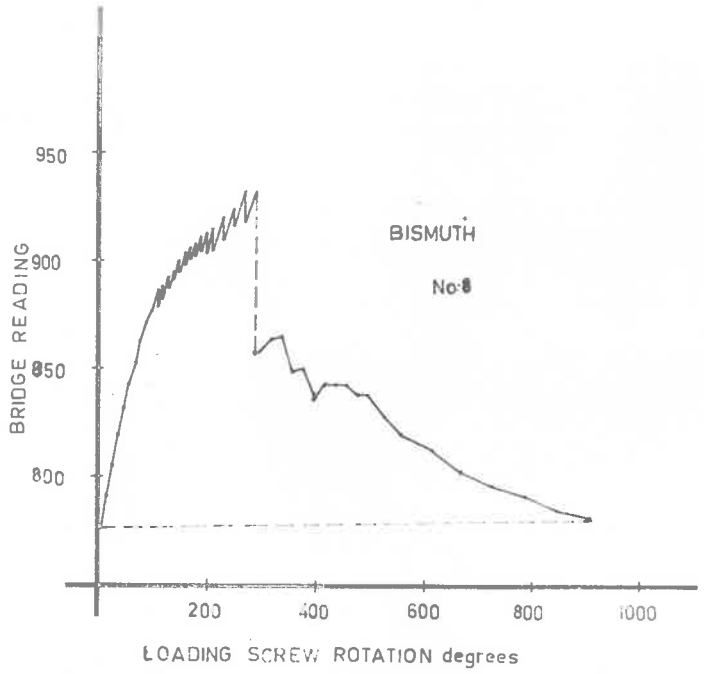

FIGURE 5.120.

FIG. 5.132 PHOTOGRAPH. FRACTURE SURFACE OF SPECIMEN 1, TAKEN IN DAYLIGHT, (8x).

FIG. 5.133 MICROGRAPH. FRACTURE SURFACE OF THE SECOND KIND ON SPECIMEN 1. NOTE CLOSE SPACING OF SECONDARY FRACTURE LINES, (75x).

FIG. 5.134 MICROGRAPH. FRACTURE SURFACE OF THE SECOND KIND ON SPECIMEN 1. NOTE WIDE BAND TRAVERSING SECONDARY FRACTURE LINES, (75x).

FIG. 5.135 MICROGRAPH. FRACTURE SURFACE OF THE FIRST KIND ON SPECIMEN 1. NOTE MULTIPLICITY OF CLEAVAGE STEP JUNCTIONS AND TWIN BANDS ON WHICH THERE ARE NO NEW LINE MARKINGS, (75x).

FIGURE 5.132.

FIGURE 5.133.

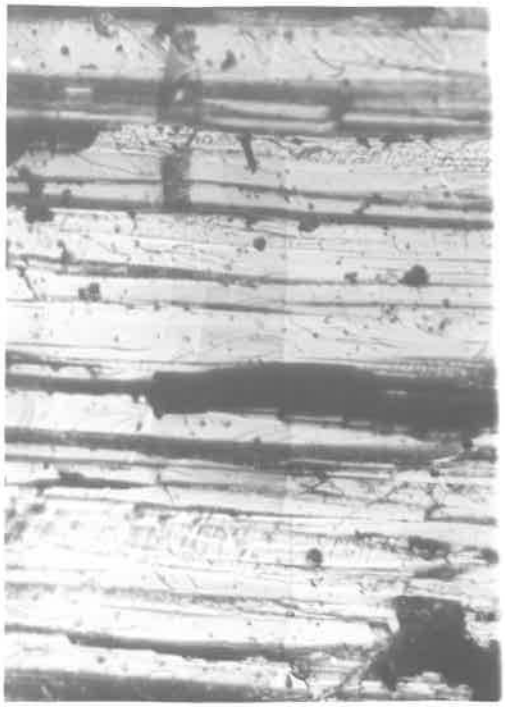

FIGURE 5.134.

FIGURE 5.135.

FIG. 5.136 PHOTOGRAPH. FRACTURE SURFACE OF SPECIMEN 2, (8x).

FIG. 5.137 PHOTOGRAPH. FRACTURE SURFACE OF SPECIMEN 3, TAKEN IN DAYLIGHT, (8x).

FIG. 5.138 PHOTOGRAPH. FRACTURE SURFACE OF SPECIMEN 4, TAKEN IN DAYLIGHT, (8x).

FIG. 5.139 PHOTOGRAPH. FRACTURE SURFACE OF SPECIMEN 5, TAKEN IN DAYLIGHT, (8x).

FIGURE 5.136.

FIGURE 5.137.

FIGURE 5. 138.

FIGURE 5.139.

FIG. 5.140 MICROGRAPH. FRACTURE SURFACE OF THE FIRST KIND ON SPECIMEN 5. NOTE STAIRWAY-LIKE APPEARANCE OF CLEAVAGE STEP LINES. (75x).

FIG. 5.141 MICROGRAPH. FRACTURE SURFACE OF THE SECOND KIND ON SPECIMEN 5. NOTE BANDS TRAVERSING SECONDARY FRACTURE LINES, (37x).

FIGURES 5.142 AND 5.143
PHOTOGRAPHS. DEFORMATION MARKINGS ON THE POLISHED SIDES OF SPECIMEN 6_a, (4x).

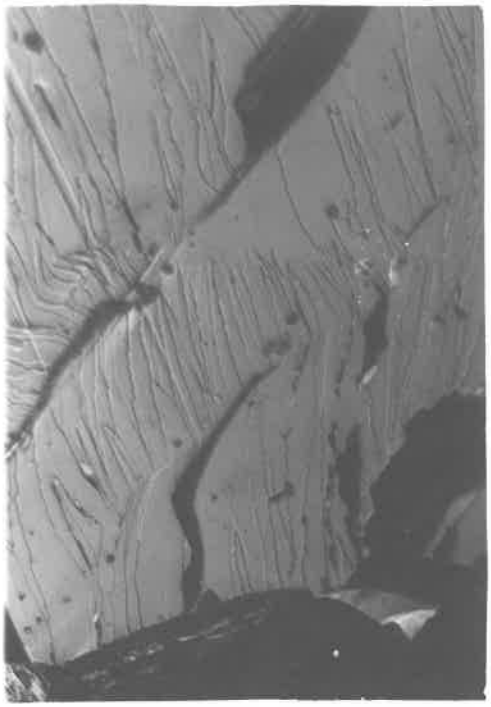

FIGURE 5.140.

FIGURE 5.141.

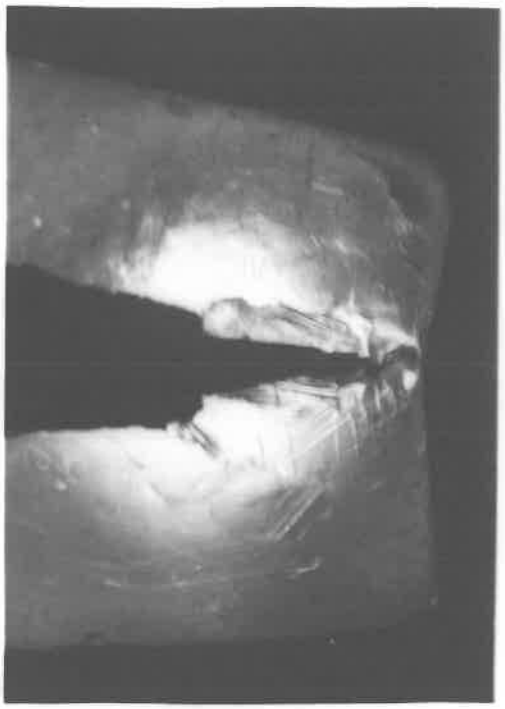

FIGURE 5.142.

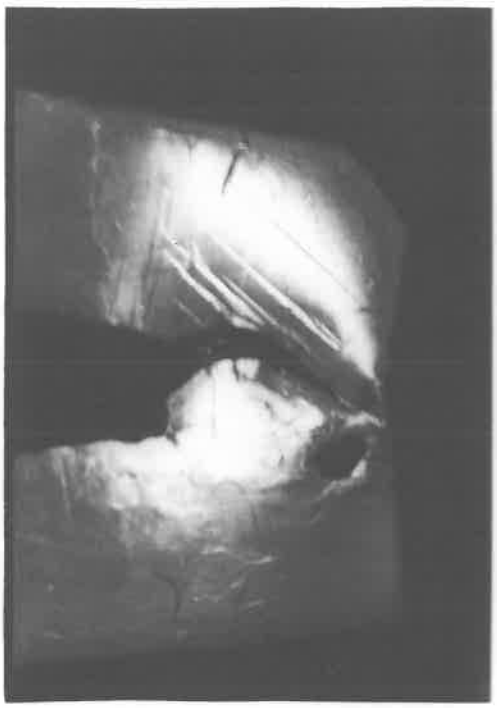

FIGURE 5.143.

FIG. 5.144 AND FIG. 5.145
PHOTOGRAPHS. DEFORMATION MARKINGS ON THE POLISHED SIDES OF SPECIMEN 6_b, ETCHED AFTER DEFORMATION, (4x).

FIG. 5.146 PHOTOGRAPH. FRACTURE SURFACE OF SPECIMEN 7, TAKEN IN DAYLIGHT, (8x).

FIG. 5.147 MICROGRAPH. FRACTURE SURFACE OF THE SECOND KIND ON SPECIMEN 7. NOTE CONTOUR LINES CURVING THROUGH 180°, (75x).

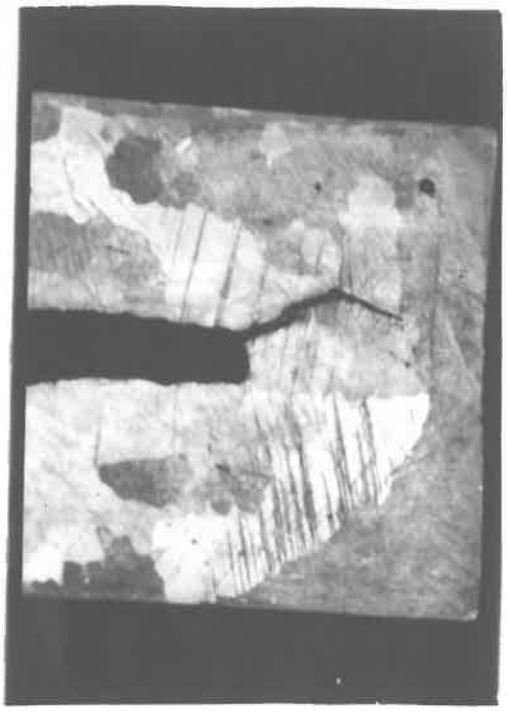

FIGURE 5.144.

FIGURE 5. 145.

FIGURE 5.146.

FIGURE 5.147.

FIG. 5.148 PHOTOGRAPH. FRACTURE SURFACE OF SPECIMEN 8, TAKEN IN DAYLIGHT, (8x).

FIG. 5.149 PHOTOGRAPH. FRACTURE SURFACE OF SPECIMEN 9, TAKEN IN DAYLIGHT, (8x).

FIG. 5.150 MICROGRAPH. FRACTURE SURFACE MARKINGS IN REGION 1 OF THE FRACTURE SURFACE ON SPECIMEN 9, (75x).

FIG. 5.151 MICROGRAPH. FRACTURE SURFACE [illegible] OF THE FIRST KIND; REGION 2 OF THE FRACTURE SURFACE ON SPECIMEN 9, (37x).

FIGURE 5.148.

FIGURE 5.149.

FIGURE 5.150.

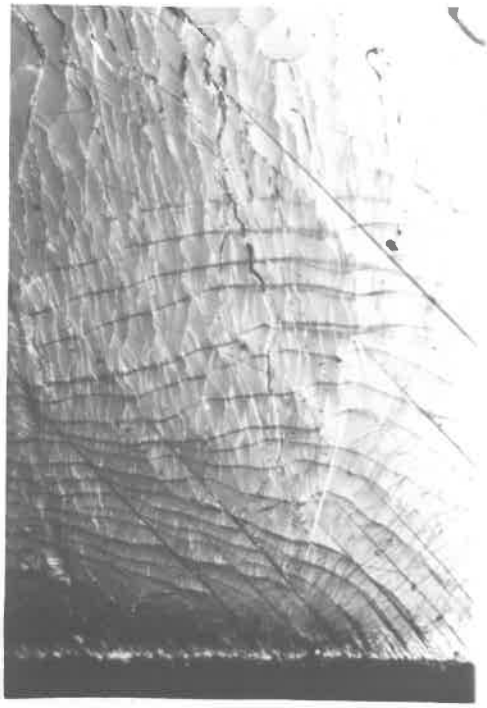

FIGURE 5.151.

FIG. 5.152 MICROGRAPH. CONTOUR LINES TERMINATING ON THE BOUNDARY OF THE FRACTURE SURFACE OF SPECIMEN 9,REGION 2, (300x).

FIG. 5.153 MICROGRAPHS. THE CONTOUR LINES AND CLEAVAGE STEP LINES ARE APPROXIMATELY PERPENDICULAR TO EACH OTHER. REGION 2 ON THE FRACTURE SURFACE OF SPECIMEN 9, (300x).

FIG. 5.154 MICROGRAPH. SINUSOIDAL UNDULATIONS OF THE CONTOUR LINES. ADJACENT CONTOUR LINES ARE ONE HALF OF ONE WAVELENGTH OUT OF STEP WITH EACH OTHER. REGION 5, SPECIMEN 9. (37x).

FIG. 5.155 MICROGRAPH. THE EFFECT OF A SECONDARY FRACTURE ON THE CONTOUR LINES. REGION 4, SPECIMEN 9, (75x).

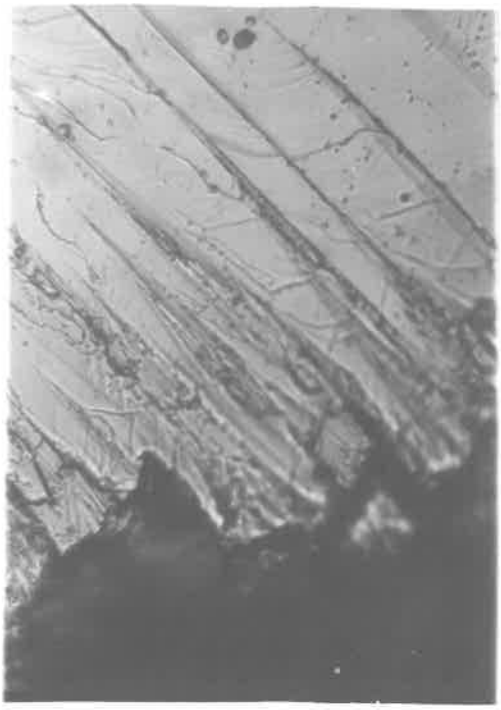

FIGURE 5.152.

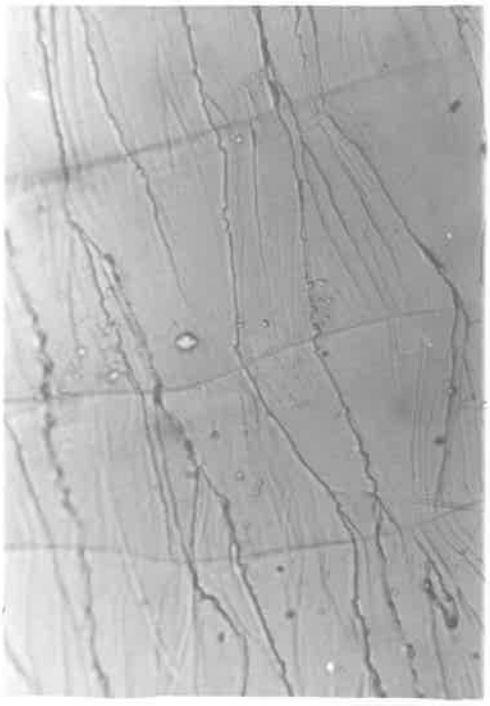

FIGURE 5.153.

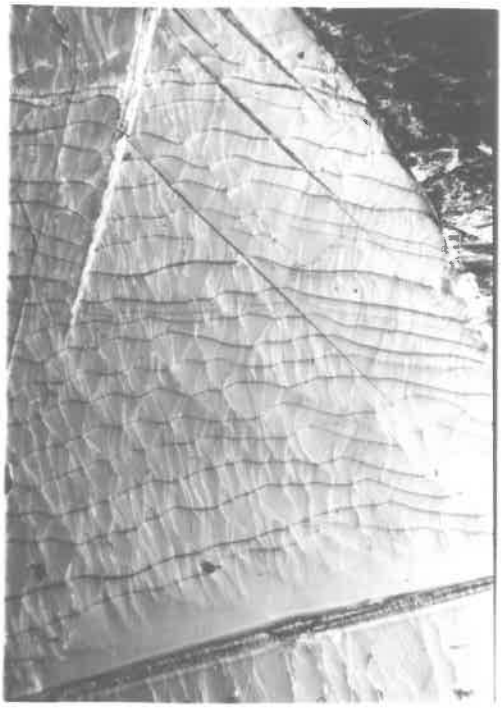

FIGURE 5.154.

FIGURE 5.155.

FIG. 5.156 MICROGRAPH. PORTION OF SURFACE SHOWN IN FIGURE 5.155 MAGNIFIED SHOWING SECONDARY FRACTURE (DARK BAND) , (300x).

FIG. 5.157 MICROGRAPH. THE TRAILING PORTIONS OF THE CONTOUR LINES TEND TO WIDEN INTO BANDS. REGION 4, SPECIMEN 9, (300x).

FIG. 5. 158 MICROGRAPH. WHEN THE FRACTURE ENTERS REGION 4 FROM REGION 5 (WHERE THERE ARE NO CONTOUR LINES), THE FIRST CONTOUR LINES HAVE THE APPEARANCE OF BANDS. SPECIMEN 9, (37x).

FIG. 5.159 MICROGRAPH. THE SURFACE MARKINGS IN THE VICINITY OF A SECONDARY FRACTURE, REGION 3, SPECIMEN 9. (300x).

FIGURE 5.156.

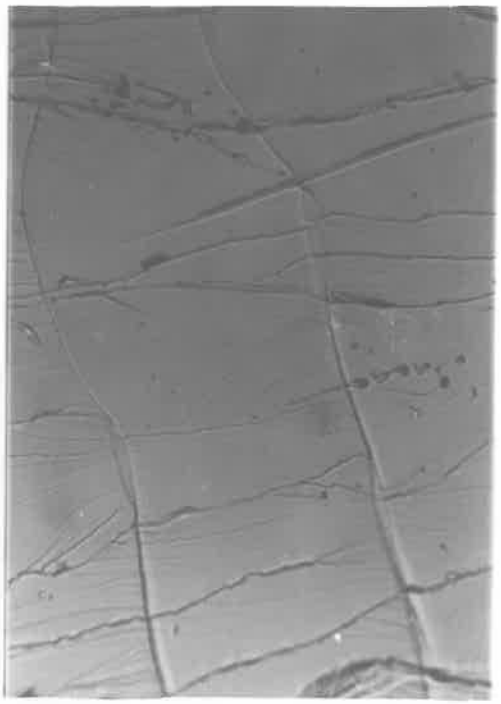

FIGURE 5.157.

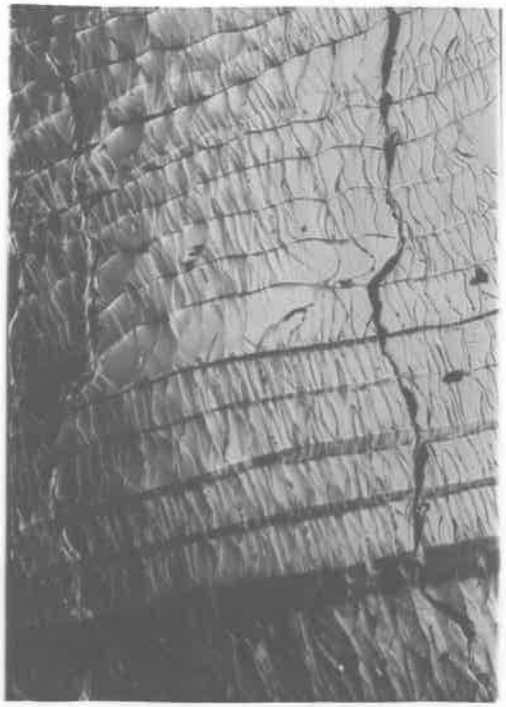

FIGURE 5.158.

FIGURE 5.159.

FIG. 5.160 MICROGRAPH. A SERIES OF CONTOUR LINES THAT BEGIN AND END AT THE BOUNDARY BETWEEN THE CRYSTALS OF SPECIMEN 9; REGION 9. (37x).

FIG. 5.161 MICROGRAPH. SHOWING THE TERMINATION OF THE CONTOUR LINES OF FIGURE 5.160. (75x).

FIG. 5.162 MICROGRAPH. FRACTURE SURFACE OF THE SECOND KIND, SPECIMEN 9. THE APPEARANCE OF THE SURFACE BETWEEN TWO SECONDARY FRACTURE LINES. (75x).

FIG. 5.163 MICROGRAPH. FRACTURE SURFACE OF THE SECOND KIND, SPECIMEN 9. SMALL SECONDARY FRACTURES ARE REVEALED BY BANDS OF MARKINGS. (300x ϕ.

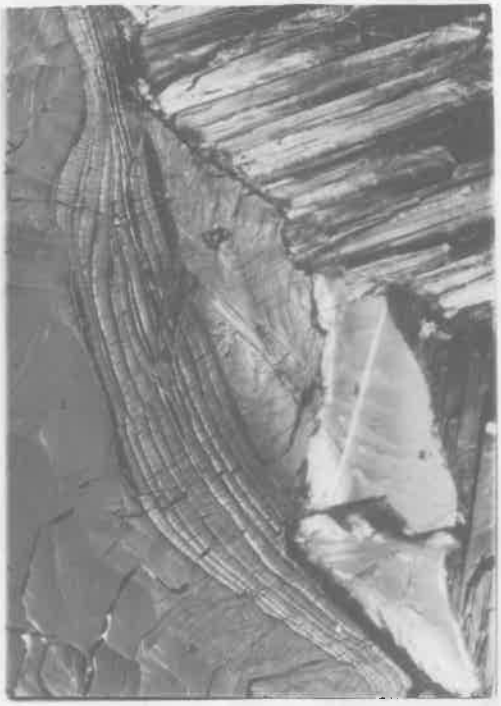

FIGURE 5.160.

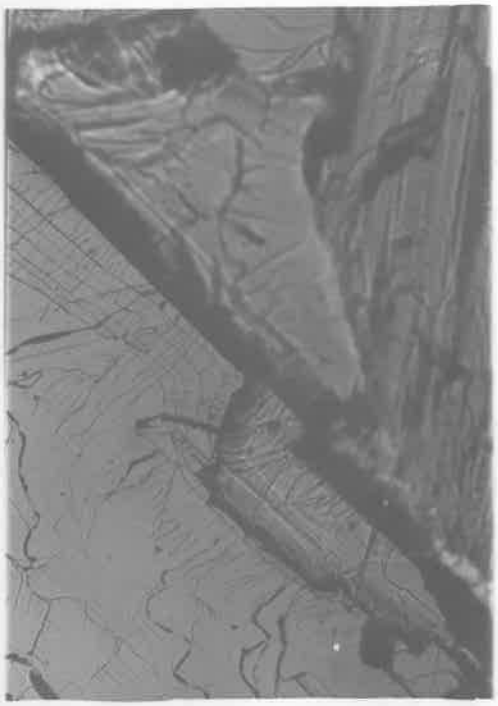

FIGURE 5.161.

FIGURE 5.162.

FIGURE 5.163.

FIG. 5.164 MICROGRAPH. FRACTURE SURFACE OF THE SECOND KIND. CONTOUR LINES WIDEN INTO BANDS. SPECIMEN 9, (300x).

FIG. 5.165 MICROGRAPH. FRACTURE SURFACE OF THE SECOND KIND. CONTOUR LINES ARE ABSENT. DENSITY OF CLEAVAGE STEP LINES IS LOWER. SPECIMEN 9, (300x).

FIG. 5.166 MICROGRAPH. FRACTURE SURFACE OF THE SECOND KIND. KINKED SECONDARY FRACTURES. SPECIMEN 9, (300x).

FIG. 5.167 MICROGRAPH. FRACTURE SURFACE OF THE SECOND KIND. A STUDY OF A CONTOUR LINE BAND. SPECIMEN 9, (300x).

FIGURE 5.164.

FIGURE 5.165.

FIGURE 5.166.

FIGURE 5.167.

FIG. 5.168 MICROGRAPH. FRACTURE SURFACE OF THE SECOND KIND. SPECIMEN 9. TWIN BANDS WITH THEIR OWN LINE MARKINGS. (300x).

FIGURES 5.169 AND 5.170
PHOTOGRAPHS. FRACTURE SURFACE OF SPECIMEN 9. DIRECTIONAL ILLUMINATION TO REVEAL TWIN BANDS ON THE FRACTURE SURFACE OF THE FIRST KIND. (4x).

FIG. 5.172 MICROGRAPH. FRACTURE SURFACE OF THE FIRST KIND, SPECIMEN 9. THE APPEARANCE OF REGION 3. CONTOUR LINES ARE ABSENT. (37x).

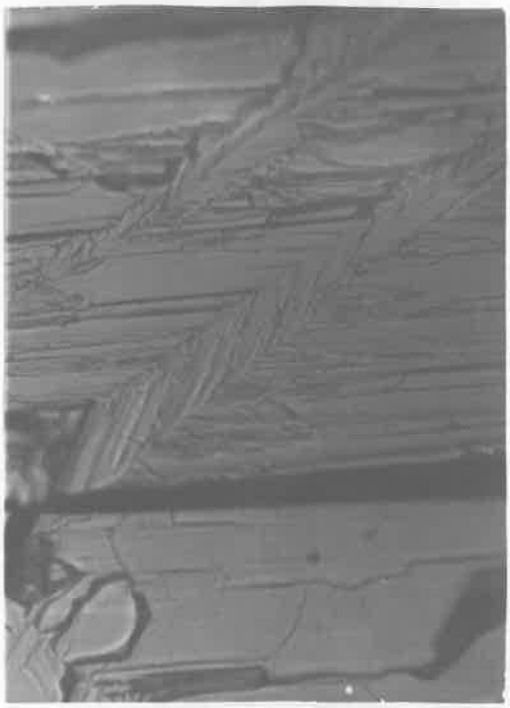

FIGURE 5.168.

FIGURE 5.169.

FIGURE 5.170.

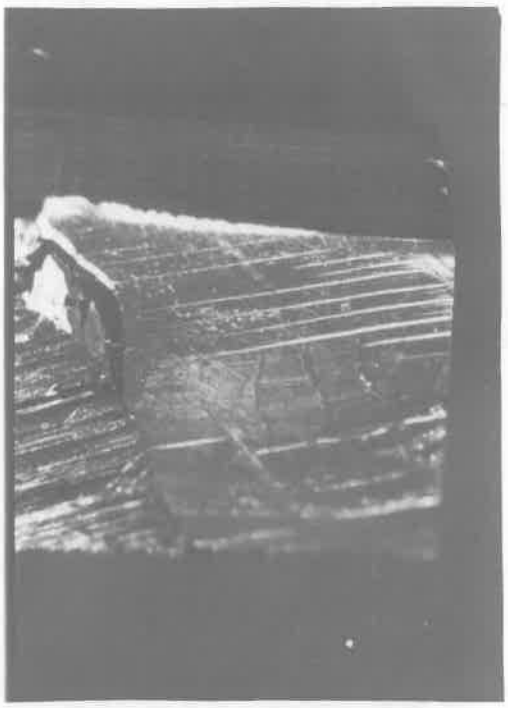

FIGURE 5.172.

FIGURES 5.173AND 5.174
PHOTOGRAPHS. THE DEFORMATION MARKINGS ON THE POLISHED SIDES OF SPECIMEN 9 WHICH WAS FRACTURED AT ROOM TEMPERATURE. (2x).

THE FRACTURE SURFACES OF THE TWO FRAGMENTS OF SPECIMEN 9.

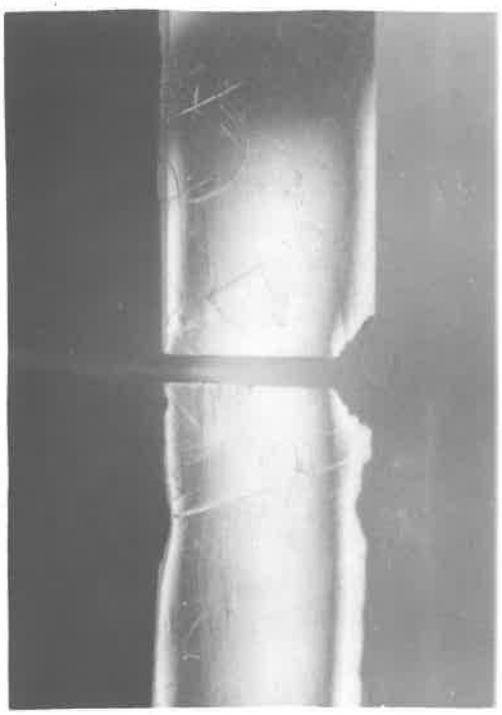

FIGURE 5.173.

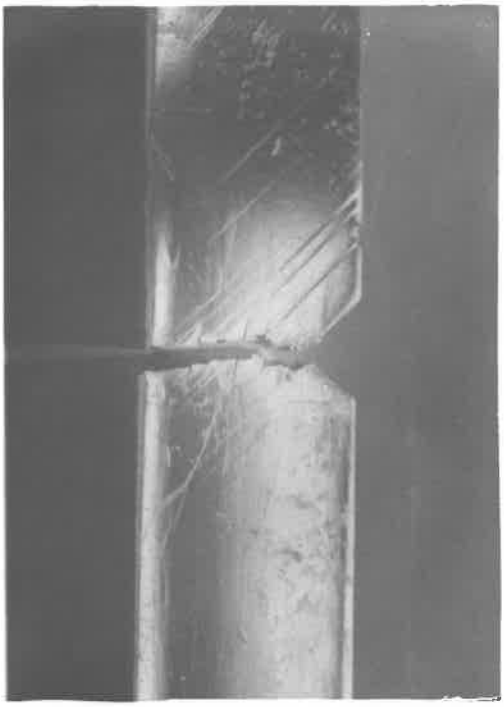

FIGURE 5.174.

FIG. 5.175 PHOTOGRAPH. THE FRACTURE SURFACE OF SPECIMEN 10, TAKEN IN DAYLIGHT. (8x).

FIGURES 5.176 AND 5.177
MICROGRAPHS. FRACTURES OF THE SECOND KIND ON SPECIMEN 10. THE SECONDARY FRACTURES AND CONTOUR LINES ARE MORE CLOSELY SPACED THAN IN THE CASE OF SPECIMEN 9. (75x).

FIG. 5.178 MICROGRAPH. A FRACTURE SURFACE OF THE SECOND KIND. INTERACTION BETWEEN A TWIN BAND AND THE REMAINDER OF THE CRYSTAL RESULTING IN SECONDARY FRACTURES. (75x).

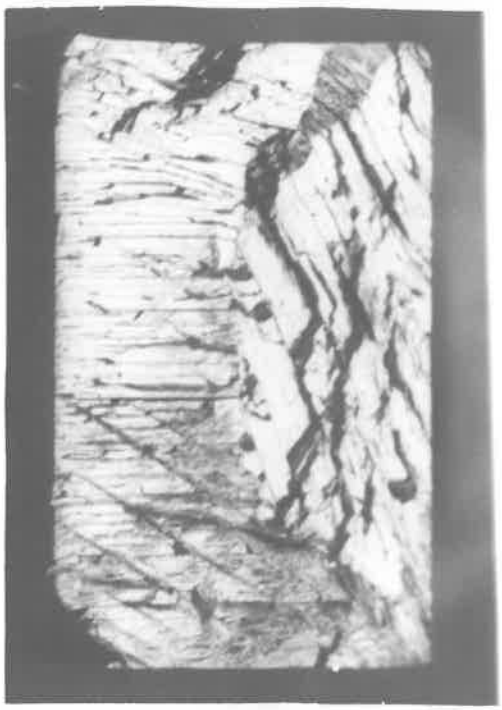

FIGURE 5.175.

FIGURE 5.176.

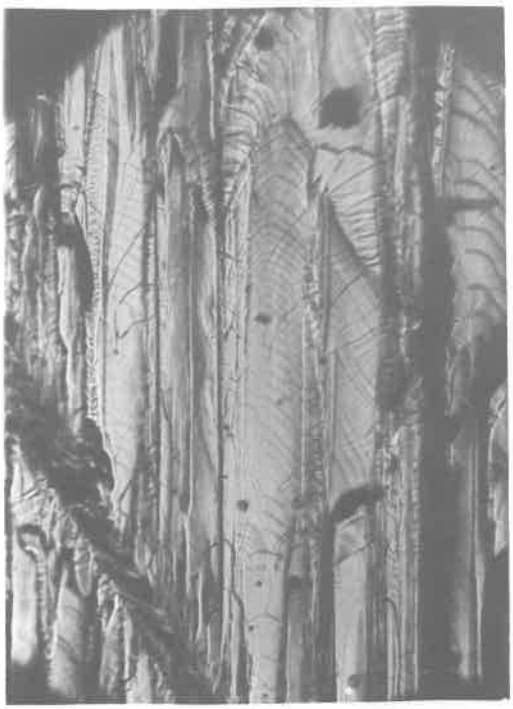

FIGURE 5.177.

FIGURE 5.178.

FIG. 5.179 MICROGRAPH. FRACTURE SURFACE OF THE SECOND KIND, SPECIMEN 10. TWIN BANDS WITH AND WITHOUT A LINE STRUCTURE. (75x).

FIG. 5.180 MICROGRAPH. FRACTURE SURFACE OF THE SECOND KIND, SPECIMEN 10. ZIG-ZAG PATTERNS PRODUCED BY TWIN BANDS (75x).

FIGURES 5.181 AND 5.182
MICROGRAPHS. FRACTURE SURFACES OF THE SECOND KIND, SPECIMEN 10. IRREGULAR CONTOUR BINE PATTERNS. (75x).

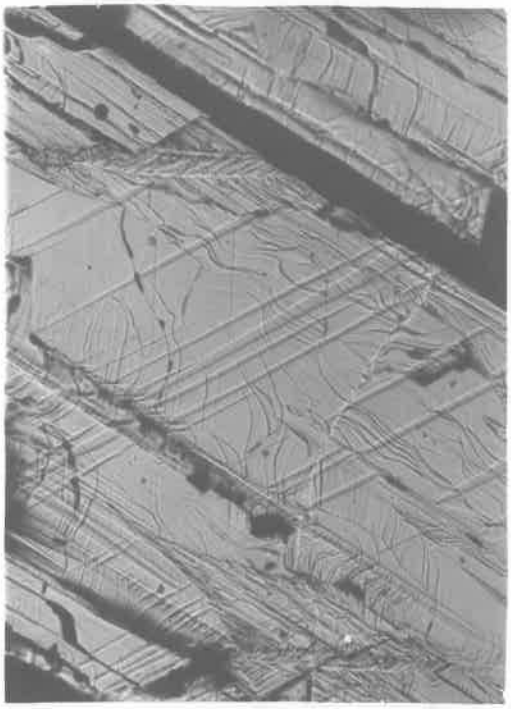

FIGURE 5.179.

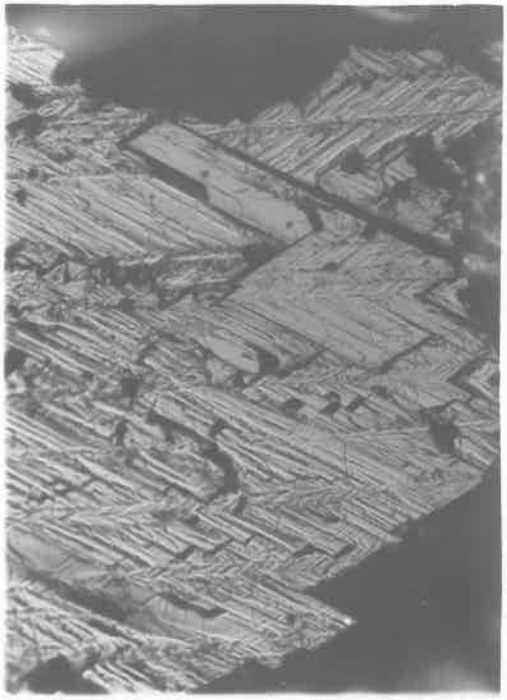

FIGURE 5.180.

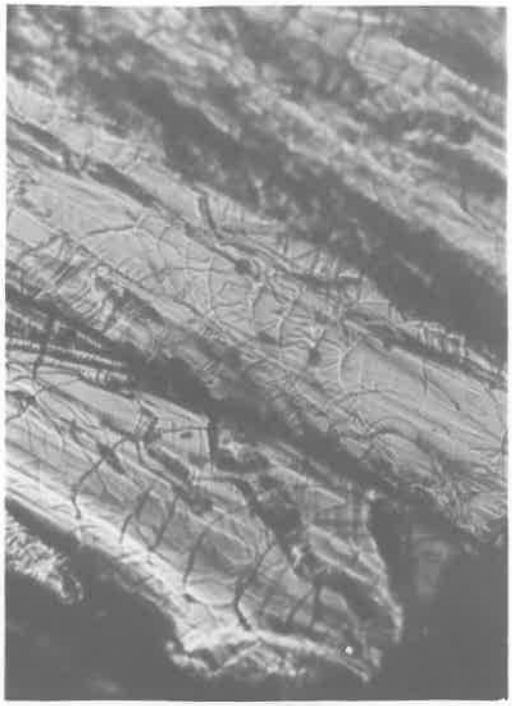

FIGURE 5.181.

FIGURE 5.182.

FIGURES 5.183 AND 5.184
PHOTOGRAPHS. DEFORMATION MARKINGS ON THE POLISHED SIDES OF SPECIMEN 10, WHICH WAS FRACTURED AT ROOM TEMPERATURE. (4x).

THE FRACTURE SURFACES OF THE TWO FRAGMENTS OF SPECIMEN 10.

FIGURE 5.184.

FIGURE 5.183.

5.3 MICRO-INDENTATION TESTS

Experiments on whiskers and metal filaments have been performed by various workers.[45,52] These provide some factual data about the behaviour of crystals of small cross-section.

The present experiment was designed to investigate the properties of a small portion of a relatively large crystal. A sharp needle was brought against the surface of the crystal being investigated. By this means, a small volume of crystal could be subjected to a high stress, the parameters of interest being the yield stress in the vicinity of the needle point, and the deformation pattern obtained when the needle penetrates.

The current deformation theory is based on the concept of dislocation. In a severely deformed crystal, the dislocation density is in the region of 10^{12} lines per sq. cm. In a carefully prepared crystal, the density can easily be kept below 10^{8} lines per sq. cm. If the surface of the crystal whose dislocation density is 10^{6} lines per sq. cm. is probed with a needle of tip radius 10^{-4} cm., then one can expect the needle to encounter dislocation-free zones, of dimension 10 or more times the tip radius, quite frequently.

This experiment was designed initially to probe crystal surfaces with a dislocation spacing greater than the needle tip radius by a factor of the order of 10 or more.

A suitable crystal surface had to be prepared by a method that did not increase the density of dislocations. This may be done by chemical and electrolytic polishing of a crystal. It was considered at that time that preparation of a crystal surface by cleavage would not only provide a surface with the same dislocation density as the bulk of the undisturbed crystal, but in addition, make available a crystallographic surface.

Large crystals of zinc grown during the preparation of zinc specimens for the splitting tests were already available. They were cleaved at room temperature and the surfaces so produced were used in the indentation tests.

In order to explain some of the observations made during the splitting tests, the writer has put forward the hypothesis that glide (i.e. dislocations) may be nucleated by a crack. According to this hypothesis, a cleavage surface will not possess a dislocation density similar to that of the bulk of the undisturbed crystal. As a consequence experiments in which cleaved surfaces were employed can be expected to yield results that are

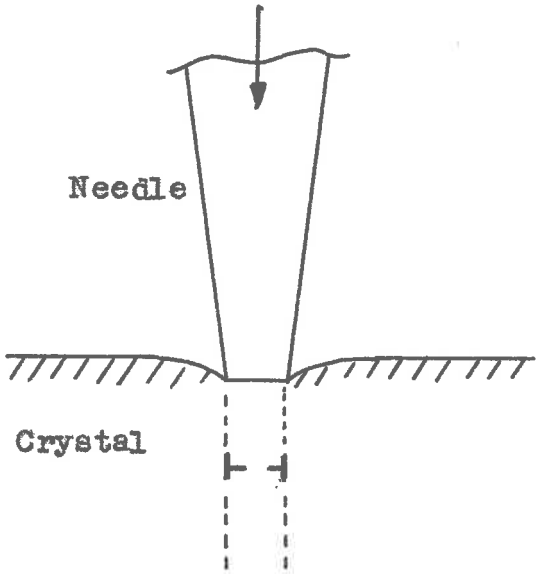

FIG. 5.185) Accomodation by Prismatic Dislocations

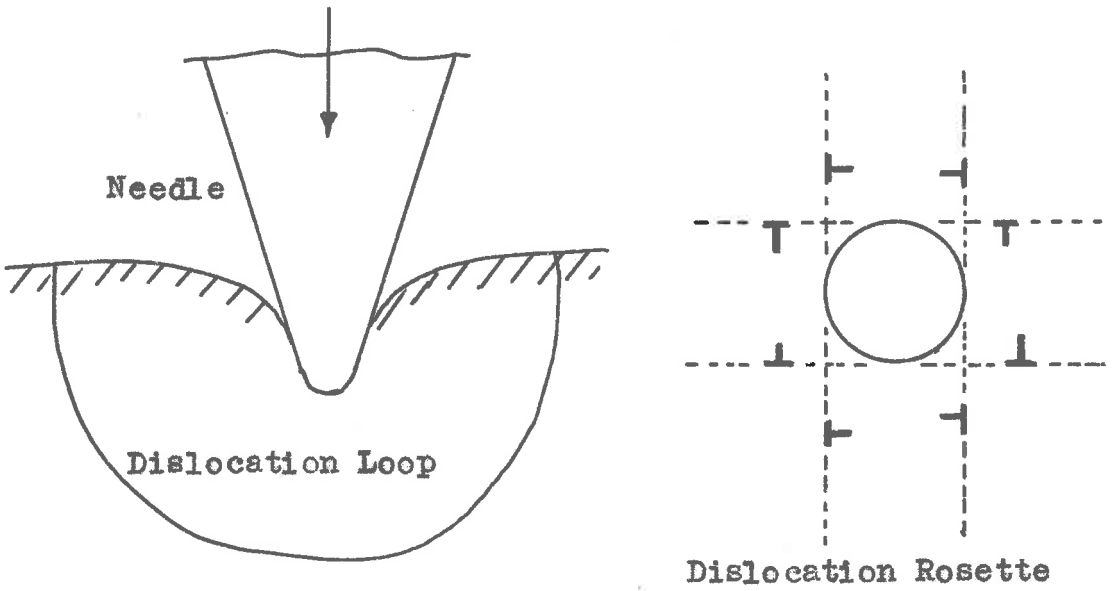

FIG. 5.186) Accomodation by normal Dislocations

FIGS. 5.185 and 5.186 Two Ways in which a Crystal can accomodate a Needle by Plastic Deformation.

relevant to this hypothesis.

If a needle is brought against the surface of a dislocation-free crystal, then any plastic penetration will be accompanied by the nucleation of dislocations. The needle is assumed to retain its shape so that it only deforms elastically.

There are two ways in which the crystal can accommodate the needle through dislocation nucleation. These are: by the formation of prismatic loops as shown by Figure 5.185 or by the formation of half-loops on at least two glide systems as shown by Figure 5.186.

The second process results in the formation of dislocation rosettes such as those found by Gilman and Johnston.[24] These workers pressed a steel ball against the surface of a dislocation-free LiF crystal and etched to reveal any dislocations that may have appeared. This substantiates the existence of such half-loops. If prismatic dislocation loops were also formed they would not have been detected by this etch.

5.3.1 Apparatus and Procedure

Two kinds of needles were prepared: steel and glass. The steel needles were obtained in the form of ordinary sewing needles about $^{3}/_{40}$th inch in diameter and polished to a finer point. This was done in a number of stages from a coarse initial grind on 300 grade metallurgical paper to a polish with medium carborundum polishing powder, this stage being performed on a polishing machine.

The glass was obtained in the form of rods $^{3}/_{32}$th inch in diameter. The rod was drawn to a point by heating in a narrow flame and pulling at the appropriate moment. The rod would generally draw down to a fibre a few thousandths of an inch in diameter. This fibre was broken off just ahead of the apex of the tapering portion and polished on the polishing machine with a course grade of corundum.

There appears to be a limit to the tip radius that may be obtained by this procedure. This limit seems to be 0.00005 inch, and is probably set by the soft polishing cloth used. A more rigid lapping surface would probably make it possible to attain even finer radii.

With the optical microscope available, the writer could expect to resolve two points 10^{-5} inch apart. To

produce indentations of this order of magnitude would involve considerable difficulty in finding them and even more in measuring them. Needles with a tip radius of 5×10^{-5} inch were therefore considered to be sufficiently sharp.

Two loading durations were considered. On the one hand, the needle was to be projected against the specimen with a known velocity. The load duration would then be of the order of the time taken by a pressure signal leaving the tip of the needle to travel to the other end and come back. The magnitude of the load can also be computed. An analysis of such an impact is presented in Appendix 9.1 in which the shape of the stress-time curve is also derived. This implies a loading duration in the region of 10^{-5} second.

The second loading interval was to be of the order of one second. The needle was to be brought into contact with the surface being investigated at a velocity so low that impact effects are negligible. The load was known and the specimen was to be examined subsequently to find out which loading condition produced an indentation. Those loads which do not produce an indentation leave no visible mark. The success of this experiment depends on

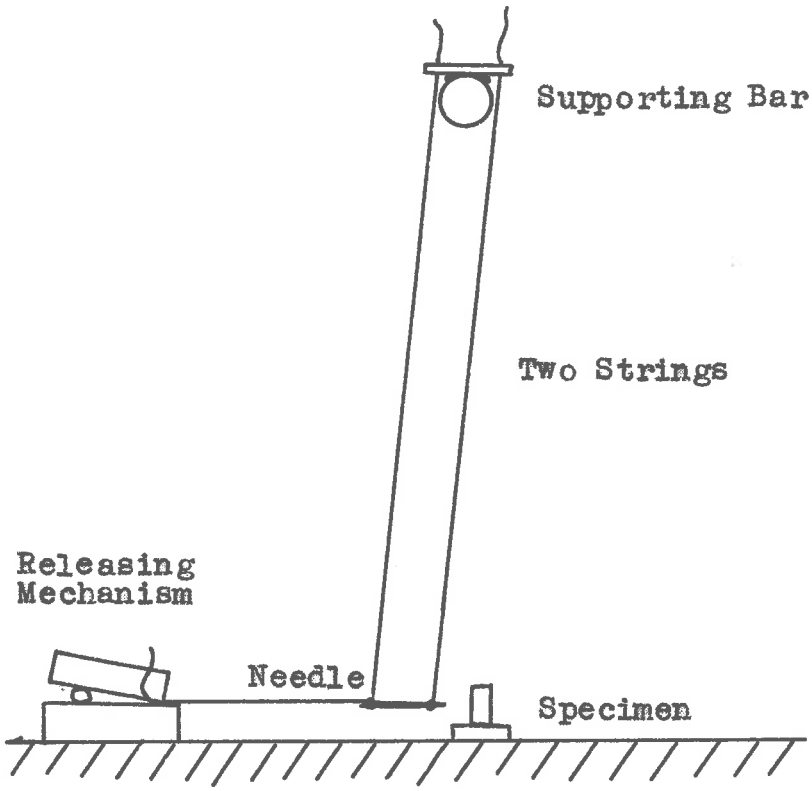

FIG. 5.187 The Dynamic Pendulum Indentation Apparatus.

arranging the location of the indentation in such a manner that from the indentations the probable location of points where no indentations were produced could be predicted, and the area subjected to careful examination. This series would also furnish information on the variation, if any, of the yield stress with the size of the indentation.

Impact experiments were performed in two ways. Initially the needle was suspended on two light strings as shown in Figure 3.407. The needle was pulled back by a third string and clamped under a weight. When all motion had been damped out, the weight was lifted and the needle moved off to impact on the specimen. A scale along the path of the needle (in this case graph paper) permits one to obtain a rebound of the needle.

Although the specimen is not moved between successive impacts the transverse freedom of the needle ensures that impact in the same region of the specimen is highly unlikely.

The potential energy of the needle is proportional to the square of the displacement of the needle from its neutral point (for small displacements). Thus a rebound distance of 1/10 impact distance represents 1/100 of the impact energy. The pendulum is therefore well adapted to

the measuring of small rebound energies.

Unfortunately, the strings which suspend the needle also set a lower limit to the velocities at which meaningful rebound readings can be expected. On the one hand there is the damping due to the air through which the string moves. Conversely, a slight air current can have a large effect on the velocity of the needle. These problems could be solved by enclosing the string and calibrating the system by finding the rate of decay of free pendulum oscillation of the needle.

The second problem is concerned with the string inertia. When the needle stops on impact, the string continues to move. As it does so, it bows out and is brought to rest only when the string tension has reached a sufficient value. The duration of the actual impact is too short to be affected, but a portion of the rebound energy of the needle is converted into vertical motion, which is therefore lost, and the change in momentum of the string is provided by the rebounding needle. This could also be allowed for. But when the needle has a rebound momentum less than the forward momentum of the string, then the needle can not rebound at all and no measurement is possible. A more detailed analysis of this limitation

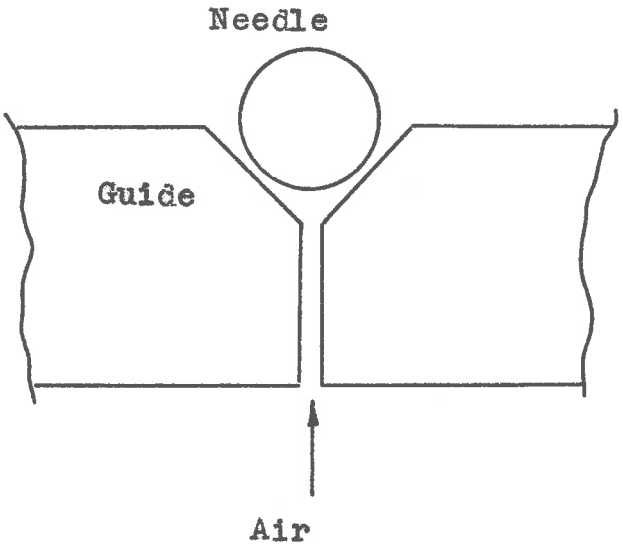

FIG. 5.188 The Inclined Plane Apparatus in which the Needle is supported by an Air Cushion.

on the dynamic pendulum system is presented in Appendix 9.2.

In preliminary tests it was found that while a glass surface gave very elastic rebounds, and steel surfaces a measureable value, zinc specimens which were of greatest interest failed to give a rebound even with string lengths of 60 inches and a pre-impact travel of ½ inch or a pendulum length of 22 inches and a pre-impact travel of 0.020 inch.

The dynamic pendulum apparatus was abandoned. Another method of guiding the needles was adopted. This apparatus consists essentially of an inclined plane. The friction between the incline and the needle was reduced by supporting the needle on an air cushion. The way in which the needle was supported is indicated by Figure 5.160. The guide is mounted on a flat plate with three levelling screws. The procedure was to place the needle onto the guide a specified distance from the specimen, apply air so that the needle is free to slide and cut it off when the needle has reached the peak of the rebound. The rebound distance could then be read at leisure. Air was supplied by a vacuum cleaner. Rubber tubing conveyed the air to the apparatus. The flow could be cut off by squeezing the tube between the fingers. The acceleration of the needle was found by measuring the

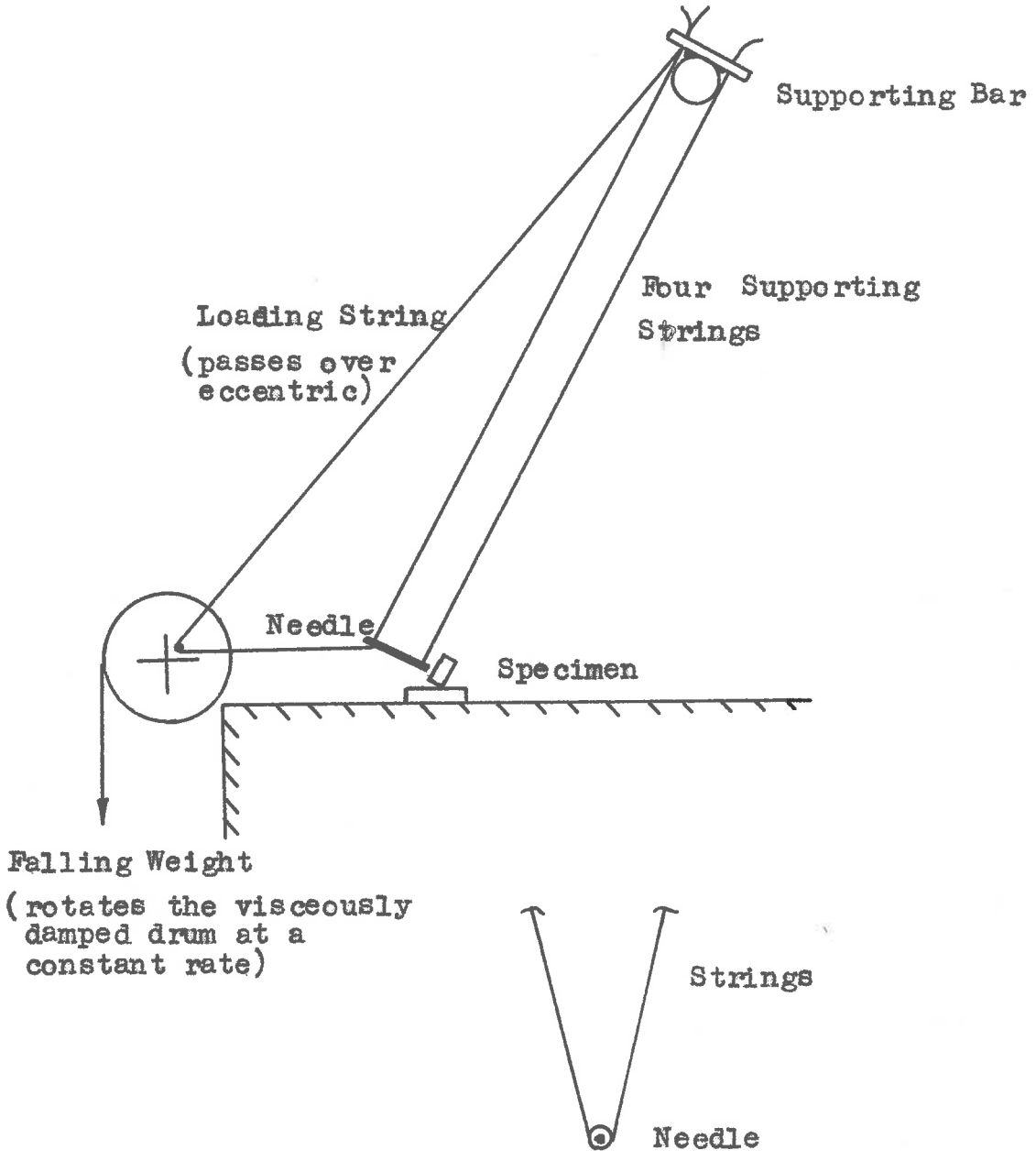

FIG. 5.189 The Static Indentation Apparatus.

time taken by the needle to impact on the specimen from various distances. The lowest practical velocities were about 1 inch per second.

This method of projecting the needle had two shortcomings. The needle had a tendency to spin about its longitudinal axis and with very low inclinations it would move back and forth along the guide in a random manner. The end of the guide behaved differently from the main part, which meant that a needle travel of ½ inch or less had doubtful significance. This precluded the use of a microscope and short needle travel. Another factor against short travel is its short duration (with a pendulum the period is independent of the amplitude), making measurement more difficult.

The requirements of the static loading experiment were less difficult to meet. The needle had to be brought against the specimen at a velocity so low that impact effects are negligible. The static load had to be capable of variation over a wide range, and of being measured with at least two-figure accuracy.

The apparatus finally adopted is shown in Figure 5.189. The needle is supported by four strings, which restrains transverse motion, and drawn back a given distance from the neutral point. If the direction of the needle is

perpendicular to the supporting strings, then the force with which it bears against a surface is given by the expression

$$P = \frac{W \cdot x}{l} \qquad \ldots\ldots (5.36)$$

where W is the weight of the needle

x is the horizontal displacement from the neutral point

l is the string length.

Another string is attached to the blunt end of the needle, passed over an eccentric and secured at the supporting bar. By pulling in the positioning string, the needle could be brought back to any desired displacement. The supporting bar was then rotated to bring the needle axis normal to the strings and minor adjustments to the positioning string made.

The eccentric is rotated by a falling weight, the rotational speed being limited by a viscous damper. When the eccentric is rotating, the needle moves back and forth a distance of about $\frac{1}{2}$ inch. At the extremities of the needle travel, its velocity is very small. The position of the needle is so adjusted that it makes contact with the specimen near the lower limit of its travel. The period of rotation of the eccentric is 10 seconds, so that

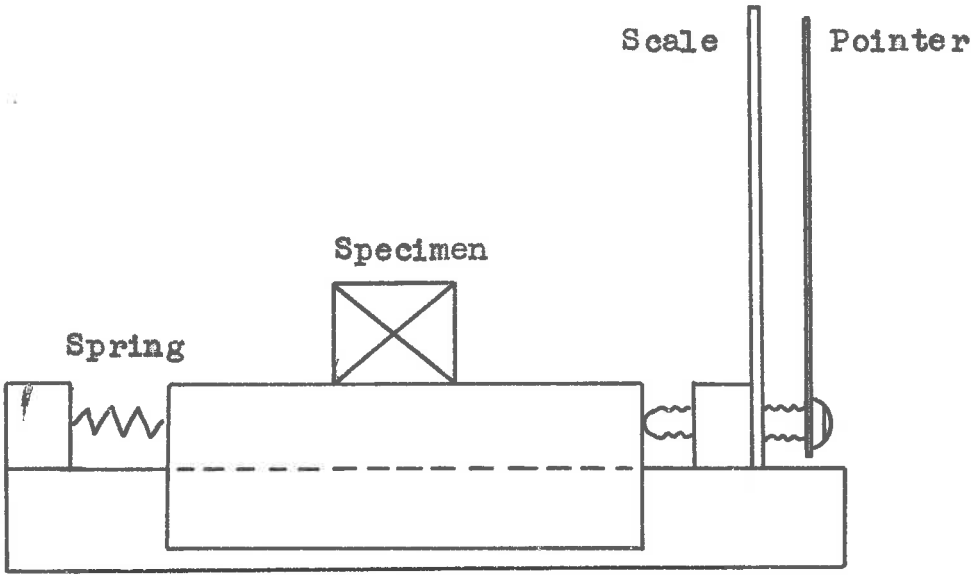

FIG. 5.190 The Apparatus for the transverse Translation of the Indentation Specimens.

needle speeds of 1/500 inch per second at the moment of contact are quite feasible.

To vary the static load, stirrups of thick copper wire were hung from the needle. When the apparatus is set up on a table the falling weight can turn the eccentric about six times before coming to rest on the floor. This made it possible to obtain five loadings at a given load in succession. The device shown in Figure 5.190 was used to displace the specimen transversely so that needle contact could take place at five points a controlled distance apart.

After each of these loading runs the needle load was varied by adding or removing a stirrup and the experiment repeated.

The experiment was performed at room temperature and under liquid air. In the latter instance, the specimen was placed into a container which was then filled with the liquid until the specimen and needle were submerged. The specimen was displaced transversely by shifting the container. In this case the load was changed after each loading, and the container was displaced before repeating the loading run. Between successive loadings, the reduction of needle load caused a slight change in string length sufficient to displace successive loading points from each other.

5.3.2

Results

It was found that with zinc specimens, no measurable rebound was obtained with a pre-impact travel of the needle of 0.020 inch and a pendulum length of 22 inches.

The needle had a length of 45 mm. and a diameter of 0.8 mm., the tip radius being 1.3×10^{-4} cm.

An analysis of an impacting needle is presented in Appendix 9.1. For the present purpose, the simplified expression (9.5) will suffice. The stress concentrating factor due to the taper at the needle, R, is approximately

$$R = \left(\frac{\text{needle shank radius}}{\text{needle tip radius}}\right)^2 = \left(\frac{4 \times 10^{-2}}{1.3 \times 10^{-4}}\right)^2 = 9.5 \times 10^4 \qquad \ldots\ldots (5.37)$$

Whence, the stress at the needle tip

$$\sigma = 9.5 \times 10^4 \times 0.09 \times 7.9 \times 5 \times 10^5 \text{ dynes/cm}^2 \qquad \ldots\ldots (5.38)$$

$$\sigma = 3.4 \times 10^{10} \text{ dynes/sq.cm.} \qquad \ldots\ldots (5.39)$$

This is a computation based on the assumption that the needle encounters a rigid obstacle. If the

surface yields, the stress is clearly less. Consequently the only conclusion that can be drawn is that zinc yields at a stress lower than 3.4×10^{10} dynes/sq.cm. Since the rebound is smaller than 0.002 in., the stress at the needle tip will be less than about 4×10^{9} dynes/sq.cm.

The static tests produced a greater body of results. The indentations were located on the specimen surfaces and photographed at a magnification of 120x. Further magnification by projecting against a wall made it possible to read the diameter of the indentation with a ruler.

The results obtained during one such series are presented in Table 5.1B. This test was performed at room temperature, the specimen surface being prepared by carefully cleaving a zinc crystal at room temperature. The pendulum length was 16.5 in. and the displacement of the needle from the mean was 3.0 in.

TABLE 5.12 Results of Static Load Indentation Test Performed at Room Temperature

Stirrup weight 2.85 gm., needle 0.62 gm.

No. of Stirrups	Active Component gms.	Indentation Area (Average) sq.cm.	Nominal Stress gm/sq.cm.	Remarks
6	3.22	0.61×10^{-6}	5.3×10^{6}	
5	2.70	0.67×10^{-6}	4.0×10^{6}	
4	2.18	0.37×10^{-6}	5.8×10^{6}	Average value 4.97×10^{6} gm/sq.cm.
3	1.67	0.37×10^{-6}	4.5×10^{6}	
2	1.15	0.23×10^{-6}	4.9×10^{6}	
1	0.63	0.12×10^{-6}	5.4×10^{6}	
0	0.113	-	-	Indentations not found

As the indentations were generally elongated, two perpendicular diameters were measured, the maximum and minimum, the area was computed by treating the indentation as an ellipse, the readings being inserted for the major and minor axes.

No indentations were found for the smallest loading force of 0.11 gm., which would exert a bearing stress of approximately 2×10^{6} gm/sq.cm. if the area of

contact is taken to be the area of a circle with radius equal to the radius of the needle tip.

The computed nominal stress values do not exhibit a trend in that the stress for the smaller indentations is equal to that at which the larger indentations are formed.

TABLE 5.13 Results of Static Load Indentation Test Performed under Liquid Air

Pendulum length 24½ in.
Displacement 13 in.
Stirrup weight 1.42 gm., needle 0.62 gm.

No. of Stirrups	Active Component of Load gm.	Average Area of Indentation $cm.^2$	Nominal Stress gm/sq.cm.
5	7.7	0.36×10^{-6}	1.5×10^{7}
4	6.3	0.26×10^{-6}	1.9×10^{7}
3	4.9	0.22×10^{-6}	1.4×10^{7}

During the low temperature test, seven loading runs were taken. There are six load values in each run so that the needle was brought against the specimen 42 times. Only 17 indentations were found however. The indentations were scattered in this case so that the points obtained during a particular loading run could not be separated from the remainder. The seven largest

indentations were therefore assumed to be due to the greatest load and so on.

The results of Table 5.13 indicate that the stress is again independent of the size of the indentation. The average stress is about three times greater than the average for the room temperature test.

The appearance of the surface around the indentation does not lend itself readily to photography. Sketches of typical indentation markings are therefore presented in Figures 5.191 to 5.193. There is a distinct dissimilarity between the indentations produced by a static load and indentations of comparable size but produced dynamically both at room temperature.

The twin bands near the static indentation are shorter, and the deformation around the indentation is continuous (no slip bands) and close to the boundary of the indentation. The dynamic indentation on the other hand has large twin bands, and a series of slip bands of hexagonal appearance around the indentation and extending a considerable distance (more than 5 diameters) on either side of the indentation.

Dynamic indentations obtained with a needle of higher velocity show more penetrating twin bands radiating out in six directions at 60° to each other, of which two collinear systems have more twin band area than the others.

The hexagonal slip lines are also present, extending as far as the twins.

Figure 5.19A shows a typical indentation obtained at high velocity (about 100x the energy of the low velocity indentation), which are more amenable to photographic reproduction.

The indentations obtained at low temperature with a static load, differ from those obtained at room temperature in the appearance of the deformation band and the starting point and angular relationship of the twins.

5.3.3

Discussion of Results

From the dynamic loading test results it was calculated that the yield stress of the specimen under dynamic conditions was less than about 4×10^6 gm/sq.cm. The yield stress value for the room temperature static test was found to be 5×10^6 gm/sq.cm. These two values are of the same order, and suggest that the yield stress is not affected by the load duration. The appearance of the specimen surface around the indentation is not the same for these two load durations. The main difference is that in the dynamic case the deformation around the indentation was concentrated into two twins and a series of hexagonal glide bands, which are found up to several diameters from the indentation. In the static load case the twin bands are still there but the hexagonal glide bands have disappeared. The volume of crystal displaced from the indentation seems to be piled up on either side as Figure 5.192 suggests.

The markings around indentations obtained at low temperature with a static load are different from those around the room temperature and dynamic indentations. The twin bands are no longer in line, and a wide glide band that will not resolve into finer bands is the only other evidence of deformation.

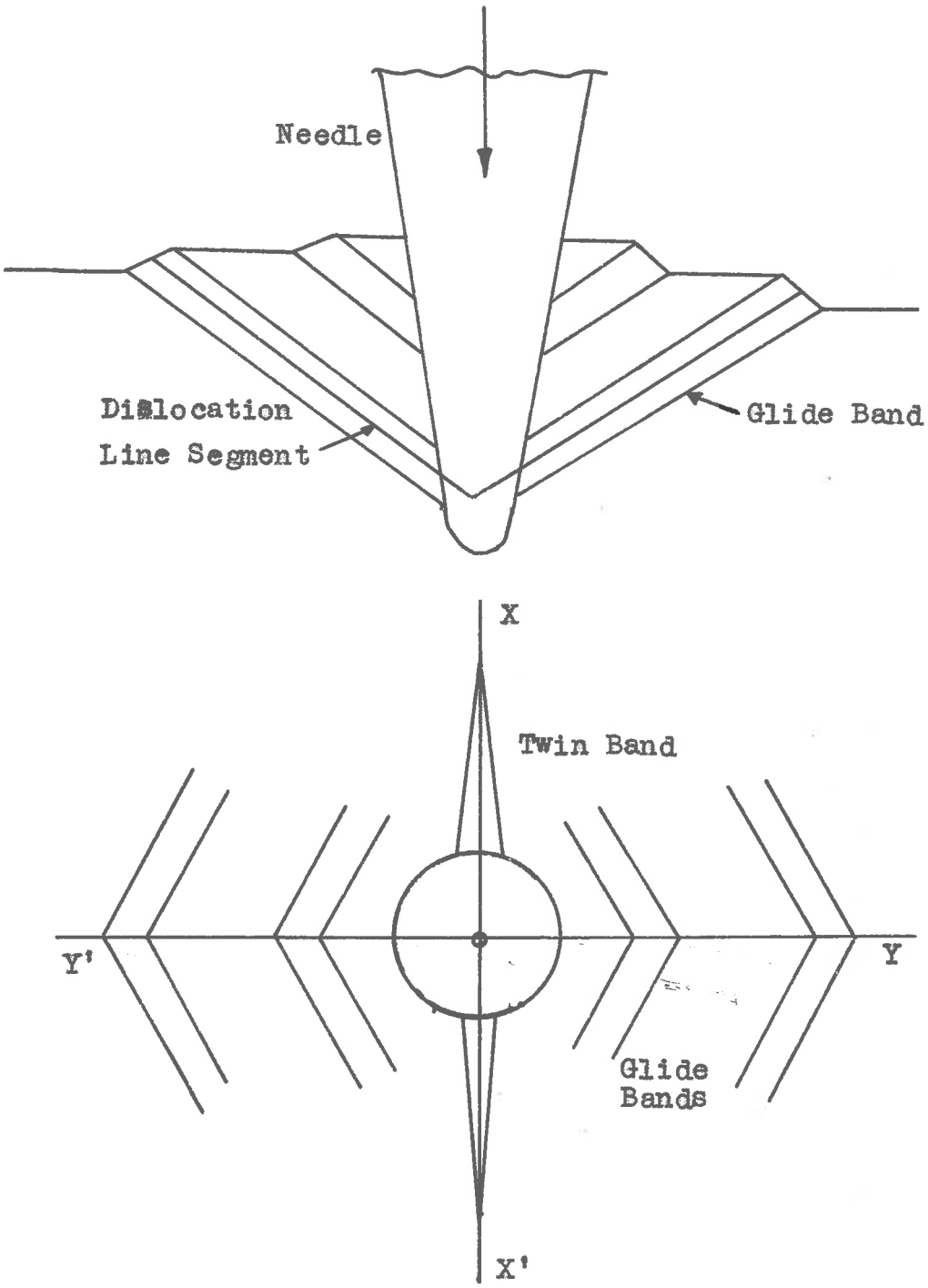

FIG. 5.195 Interpretation of the Patterns of Figure 5.191.

It seems reasonable that the high energy indentations will exhibit every possible mode of deformation. Twin bands radiate out in six equally spaced directions, and glide bands can form hexagonal outlines around the indentations although this hexagon is not completed around any one indentation.

The twin bands have an appearance that is very similar to the dislocation rosettes referred to earlier. The glide bands, however, suggest an entirely new deformation mode. This is illustrated in Figure 5.19b. The widening of the indentation along the OX and OX' direction is by the glide bands shown. It appears that dislocations which occur simultaneously on two planes can move together, resulting in a 60^{0} bend in the glide band. At the ends of these glide bands dislocation lines terminate. They are connected in the manner shown in part (a) of the Figure. While these dislocation loops can expand in the OX and OX' directions, they do so at a considerable depth. Near the surface, accomodation in these directions is therefore by twinning.

According to this interpretation, the greater concentration of glide for the static loading at both temperatures implies that not all the events that must

necessarily occur in order to accommodate the needle are visible. It is possible that accommodation of the type indicated in Figure 5.186 occurs in these instances.

Figure 5.193 shows a glide band on one side of the indentation only, the twins beginning on the opposite boundary of the indentation. Small scale accommodation (to accommodate the shape of the needle) of the type indicated in Figure 5.186 is likely in this case.

Twin bands are more plentiful around the high energy dynamic indentations. If the region under strain is large, twinning seems to occur more readily than when it is small, even if the stress in both cases is the same. This may be taken to imply that twinning is propagated more readily than glide. Thus, if glide appears at a lower stress than twinning, the smaller indentations will have fewer twin bands than the larger ones. This hypothesis is supported by the great length even of narrow twin bands on the zinc cleavage surfaces.

The specimen surfaces were on the basal plane consequently the glide bands represent non-basal glide, and the stress values obtained give some indication of the stress necessary to maintain non-basal glide.

The threefold increase of the stress at liquid air temperature suggests that at reduced temperature the

stress to move dislocation is higher. It does not appear likely that room temperature has a significant effect on the dislocation nucleating mechanism. Cold worked zinc anneals at room temperature. It is not surprising that thermal assistance to the motion of dislocation should be significant. If this is so, then the yield stress is glide not nucleation controlled.

Examination of the indentation markings suggests that temperature affects the stress reading by also influencing the inclination of the glide plane to the specimen surface. If this angle of inclination is small, surface markings a considerable distance from the indentation are found. From this the order of the indentations in decreasing inclination is: static room temperature, static low temperature and dynamic room temperature.

Assuming that the influence of temperature is due to the occasional high thermal energy, E, that may be associated with a particular group of atoms, the frequency of such high energy values is

$$\nu \propto e^{\frac{-E}{kT}} \qquad \ldots\ldots (5.40)$$

where E is the energy

k Boltzmann's constant

T absolute temperature.

At two temperatures, T_1 and T_2, the frequencies have the ratio

$$\nu_1 / \nu_2 = e^{-\frac{U}{k}\left(\frac{1}{T_1} - \frac{1}{T_2}\right)} \quad \text{..... (5.14)}$$

In two intervals of equal duration at different temperatures, the ratio of the number of random events is given by the above expression.

In two intervals of different duration performed at the same temperature

$$\frac{n_1}{n_2} = t_1/t_2$$

where t_1, t_2 are the load durations.

The dynamic indentation may be taken as being equivalent to a low temperature static indentation. The equivalent temperature T_2 is defined by the expression

$$\frac{T_1}{T_2} = 1 + \frac{k}{U} T_1 \ln \frac{t_2}{t_1} \quad \text{..... (5.15)}$$

where t_1 is the static load duration and

T_1 is the temperature at which both static and dynamic tests are actually performed.

If the static load duration is 1 sec., the dynamic duration 10^{-3} sec., and the room temperature 290°K, the

equivalent temperature

$$\frac{T_1}{T_2} = 1 + \frac{k T_1}{E} (11.51) \qquad \ldots\ldots (5.43)$$

Hence if $\frac{E}{kT} = 10, 5, 2$

$T_2 = 135^\circ K, 58^\circ K, 43^\circ K$ respectively.

The interesting aspect of this is that as the activation energy, E, tends towards the thermal mean kT, the equivalent temperature tends towards zero.

The deformation markings around the low temperature static indentations are more extended than those around the room temperature indentations. The markings around the dynamic indentations differ more from those around the low temperature static indentations than the two static indentations differ from each other. This suggests an equivalent temperature even lower than 90°K (the temperature of liquid air), and a corresponding activation energy of less than 0.2 e.v.

The nominal stress is measured at values as high as 1.4×10^7 gms/sq.cm. This represents an elastic strain of 1.4×10^{-2} in zinc ($E = 10^9$ gms/sq.cm.). When compared with the yield strain of 10^{-5} for basal glide at room temperature (using macroscopic specimens), the increase is by a factor of 700. The static load indentations do not show any dependence of yield stress on

indentation size. The temperature dependence of the yield stress suggests that the flow stress is determined by the stress required to move a dislocation. (It is assumed that any dislocation nucleating mechanism is relatively insensitive to temperature). If this is the case, then the indentation experiments have measured the flow stress for non-basal glide.

On the other hand, if a dislocation nucleating mechanism is activated and if such a mechanism is temperature sensitive, then the yield stress measured by the indentation experiments may be the stress at which this nucleation takes place.

While the indentation experiments give a nominal stress value, the question of the maximum local stress remains unanswered. There are two reasons for assuming that the maximum stress does not exceed the nominal stress by a large factor. A large stress would have deformed the needle. The needle contains a high density of dislocation and the small-scale flow stress would not differ greatly from the large-scale value. A large elastic strain in the zinc would become apparent, when the needle is removed, as an irregularity in the indentation. The indentation surface is noted to be smooth, rounded and the same for all indentations of the same size. A conical needle with a round tip activates many glide planes in

the specimen if it is to conform to the needle. This means that dislocations must be nucleated simultaneously in many places; the result being that large stress variations at the needle-specimen interface are unlikely.

In the discussion of the splitting experiments performed on zinc, the hypothesis was put forward that during cleavage dislocations are introduced into the specimen. Two deformation markings - the twin bands and the hexagonal glide bands - can not be ascribed to crack-nucleated glide. An explanation of the deformation markings around indentations in terms of these dislocations only is therefore only partial.

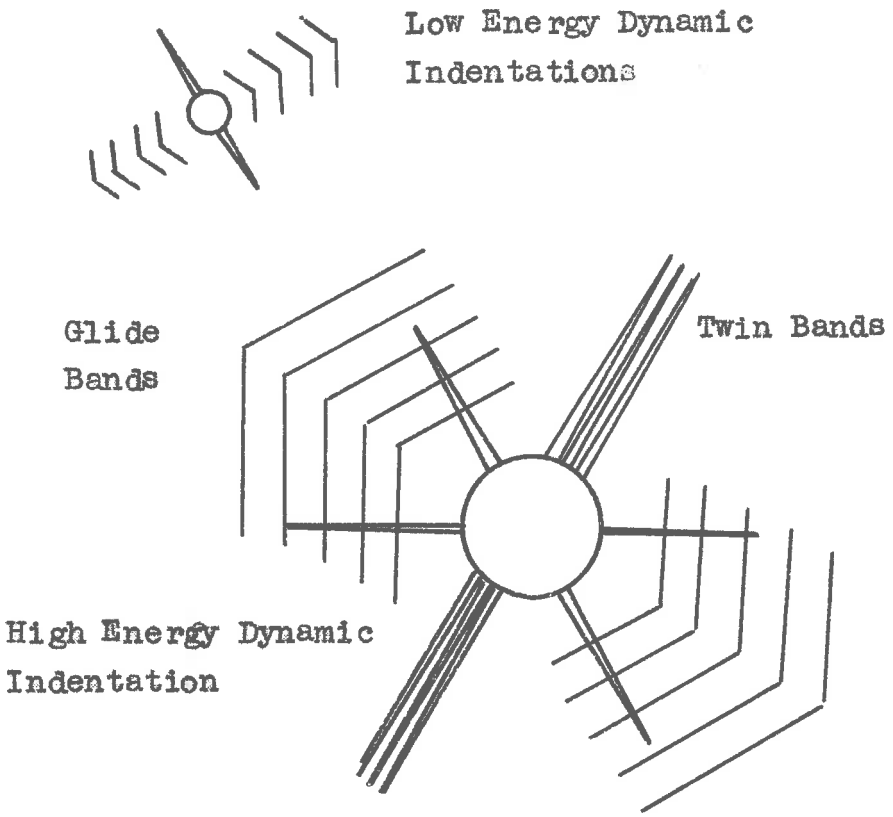

FIG. 5.191 Deformation Patterns around Dynamic Indentations obtained at Room Temperature.

Note the relative Orientation of the Deformation Patterns of the high and low Energy Indentations.

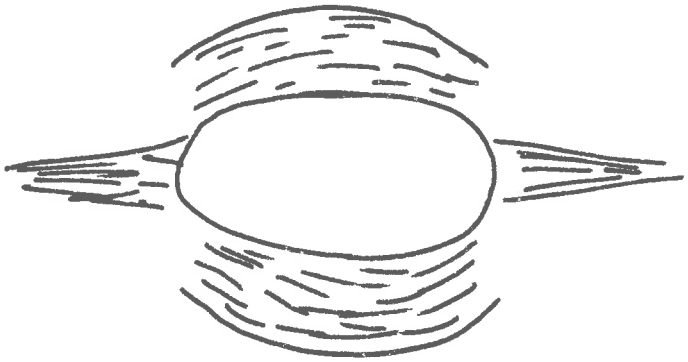

The marked Areas appear as dark Shading under the Microscope.

FIG. 5.192 The Deformation Pattern around a Static Indentation obtained at Room Temperature.

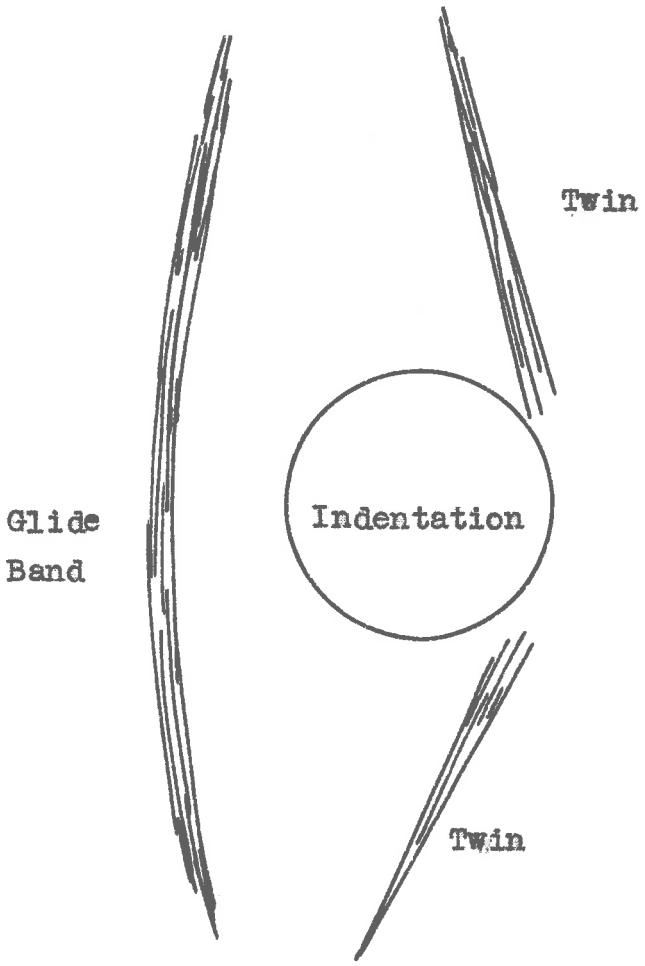

FIG. 5.193 The Deformation Pattern near a Static Indentation obtained at -186°C.

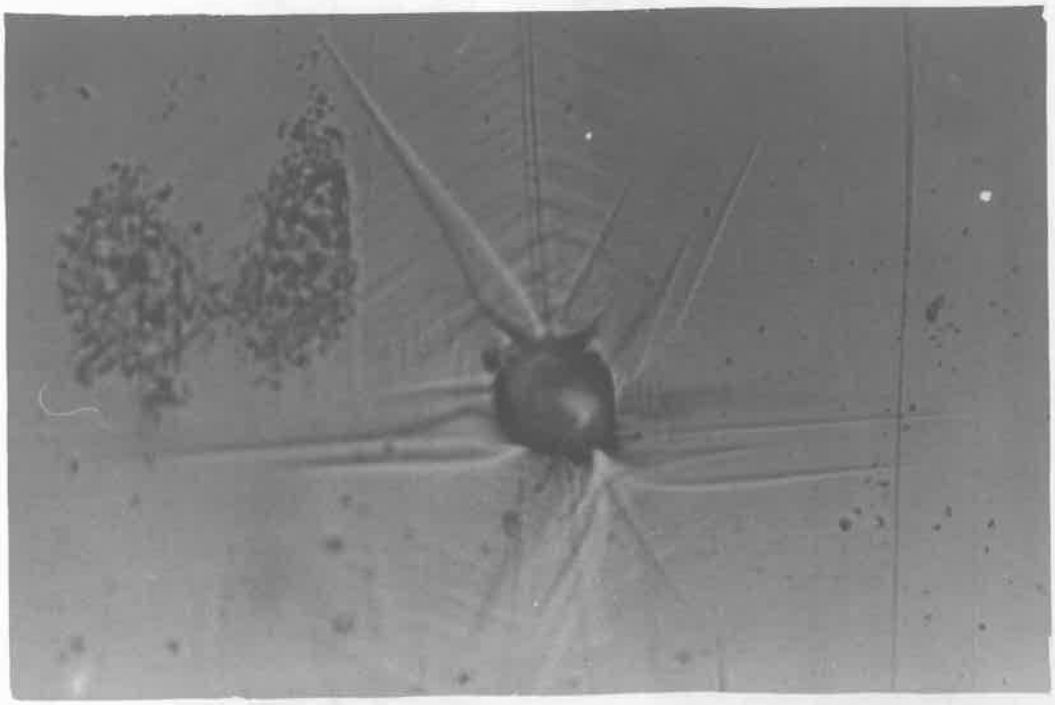

FIG. 5.194a MICROGRAPH, 40x OBJECTVE. A HIGH ENERGY DYNAMIC INDENTATION OBTAINED AT ROOM TEMPERATURE, (600x).

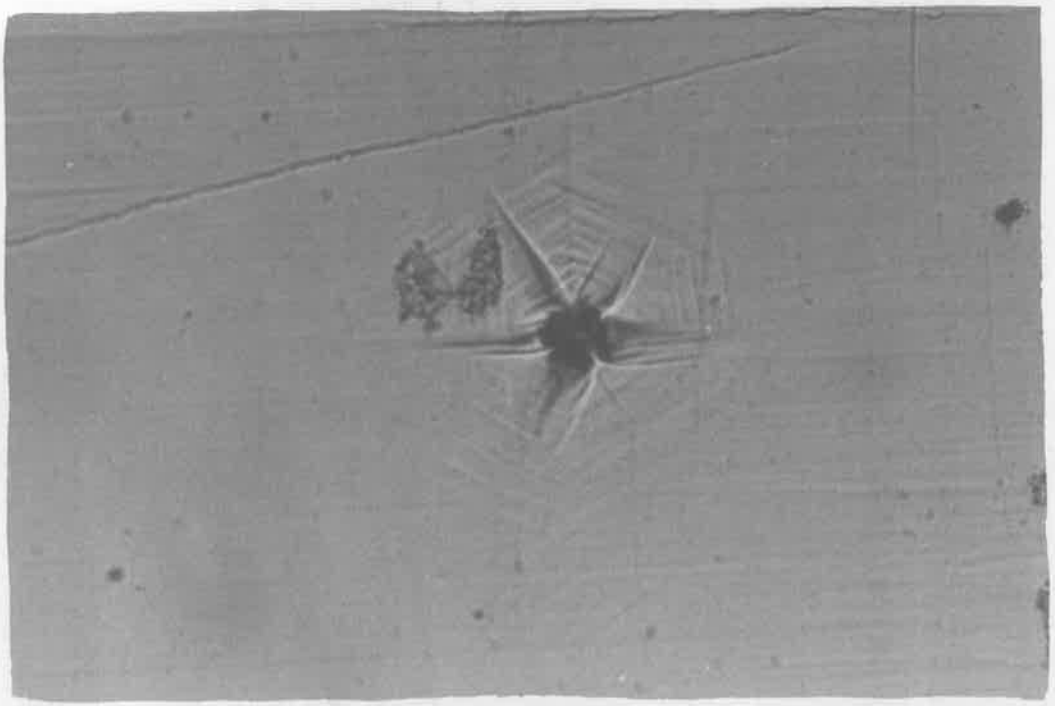

FIG. 5.194b MICROGRAPH, 10x OBJECTIVE. THE SAME INDENTATION SEEN THROUGH ANOTHER MICROSCOPE OBJECTIVE, (300x).

6.0 GENERAL DISCUSSION OF EXPERIMENTAL RESULTS

In the preceding section, the development of the Dislocation Theory of Deformation, its shortcomings, an alternative nucleation hypothesis, and the results of a series of experiments were considered.

The nucleation hypothesis proposed in section 4 will now be applied in greater detail to the experimental results presented in section 5.

A summary of the surface energy values obtained for the various specimens is presented in Table 6.1. It is seen that these values are in the region of 1000 times greater than the surface energy of the molten metal, which is taken to be a good approximation to the solid surface energy value.

A mechanism capable of absorbing all this energy has already been proposed. It was suggested that the stress field around a crack causes the nucleation of glide on glide planes that intersect the surfaces produced by the crack. This glide is energized by the concentrated stress in the neighbourhood of the crack root, with the result that the stress field becomes less intense, and the crack ceases to be propagated.

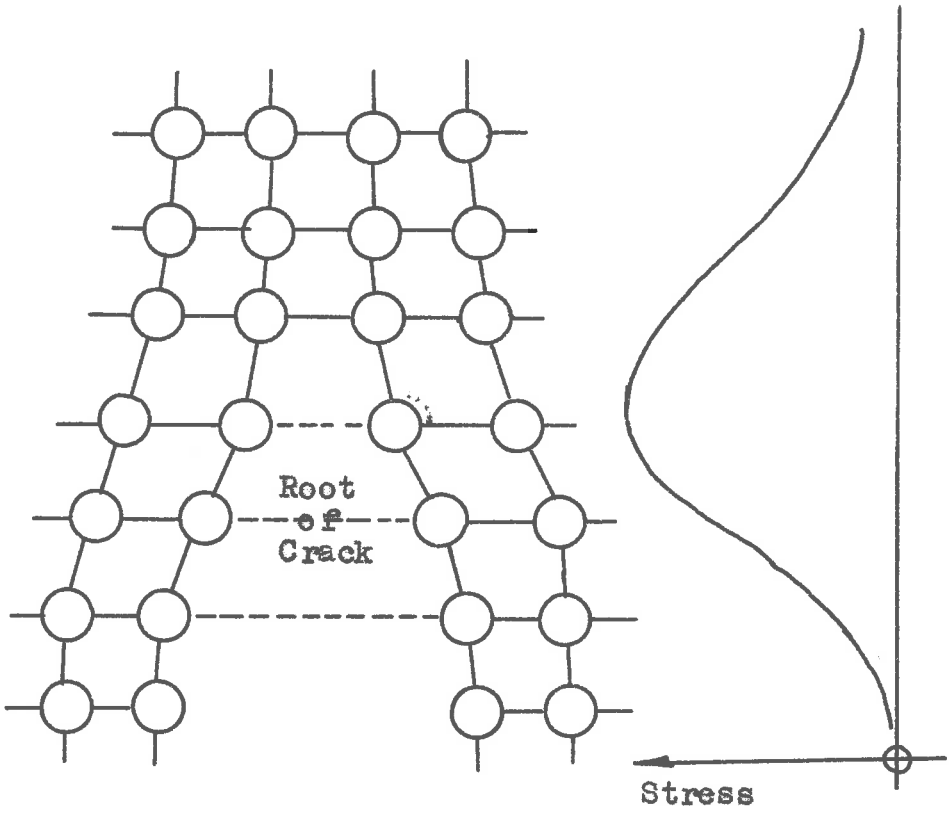

FIG. 6.1 The Root of a Crack in a real Crystal according to the Concepts of the current Theory of Deformation.

TABLE 6.1 Summary of Surface Energy Results

Specimen	Test Temp.	Average Nominal Surface Energy in lb/in^2	"True" Surface Energy in lb/in^2	Ratio Nominal/ "True"	Remarks
T.C.H. Steel	15°C	2.30	8.4×10^{-3}	270	
T.C.H. Steel	-70°C	3.65	8.4×10^{-3}	430	
Mild Steel	-196°C	32.7	8.4×10^{-3}	3900	Furnace cooled
Mild Steel	-196°C	30.3	8.4×10^{-3}	3600	Water quenched
Mild Steel	-196°C	16.9	8.4×10^{-3}	2000	As-machined
Zinc	-196°C	4.28	4.3×10^{-3}	1000	
Bismuth	-196°C	1.03	2.1×10^{-3}	490	
Bismuth	15°C	7.00	2.1×10^{-3}	3300	

*Liquid surface tension values, p. 200, "Metals Handbook" A.S.M., 1948 Edn.

6.1 The Current Theory of Cracks and Fracturing

The mechanism basic to the current theory of fracturing is the crack. When a crystal fractures, new surfaces are formed. The region in which these surfaces are being produced is described as the root of the crack. This process is illustrated in Figure 6.1, which shows two layers of atoms being seperated by a high stress. This high stress value is generated by the crack itself.

It follows that in a perfect lattice where cracks are absent fracture cannot be expected until a stress comparable to the stress at the root of the crack has been imposed on the specimen. Crystals generally fail at stresses far lower than this value.

The position as regards fracture is therefore analogous to that regarding shear deformation. A theory that explains the low fracture strength of materials will take one of two forms:

(1) The crack or a suitable weakness is present in the crystal when stress is applied.

(2) A crack is generated when the crystal is placed under stress.

The theory proposed by Griffith[1] belongs to the first group. The hypothesis that metallic crystals contain cracks, or weaknesses that can release a crack at moderate applied stress is not used in interpreting the brittle behaviour of metallic crystals.

Theories of the second kind have dislocations as the active factor in generating a crack.

Koehler,[53] Mott[54] and Stroh[55] have suggested that a crack may be released by a piled-up group of dislocations.

Fujita[36] (and others before him) has put forward another hypothesis according to which dislocations of opposite sign on parallel planes a few atomic diameters apart, annihilate each other, forming an elongated void. This void eventually releases a crack.

In view of the writer's hypothesis on crack-nucleated glide, it is important to know the shear stress values that can be expected to occur near the root of a crack. Clearly, if the shear stress at the crack root exceeds the stress at which dislocations are nucleated in a crystal (which has been calculated at $\mu/30$), then a pure crack will not be propagated at all, for as soon as a crack appears, the accompanying stress pattern gives rise to dislocations that reduce the stress concentration factor, and so on.

The Crack-Nucleation Glide Hypothesis can be interpreted by use of the current theories of fracture and dislocation. No one, to the writer's knowledge, has examined the possibility that the stress field around a crack may nucleate dislocations.

This glide nucleation mechanism will have its effect on the brittleness or otherwise of any given material. The stress required to propagate a fracture in which glide is nucleated will be higher than the stress

required to propagate a pure crack in the same material. Materials in which the crack nucleates glide will have an apparent surface energy that may be many times the true surface energy.

Thus, a material can fracture only if a suitable crack can be generated, and if the applied stress is sufficient to supply the energy required by the nucleation processes as well as the energy associated with the new surface being formed.

Experience with mild steel, tool steel, zinc and bismuth suggests that if the crack nucleated glide mechanism exists at all, it is a uncommon occurrence. Consequently hypotheses of crack generation such as those of Koehler etc. and Fujita, referred to above, would probably become unacceptable.

The frequency with which dislocations are nucleated would depend on the magnitude by which the shear stress near the crack exceeds the nucleation stress for dislocations. Once such a dislocation line has been nucleated, the root of the crack has undergone a radical change. When the nucleated dislocation has moved away far enough, shear stress values can be high enough to generate another dislocation (or a pair of dislocations).

In this way an array of dislocations can build up until the back stress from this array is such that nucleation ceases. Thus the tensile stress level can build up to a value where a crack can be nucleated. This crack will be able to penetrate some distance, of the order of the total glide before it is again arrested.

If the lattice strongly resists the motion of these nucleated dislocations then the array will not penetrate deeply and the number of dislocations in this array will be relatively small. The energy absorbed by the nucleated dislocations will then be relatively small.

If the nucleation stress is much smaller than the shear stress near a crack, the crack will be arrested more frequently than would be the case if these quantities were nearly equal.

If a crack propagates so rapidly that the dislocations nucleated in its stress field do not have time to move away, then the number of nucleated dislocations is reduced by what may be called dynamic back-stress.

The sequence of events will be as follows. A crack is arrested by nucleated glide, and an array of

dislocations develops. As this process continues, a relatively large volume of crystal is thrown under a tensile stress which finally reaches a level at which a new crack is nucleated. The nucleated crack moves very rapidly at first and glide nucleation is limited. As the crack enters regions of lower stress, the glide nucleation will eventually bring it to rest. An array is now established and the process repeated.

6.2 The Interpretation of the Crack-Nucleated Glide Hypothesis by using the Temporary Electron State Hypothesis

According to the Temporary Electron State Hypothesis, a tensile void is nucleated spontaneously in a lattice under tensile stress.

This tensile void becomes a crack when the applied stress is large enough to develop it. As the void develops, the stress pattern around its periphery gradually tends towards the pattern around a true crack. This stress pattern involves large shear stress values on which shear voids can be nucleated and developed. These shear voids generate dislocations which reduce the stress concentration factor near the crack root, and so increase the overall stress that must be applied if the fracture is to be propagated.

One difference between the predictions about the crack nucleation process when the current theory is applied and when the hypothesis is applied is that successive glide planes will be separated by a distance of the order of the void dimension in the latter case. This difference is marginal for the current theory also predicts large arrays separated by distances of many atomic diameters.

It is the development of secondary fractures on

the zinc and bismuth specimens which points more strongly to the proposed hypothesis. These secondary fractures lie in the same plane as the dislocation arrays, i.e. the glide plane.

According to the proposed hypothesis, the dislocation arrays on the glide planes will attract a void which can open up under a tensile stress. If several secondary fractures are propagated simultaneously, the amount of nucleated glide will be reduced, and the process is favoured.

The theory proposed by Koehler[53] and others analyzes the nucleation of cracks by dislocation arrays, but these cracks will not lie in the plane of the arrays which nucleated them. In this respect the proposed hypothesis stands on its own.

An explanation for the contour lines in terms of thermal resistance to the motion of the dislocations has already been presented.

The reduction of the surface energy of the fracture at reduced temperature for bismuth can also be explained in terms of increased resistance to the motion of dislocations.

The behaviour of the tool steel is opposite to that of bismuth in that the surface energy of the low

temperature specimens is higher. This implies that thermal activation does not assist the dislocation in this steel significantly. At reduced temperature the stress to nucleate cracks and dislocations is higher, as explained previously (section 4). When dislocations are nucleated, they penetrate further into the crystal, or conversely, if their penetration is limited by the crystal dimension, the array becomes denser.

For the steel specimens the crack propagation rate was found to be stress dependent. From the results it appeared that there is a stress below which the fracture is immobile. At stress levels slightly above this, the rate of propagation of the crack increases rapidly with increasing stress. The stress dependence of the fracture velocity was found to disappear at -78°C. This may be interpreted as follows.

At room temperature the stress to nucleate dislocations is lower than at reduced temperature. Thus, it is possible that at room temperature the shear stress is so low that the dislocations require some thermal assistance, particularly to pass impurities and so on. At the reduced temperature the stress is higher and thermal activation is not needed to overcome the same obstacles.

It should be noted that this thermal activation is relatively minor and does not affect the validity of the explanation for the higher surface energy at low temperature.

6.3 An Interpretation of the Results obtained from the Indentation Experiments

The results of the indentation tests are summarized briefly in Table 6.2.

TABLE 6.2

Test condition	Nominal Stress gm/cm^2	Strain	Remarks
$-196^{\circ}C$	5×10^{6}	5×10^{-3}	Static
$15^{\circ}C$	1.4×10^{7}	1.4×10^{-2}	Static
$15^{\circ}C$	$<4 \times 10^{9}$	$<4 \times 10^{-3}$	Dynamic

These results compare well with the results of Price[45,46], who tested platelets and whiskers in the range 0.05μ to 0.5μ and obtained elastic strains of $2-10 \times 10^{-3}$. The dimension of the indentations was in the region 1μ.

Price considered that his specimens were dislocation free. It was indicated in section 5.3 that because of the complex deformation around an indentation, dislocation nucleation is to be expected, even if dislocations have been introduced during the cleavage process.

A considerable interval of time elapsed between the preparation of the cleavage surfaces and the test (several months) so that many of the surface

dislocations will doubtless have annealed out of the crystal.

Both the work of Price and the indentation results indicate that a nucleation process is active and that this process may operate at different stress levels under different conditions.

According to the current theory of deformation, these stress levels are still too low for glide nucleation. Consequently a generating mechanism which makes use of existing dislocations must be sought in applying this theory. Price found that deformation always began at the most highly stressed point, and indentation results indicated complex deformation patterns. In both cases, suitable generators must be present in a small volume of crystal, and in both cases, this is improbable.

6.4 Conclusion

It is unfortunate that a crack nucleated glide mechanism can be put forward in terms of the concepts of the current theory as well as those of the proposed theory.

One important point on which the predictions of the two mechanisms differ is the secondary fracture process. Here the result is in favour of the proposed hypothesis.

The indentation experiments can also be interpreted more readily in terms of the proposed hypothesis.

While these experimental results certainly do favour the proposed hypothesis, it cannot unfortunately be said that the issue between a nucleation theory and a non-nucleation theory of deformation has been decided with anything like a satisfactory degree of certainty.

7.0 GENERAL CONCLUSIONS

The purpose of the writer while embarking on this project was to investigate the elastic and post-elastic behaviour of metals. In the course of his reading he concluded that a nucleation hypothesis should be sought.

When one considers that a given piece of metal is defined by a host of variables - a variable which defines the element, several others which define impurities, the previous stress, strain and temperature history of the specimen, and further parameters that define the nature of the experiment being performed, one may despair of obtaining a significant proportion of the total experimental data available.

Experience shows that these numerous parameters have their effect on a limited number of mechanical properties. There are not likely to be many hypotheses of deformation which are consistent with general physical principles and also make it possible to interpret these mechanical properties in terms of the hypothesis. The other variables can then be considered, and if more than one hypothesis is available, the one that fits experimental results best can be selected.

In this dissertation the writer set out to show that a search for a nucleation hypothesis is justified. He did this by citing the experimental results obtained by other workers, putting forward a nucleation hypothesis and examining the application of this hypothesis in explaining various mechanical properties. Finally, the hypothesis was tested by using it to interpret experimental results obtained by the writer.

This nucleation hypothesis was found to be particularly useful in explaining the behaviour of dislocation free crystals, the phenomenon of delayed yielding, and the phenomenon of secondary fractures that are frequently associated with fracture processes.

These results are significant, and show that this hypothesis, or at least a hypothesis of this kind, i.e. a nucleation hypothesis, deserves serious consideration.

Another important development that has emerged from this investigation, is a hypothesis that explains the melting process. The current theory of deformation does not lend itself to an explanation of this phenomenon, and so it has generally been neglected. This act of expediency is hardly justifiable, for the latent heat of fusion and the melting point of a material and its yield strength for example are related, as Furth[23] has pointed out.

An important application of a satisfactory deformation hypothesis is in predicting the conditions for a material of high strength or any other particular property. Hitherto such developments have been largely empyrical. If, for example, one could find a way in which the nucleation process can be inhibited, materials of high strength (though not necessarily brittle) and high melting point would result. A ductile material with a yield strength of 10^6 p.s.i. say and a melting point of several thousand degrees centigrade would be an extremely valuable engineering material.

Before such developments can be expected, however, a full theoretical appreciation of the nucleation process is necessary. It is possible that when the process of deformation is fully understood, the limits to the various material properties will also be apparent.

It is the writer's thesis that the search for a nucleation process is justified, and that such a process will probably have the general characteristics of the Temporary Electron State Hypothesis described in section 4.

6.0 BIBLIOGRAPHY

1. A.A. Griffith, Phil.Trans.Roy.Soc.(London), A221, 1921, pp. 163, "The Phenomenon of Rupture and Flow in Solids."

2. M. Polanyi, Zeitschrift fur Physik, V.89, P. 660, 1934. "Uber eine Art Gitterstorung, die einen Kristall plastisch machen konnte."

3. L. Prandtl, Z.a.f.a.m.Math.u.Mech., 8, 85-106, 1928.

4. M. Polanyi, Z.a.f.Krist.u.Mineralogie, 61, 1924, 49. "III Deformation von Einkristallen."

5. M. Dehlinger, Annal.Physik, 5, 1929, 2/749. "Zur Theorie der Rekristallisation reiner Metalle."

6. G.I.Taylor, Proc.Roy.Soc.(London), A145, 362, 1934. "The mechanism of Plastic Deformation of Crystals." I.

7. E.Orowan, Z.a.f.Phys. 89, 1934, 605, 614, 634. "Zur Kristallplastizitat I Temperaturplastizitat u. Beckersche Formel II Die Dynamische Auffassung der Kristallplastizitat III Uber den Mechanismus des Gleitvorganges."

8. R.Becker, Physic Z.a. XXVI, 99, 1925. "Uber die Plastizitat amorpher und Kristalliner festen Korper."

9. W. Rosenhain and D. Ewen, Jour.Inst.Met., 8, 149, 1912.
"Intercrystalline Cohesion in Metals."

10. M. Polanyi, Z.S.f Physik, 6/7, 1921, 323.
"Uber die Natur des Zerreibvorganges."

11. M.Zwicky, Physik. Z.S. 24, 1923, 131.
"Die Reibfestigkeit von Steinsalz."

12. J.J. Gilman, Jour.Appl.Phys. V.31, 1960, 2208.
"Direct Measurements of the Surface Energies of Crystals."
P.B. Hirsh, Metallurgical Review, V.4, 1959, 101.
"Direct Experimental Evidence for Dislocations."

13. F. Seitz and T.A. Read, Jour.Appl.Phys. 12, 1941, 100.
"Theory of the Plastic Properties of Solids."

14. F.C.Frank and W.T. Read,Jr., Phys.Rev. 79, 1950, 722.
"Multiplication Process for Slow Moving Dislocations."

15. N.F. Mott, Proc.Phys.Soc. 64, 1951, 381.
"The Mechanical Properties of Metals."

16. A.H. Cottrell, Clarendon Press, Oxford 1953, p. 191.
"Dislocations and Plastic Flow in Crystals."

17. A.H. Cottrell and B.A. Bailby, Phys.Soc.Lond. A62, 1949, 49.
"Dislocation Theory of Yielding and Strain Ageing of Iron."

18. J.C. Fisher, Trans. A.S.M. 47, 1955, 451.
"Application of Cottrells' Theory of Yielding to Delayed Yielding in Steel."

19. D.O. Thompson and D.K. Holmes, Jour.Appl.Phys. 30, 1959, 525.
"Dislocation Contribution to the Temperature Dependence of the Internal Friction and Youngs' Modulus of Copper."

20. K. Lucke and A. Granato, International Conference on Dislocations and Mechanical Properties of Crystals, 1957, pp. 425.
"Internal Friction Phenomena due to Dislocations."

21. N.F. Mott and F.R.N. Nabarro, Report on Strength of Solids (London; Phys.Soc.), 1, 1948.

22. G.L. Smith, Proc.Phys.Soc. 61, 1948, 201.

23. R. Furth, Proc.Roy.Soc.London. A.177, 1940-1, 217.
"A Thermodynamical Theory of the tensile strength of isotropic bodies."

24. G. Liebfried u.K. Lucke, Z.f.d. Physik. 126,1949,450.
"Uber das Spannungfeld einer Versetzung."

25. W.L. Bragg and J.F. Nyl, Proc.Roy.Soc.(London), A190, 1947, 474.
"A Dynamical Model of a Crystal Structure."

26. P.B. Hirsch, Metallurgical Reviews, 4/14, 1959, 101.
"Direct Experimental Evidence of Dislocations."

27. J.J. Gilman et al., Jour.Appl.Phys. 29, 1958, 747.
"Dislocation Etch Pit Formation in Lithium Fluoride."

28. J.J. Gilman and W.G. Johnston, Jour.Appl.Phys. 31, 1960, 687.
"Behaviour of Individual Dislocations in Strain Hardened LiF Crystals."

29. J.J. Gilman and W.G. Johnston, International Conference on Dislocations and Mechanical Properties of Crystals, 1957, p. 116.
"The Origin and Growth of Glide Bands in LiF Crystals."

30. W.G. Johnston and J.J. Gilman, Jour.App.Phys. 30, 1959, 129.
"Dislocation Velocities, Dislocation Densities and Plastic Flow in Lithium Fluoride Crystals."

31. W.G. Johnston and J.J. Gilman, ibid, 31, 1960, 632.
"Dislocation Multiplication in Lithium Fluoride Crystals."

32. W.C. Dash, Journ.Appl.Phys. 27, 1956, 1193.
"Copper Precipitation on Dislocations in Silicon."

33. W.C. Dash, Journ.Appl.Phys. 30, 1959, 459.
"Growth of Silicon Crystals Free from Dislocations."

34. Z.J. Pholen et al. Proc.Roy.Soc.(London), A240, 1957, 524.
"Dislocations and stacking faults in stainless steel."

35. F.D. Rosi and C.H. Mathewson, Trans.A.I.M.E. 188, 1950, 1159.

36. A.F. Brown, Advances in Physics, 1, 1952, 427.
"Surface Effects in Plastic Deformation of Metals."

37. J.T. Fourie and H.G.F. Wilsdorf, Acta Met. 7,1959,339.
"A Study of Slip Lines in α-Brass as Revealed by the Electron Microscope."

38. A.F. Brown and R.W.K. Honeycombe, Phil.Mag. 42, 1951, 1146.
"Micro Slip in Metal Crystals."

39. H.W. Paxton, N.A. Adams and T.B. Massalski, Phil.Mag. 43, 1952, 257.
"Some Observations on Slip Lines in Iron."

40. A. F. Brown, J.Inst.Metals. 80, 1951, 115.

41. R.W. Cahn, J.Inst.Metals. 79, 1951, 129.

42. D.S. Wood and D.S. Clark, Trans.A.S.M. 44, 1952, 726.
"Delayed Yielding in annealed steels at very low Carbon and Nitrogen Content."

43. H.R. Pfeiffer, Acta Met. 9, 1961, 735.
"Concerning delayed yielding in b.c.c. metals (1)".

44. M.J. Whelan, Proc.Roy.Soc. A240, 1957, 524.
"Dislocations and Stacking Faults in Stainless Steel."

45. P.B.Price, Phil.Mag., 5, 1960, 873.
"Pyramidal Glide and the Formation and Climb of Dislocation Loops in Nearly Perfect Zinc Crystals."

46. P.B. Price, Phil.Mag., 6, 1961, 449.
"On Dislocation Loops in Zinc Crystals during Low Temperature Pyramidal Glide."

47. W.G. Dash, International Conference on Dislocation and Mechanical Properties of Crystals, 1957, 116.
"The Observation of Dislocations in Silicon."

48. D.F. Stein and J.R. Low, Jour.Appl.Phys. 31, 1960, 362.
"Mobility of Edge Dislocations in Silicon-Iron Crystals."

49. J.S. Ericson, Jour.Appl.Phys. 33, 1962, 2499.
"Mobility of Edge Dislocations on Slip Planes in 3.25% Silicon Iron."

50. J.L. Powell and B. Crasemann, "Quantum Mechanics", Addison-Wesley, 1961.

51. C.S. Barrett, Structure of Metals, McGraw-Hill, 1952.

52. S.S. Brenner, Jour.Appl.Phys. V.27, 1956, 1484.
"Tensile Strength of Whiskers."

53. J.S. Koehler, Phys.Rev. 85, 1952, 480.
"Production of Large Tensile Stresses by Dislocation (L)"

54. N.F. Mott, Proc.Roy.Soc. A220, 1953, 1.
"Dislocations, Plastic Flow and Creep."

55. A.N. Stroh, Proc.Roy.Soc. A223, 1954, 404.
"The Formation of Cracks as a Result of Plastic Flow."

56. F.E. Fujita, Acta Met. 6, 1958, 543.
"Dislocation Theory of Fracture of Crystals."

57. P.W. Bridgeman
"Studies in Large Plastic Flow and Fracture."

58. Makin - reported by Andrade[60] pp. 138-9.

59. M.Meshii and J.W. Kaufman, Acta Met. 7, 1959, 180.
"Quenching Studies on Mechanical Properties of Pure Gold."

60. E.N. DeC. Andrade, Institute of Metals, No. 13, 1953, 133.
Symposium: "Properties of Metallic Surfaces".

61. F. Blaha and B. Langenecker, Acta Met. 7, 1959, 93.
"Plasticitats Untersuchungen von Metallkristallen im Ultraschallfeld."

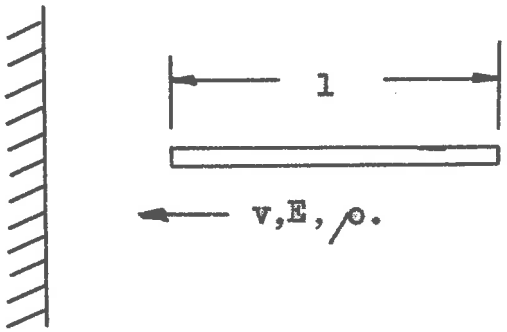

FIG. 9.1 A blunt Needle impacting against a rigid Wall.

9.0 APPENDIX

9.1 Analysis of an Impacting Bundle

Consider the case of a uniform rod of length L, and Elastic Modulus E, colliding with a rigid surface at velocity v, Figure 9.1. When the leading surface of the rod comes into contact with the rigid surface, it stops. A moment later the layer behind it stops and so on. A pressure pulse begins at the front of the rod and travels towards the back. Behind the pressure pulse, the rod is at rest relative to the surface. In front of this pressure front, the rod is still moving at velocity v. The stress in the leading part of the rod and all other parts behind the shock wave is related to the various parameters by the relationship

$$\sigma = v \rho c \qquad \ldots\ldots (9.1)$$

where ρ is the density of the material of the rod and c the velocity of sound.

When the shock has reached the end of the rod the whole rod will be at rest. If the compression of the rod was purely elastic, then all of the kinetic energy has been converted to elastic energy and the stress in the rod is given by the relationship

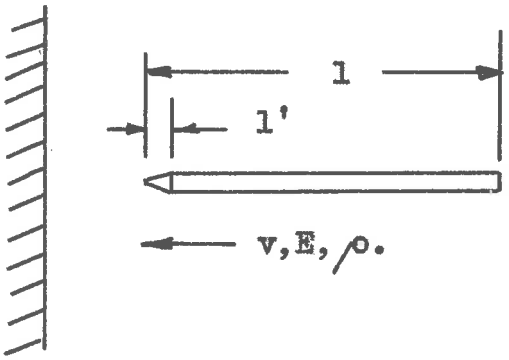

FIG. 9.2 A pointed Needle impacting against a rigid Wall.

$$\tfrac{1}{2}\ \sigma^2/E = \tfrac{1}{2}\ \rho v^2 \qquad \text{..... (9.2)}$$

$$\text{i.e.} \qquad \sigma = \sqrt{\frac{E}{\rho}} \cdot v\rho \qquad \text{..... (9.3)}$$

Equation 9.3 is of the same form as 9.1, giving the well-known relationship

$$c = \sqrt{\frac{E}{\rho}} \qquad \text{..... (9.4)}$$

which is to be expected since the interaction is purely elastic. It is interesting to note that if the shock wave in the rod is plastic, equation 9.1 will immediately give its velocity, for σ is then known.

Consider next a rod with a tapered front, Figure 9.2. This has two effects. The shock wave stress increases in time, and when the tapered portion has come to rest, the stress at the narrowed front has been concentrated and may be expressed by

$$\sigma = R\, v\, \rho c \qquad \text{..... (9.5)}$$

where R is the ratio of the area of the rod to the area of the loading surface. This equation is only valid if the shock pulse has left the tapered section before the loading part of the pulse (which is negative) has returned.

For a tapered needle, the shape of the shock wave is clearly important. Only an approximate analysis is considered here. It is assumed that the tapered section represents only a small portion of the total length of the needle.

The velocity of the needle at the large end of the tapered section may be described by the expression

$$v - v_t = \frac{\sigma_t}{\rho c} \qquad \text{..... (9.6)}$$

where v and σ_t are local values.

Let the stiffness of the tapered section be K and assume that the velocity of sound in this section is infinite. The stress at the large end of the tapered section is therefore also defined by

$$\sigma_t = \frac{K\delta}{a} \qquad \text{..... (9.7)}$$

where δ is the distance by which the tapered section is being compressed, and 'a' is the area of the rod.

Equation 9.6 may be rewritten in the form

$$v_t = \frac{\sigma_m - \sigma_t}{\rho c} \qquad \text{..... (9.8)}$$

where $\sigma_m = v \rho c$.

Differentiating 9.7, with respect to time

$$\frac{d\sigma_t}{dt} = \frac{K}{a}\frac{d\delta}{dt} \qquad \ldots\ldots (9.9)$$

$$= \frac{K}{a} v_t \qquad \ldots\ldots (9.10)$$

Inserting 9.8,

$$d\sigma_t = \frac{K}{a\rho c}(\sigma_m - \sigma_t)\,dt \qquad \ldots\ldots (9.11)$$

The initial value of the stress is not zero, for when the tapered section strikes the wall, a local stress of σ_m is generated, which diminishes in magnitude as the shock travels along the tapered section. At the large end of the taper, the stress value has been reduced to

$$\sigma_o = \frac{1}{K}\sigma_m \qquad \ldots\ldots (9.12)$$

The solution of equation 9.11 takes the form

$$\frac{\sigma_R}{R(\sigma_m - \sigma_t)} = e^{\frac{Kt}{a\rho c}} \qquad \ldots\ldots (9.13)$$

which may be rewritten

$$\frac{\sigma_t}{\sigma_m} = 1 - \frac{1}{K} e^{-\frac{Kt}{a\rho c}} \qquad \ldots\ldots (9.14)$$

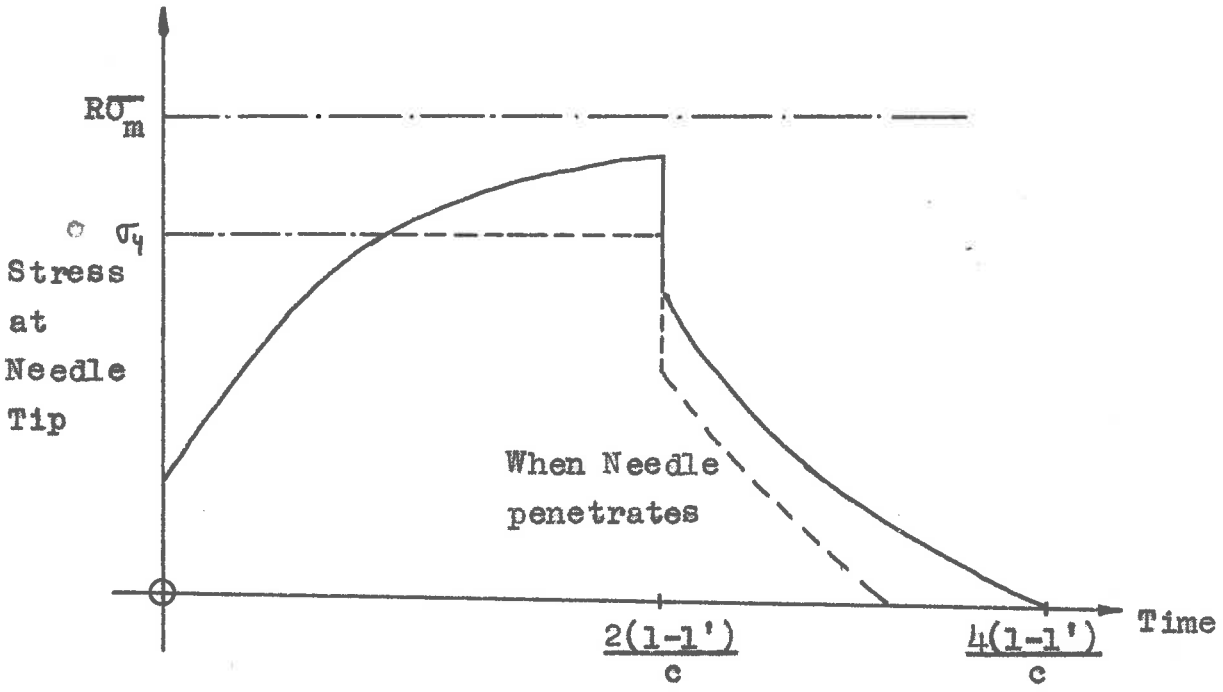

FIG.

FIG. 9.3 The Variation in Time of the Stress at the Pointed Tip of an impacting Needle.

and indicates clearly that σ_t tends towards the maximum asymptotically in time. The stress at the tip of the needle is magnified by the factor R, and is given by the expression

$$\sigma' = \sigma_m\left(R - e^{-\frac{Kt}{\eta\omega}}\right) \qquad \ldots\ldots (9.15)$$

A plot of the stress variation at the needle tip is shown in Figure 9.1.

In this analysis the conical section was treated as a mass-less elastic member with stiffness K. It follows that this analysis is valid only as long as this approximation holds. The effect of the mass of the tapered section is to add an additional inertia force. A correction could be applied, but this is unnecessary, for if the same needle is used the calculated stress at which the specimen yields is in error by the same proportion in all instances and useful comparisons can still be made.

Another reason for neglecting the correction for the inertia of the tapered section is that the specimen surface is not rigid. This reduces the apparent stiffness of the tapered section, and counteracts the effect of the mass of the tapered section.

When the needle has penetrated the specimen surface, the situation is modified in that the stress at the needle

tip does not exceed the local stress on the specimen at which it yields. The stress-time plot for a penetrating needle is shown by the dashed curve of Figure 9.3. It is apparent that if the rebound energy is measured then a plot of rebound energy vs. incident energy will make it possible to determine the point at which the needle just penetrates, and so calculate the yield stress.

9.2 The Limitations of the Isonomic Pendulum

Consider the pendulum system of Figure 5.187 in which there are two strings of length l and total mass m_s. The mass of the needle is m_n, and the impact velocity of the needle is v_i.

The total momentum of the string is

$$p_s = \tfrac{1}{2} m_s v_i \qquad \ldots\ldots (9.16)$$

Let the rebound velocity of the needle be v_r. Assume that the change in momentum of the string occurs immediately after the rebound. When this has happened, the needle velocity is v_r'. Equating the momentum before and after distribution to the string, one obtains

$$v_p = (1 + \tfrac{1}{2}\,\frac{m_s}{m_n})\,v_p' + \tfrac{1}{2}\,\frac{m_s}{m_n}\,v_i \qquad \text{..... (3.17)}$$

The limit is set by

$$v_p' = 0 \text{ whence}$$

$$v_{p\,lim} = \tfrac{1}{2}\,\frac{m_s}{m_n}\,v_i \qquad \text{..... (3.18)}$$

If v_p/v_i is defined as the rebound coefficient then it is apparent that the ratio of the mass of string to the mass of the needle determines the lowest rebound coefficient that can be measured.

Now the impact velocity v_i is determined by the properties of the needle and the material being tested. For a soft material such as wax, it is very low.

To obtain a rebound distance measurable with the unaided eye, the pre-impact travel of the needle must be at least $\frac{1}{4}$ inch. Consequently low values of v_i mean long strings with a concequent increase in string mass and air damping.

In addition, these small displacements require very delicate needle releasing devices.

An obvious improvement is to reduce the needle travel and observe its motion with a suitable microscope. Such an instrument permits one to use a pre-impact travel

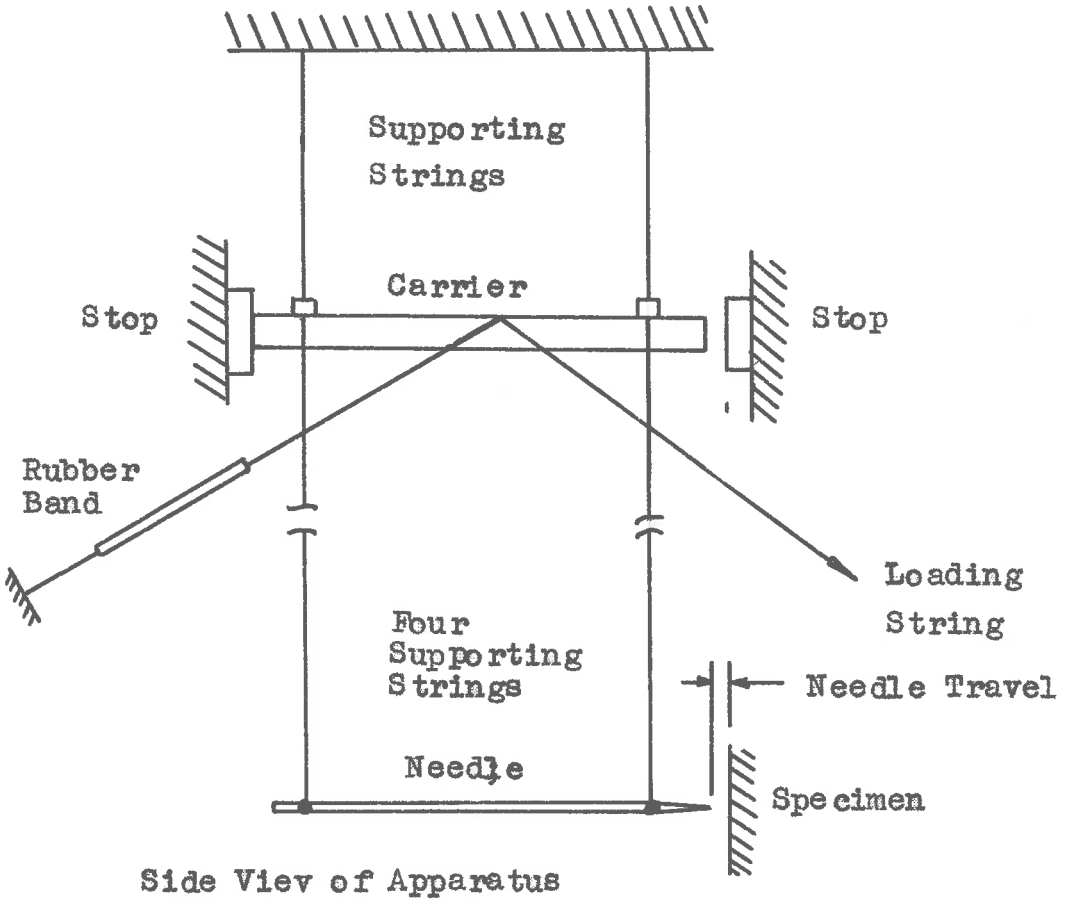

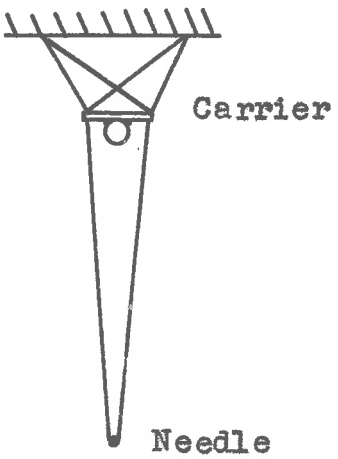

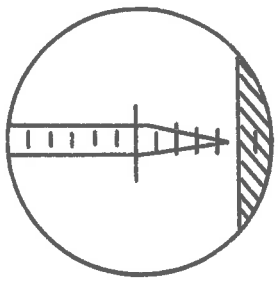

FIG. 9.4 The Improved Dynamic Pendulum Apparatus.

of 0.010 inch only, resulting in a significant reduction of the string length and a corresponding improvement of the performance of the apparatus.

The apparatus presented in Figure 9.4 was an attempt to examine zinc with very low impact energies. Four strings from a rigid support support a carrier and a needle. The carrier is stabilized by two additional strings, which completely remove transverse motion, as shown in the Figure. An elastic string keeps the carrier against one stop. A second string enables the operator to pull the carrier over against the other stop. The specimen is so positioned that the needle would just touch it when it comes to rest after the carrier is pulled over to the second stop.

The procedure is to let the needle come to rest with the carrier against the first stop. The carrier is pulled over quickly and the rebound of the needle is measured. The needle is calibrated by removing the specimen and noting the amplitude of the first free half swing.

It was found that the needle was readily disturbed by the slightest air turbulence, even that due to convection past the operator's body. Zinc, however, showed no rebound for a pendulum length of 22 inches and a displacement of 0.020 inch.

9.3 A SIMPLIFIED MODEL OF THE METALLIC CRYSTAL.

It is postulated that the metallic crystal may be looked upon as an aggregate of positive ions arranged in a regular way and held in place by electrons moving through the lattice.

At equilibrium the electrostatic attraction between ions and electrons is just balanced by the kinetic pressure of the moving electrons.

For stability, the electron pressure must exceed the electrostatic cohesion if the volume of the aggregate is reduced and vice versa if the volume is increased.

Another simplifying assumption made is that the ions do not obstruct the electrons in their motion through the lattice. The electrons are, of course, reflected at the crystal boundaries. A suitable model for the electrons is to imagine them as being contained in a box whose boundaries conform to those of the crystal. Since the charge of the electrons in the crystal is neutralized, the particles in the box may be treated as being without charge but similar in every other respect to electrons.

9.3.1 Quantum Restrictions on a Particle moving between Two Reflecting Walls

A particle of mass m, and velocity v_x is moving

back and forth between two walls a distance 'a' apart, at which it undergoes elastic reflection.

A periodic motion is subject to the quantum restriction (equation (1-39)[50],

$$J = n\,h \quad \text{where} \qquad \ldots\ldots 9.19$$

$$J = \oint p_x\, d_x \qquad \ldots\ldots 9.20$$

$p = m\,v_x$, n is an integer and h is Planck's constant.

For the present case

$$\oint p_x\, d_x = 2\,m\,v_x\,a$$

whence

$$2\,m\,v_x\,a = n_x\,h \qquad \ldots\ldots 9.21$$

Since the electron may occupy any one of these states, a single electron would take n=0. With two electrons the state n=0 is filled because each has opposite spin. With four electrons the states n=0 and n=1 will be filled and so on.

It may be noted that if the reflecting walls are moved together or apart, the state of any electron moving between them is not disturbed if $v_x \gg |da/dt|$.

That is, 'n' in equation 9.21 remains constant.

Differentiating equation 3 one obtains

$$a\,d v_x + v_x\,da = 0 \qquad \text{..... 9.22}$$

The period of one round trip by the electron is $2a/v_x$. In this interval 'a' changes by $(da/dt)2a/v_x$

i.e. $$\delta a = \frac{da}{dt} \cdot \frac{2a}{v_x} \qquad \text{..... 9.23}$$

In the same interval

$$\delta v_x = -\frac{2dv}{dt} \qquad \text{..... 9.24}$$

and if these quantities are substituted into equation 9.22 the equation remains valid, indicating that n remains constant.

9.3.2 Quantum Restrictions on Particles in a Box

Given a rectangular box of dimensions a, b and c in the coordinate directions x, y and z. A particle in this box will generally have three components of velocity v_x, v_y and v_z which are independent of each other. Consequently it can execute three independent periodic motions, each of which conforms to the quantum restriction expressed in equation 9.21.

The particles in this box will naturally arrange themselves in those stable states which permit the total energy of the system to be a minimum. For any particle the kinetic energy E is given by

$$E = \tfrac{1}{2} m v^2 = \tfrac{1}{2} m (v_x^2 + v_y^2 + v_z^2)$$

$$= \frac{1}{2m} (p_x^2 + p_y^2 + p_z^2) \qquad \text{..... 9.25}$$

where $p_x = m v_x = n_x h/2a$

$p_y = m v_y = n_y h/2b$

$p_z = m v_z = n_z h/2c$

$$\therefore \quad E = \frac{h^2}{2m} \left(\frac{n_x^2}{4a^2} + \frac{n_y^2}{4b^2} + \frac{n_z^2}{4c^2} \right) \qquad \text{..... 9.26}$$

It will be noted that p_x, p_y and p_z increase in units of $h/2a$, $h/2b$ and $h/2c$ respectively. Each particle has a vector p which is the vector sum of the three components p_x, p_y and p_z. If this vector is drawn from an origin, it ends at one intersection point of a three dimensional line grid which has the intervals $h/2a$, $h/2b$, or $h/2c$ in the three component directions. The various possible momentum vectors can therefore be represented by points in this grid.

It follows that the total energy of N particles in the box is a minimum if their corresponding points in the grid are contained by a spherical surface below which all available grid points are occupied.

The volume of this space is

$$V' = \frac{1}{8}\left(\frac{4}{3}\pi p_{max}^3\right) \qquad \text{..... 9.27}$$

for only positive values of n_x, n_y and n_z are relevant. The volume per grid point V" is

$$V'' = \frac{h}{2a} \cdot \frac{h}{2b} \cdot \frac{h}{2c} = \frac{h^3}{8abc}$$

so that the number of grid points occupied is

$$\frac{N}{2} = \frac{V'}{V''} = \frac{\pi p_{max}^3}{6} \cdot \frac{8abc}{h^3}$$

$$\frac{N}{2} = \frac{4}{3}\,\frac{\pi abc\, p_{max}^3}{h^3}$$

abc is the volume V of the crystal, whence

$$\frac{N}{2} = \frac{4\pi V p_{max}^3}{3h^3} \qquad \text{..... 9.28}$$

The number of electrons N is equal to twice the number of grid points.

It follows also that

$$p_{x\,max} = p_{y\,max} = p_{z\,max} = p_{max}$$

whence $$n_x = \frac{2a\,p_{max}}{h}$$

$$n_y = \frac{2b\,p_{max}}{h} \qquad \ldots\ldots 9.29$$

$$n_z = \frac{2c\,p_{max}}{h}$$

The total energy of the particles in the box may be found as follows.

The volume of the element between the surfaces of radii p and p+dp is dV

$$dV = \tfrac{1}{8}\,4\pi p^2 dp \qquad \ldots\ldots 9.30$$

the number of grid points is $\frac{dV}{abc}$

$$d\left(\frac{N}{2}\right) = \frac{4\pi p^2 dp.dV}{2h^3}$$

$$dN = \frac{2.4\pi p^2 V dp}{h^3} \qquad \ldots\ldots 9.31$$

The energy of each particle with momentum p is $\frac{p^2}{2m}$ so that the energy of the particles in the momentum range p+dp is

$$\frac{p^2}{2m}\,dN = \frac{8\pi m^2 V dm}{h^3} \cdot \frac{p^2}{2m}$$

$$\frac{dE}{dm} = \frac{8\pi V m^4 dm}{2mh^3} \qquad \ldots\ldots 9.32$$

From the definition

$$\bar{E} = \int_0^{p_{max}} dE$$

$$= \int_0^{p_{max}} \frac{8\pi V}{2mh^3} \cdot p^4 dp$$

$$\bar{E} = \frac{4\pi V p_{max}^5}{5mh^3} \qquad \ldots\ldots 9.33$$

Now the kinetic pressure $\bar{p} = \frac{dE}{dV}$

$$\therefore \quad \bar{p} = \frac{4\pi p_m^5}{5mh^3} + \frac{4\pi \cdot 5p_m^4}{5mh^3} \frac{dp_m}{dV}$$

$$\bar{p} = \frac{4\pi p_m^5}{5mh^3}\left(1 + \frac{V}{p_m}\frac{dp_m}{dV}\right) \qquad \ldots\ldots 9.34$$

From equation 11

$$p^3_{max} = \frac{3Nh^3}{8\pi V} \qquad \text{..... 9.35}$$

and $$3p^2_{max}\, d(p_{max}) = -\frac{3Nh^3}{8\pi} \cdot \frac{1}{V^2}\, dV \qquad \text{..... 9.36}$$

whence

$$\frac{dp_{max}}{dV} = -\frac{h^3}{3\pi V^2 p^2_{max}} \qquad \text{..... 9.37}$$

$$\frac{dp_{max}}{dV} = -\frac{p_{max}}{3V} \qquad \text{..... 9.38}$$

Equation 9.30 becomes

$$\bar{p} = \frac{4\pi V^5 m}{5nh^3} (1 - \tfrac{1}{3})$$

$$\bar{p} = \frac{8\pi p^5_m V}{15nh^3} \qquad \text{..... 9.39}$$

This equation can be converted into a more convenient form by using equation 9.28

$$\bar{p} = \frac{3^{2/3}}{20m\pi^{2/3}} h^2 \left(\frac{N}{V}\right)^{5/3} \qquad \text{..... 9.40}$$

9.3.3 The Electrostatic Cohesion in a Metallic Crystal

To compute the cohesive pressure in the metallic crystal, a simplified model will be considered. While metals generally have the close-packed structure, a simple cubic lattice will be considered here.

Instead of moving electrons, the negative charges are taken to be equally distributed amongst all the points which are midway between two ions.

In the simple cubic structure each ion is surrounded by six such points. If the ion is singly ionised, one sixth of the electronic charge is taken to be located at each of these points.

Each point of negative charge is situated midway between two ions. Hence, the total electronic charge at these points is the sum of the contributions made by these ions, namely one third of the electronic unit charge.

Each ion in the cubic lattice is surrounded by six regularly spaced ions at a distance 'r' and six points of negative charge of magnitude $\frac{1}{3}e$ at a distance of $\frac{1}{2}r$.

The ion attracts each point of charge with a force

$$f_1 = \frac{K \cdot e \cdot 12}{(\frac{1}{2}r)^2} = \frac{48Ke^2}{3r^2} \qquad \text{..... 9.41}$$

Each negative charge is repelled by the other five charges in a direction opposite to the attraction of the ion with a force

$$f_2 = \frac{4 \cdot K \cdot (\frac{1}{2}e) \cdot 1(e)}{\sqrt{2} \cdot (\frac{1}{\sqrt{2}}r)^2} + \frac{K(\frac{1}{2}e)^2}{r^2}$$

$$f_2 = \frac{(4\sqrt{2}+1)}{8} \cdot \frac{Ke^2}{r^2} \qquad \text{..... 9.42}$$

whence the net inwards acting force is

$$f_a = \frac{9.60\,Ke^2}{r^2} \qquad \text{..... 9.43}$$

This point is surrounded by other charges of both signs. To a first approximation the effect of these charges may be assumed to cancel out. Hence, the force with which each negative charge is pulled towards

its nearest ions is 'f_a' and this is the magnitude of the force pulling the ions together.

The net inter-ionic attraction, 'f_a' is equivalent, in the simple cubic lattice, to a cohesive stress

$$P_c = \frac{f_a}{r^2} = \frac{0.6\,Ke^2}{r^4} \qquad \ldots\ldots 9.44$$

If N' ions arranged in the simple cubic manner occupy a volume V then

$$\frac{N'}{V} = \left(\frac{1}{r}\right)^3 \qquad \ldots\ldots 9.45$$

whence

$$P_c = 0.60\,Ke^2 \left(\frac{N'}{V}\right)^{4/3} \qquad \ldots\ldots 9.46$$

If the analysis had been performed with a more precise model equation 9.46 would retain its general form, but the numerical constant would be changed, and terms of higher order would also appear.

If the ions are doubly ionised, the interacting forces are doubled and the same factor must be inserted into equation 9.46.

9.3.4 The Stability of the Metallic Crystal

The kinetic pressure of the electrons in the metallic crystal is given by equation 9.40, which is presented in simplified form below

$$\bar{p} = K_p \left(\frac{N}{V}\right)^{5/3} \qquad \text{..... 9.47}$$

The expression for cohesive pressure, as derived from equation 9.46 takes the form

$$P_c = K_c \; n^{-\frac{1}{3}} \left(\frac{N}{V}\right)^{4/3} \qquad \text{..... 9.48}$$

where n is the number of free electrons per atom,

$$K_p = \frac{3^{2/3} h^2}{20m\pi^{2/3}} \quad \text{and}$$

$$K_c = 0.60 \, K_e^2$$

It is immediately obvious that these two pressures are equal at one point only and that if the volume of the crystal is reduced below the equilibrium value, the kinetic pressure is the larger and vice versa, which is the requirement for stability of the crystal.

The elastic bulk modulus of the crystal is

$$B = \frac{1}{V} \frac{dp}{dV} = \frac{1}{V}\left(\frac{d\bar{p}}{dV} - \frac{dp_c}{dV}\right) \qquad \text{..... 9.49}$$

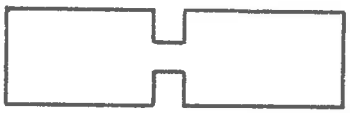

FIG. 9.5 The Intemediate Shear Rate Test Specimen.

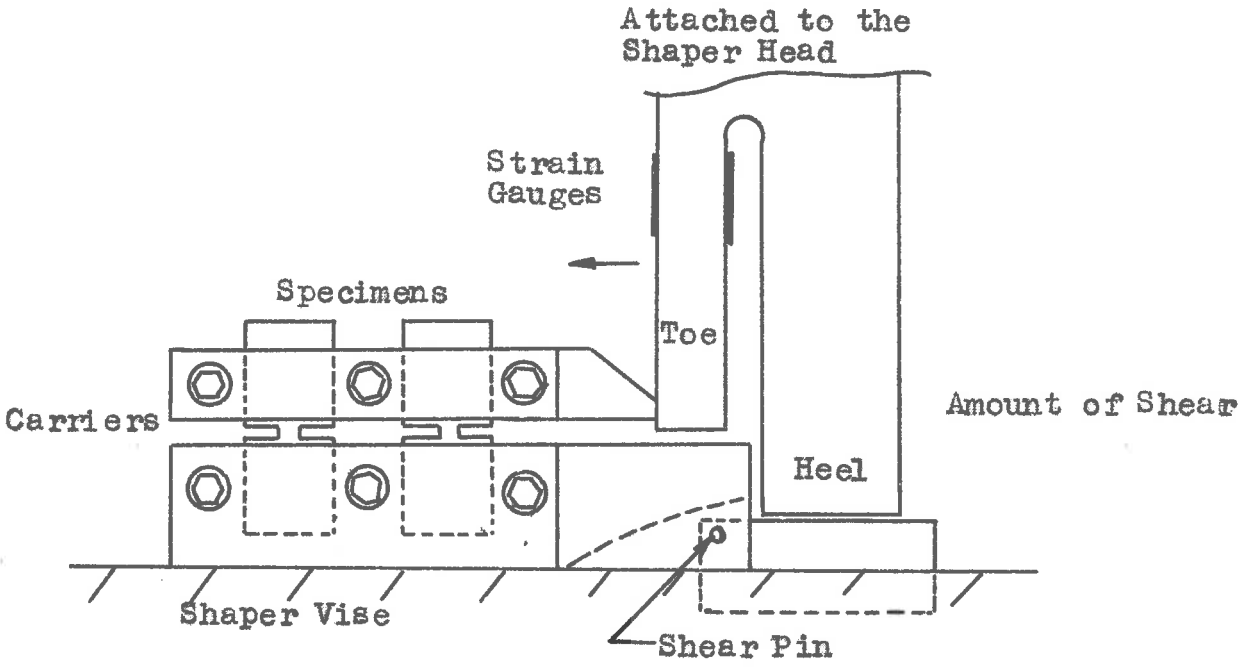

FIG. 9,6 The Intermediate Shear Rate Test Apparatus.

9.4 The Shear Test Apparatus

The shear deformation test was to have been performed for strain rates of 0.1 per second to 10^5 per second. Three kinds of apparatus, for the ranges 0.1-10, $10-10^3$ and 10^3-10^5 were to be employed.

9.4.1 The Intermediate Shear Rate Apparatus

These tests were performed on a shaper. The specimen is presented in Figure 9.5, and the apparatus is shown in Figure 9.6. The specimens are clamped onto the upper and lower carrier. The lower carrier is attached to the shaper vice by a pin which passes through the lower carrier and a hole near the edge of a piece of mild (or other) steel about 0.050 inch thick, clamped by the vice.

The loading device replaces the cutting tool that is normally mounted on the shaper head. The toe on this device is a cantilever with strain gauges attached. The heel is more rigid.

The procedure is to mount the apparatus on the shaper, select a shaper head speed and then take the head through a single stroke. The heel first makes contact with the upper carrier and brings it to the slider head velocity. The lower carrier is still fixed and

the relative motion appears as shear deformation in the specimens. The heel then makes contact with the lower carrier and releases it by shearing through the restraining plate. The carriers are collected in a box packed with rags and cotton-wool.

The apparatus is set up by mounting the lower carrier on the vice with the specimens clamped in. The heel of the loading device is now brought within a pre-determined distance of the lower carrier (as measured by suitable spacers). The upper carrier is shifted until it touches the toe of the loading device and clamped onto the specimens. The vertical displacement between the two carriers is maintained by another spacer which is removed after the upper carrier is clamped.

The signal from the strain gauges is recorded by pen recorder or by photographing a C.R.O.-trace.

The apparatus for calibrating the toe is shown in Figure 9.7. The procedure is self evident.

9.4.2 High Shear Rate Apparatus

The specimen, and the manner in which it is deformed, can be seen from Figure 9.8. The loading head strikes the centre of the specimen first, causing shear deformation. The specimen is then released when the

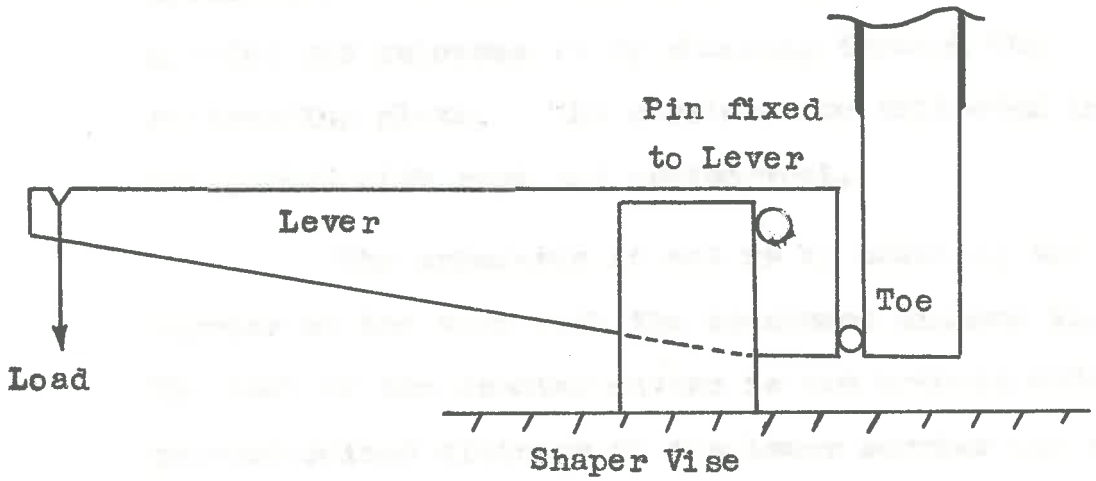

FIG. 9.7 Calibration of the Intermediate Shear Rate Loading System.

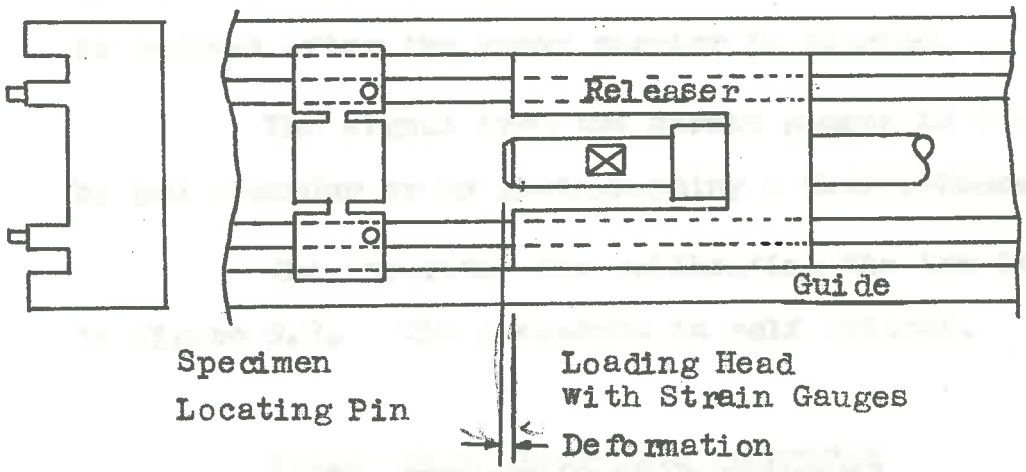

FIG. 9.8 The Specimen loading Arrangement for the high and low Rate Shear Test Apparatus.

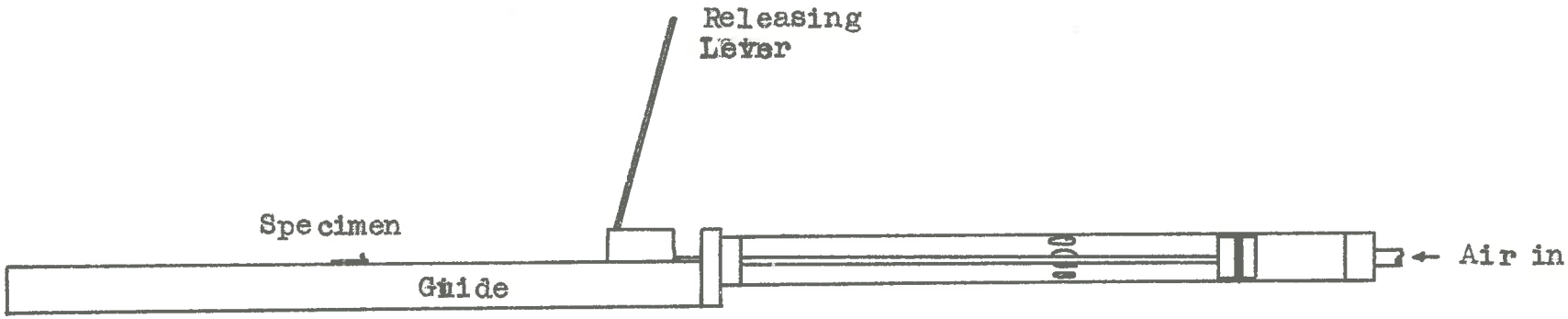

FIG. 9.9 The High Rate Shear Test Apparatus.

heels force the specimen away from the loading pins by shearing through the holes. The specimen is caught in a box packed with waste.

The whole rig, Figure 9.9, illustrates the way in which the loading device is accelerated. Air pressure builds up behind the driving piston, and when the loading device is released it is accelerated by the air under pressure. When the piston has travelled half-way along the cylinder, it passes vents and from there on the pressure in front of the piston builds up, and it is slowed down.

Strain gauges mounted on the loading head measure the force during the deformation process.

9.4.3 Low Shear Rate Apparatus

The high shear rate apparatus may be used to obtain very low loading head velocities by using oil as the working fluid. Oil from a high pressure source is passed through a high hydraulic resistance and into the space normally filled by the driving air. The loading can be terminated at will, and the specimen releasing mechanism which operates during high rate tests is no longer necessary.

9.4.4 Shear Tests at High and Low Temperatures

The specimen can be thermally insulated from the guide, so that for the high and low rate tests at least, it may be tested at high or low temperatures. The additional apparatus required is a heater or cooler which is brought into contact with the specimen, and removed just before testing, during high rate tests, and held in contact with the specimen during low rate tests.